Properties of Plant Fiber Yarn Polymer Composites

An Experimental Study

Madsen, Bo; Lilholt, Hans; Damkilde, Lars; Hoffmeyer, Preben; Thomsen, Anne Belinda

Publication date:
2004

Document Version
Publisher's PDF, also known as Version of record

BYG·DTU

Bo Madsen

Properties of Plant Fibre Yarn Polymer Composites

An Experimental Study

TECHNICAL
UNIVERSITY
OF DENMARK

Report
BYG·DTU
R-082
2004
ISSN 1601-2917
ISBN 87-7877-145-5

SUMMARY

The evolutionary history of plants means that the mechanical properties of their load-bearing elements, i.e. the plant fibres, are highly optimised with respect to the mechanical requirements of plants. Moreover, plant fibres themselves can be thought of as composite materials, but with a structure far more complex than any man-made composites. Thus, in addition to the attractive mechanical properties of plant fibres, they might as well provide insight into form and function of a sophisticated composite material.

The use of plant fibres as reinforcement in composite materials is finding increasing interest in the automotive and building industry, and the properties of plant fibre composites have been addressed in numerous research studies. The work has so far mainly been focused on plant fibre composites with a random fibre orientation, and therefore with moderate mechanical properties. To explore the full reinforcement potential of plant fibres requires however that the fibres are aligned. Presented in this study are experimental investigations of the properties of aligned plant fibre composites based on textile hemp yarn and thermoplastic matrices.

The characteristics of textile hemp yarn have been investigated. The fibres are well separated from each other; i.e. only few fibres are situated in bundles. The twisting angle is low; i.e. about 15° for the outermost fibres in the yarn. The water sorption capacity of the fibres is much reduced in comparison to raw hemp fibres. Stiffness and ultimate stress of the fibres are estimated from composite data in the ranges 50-65 GPa and 530-650 MPa, respectively. These findings show that textile hemp yarn is well suited as composite reinforcement.

The volumetric interaction in aligned hemp yarn composites have been investigated. A model is presented to predict the relationship between fibre volume fraction and porosity. The porosity content is well predicted from experimentally determined parameters such as fibre luminar dimensions and fibre compactibility. In particular, the latter parameter is found to be important. Composite porosity starts to increase dramatically when the fibre volume fraction approaches a certain maximum value, which is accurately predicted by the compactibility of the fibres.

The water sorption properties of aligned hemp yarn composites have been investigated. Water diffusion is non-Fickian, and is characterised by so-called two-stage diffusion behaviour, which is a well-known phenomenon in synthetic fibre composites. The rate of water diffusion is largest in the axial direction along the fibres, and is not identical in the two transverse directions. These

anisotropic water diffusion properties imply that different diffusion coefficients must be assigned to the three directions. The dimensional swelling/shrinkage of the composites at the two humidities 35 and 85 % RH, with respect to a reference humidity of 65 % RH, is relative small. The dimensional swelling/shrinkage in the transverse directions is less than ±1 %, whereas the dimensions in the axial direction are almost unchanged. For composites with high fibre content, the dimensional swelling/shrinkage is well predicted from the product of density and water content of the composites. This simple predictability of the water-related dimensional changes is beneficial with respect to an industrial use of aligned plant fibre composites.

The tensile properties of aligned hemp yarn composites have been investigated. For composites with fibre volume fraction in the range 0.30-0.34, stiffness is in the range 16-20 GPa and ultimate stress is in the range 190-220 MPa. Generally, these properties are superior to previously reported properties of aligned plant fibre composites (with a comparable fibre volume fraction). The investigations included a number of relevant parameters: testing direction, yarn type, matrix type, fibre volume fraction, process temperature and conditioning humidity. The tensile properties of the composites are highly affected by the testing direction; e.g. axial ultimate stress is reduced from 205 to 125 MPa at an off-axis angle of only 10°. The off-axis properties are well modelled by a planar model of a homogenous and orthotropic material. The reinforcement efficiency is different between types of hemp yarn. Even for two batches of the same type of hemp yarn, but bought separately in time, the reinforcement efficiency is not identical. This underlines a critical aspect in the use of plant fibres; i.e. their properties are less controllable in comparison to the properties of synthetic fibres. The axial tensile properties of the composites are affected only little by the degree of fibre/matrix compatibility. Even for composites with a strong fibre/matrix bonding, no clear improvement in axial properties are observed, but the failure characteristics of the composites are changed dramatically. A model is presented to predict the tensile properties of the composites as a function of the fibre volume fraction. Axial stiffness and ultimate stress are well predicted by the model. The model includes the effect of porosity, and demonstrates how tensile properties of the composites are reduced when the porosity is increased. The process temperature is mainly affecting axial ultimate stress of the composites; e.g. when the process temperature is increased from 180 to 220 °C, axial ultimate stress is decreased from 240 to 170 MPa. The results emphasize the importance of a low process temperature. The conditioning humidity is mainly affecting axial stiffness and strain at ultimate stress of the composites; e.g. when the conditioning humidity is increased from 35 to 85 % RH, axial stiffness is decreased from 18 to 14 GPa, and axial strain at ultimate stress is increased from 0.026 to 0.037. The results underline that plant fibre composites need to be carefully conditioned before testing in order to compare results between series of experiment.

RESUMÉ

Den evolutionære udvikling af planter betyder at deres last bærende elementer, dvs. plantefibre, besidder mekaniske egenskaber som er optimeret i forhold til efterkomme de mekaniske krav som stilles af planterne. Plantefibre kan herudover betragtes som værende en form for kompositmateriale, men med en struktur som er langt mere kompliceret end syntetiske kompositter. Plantefibre besidder således ikke kun attraktive mekaniske egenskaber, men kan også tjene til at bibringe en forståelse for form og funktion af et sofistikeret kompositmateriale.

Interessen for anvendelse af plantefibre som forstærkning i kompositmaterialer er stigende i bil- og byggeindustrien og egenskaberne af plantefiberkompositter er beskrevet i et stort antal videnskabelige studier. Indtil videre har fokus hovedsageligt været på plantefiberkompositter med en tilfældig fiberorientering, og derfor med moderate mekaniske egenskaber. For at undersøge plantefibrenes fulde forstærkningspotentiale er det imidlertid nødvendigt at fibrene er ensrettede. Dette studie præsenterer eksperimentelle undersøgelser vedrørende egenskaberne af ensrettede plantefiberkompositter baseret på tekstilhampegarnfibre og termoplastiske matricer.

Egenskaberne af tekstilhampegarn er blevet undersøgt. Fibrene er fortrinsvist adskilt fra hinanden (dvs. kun få fibre optræder i bundter). Snoningsvinklen i garnet er lav (omkring 15° for de yderste fibre i garnet). Vandsorptionskapaciteten for fibrene er lav i forhold til ubehandlede hampefibre. Fibrenes stivhed og brudspænding er estimeret på baggrund af kompositdata til henholdsvis at være i områderne 50-65 GPa og 530-650 MPa. Disse resultater viser at hampegarn er velegnet som forstærkning af kompositmaterialer.

En model er udviklet til at forudsige den volumetriske interaktion i hampegarnkompositter. Forudsigelsen af kompositternes porøsitet er god, og er modelleret på baggrund af en række eksperimentelle parametre såsom størrelsen af lumen i fibrene og fibrenes sammentrykkelighed. Specielt fibrenes sammentrykkelighed er en vigtig parameter. Porøsiteten stiger dramatisk når fibervolumenfraktionen nærmer sig en given maksimum værdi som præcist kan forudsiges udfra fibrenes sammentrykkelighed. Den præsenterede model er et godt redskab til at forudsige forholdet mellem fibervolumenfraktion og porøsitet i plantefiberkompositter.

Vandsorptionsegenskaberne af ensrettede hampegarnkompositter er blevet undersøgt. Resultaterne viser at diffusionen af vand afviger fra Ficksk diffusion, og er karakteriseret ved et såkaldt totrins diffusionsmønster, hvilket er et velkendt fænomen indenfor syntetiske fiberkompositter.

Diffusionshastigheden i kompositterne er størst i den aksiale retning langs fibrene, men er ikke ens i de to tværgående retninger. De fugtbetingede dimensionsændringer af kompositterne ved luftfugtighederne 35 og 85 % RF, i forhold til en reference luftfugtighed på 65 % RF, er relative små. Dimensionsændringerne i de tværgående retninger er mindre end ± 1 %, hvorimod dimensionerne i den aksiale retning nærmest er uændret. De fugtbetingede dimensionsændringer for kompositter med en højt fiberindhold kan estimeres udfra produktet af densitet og vandindhold af kompositterne. Denne enkle metode til at forudsige de fugtbetingede dimensionsændringer er fordelagtig i forhold til en industriel anvendelse af ensrettede plantefiberkompositter.

Trækegenskaberne af ensrettede hampegarnkompositter er blevet undersøgt. Stivhed og brudspænding er henholdsvist målt i områderne 16-20 GPa og 190-220 MPa for kompositter med en fibervolumenfraktion i området 0.30-0.34. Disse trækegenskaber er generelt bedre end tidligere publiceret trækegenskaber for ensrettede plantefiberkompositter (men en sammenlignelig fibervolumenfraktion). En antal relevante parametre er inkluderet i undersøgelserne: trækretning, garntype, matrixtype, fibervolumenfraktion, proces-temperatur og konditioneringsfugtighed. Trækegenskaberne er i høj grad påvirket af trækretningen; f.eks. er den aksiale brudspænding reduceret fra 205 til 125 MPa ved en off-axis vinkel på kun 10°. Relationen mellem trækretning og trækegenskaber er modelleret på basis af en plan model af et homogent og orthotropisk materiale. Forstærkningsgraden for forskellige hampegarntyper er ikke ens. Dette gælder selv for to partier af den samme hampegarntype indkøbt med 2 års mellemrum. Egenskaberne af plantefibre er således ustabile i forhold til syntetiske fibres stabile egenskaber. Affiniteten mellem fibre og matrix har kun en lille betydning for kompositternes aksiale trækegenskaber. Dette gælder selv for kompositter med en stærk binding mellem fibre og matrix, selvom brudmønsteret i disse kompositter er markant ændret. En model er udviklet til at forudsige trækegenskaberne af kompositterne som funktion af fibervolumenfraktionen. Forudsigelsen af kompositternes aksiale stivhed og brudspænding er god. Kompositternes porøsitet indgår som en parameter i modellen, og det påvises at trækegenskaberne forringes når porøsiteten stiger. Proces-temperaturen påvirker hovedsageligt kompositternes aksiale brudspænding; f.eks. bliver den aksiale brudspænding reduceret fra 240 til 170 MPa når proces-temperaturen øges fra 180 til 220 °C. Konditioneringsfugtigheden påvirker hovedsageligt kompositternes aksiale stivhed og brudtøjning; f.eks. bliver den aksiale stivhed reduceret fra 18 til 14 GPa når konditioneringsfugtigheden øges fra 35 til 85 % RF, og samtidig bliver den aksiale brudtøjning forøget fra 0.026 til 0.037. Dette understreger vigtigheden af at plantefiberkompositter konditioneres under kontrollerede klimatiske forhold inden de testes.

PREFACE

This thesis is submitted as a partial fulfilment of the requirements for the Danish Ph.D. degree. The study was carried out during 2000 to 2003 at the Department of Civil Engineering (BYG), Technical University of Denmark. Part of the experimental research has been carried out at the Materials Research Department (AFM), Risoe National Laboratory and at the Plant Research Department (PRD), Risoe National Laboratory.

The project was financially supported by the Danish Research Councils (project: "Characterisation and application of plant fibres for new environmentally friendly products"), and by the Danish Research Agency of the Ministry of Research (project: "High performance hemp fibres and improved fibre network for composites"). Moreover, the project was partly supported by the Engineering Science Centre for Structural Characterization and Modelling of Materials.

The study has been supervised by:

Associate Professor, Ph.D., Preben Hoffmeyer (BYG)	Main supervisor
Associate Professor, Ph.D., Lars Damkilde (BYG)	Co-supervisor
Senior Scientist, Ph.D., Hans Lilholt (AFM)	Co-supervisor
Senior Scientist, Ph.D., Anne Belinda Thomsen (PRD)	Co-supervisor

I wish to acknowledge my supervisors for their encouraging support and inspiration, and for giving me the freedom to choose the subjects of my interest. Especially, I am grateful for the many fruitful discussions of the applied experimental procedures and the obtained results.

Furthermore, I would like to express my gratitude to Tom Løgstrup Andersen for advices on composite processing methods, Henning Frederiksen for the determination of composite physical properties, Ulla Gjøl Jacobsen for assistance in the studies of water sorption, Claus Mikkelsen for technical assistance, Tomas Fernquist for guidance in the chemical work, Frants Torp Madsen for helping me with the measurements of yarn tensile properties, David Plackett for inspiring discussions, and Peter Szabo for providing me with the opportunity to measure thermoplastic rheological properties at the Danish Polymer Centre, Technical University of Denmark.

CONTENTS

1 INTRODUCTION

The potential of plant fibres as reinforcement in composite materials have been well recognized since the Egyptians some 3,000 years ago used straw reinforced clay to build walls. The current application of plant fibres in composites is mainly non-structural components with a random fibre orientation used by the automotive and building industry (Broge 2000, Clemons 2000, Karus et al. 2002, Parikh et al. 2002). This application of plant fibres is however primarily driven by price and a compulsory demand of ecological awareness, and to a lesser extent by the reinforcement effect of the fibres (Bledzki et al. 2002, Kandachar 2000). Thus, the next step is to attract industrial interest in the use of plant fibres in load-bearing composite components as a natural alternative to the traditionally applied synthetic fibres (e.g. glass fibres). One of the main barriers to overcome is control of fibre orientation (i.e. alignment of the fibres), to ensure that the fibre mechanical properties are most efficiently utilized, and that the maximum obtainable fibre content is high. In the textile industry a wide range of techniques for the alignment of plant fibres have since long been developed and optimised to produce yarns with highly controlled fibre orientations (Klein 1998). Therefore, by applying textile plant fibre yarns for composite reinforcement, the full potential of plant fibres can be explored, and form the necessary basis whereupon the prospective of plant fibres in structural composite components can be identified.

Various types of plant fibre yarns are commercially available, such as cotton, jute, flax and hemp yarns. Cotton yarn is by far the most widely supplied type. Despite its dominant position in the plant fibre market and its lower price, the large environmental impact of cotton cultivation (Robinson 1996), makes cotton a less appropriate "green" candidate for composite reinforcement. In contrast, hemp is an upcoming European industrial crop (Karus et al. 2002), which can be grown with a low consumption of fertilizers and virtually no pesticides (Robinson 1996), and with good mechanical fibre properties (Lilholt and Lawther 2000). Therefore, hemp yarn was the preferred yarn type in the presented study.

Thermoplastics were selected as matrix materials, and this is in agreement with the general trend for industrially fabricated plant fibre composites, where thermoplastics are increasingly being used in preference to thermosettings (Clemons 2000, Karus et al. 2002). Thermoplastic matrix composites offers several advantages over their thermosetting counterparts: (i) they are easier to recycle, (ii) they are faster to process (i.e. no extra time for curing), (iii) they are fabricated by a cleaner process technique (e.g. no toxic by-products), and (iv) they are less expensive. However, there is a number of disadvantages of thermoplastics, which are more technically oriented, and are directed in

particular towards their use in plant fibre composites: (a) their high viscosity, (b) their high melting temperature, and (c) their low polarity. Accordingly, for plant fibre composites with a thermoplastic matrix special attention must be paid to the effect of (a) composite porosity, (b) process temperature, and (c) fibre/matrix compatibility.

1.1 OBJECTIVES

The overall objective is to achieve an improved understanding of composite properties in the special case where the fibre part is represented by plant fibres. Previously, much research has been undertaken with the exact same objective, but based on plant fibre composites with a random fibre orientation (see reviews in Robson et al. 1993, Mohanty et al. 2001, Eichhorn et al. 2001, Bledzki et al. 2002). However, if the fibres are aligned, the interfering effect of a non-uniform fibre orientation distribution is excluded, and this makes it less complicated to analyse fibre properties in relation to composite properties. Thus, an aligned fibre orientation is beneficial to point out the critical parameters in plant fibre composites in general. Furthermore, the properties of aligned plant fibre composites must be considered to form the necessary foundation, if the properties of composites with a more complex fibre orientation distribution are to be satisfactorily predicted.

The overall objective is to study the water sorption properties and mechanical properties of aligned plant fibre yarn composites. Water sorption in plant fibre composites is a field where only little work has been done. Nevertheless, it is frequently quoted that the large water sorption capacity of plant fibres is a central aspect in relation to the dimensional stability of the composites. Measurements of mechanical properties are limited to tensile tests, which is the testing approach that is most appropriate to analyse fibre properties in relation to composite properties. This study aims at investigating the effect of a range of relevant parameters such as yarn type, thermoplastic matrix type, fibre content, process temperature and conditioning humidity.

Porosity is an unavoidable part in all plant fibre composites, but this topic has so far only received limited attention. Thus, there is a need for a proper documentation of the influence of porosity on composite properties.

Another important topic is the natural origin of plant fibres which implies that fibre properties are not strictly controlled, but they are likely to vary from year to year caused by the actual weathering conditions during growth of the plants. Thus, constant product quality cannot be guaranteed. In contrast, the properties of synthetic fibres are much more controllable. This problem was addressed

in the investigations by applying two batches of the same hemp yarn type, but bought separately in time.

1.2 OUTLINE

The report consists of 6 chapters. The layout is in principle as a traditional academic report presenting experimental results. In this chapter, Chapter 1, a general introduction to the subject is given, in addition to the objectives and the outline of the report.

Chapter 2 addresses the relevant background of the performed work. It is intended to provide the necessary detailed insight in issues directly related to the experimental work. The purpose of this chapter is also to provide a broad understanding of plant fibres and their composites.

Materials and methods are presented in Chapter 3.

In Chapter 4, the obtained experimental results are presented and discussed in relation to existing knowledge and previously reported results. This chapter forms the central part of the report and it consists of 5 sections with a number of subsections within each section. It has been attempted to supply each subsection with a short introduction concerned with the specific issue, and as such this is complementary to the background descriptions in Chapter 2. The content of the 5 sections is briefly described here:

- The measured characteristics of plant fibre yarns are presented in Section 4.1. The yarns were characterised with respect to (i) chemical properties, (ii) physical properties, (iii) water sorption properties, and (iv) mechanical properties. These results form an important basis for the analysis of composite properties as given in Sections 4.4 and 4.5.
- Section 4.2 gives a summary of Paper III, which is concerned with the compactibility of plant fibre assemblies. This provides information of the maximum obtainable fibre volume fraction of composites fabricated at a given consolidation pressure, and this is closely correlated with the predictions of composite porosity in Section 4.3.
- A model of composite volumetric interaction is presented in Section 4.3. The prediction of composite porosity is a central element in the model. The model is improved in relation to the work presented in Paper II.
- Section 4.4 presents the results of composite water sorption. The section is divided into 5 subsections concerned with non-equilibrium water content, and equilibrium water content and

dimensions. Only one type of hemp yarn was used as composite reinforcement, but the fibre weight fraction was varied, as well as the type of thermoplastic matrix.

- The results of composite tensile properties are given in Section 4.5. The work of Paper I is included in this section. The results are analysed in relation to the 7 parameters of the investigations (e.g. yarn type, matrix type and process temperature). The analysis of each parameter is confined to a single subsection.

Chapter 5 presents the main conclusions of the investigations.

Finally, based on the results and considerations in this study, a number of issues are proposed for future work in Chapter 6.

2 BACKGROUND

2.1 PLANT FIBRE STRUCTURE

In terms of taxonomy, plants belongs to the one of the five kingdoms of living organisms which is denoted Plantae. This kingdom includes most of the algaes and all green plants, i.e. mosses, ferns, gymnosperms (e.g. softwood) and angiosperms (e.g. hardwood and annual plants). At the cellular level one of the main features distinguishing plants from the animal kingdom is the presence of a rigid *cell wall* surrounding the cells. In a special type of plant cells, the cell walls are enlarged and this makes these cells responsible for the good structural integrity of plants. The physical dimensions of these cells vary between different plants (Table 2.1), but their overall shape is most often elongated with a high aspect ratio (length/diameter ratio), and they are therefore denoted *fibres* (Figure 2.1). Accordingly, the term *plant fibre* refers to a single cell that provides mechanical stability to the plant. This broad definition covers a range of fibres located a different parts of the plants, e.g. bast fibres from hemp, leaf fibres from sisal and seed fibres from cotton.

In living plants, when the plant fibres are fully developed, their intracellular organelles start to degenerate resulting in fibres having an empty central cavity, the so-called *lumen*. This makes these cells suitable for transport of water and nutrients. The actual size of the lumen varies considerably both within and between fibre types. Hemp and flax fibres have small luminar dimensions, whereas the luminar dimensions in jute and sisal fibres are relatively larger (Perry 1985). In wood fibres, the luminar area is between 20 and 70 % of the fibre cross-sectional area (Siau 1995).

The major part of research has been done on fibres from wood, and most of the available results and theories are therefore based on this type of fibres. However, with some modifications, it is assumed that the observations made on wood fibres can be applied to fibres from other plants as well. Throughout this report, if not otherwise noted, the term plant fibre will refer to non-wood fibres, and in particular it will refer to bast fibres from hemp.

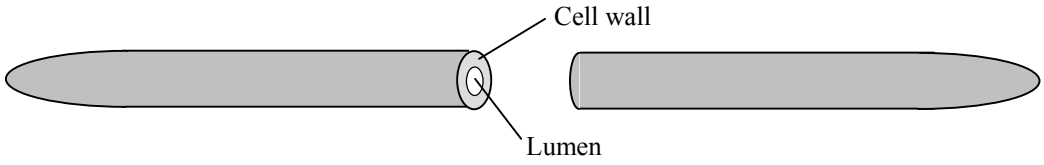

FIGURE 2.1. *Drawing of a plant fibre.*

TABLE 2.1. *Mean dimensions of various plant fibres. In brackets are given the range of variation. Data on non-wood fibres are from Bledzki et al. (2002) and data on wood fibres are from Lilholt and Lawther (2000).*

Plant	Fibre type	Dimensions				Aspect ratio
		Length (mm)		Diameter (μm)		
Hemp	Bast	25	(5-55)	25	(10-51)	1000
Flax		33	(9-70)	19	(5-38)	1750
Jute		2	(2-5)	20	(10-25)	100
Ramie		120	(60-250)	50	(11-80)	2400
Sisal	Leaf	3	(1-8)	20	(8-41)	150
Cotton	Seed	18	(10-40)	20	(12-38)	900
Wheat	Stem	1.4	(0.4-3.2)	15	(8-34)	90
Softwood (e.g. spruce)	Tracheid	3.3		33		100
Hardwood (e.g. beech)		1.0		20		50

2.1.1 Cell wall composition

The cell wall of plant fibres is mainly composed of three large polymers: cellulose, hemicellulose and lignin. These polymers differ in molecular composition and structure and therefore they display different mechanical properties as well as different water sorption properties. The content of the three polymers is highly variable between plant fibres (Table 2.2).

TABLE 2.2. *Chemical composition of the cell wall in different plant fibres. Data are from Bledzki et al. (2002).*

Plant	Fibre type	Cell wall chemical composition (w%)		
		Cellulose	Hemicellulose	Lignin
Hemp	Bast	57-77	14-17	9-13
Sisal	Leaf	43-62	21-24	7-9
Cotton	Seed	85-96	1-3	0.7-1.6
Wheat	Stem	29-51	26-32	16-21
Wood	Tracheid	38-49	7-26	23-34

Cellulose is a non-branched polysaccharide made up of the cellobiose monomer, which consists of two glucose units covalently bound to each other by a glycosidic carbon (1-4)-linkage (Figure 2.2). The glucosidic linkage is β configured and this allows cellulose to form a flat and ribbon like long straight chain, which for wood fibres is having an average length of 5 μm corresponding to a degree of polymerisation (i.e. glucose units) of 10,000 (Siau 1995). This molecular linearity makes

cellulose highly anisotropic with a theoretical strength of about 15 GPa in the chain direction (Lilholt and Lawther 2000).

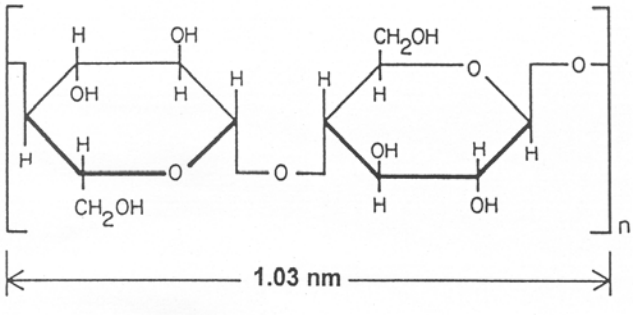

FIGURE 2.2. *Chemical structure of the repeating cellobiose unit in cellulose. From Siau (1995).*

Cellulose is synthesised by cellulose synthase, an enzyme complex located in the cell membrane, which simultaneous synthesise a number of parallel cellulose chains forming an elementary fibrillar unit, called a *micellar strand* (Salisbury and Ross 1992) (Figure 2.3). Several of these strands are most often combined into a larger *microfibril*, which conventionally is considered to be the smallest unit of cellulose chains. The number of cellulose chains in a microfibril varies between 30 and 200 depending on the type of plant fibre. The synthesis of a microfibril comprises a number of cellulose synthases working together in a coordinated manner (O'Sullivan 1995). In some regions of the microfibrils the molecular structure is highly ordered by intermolecular hydrogen bonds linking the cellulose chains together in a crystalline arrangement, and accordingly, the ordered regions are denoted *crystalline regions* and the less ordered regions are denoted *amorphous regions*. In one theory, the so-called *fringe-micellar theory,* the amorphous regions are thought to be located inside the microfibrils where the ends of single cellulose chains are disrupting the crystalline arrangement (Siau 1995) (Figure 2.4). In another theory the amorphous regions are thought to merely reflect the higher free energy of cellulose molecules at the surface of the microfibrils (O'Sullivan 1995). The degree of crystallinity varies with the type of plant fibre; e.g. for wood fibres it is between 60 and 70 % (Siau 1995), whereas it is between 40 and 45 % for cotton fibres (O'Sullivan 1995). Moreover, physical and chemical treatments of plant fibres are known to change the degree of crystallinity (Zeronian et al. 1990, Bhuiyan and Sobue 2001).

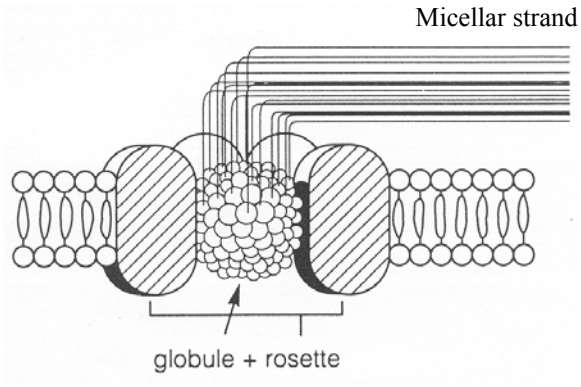

FIGURE 2.3. *Section of a plant fibre cell membrane showing a cellulose synthase enzyme complex synthesising a micellar strand. From Salisbury and Ross (1992).*

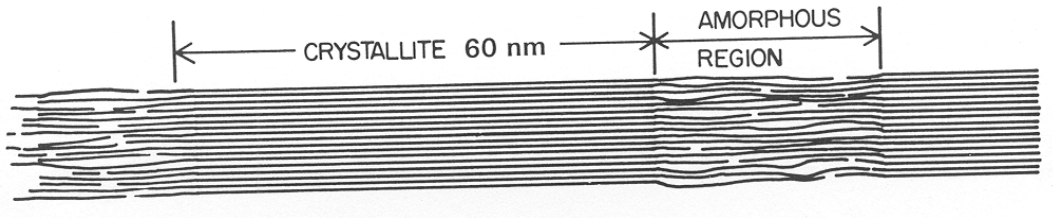

FIGURE 2.4. *Depiction of the fringe-micellar theory showing how crystalline and amorphous regions are repeatedly located next to each other along the cellulose microfibril. From Siau (1995).*

Hemicellulose is a heterogeneous group of polysaccharides with a composition that varies between different types of plant fibres and includes a range of carbohydrates, such as glucose, galactose, mannose, xylose and arabinose. Compared to cellulose, the hemicellulose polymers are generally characterised by being short (a maximum of 150 units), non-linear and more branched. Examples of hemicelluloses are: (i) branched chains, such as carbon (1-4)-linked xyloglucan or galactoglucamannan, (ii) unbranched chains, such as carbon (1-4)-linked xylan or mannan, and (iii) chains of carbohydrate units that are carbon (1-3)-linked and therefore are forming a helical structure (O'Sullivan 1995).

Lignin is a highly branched polymer composed of phenylpropane units organised in a very complex three-dimensional structure. In a chemical sense, lignin is rather reactive and therefore any method applied to extract lignin from plant fibres is affecting its molecular composition and structure.

2.1.2 Cell wall organization

The exact structural organization of the chemical constituents in the cell wall is a much-debated subject, however it is generally accepted that the three major polymers are not uniformly mixed, but are arranged in separate entities (Figure 2.5). The hemicellulose polymers are thought to be bound

to the cellulose microfibrils by hydrogen bonds forming a layer around the fibrils, and these cellulose/hemicellulose units are then encapsulated by lignin.

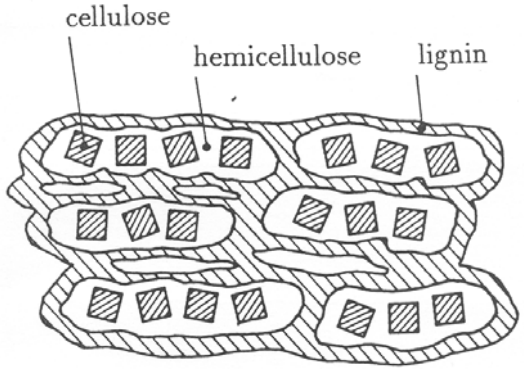

FIGURE 2.5. *Model of the structural organisation of the three major constituents in the cell wall of wood fibres. From Wadsö (1993).*

In addition to the organisation of the chemical constituents, the structural complexity of the cell wall is increased by being organised into a number of layers differing by the angle of the cellulose microfibrils to the longitudinal fibre axis, the so-called *microfibril angle* (Figure 2.6). During growth of a plant fibre, the cell wall consists only of one layer, the so-called *primary layer*. The microfibrils in the primary layer are deposited predominantly in the transverse direction, and because of the restraining effect of the microfibrils, this makes the fibre grow in the longitudinal direction. However, as the fibre is elongating the early deposited fibrils are being reoriented into the longitudinal direction and consequently when growth ends, the fibril orientation in the primary layer is not confined to a single direction. This generally accepted model of plant fibre growth is called *the multi-net model* (Niklas 1992).

In the classical interpretation of the deposition of the cell wall after growth has terminated, the distinction is made between three *secondary layers* denoted S1, S2 and S3. In these layers the microfibrils are arranged in helixes coiling around the longitudinal axis of the fibre with a constant angle within each layer but with large angular shifts between the layers. The microfibril angle in the S1 and S3 layers is large, meaning that the fibrils are oriented nearly transverse to the fibre axis. The microfibril angle in the S2 layer is small, and therefore these fibrils are oriented more parallel to the fibre axis. In wood fibres, the microfibril angle in the S2 layer is in the range 3-50° and in bast fibres it is below 10° (see Table 2.5, p. 20). Since the S2 layer is by far the thickest layer, including about 60-80% of the cell wall in wood fibres (Siau 1995), the small angle of the microfibrils in this layer dictates the overall anisotropic properties of the fibres. This rather simple model of the fibril orientation in the secondary layers has however been questioned by some recent

studies indicating the existence of intervening layers with a gradual change of the microfibril angle forming a so-called helicoidal structure (Neville 1993).

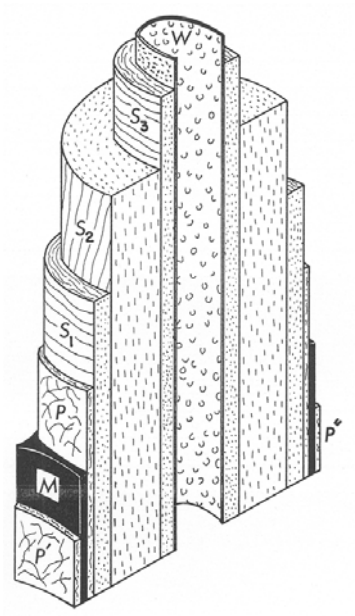

FIGURE 2.6. *Cell wall layers in a plant fibre. M is the middle lamella connecting the fibres in the plant, P is the primary layer, S1, S2 and S3 are the three secondary layers, and W is the cell membrane. From Siau (1995).*

2.2 PLANT FIBRE WATER SORPTION

The large water sorption capacity of plant fibres is an essential aspect of plant fibre composites. To achieve an understanding of water sorption in the composites requires necessarily an understanding of water sorption in the fibres themselves. However, only little information is presented on this subject in the existing literature concerned with plant fibre composites. In contrast, in the field of wood technology much research has been addressed to wood fibre water relations, and the succeeding subsections are based on this work.

2.2.1 Physics of water

Basic knowledge of the physics of water is essential in relation to water sorption in plant fibres. The water molecule is made from one oxygen atom and two hydrogen atoms held together by polar covalent bonds. The polarity arises from the high electronegativity of the oxygen atom relative to the hydrogen atoms, which causes the electrons of the covalent bonds to be located at a position statistically closer to the oxygen than to the hydrogens. As a result, the covalent bonds are about 40 % ionic in character. The asymmetrical distribution of charges in water is the basis of formation of

hydrogen bonds between water molecules, but also between water molecules and polar groups in other molecules, such as the hydroxyl groups (-OH) in the cell wall polymers of plant fibres.

To view the charge distribution within a water molecule various models have been proposed of which the so-called ST2 model is a relative simple but descriptive model (Israelachvili 1991) (Figure 2.7A). The ST2 model shows how two negative and two positive charges are located along four tetrahedral arms radiating out from the centre of the oxygen atom with a mutual angle of 109°. Thus, the water molecule can participate in four hydrogen bonds, and this allows for a tetrahedral arrangement of water molecules to be formed (Figure 2.7B). This three-dimensional arrangement is the main explanation for many of the special physical properties of water (e.g. high melting and boiling point) compared to other molecules with similar low molecular weight and high polarity.

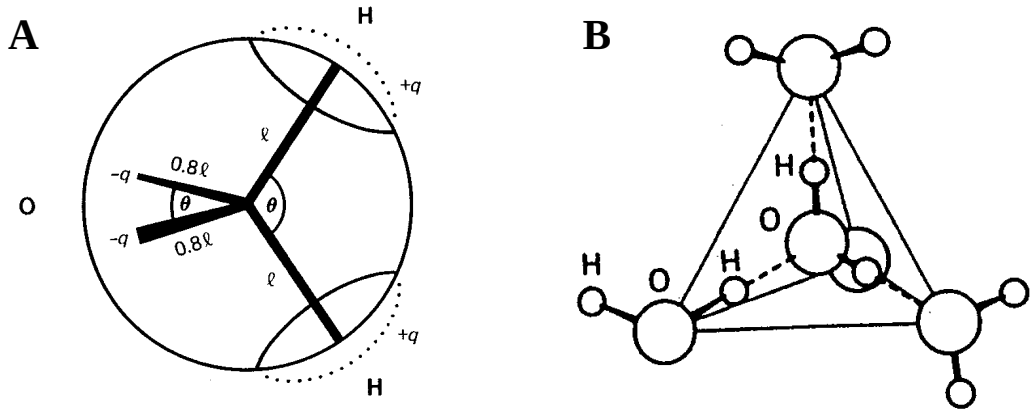

FIGURE 2.7. *(**A**) The water molecules shown by the ST2 model (q=0.24 e; l=0.1 nm; θ=109°). (**B**) The tetrahedral hydrogen bonded structure of water molecules. From Israelachvili (1991).*

The strength of the hydrogen bonds between water molecules is relatively low (about 20 kJ/mol compared to about 500 kJ/mol for covalent bonds) and because of molecular vibrations, the hydrogen-bonded structure is highly labile with a constant formation and breaking of bonds (Israelachvili 1991). Therefore, no specific water molecules are bound to one another for more than a relative short time, yet a statistically constant fraction of molecules is joined together at all times at a given temperature. By changes in temperature (the level of molecular kinetic energy), the lifetime of the hydrogen bonds are changed and the equilibrium condition between fractions of hydrogen bound water molecules and free water molecules are changed accordingly. Hydrogen bound water molecules are defined as *liquid water* and free water molecules are defined as *water vapour*. The fraction of water vapour is extremely small compared to the fraction of liquid water, even at the boiling point the ratio is only 2 molecules per million (Skaar 1972). This small fraction of water vapour exerts a pressure denoted as the *saturated vapour pressure*, which is an indirect

expression for the equilibrium condition that exists between fractions of liquid water and water vapour at a given temperature. Except in closed systems, the *actual vapour pressure* of the atmosphere is below the saturated vapour pressure and therefore liquid water is constantly vaporised. Normally, air humidity is measured in terms of the *relative humidity* (RH), which is defined as the ratio of the actual vapour pressure (p) and the saturated vapour pressure (p_*):

$$RH = 100 \frac{p}{p_*} \tag{2.1}$$

As mentioned above, the actual vapour pressure above an air-water interface will tend to move towards the saturated vapour pressure. However, when water is trapped in small spaces, the saturated vapour pressure is depressed. This is an important phenomenon in relation to water sorption in porous materials, such as plant fibres, and will subsequently be explained. The affinity between liquid water and a solid material is characterised by the *contact angle* at the water-material interface, and the material is denoted *hydrophilic* when the angle is below 90° and *hydrophobic* when the angle is above 90°. This can be recognised by observing the water surface close to the walls of a container; if the container is made of a hydrophilic material (e.g. glass) the surface will be curved in a downward direction with an angle given by the contact angle. By decreasing the radius of the container into capillary dimensions (<100 μm) it can visualised that the water surface, the so-called *meniscus*, will attain a concave curved shape between the walls of the capillary and that the radius of the curvature will depend on the contact angle (Figure 2.8). The curvature of a capillary meniscus will shift the equilibrium condition between liquid water and water vapour towards liquid water and thereby depress the saturated vapour pressure. Moreover, the increased area of the curved meniscus relative to the flat meniscus represents an amount of work, which is equal to the difference in hydrostatic pressure above and below the meniscus. The hydrostatic pressure is higher above the meniscus, which means that capillary water is in tension. In relation to *capillary water sorption* in plant fibres, this will tend to decrease the overall dimensions of the fibres. In Table 2.3 some numerical examples are presented of the relationship between the capillary radius, the fractional depression of the saturated vapour pressure and the capillary pressure. The table shows that only capillaries with radii smaller than about 10 μm will notably depress the saturated vapour pressure and exert any capillary pressure. It can be realised that if the ambient relative humidity is exceeding the fractional depression of the saturated vapour pressure, water vapour will condense into liquid water; e.g. at an ambient relative humidity of 0.95 water vapour will condense into capillaries with radii below 0.020 μm.

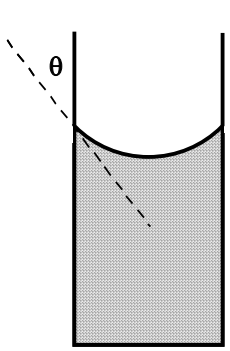

FIGURE 2.8. *Drawing of a capillary meniscus. θ is the contact angle between water and the material of the capillary wall.*

TABLE 2.3. *Relationship between capillary radius, fractional depression of the saturated vapour pressure and capillary pressure. Data are from Skaar (1972) and are based on the Kelvin equation and the capillar-pressure equation.*

Capillary radius (μm)	Fractional depression of p_*	Capillary pressure (kPa)
	1.0000	0
10.4	0.9999	15
1.0	0.999	140
0.103	0.99	1400
0.034	0.97	4200
0.020	0.95	7100
0.012	0.92	11600
0.010	0.90	14600

2.2.2 Water sorption

The traditional definition of water content in plant fibres is based on gravimetric measurements of the dry fibre mass (m_0) and the moist fibre mass (m_{RH}):

$$u_{RH} = \frac{U_{RH}}{100} = \frac{m_{RH} - m_0}{m_0} = \frac{m_w}{m_0} \tag{2.2}$$

where u is fractional water content, U is water content in percentage (%), m_w is mass of sorped water, and the subscript RH denotes that the moist fibre mass is determined at a given ambient relative humidity.

Water can exist in plant fibres in three different forms: (i) water bound by hydrogen bonds to the various sorption sites in the cell wall, subsequently referred to as *bound water*, (ii) free liquid water

in the fibre cavities (e.g. the luminar space), subsequently referred to as *free water*, and (iii) water vapour in the fibre cavities (Skaar 1988). Because of the low density of water vapour, the mass of the third form is negligible and its contribution to the water content is ignored.

The water content of plant fibres in living plants can be very high (U>>100 %), and this so-called *green water content* is mainly based on free water, and to a lesser extent on bound water. When a plant dies and the plant fibres are exposed to the atmosphere (with a vapour pressure below the saturated vapour pressure), the free water, which represents a higher energetic state than the bound water, will vaporise into water vapour before the cell wall loses any bound water. The water content at which the plant fibre is fully saturated with bound water, but contains no free water is denoted the *fibre saturation point* (U_{fs}), which for wood fibres ranges from 25 to 35 % (Siau 1995). The definition of the fibre saturation point is strictly theoretical since there are no definite methods to measure the two forms of waters individually. Moreover, it is generally believed that bound water and free water exist together over a wide range of water contents and therefore the shift does not occur at a single point. Anyway, the fibre saturation point, as a conceptual definition, forms an important basis of the understanding of water in plant fibres.

Bound water is confined to the polar groups in the fibre cell wall, which are mainly the hydroxyl groups of the cell wall polymers. Hemicellulose is not forming a highly ordered intermolecular structure, and therefore most of the hydroxyl groups of the carbohydrate units are not occupied by interchain hydrogen bonds. Thus, hemicellulose is the cell wall polymer with the largest water sorption capacity. The hydroxyl groups in the crystalline regions of cellulose are bonded to hydroxyl groups of neighbouring cellulose chains, and the water sorption capacity of cellulose is therefore limited, and confined to the amorphous regions. The cell wall polymer with the lowest sorption capacity is lignin. It has been shown for wood that the water sorption capacity can be calculated as a linear mixture of the sorption capacities of its chemical constituents (Skaar 1972, Salmén 1997). Thus, water sorption can be notably reduced if the content of hemicellulose is lowered, which is indicated in this study to occur as a result of alkalisation and thermal exposure (see Subsection 4.1.6). However, water sorption can as well be reduced by substitution of less polar groups for the hydroxyl groups, and this is the underlying principle in acetylation (Rowell 1986), silanization (Gassan and Bledzki 1999b) and formaldehyde treatment (Hua et al. 1987).

The amount of bound water in the fibre cell wall is strongly influenced by the relative humidity of the surroundings. This can be recognised from some thermodynamic considerations based on Skaar (1972) and Siau (1995). The thermodynamic criteria for an equilibrium condition states that *a system is in equilibrium with its surroundings when there is no more change in free energy*. This means that the free energy of bound water is identical to the free energy of the surrounding water

vapour (at the equilibrium condition). Water vapour obeys the ideal gas law and the product of pressure and molar volume of water vapour is therefore constant. Accordingly, since the actual vapour pressure is below the saturated vapour pressure, the molar volume is larger and this corresponds to an amount of work performed by the unsaturated vapour; i.e. the amount of available energy to do work (i.e. the free energy) is lowered. Therefore, unsaturated water vapour is representing a relatively lower free energy. Water will always move into regions of lower free energy. This means that the amount of bound water is decreased when the free energy of the surrounding water vapour is decreased relatively to the free energy the saturated water vapour (i.e. the relative humidity is decreased). The amount of free water in the fibre cavities too is a function of the relative humidity. The higher the relative humidity, the larger the dimensions of the capillary cavities that are filled with free water (see Table 2.3, p. 13).

A plot of the equilibrium water content against the relative humidity at isothermal conditions is called a *sorption isotherm* (see Figures 2.9 and 2.10). The sorption isotherm for plant fibres is characterised by a sigmoidal profile, the exact shape of which depends on the physical and chemical characteristics of the fibres. In addition to the relative humidity, the equilibrium water content in plant fibres is to a lesser extent affected by a few other external factors, where the most important are: (i) *temperature*, (ii) *history of relative humidity exposures*, and (iii) *mechanical stress*. The effect of these factors will briefly be described.

By increasing the actual temperature of the isothermal condition, the water content at a given relative humidity is reduced and the sorption isotherm is shifted in a downward direction (Figure 2.9). The effect is fully reversible, and can be explained by the thermodynamic relationship between bound water and the surrounding water vapour. When the temperature is increased, the free energy of unsaturated water vapour is furthermore decreased relative to the free energy of saturated water vapour. Therefore, the amount of bound water is reduced (Siau 1995). It can be calculated that the actual and the saturated vapour pressures approximately doubles with each 10 °C rise in temperature for a given relative humidity. Figure 2.9 shows that the water content decreases by less than 1 % with a similar change in temperature. This demonstrates that the water content is more strongly correlated to the ratio of the actual and saturated vapour pressure (i.e. the relative humidity) than to their absolute values.

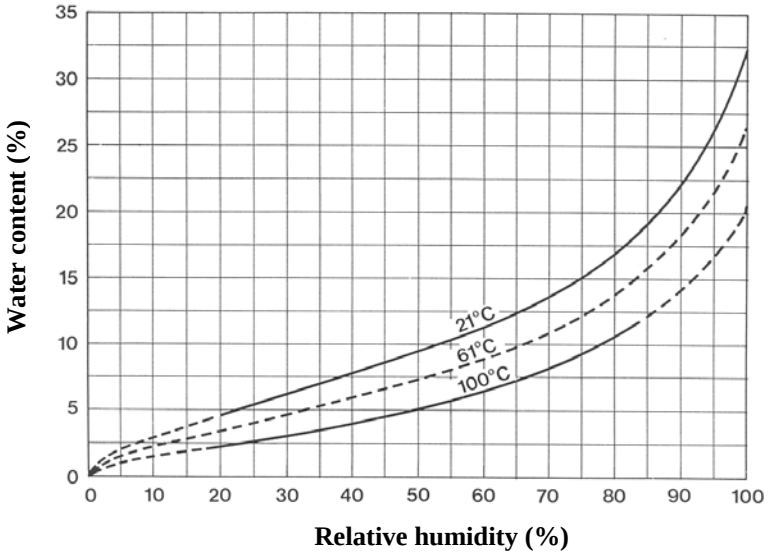

FIGURE 2.9. *The effect of temperature on the sorption isotherm of wood. From Siau (1995).*

The procedure to construct a sorption isotherm is to measure the water content at an ascending or descending successive sequence of relative humidities. However, the direction of the sequence is of importance. The measured water contents of an ascending sequence, called *adsorption*, are always lower than the water contents of a descending sequence, called *desorption* (see Figure 4.8. p. 65). This phenomenon is called *hysteresis*. It has been attempted to explain the governing mechanism of hysteresis, but at present no single explanation seems to be fully satisfactory. In one explanation, the cellulose chains are thought to be bonded to each other when they loose bound water in the desorption sequence. During the subsequent adsorption sequence these sorption sites are not available until after the fibre saturation point, and the amount of adsorped water is therefore reduced (Siau 1995, Avramidis 1997). In another explanation, compressive stress is thought to be generated during adsorption because of the different water sorption capacities of the cell wall polymers, and this might reduce the water content (see below) (Siau 1995).

When compression stress is applied to a plant fibre, the water content is decreased at a given relative humidity, and likewise, if tension stress is applied to a fibre, the water content is increased (Figure 2.10). This is denoted the *Barkas-effect* (Barkas 1949). By thinking of a plant fibre as cell wall material dissolved in bound water, the phenomenon can be explained by the principles of osmosis (Skaar 1972). When a salt solution is separated from pure water by a semipermeable membrane, water will migrate through the membrane and generate an osmotic pressure. To prevent the migration of water through the membrane, a pressure must be applied to the solution that is equal to the osmotic pressure. Likewise, if a plant fibre is restrained from swelling, it will exert a swelling pressure and the amount of adsorped water is decreased. The experimentally measured swelling pressures of wood are typically much below the theoretical ones as calculated by the

osmotic-pressure equation. This is however anticipated for two reasons: (i) wood fibres are not solid, but contain empty cavities which provides space for internal swelling, and (ii) the fibre cell wall is not a material with infinite stiffness and therefore it is compressible, which means that the cell wall itself takes up some of the swelling pressure. It has been shown in a model by Barkas (1949) that when the elastic properties of the cell wall are taken into account, the swelling pressure of wood fibres can be well predicted from the fibre water content.

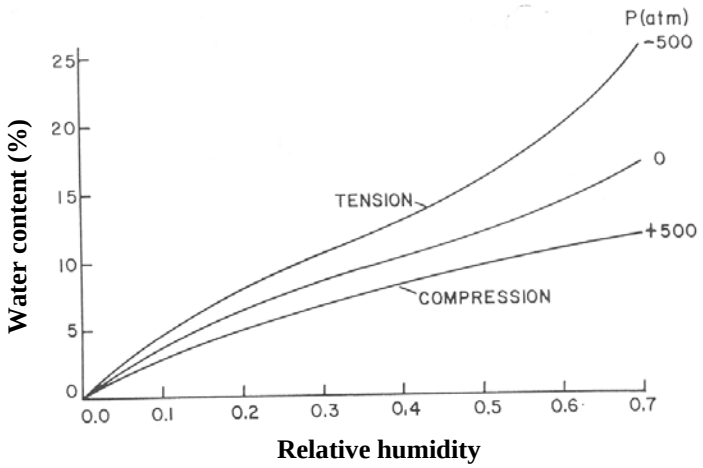

FIGURE 2.10. *The effect of hydrostatic stress on the sorption isotherm of wood (Sitka spruce). From Skaar (1972).*

2.2.3 Water related dimensional stability

A central parameter in the study of material dimensional stability is *density*, which identifies the ratio of material mass to material volume. The large water sorption capacity of plant fibres means that fibre density cannot be specified by a single value. Furthermore, their porous structure makes it necessary to distinguish between an *absolute density* of the fibre solid matter (i.e. the cell wall) and an *apparent density* that includes the central lumen of the fibres. Finally, any dimensional changes of the lumen as a consequence of water sorption directly affect the apparent density of the fibres. Thus, these three factors complicate the simple concept of density.

Whereas fibre mass is readily determined, fibre volume is more problematic to determine accurately. Typically it is determined by submerging the fibres into a medium with known density, and the fibre volume is then determined indirectly from the mass of displaced medium. However, it has been shown that the polarity of the displacement medium is affecting the determined absolute density of wood fibres (Table 2.4) (Skaar 1972). When non-polar displacement media, such as benzene or toluene, are used instead of water, the density is reduced. This phenomenon can be explained by two mechanisms:

- The low penetrability of non-polar molecules into cell wall microcavities would account for the measured larger fibre volume when a non-polar displacement medium is used.
- The compression of bound water molecules due to bonding forces makes bound water denser than liquid water, and this would account for the measured lower fibre volume when water is used as the displacement medium.

In a study by Weatherwax and Tarkow (1968) based on wood fibres from Sitka spruce, the relative importance of these two explanations was experimentally investigated. It was found that the effect of lower penetrability explained 85 % of the reduction in density, and they approximated a bound water density of 1.017 g/cm^3. Thus, bound water is having only a slightly larger density than liquid water. However, this statement is based on fully water-saturated fibres and it must be expected that bonding forces at the sorption sites are larger in more dry fibres. It follows that bound water density might be more markedly different from liquid water density at fibre water contents below the fibre saturation point. Nonetheless, since no other experimental data are available on this issue, it will subsequently be assumed that bound water density is equal to liquid water density.

TABLE 2.4. *Absolute density of fibres from three wood species determined by the use of different displacement media. From Skaar (1972).*

Wood species	Displacement medium	Absolute density (g/cm^3)
Alaska cedar	Water	1.55
	Ethanol	1.54
	Benzene	1.48
	Mineral oil	1.46
Abies grandis	Water	1.52
	Toluene	1.44
English spruce	Water	1.52
	Toluene	1.45

Principally, three possibilities can be considered for the change in luminar dimensions as an effect of water adsorption:

- The lumen may shrink, meaning that the cell wall swells into the luminar cavity, and the external dimensional changes of the fibres are therefore small.
- The lumen may remain constant, meaning that the cell wall swells outward, and the external dimensional changes of the fibres are therefore directly proportional to the volume of adsorped water.

- The lumen may swell, and this would result in maximum external dimensional changes of the fibres.

In fact, all three possibilities have been observed for wood fibres, but in general the luminar dimensions are more or less unaffected by water sorption (Skaar 1972).

Assuming that (i) the density of bound water is equal to the density of liquid water (ρ_w), and (ii) the luminar dimensions are constant, the apparent density of plant fibres with given water content ($\rho_{f\,RH}$) can be estimated:

$$\rho_{f\,RH} = \frac{m_0 + m_w}{v_0 + m_w/\rho_w} = \frac{m_0\,(1 + u_{RH})}{m_0/\rho_{f\,0} + m_0\,u_{RH}/\rho_w} = \frac{1 + u_{RH}}{1/\rho_{f\,0} + u_{RH}/\rho_w} \tag{2.3}$$

where v is volume.

2.3 PLANT FIBRE MECHANICAL PROPERTIES

As can be recognized from the description of plant fibre structure in Section 2.1, plant fibres themselves can be thought of as composite materials with the stiff and strong cellulose microfibrils embedded in a hemicellulose/lignin matrix. However, the composite structure in plant fibres is rather complex (e.g. two-phase matrix and cell wall layers). Moreover, plant fibres are part of a larger biological system, i.e. the plants, with a long evolutionary history, and their properties have therefore been highly optimised with respect to the functional requirements of plants. Thus, the study of plant fibre mechanical properties is not just an assessment of the reinforcement potential of plant fibres in man-made composites, but might as well provide insight into the form and function of a sophisticated composite material.

Based on considerations of bond energies between atoms in the molecular structure of cellulose, the theoretical stiffness and ultimate stress of crystalline cellulose loaded on the chain direction have been estimated to be in the ranges 60-120 GPa and 12,000-19,000 MPa, respectively (Lilholt and Lawther 2000, and references cited herein). Thus, these estimates can be thought of as upper limits in the tensile performance of plant fibres. A number of structural aspects serve however to restrain the practical attainable tensile properties of plant fibres: e.g. the degree of cellulose crystallinity, the microfibril angle and the cellulose content. Table 2.5 presents typical reported tensile properties of different types of plant fibres. Stiffness and ultimate stress of hemp fibres have been reported in the ranges 30-60 GPa and 300-800 MPa, respectively. It can be seen in the table that in particular the measured ultimate stress of plant fibres is much below the theoretical estimates. This might be explained by the presence of fibre defects, which has been shown to affect the failure mechanisms

in plant fibres (Eichhorn et al. 2001). The measured fibre stiffness is more closely reflecting the theoretical estimates. The observed large variation in the measured tensile properties is a typical trait for materials with a natural origin, but some variation is also added by the experimental testing procedure. The measurement of tensile properties of single plant fibres is not a simple task, and problems are especially related to fibre gripping and determination of fibre cross-sectional area. A promising method is presented in Mott (1995), in which the fibre is gripped between two epoxy droplets placed along the fibre (a ball-and-socket type gripping), and the fibre cross-sectional area at the failure region is determined with a laser confocal scanning microscope.

TABLE 2.5. *Microfibril angle and tensile properties of different plant fibres. Data for microfibril angles are from Gassan et al. (2001), except for data on softwood that are from Anagnost et al. (2002). Data for tensile properties are from Lilholt and Lawther (2000).*

Plant fibre	Microfibril angle (degrees)	Stiffness (GPa)	Ultimate stress (MPa)
Hemp	6	30-60	300-800
Flax	6-10	50-70	500-900
Jute	8	20-55	200-500
Sisal	10-25	9-22	100-800
Cotton	-	6-10	300-600
Softwood	3-50	10-50	100-170

The inclination angle relative to the fibre axis for the cellulose microfibrils is a key parameter to assess fibre tensile properties. The microfibril angle can be determined by different techniques, such as by X-ray diffraction (Entwistle and Terrill 2000) and by fungal decomposition of the non-cellulose constituents in the cell wall (Anagnost et al. 2002). The term microfibril angle refers normally to the angle in the S2 layer. Table 2.5 shows reported microfibril angles of various types of plant fibres. In hemp fibres the microfibril angle is reported to be about 6°. The microfibril angle in wood fibres is more variable (3-50°), and wood fibres are therefore suitable in order to study the correlation between fibre tensile properties and microfibril angle. Figure 2.11 is from Page et al. (1977), and it shows how stiffness of wood fibres is well correlated with the microfibril angle. At small angles (<5°) stiffness is in the range 50-80 GPa, and at large angles (40-50°) stiffness is reduced to about 20 GPa. Also shown in the figure is a theoretical model fitted to the upper limit of the experimental data. The cell wall is modelled by a planar model of a homogenous and orthotropic material (a similar approach is used in the present study to predict composite off-axis properties). The elastic constants of the wood fibre cell wall are estimated to be about 80 GPa for axial stiffness, 9 GPa for transverse stiffness, 7 GPa for shear stiffness and 0.3 for Poisson's ratio. Other models, in which the cell wall geometry and structure are more correctly modelled,

have been proposed to predict the tensile properties of plant fibres. In Gassan et al. (2001) the three cell wall layers are taken into account by using composite laminate theory. In Davies and Bruce (1997) and Gassan et al. (2001) the elliptic geometry and the central lumen are furthermore taken into account by using a laminated composite tube model.

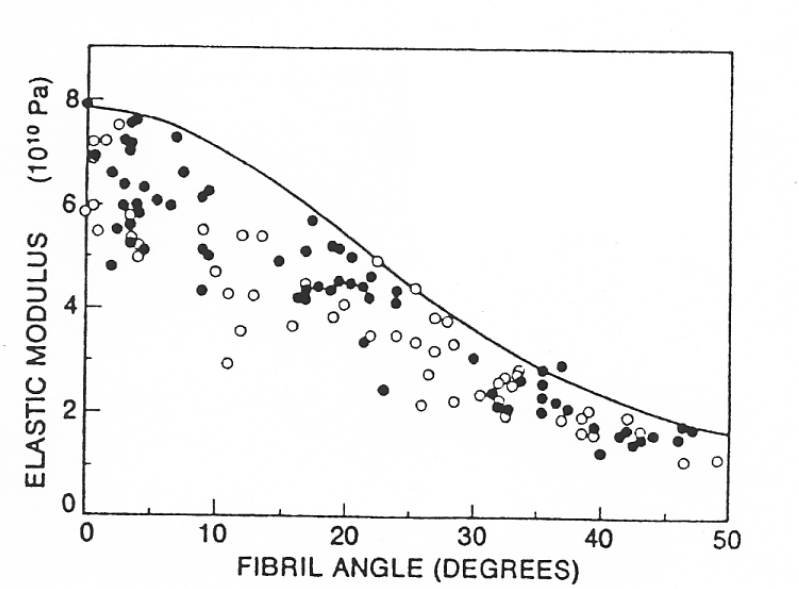

FIGURE 2.11. *Relationship between wood fibre stiffness (elastic modulus) and microfibril angle in the S2 layer. The symbols (o and •) are experimental data for fibres extracted by two different techniques. The curve is a theoretical model fitted to the upper limit of the experimental data. From Page et al. (1977).*

2.4 PLANT FIBRE PROCESSING

Since the main interest in this report is bast fibres, and in particular hemp fibres, the presented description of plant fibre processing is focused on hemp. However, when information is available only for other bast fibres, such as flax and jute, this is assumed to apply for hemp as well.

2.4.1 From plant to fibres

Hemp (*Cannabis sativa* L.) is an annual crop, which is sown in spring and harvested in autumn. The hemp plants are fast growing. They grow to a height of 2-5 m in 110 days (Figure 2.12A), which means that no weed control is needed, and that hemp yields a large amount of fibre mass per hectare (per year), which is 4 times the fibre mass of wood. Moreover, the hemp plant has just a few natural enemies in the form of insect pests, and therefore only a limited pest control is needed (Robinson 1996). The fibres are situated in bundles at the periphery of the hemp stem just beneath the epidermis (Figures 2.12B and 2.13). The fibre bundles extend continuously from bottom to top of the hemp plant, however the single fibres are smaller units with lengths in the range 5-55 mm (Bledzki et al. 2002).

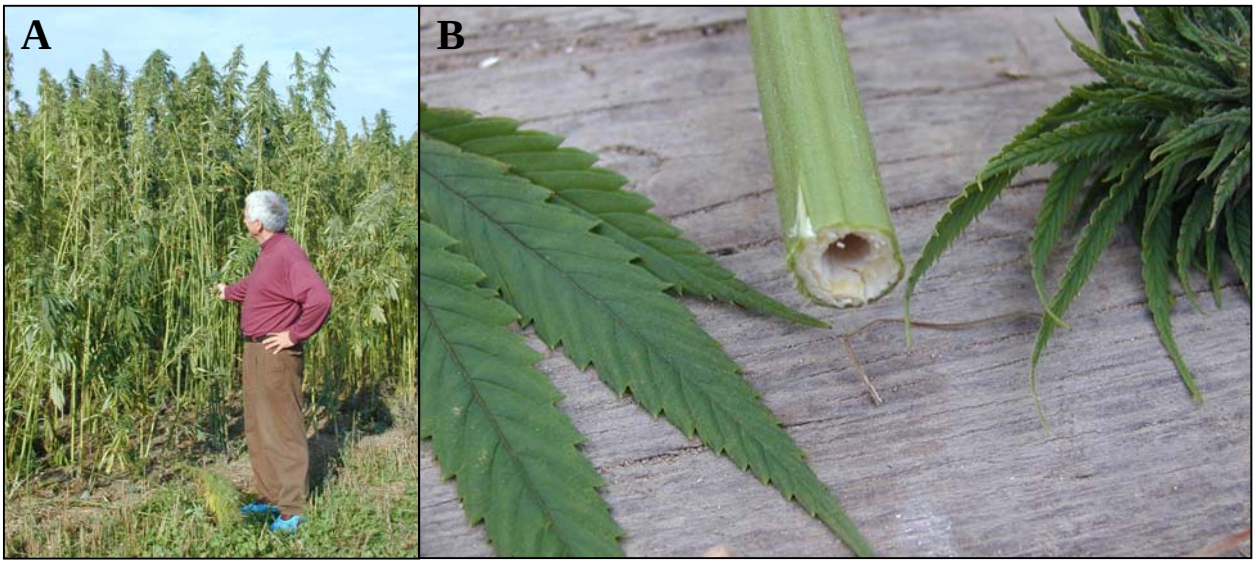

FIGURE 2.12. *(**A**) shows a hemp field with mature hemp plants. (**B**) shows a hemp stem cross-section.*

After harvesting, the fibres are separated from the plant stems by two processes: *retting* and *mechanical extraction*. The primary goal of retting is to degrade the tissue that interconnects the single fibres, i.e. the middle lamella (see Figure 2.6, p. 10). Traditionally, hemp stems are left in the field to be decomposed by microbial activity. This is denoted *dew retting*, and is a strictly natural process strongly influenced by the actual weather conditions. Alternatively, to make the retting process more controllable, the plant stems are retted in water tanks, which is denoted *water retting*. The efficiency of water retting can be furthermore improved by controlling the microbial flora (Donaghy et al. 1992). Finally, retting can also be performed on a pure *enzymatic* basis (Brühlmann et al. 2000). After retting, the fibres are extracted from the dry stems by a mechanical process. Various extraction methods can be applied (e.g. *beating*, *scutching* and *decortification*), however, the underlying principle is to break the core of the stems into small lengths, the so-called *shives* (Figure 2.13), and separate them from the fibres. In decortification, this is performed by pairs of profiled rotating rolls (Hobson et al. 2001). After retting and mechanical extraction, the yield of hemp fibres is in the range 15-30 w% (expressed as percentage of stem dry matter) (Sankari 2000).

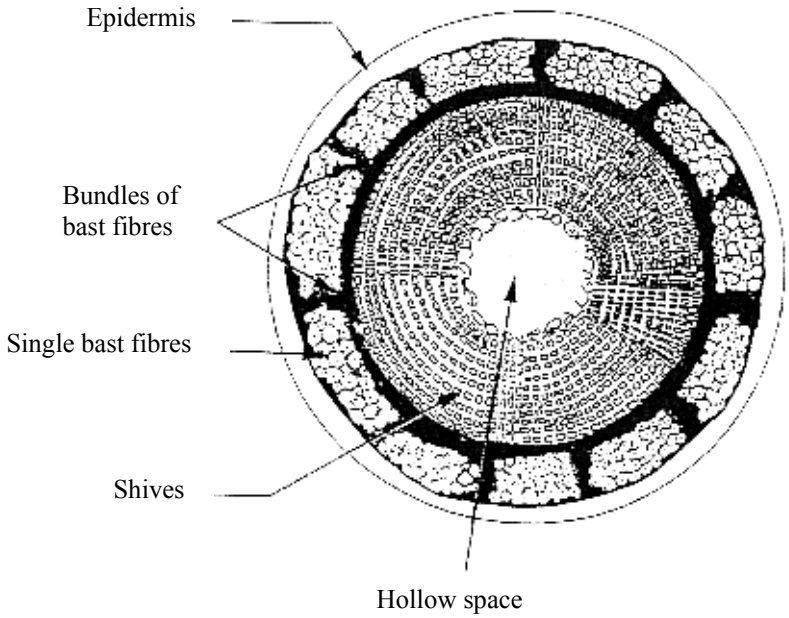

FIGURE 2.13. *Cross-section of a bast fibre stem. From Eriksen and Pallesen (2002).*

The extracted fibre material is only partially separated into single fibres, and additional treatment is performed to improve fibre separation, which is denoted *defibration.* This step is in particular important when the fibres are to be processed into yarns. In the textile industry, defibration is traditionally achieved by carding. In this process, the fibre bundles are drawn apart by toothed surfaces working against each other (Klein 1998). Moreover, *alkalisation* (or *cottonisation*) is a common chemical process, in which fibre bundles are treated with an alkaline solution (e.g. NaOH) to degrade the pectins of the middle lamella (Wang et al. 2003). This method is widely used for flax (Perry 1985). However, other methods have been used as well: e.g. *steam explosion* (Vignon et al. 1996), *ultrasound* (Keller et al. 2001) and *wet oxidation* (Thomsen et al. 1999). After defibration, the collection of fibres is referred to as a *filament*, which in a textile terminology corresponds to a *sliver*.

2.4.2 Yarn production

To minimize the variation of properties within a yarn, a high degree of yarn regularity is required, which therefore is an important indicator of yarn quality. Thus, order must be imparted to the fibre filament before twists are inserted in the spinning process. This is accomplished by the two traditional textile processes: (i) *combing* (or *hackling*), which aligns the fibres and removes a portion of the shortest fibres, and (ii) *drafting*, which straightens out the fibres and ascertains that the number of fibres in a filament cross-section is within specified limits (Klein 1998, Grosberg and Iype 1999). In combing, the filament is progressed through a series of pinned rollers that comb out the short and tangled fibres, and align the long fibres. In drafting, the filament is as well progressed

through a series of rollers (Figure 2.14). However, the rotational speed of the roller pairs is increased in the forward direction, and subsequently the filament is drawn apart. The fibres are moved relative to each other, and the fibre mass per unit filament length is reduced. This underlines the importance of an efficient defibration process. Typically, a number of filaments are fed in together in the drafting process to level out the variation in cross-sectional area along a single filament. Moreover, drafting is improved if the filaments are slightly twisted. When a filament is twisted, the twists are primarily located at thin locations where least resistance is meet. Accordingly, when draft is applied to a twisted filament, the fibres slide apart at locations of low fibre-fibre friction, which are equivalent to locations of low twist (i.e. the thick locations). Thus, drafting predominantly affects the thick locations of the filament until they approach the volume of the thin locations. After that, the twists are redistributed, and drafting affects the entire filament uniformly (Klein 1998).

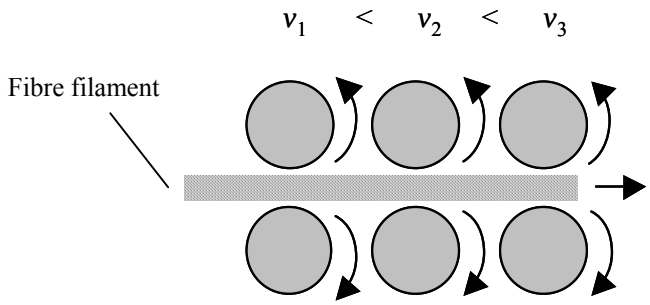

FIGURE 2.14. *The drafting process. Three pairs of drafting rollers are shown with different rotation speeds (v). Modified from Klein (1998).*

A range of different techniques exists to spin discontinuous fibres into a twisted yarn structure: e.g. *ring spinning*, *rotor spinning*, *wrap spinning* and *air-jet spinning* (Grosberg and Iype 1999). Ring spinning is however the most widely used method. Figure 2.15 illustrates the fundamental principles in ring spinning. The parallelized fibre filaments are delivered from the drafting rollers and twists are inserted by the arrangement of (i) the traveller, which freely rotates on the ring, (ii) the ring, which distribute the yarn on the bobbin, and (iii) the bobbin, which is rotating. Each rotation of the traveller inserts one twist, and the number of twists (i.e. turns) per length is controlled by varying the delivering speed of the drafting rollers and the rotation speed of the bobbin (Booth 1975):

$$\text{Twist per length (turns/m)} = \frac{\text{Rotation speed (turns/s)}}{\text{Delivering speed (m/s)}} \tag{2.4}$$

The twisting operation forces the fibres to take up a helical organization. Because of the inherent sliding friction between the fibres, the fibres are slightly extended and a pressure is exerted towards

the yarn interior. This will increase the frictional forces between the fibres and impart axial strength to the yarn (Klein 1998). Therefore, the number of twists per length (the so-called *twist number*) is a main factor determining the breaking load of a yarn; i.e. the breaking load is increased with the twist number until a maximum value, whereafter it starts to decrease. This relationship is depicted in Figure 2.16.

The fineness of plant fibre yarns cannot easily be specified with a reference to yarn diameter or number of fibres in a yarn cross-section. Instead, yarn fineness is expressed either as "mass per unit length" or as "length per unit mass", and the number is denoted *yarn count*. The applied unit of yarn count varies between fibre types and countries, but the standard unit is tex (g/1000 m) (ASTM D2260), and it specifies *yarn linear density*.

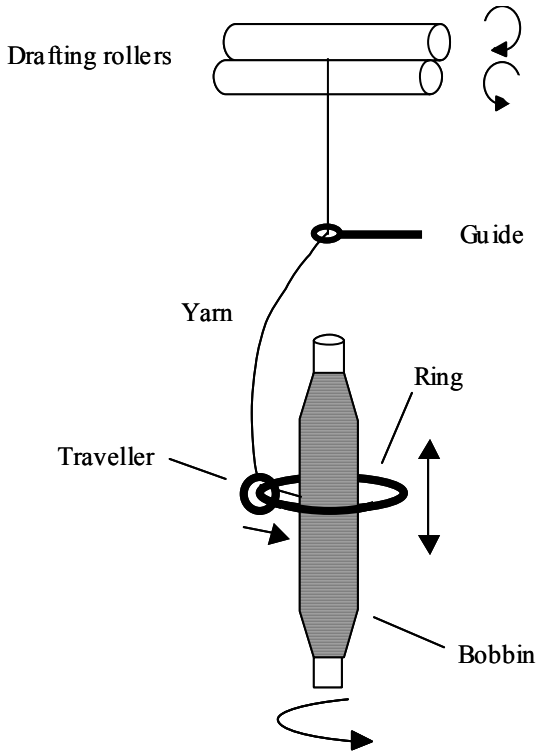

FIGURE 2.15. *The principles in ring spinning. Modified from Grosberg and Iype (1999).*

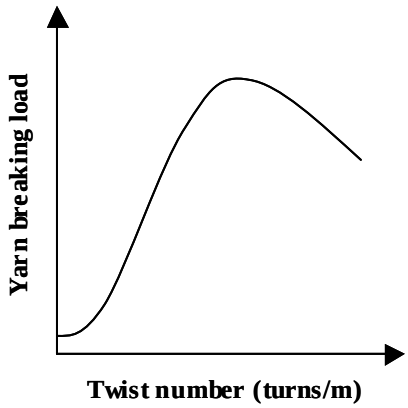

FIGURE 2.16. *The relationship between yarn breaking load and twist number. Modified from Klein (1998).*

2.4.3 Cost of fibre semi-products

The two typical semi-products of plant fibres used for reinforcement of composite materials are *raw fibres* and *non-woven mats*. The term "raw" designates that the fibres are not arranged in an assembly, but are merely an unconfigurated mass of retted (and shortened) fibres. The raw fibres are also used for processing into non-woven mats by air-laid and needle-punching techniques (Dobel 2002, Henriksen and Pallesen 2002). The planar fibre orientation in non-woven mats is uncontrolled, and is basically random.

Table 2.6 presents the general market prices for the two fibre semi-products, in addition to the price for plant fibre yarns. It shows that the market price for plant fibre yarns is relatively high, although it is strongly influenced by fibre type; e.g. the price for hemp yarn is about 5 times the price for cotton yarn, which is about 1.5 times the price for glass fibre rovings. The high price reflects the expensive processing methods governed by the demanded high quality of textile products. However, by adapting the textile processing methods to serve a composite reinforcement purpose, the price of aligned plant fibre products can expectedly be lowered, and they might then be competitive substitutes for aligned synthetic fibre products. The prices of raw fibres and non-woven mats are however competitive to their synthetic counterparts, and this forms a strong motivation for the industrial use of plant fibre composites based on these two fibre semi-products (Bledzki et al. 2002).

TABLE 2.6. *Examples of suppliers and general market prices for various types of plant and synthetic fibre semi-products. The quoted prices should only be considered as guidelines for means of comparison, since they are strongly influenced by the required quantity and quality of the products.*

Fibre type	Semi-product type	Specification	Supplier	Price (€/kg)
Hemp	Raw fibres		Hemcore Ltd (UK)	0.6
Flax	Raw fibres		Bio-7-Fibers (DK)	0.6
Glass	Chopped strands		Owens Corning (CA)	1.5
Hemp	Non-woven mat	1500 g/m^2	Bio-7-Fibers (DK)	1.8
Flax	Non-woven mat	1500 g/m^2	Bio-7-Fibers (DK)	1.8
Glass	Strand mat	150 g/m^2	Owens Corning (CA)	2.6
Hemp	Yarn	50 tex	Linificio e Canapificio (I)	16.3
Flax	Yarn	60 tex	Linificio e Canapificio (I)	11.6
Jute	Yarn	140 tex	Himanshu Jute Fab (IN)	1.6
Cotton	Yarn	50 tex	Textil Manual Goncalves (PT)	3.4
Glass	Roving	100 tex	Owens Corning (CA)	2.5
Carbon	Roving	800 tex	Toray (JP)	18.9

2.5 PLANT FIBRE COMPOSITES

The industrial use of plant fibres as reinforcement in composites is supported by a huge number of publications on the many distinctive aspects of plant fibre composites (see reviews in Robson et al. 1993, Mohanty et al. 2001, Eichhorn et al. 2001, Bledzki et al. 2002). Thus, it is well documented that plant fibres are suitable alternatives for synthetic fibres in composite materials. From an ecological point of view, the use of plant fibres is favourable because of their CO_2 neutrality, biodegradability and cleaner processing conditions. A main disadvantage of plant fibres is their natural origin, which implies an inherent large variation in fibre properties, and this is conflicting with the normal industrial demand of constant product quality. Moreover, the strong hydrophilic nature of plant fibres means that precautions must be taken to improve the water-related dimensional stability of the fibres, and to enhance the low compatibility between the fibres and the hydrophobic thermoplastic matrix.

2.5.1 Fibre/matrix compatibility

In an engineering sense, the transfer of stress from one discrete part to another depends on the interface between the parts, and this is in particular the case for composite materials. Composite interface properties depend on how closely the fibre and matrix parts are contacted by each other, i.e. the *fibre/matrix compatibility*. Intimate contact (<1 nm) is required to generate chemical bonds

(covalent, hydrogen, ionic or van der Waals) between atoms in the interface region, and as such to promote fibre/matrix bonding (or adhesion). Fibre/matrix compatibility is mainly governed by the surface polarity of the two parts. Thus, in the case of polar (i.e. hydrophilic) plant fibres and a non-polar (i.e. hydrophobic) thermoplastic matrix, the compatibility is low and this restricts fibre/matrix bonding.

The technology of synthetic fibre composites is well established, and highly specialized sizing agents have been developed to control the properties of the fibre/matrix interface (Thomason and Adzima 2001). However, the heterogeneous and inconsistent chemical structure of plant fibres makes fibre/matrix compatibilization less controllable. Even so, based on wood fibre composites, a whole range of methods have been demonstrated to enhance the compatibility between wood fibres and thermoplastics, and these have proved to be applicable to other plant fibre composites as well (see Zafeiropoulos et al. 2002b, and references cited herein). Typically, the fibres are treated chemically or physically to reduce their polarity (which as a positive side effect also lowers the water sorption capacity of the fibres). *Acetylation* is an example of a method that frequently has been used to compatibilize plant fibres (Khalil et al. 2001). In this method, the hydroxyl groups at the fibre surface are covalently bonded with acetyl groups (CH3CO) of acetic anhydride by an esterification reaction. Thus, the fibres are made less hydrophilic. This approach establishes a more intimate contact between fibres and matrix and promotes interatomic fibre/matrix adhesion by the relative weak van der Waals forces. In contrast, *coupling agents* can be used to create stronger bonds between fibres and matrix (Lu et al. 2000). A commonly applied coupling agent is *maleic anhydride* (MA). The compatibilization process includes two steps: (i) MA is reacted with the thermoplastic materials (e.g. PP) to form a reaction product (e.g. MAPP) consisting of anhydride units located along the thermoplastic carbohydrate chains, and (ii) MA is reacted with the hydroxyl groups at the fibre surface to form intermolecular covalent and hydrogen bonds (Figure 2.17). It is well accepted that this approach is suitable to improve the mechanical properties of plant fibre composites (Myers et al. 1991) (see also Table 2.7, p. 30).

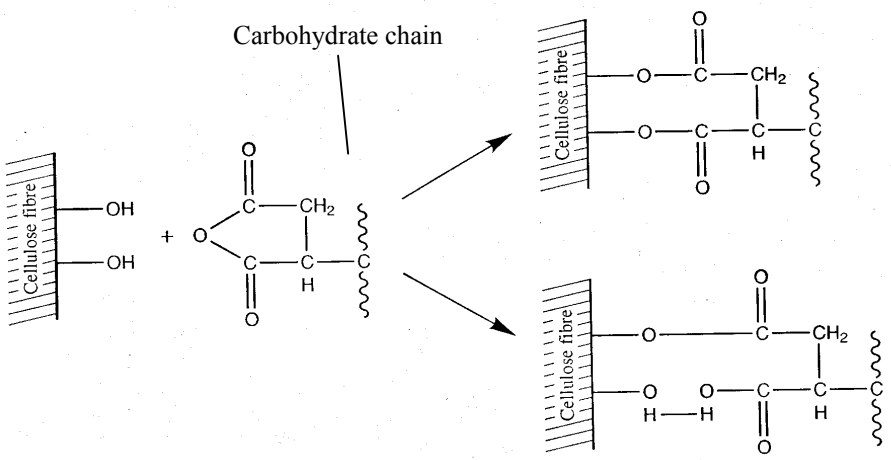

FIGURE 2.17. *Principles in the compatibilization of plant fibres with maleic anhydride. From Bledzki et al. (2002).*

2.5.2 Composite mechanical properties

Based on existing experience and knowledge of synthetic fibre composites, the mechanical behaviour of plant fibre composites have been extensively characterised and analysed. The work has mainly been addressed to measurements of pure tensile properties, as well as bending and impact properties. However, to some extent, the performed work includes also measurements of mechanical properties related to pure compression (Bisanda and Ansell 1991), fatigue (Gassan and Bledzki 1999b), and creep (Gassan and Bledzki 1999c). In addition, fibre/matrix interface properties have been investigated by microbond tests and fragmentation tests (Khalil et al. 2001, Zafeiropoulos et al. 2002a).

Table 2.7 presents typical reported tensile properties of plant fibre composites. The results reveal that composites with a random fibre orientation possess moderate tensile properties with stiffness below 6 GPa and ultimate stress below 60 MPa. Moreover, only ultimate stress is notable increased by fibre/matrix compatibilization, but the effect is relative small. It should however be mentioned that the effect of compatibilization is more pronounced for bending properties (Myers et al. 1991). Nevertheless, the table shows as expected that if the fibres are aligned, the tensile properties are considerably improved, and the obtainable fibre volume fraction is increased (see Section 4.2). The latter finding is noteworthy in relation to an ecological assessment of plant fibre composites. Thus, (partial) alignment of plant fibres would be an alternative and cleaner approach to improve composite properties, instead of treatment of fibres with chemical additives.

Also shown in Table 2.7 are typical tensile properties of glass fibre composites. This demonstrates that glass fibre composites are superior to plant fibre composites irrespective of fibre orientation, and moreover, that ultimate stress in particular is larger for glass fibre composites. Thus, the table

reveals the current status of plant fibre composites where stiffness is acceptable, but ultimate stress needs to be somewhat improved. The lower weight of plant fibre composites is usually used as an argument to compensate for their lower properties (see subsection below).

TABLE 2.7. *Typical reported tensile properties of plant fibre composites. V_f is composite fibre volume fraction. For means of comparison reported properties of glass fibre composites are included.*

Fibre type	Fibre orientation	V_f	Stiffness (GPa)	Ultimate stress (MPa)	Reference
Hemp	Random	($W_f = 0.40$)	2.7	33	Mishra et al. (2000)
		($W_f = 0.40$)*	2.4	37	
	Aligned	0.48	27.6	277	This study
Flax	Random	0.14	3.4	36	Hornsby et al. (1997b)
		0.14*	3.4	39	
	Aligned	0.51	28.7	288	This study
Jute	Random	0.30	5.2	40	Andersen and Plackett (2002)
		0.30*	5.2	61	
	Aligned	0.50	27.2	225	Roe and Ansell (1985)
Wood	Random	0.27	4.2	28	Clemons (2000)
		0.27*	4.2	52	
Glass	Random	0.20	5.4	77	Oksman (2000)
	Aligned	0.60	45.0	1020	Gamstedt et al. (1999)

* *MA was used as compatibilizing agent.*

2.5.3 Materials selection criteria based on weight

Selection of materials during product development is a process where a range of material properties (mechanical, chemical, economical and environmental) is taken into consideration. Material weight is a central selection criterion used for most industrial products, and this is especially important for products made to be transported, such as vehicles. It has been shown that the use phase of a vehicle accounts for the largest part of energy consumption and pollution (over 85 %), followed by manufacture and disposal (Kandachar 2002). Thus, any reduction in vehicle weight means energy savings and less pollution.

The lower density of plant fibres in relation to glass fibres (about 1.5 vs. 2.6 g/cm^3) is advantageous with respect to a lower composite component weight. If tensile stiffness is selected as the key mechanical parameter, and component stiffness is predetermined, it is anticipated that a composite component based on plant fibres would possess the lowest weight. However, this implies that the stiffness of plant fibres is similar to the stiffness of glass fibres, which in general is not the case.

The stiffness of glass fibres is reported to be about 75 GPa (Hull and Clyne 1996). In this study, the estimated largest value of plant fibre stiffness is about 65 GPa. Because of the difference in fibre stiffness, the anticipations of composite component weight are not that obvious. It can be recognized that a low V_f would favour the higher stiffness of glass fibres, and a high V_f would favour the lower density of plant fibres. Figure 2.18A shows the required thickness of a composite component when the component compliance is fixed at a given value. Shown are calculations for composites with a random and a unidirectional fibre orientation. Because of the lower plant fibre stiffness, the figure shows that the required component thickness is largest for plant fibre composites. However, because of the lower plant fibre density, Figure 2.18B shows that component weight is lower for plant fibre composites beyond a given threshold V_f (0.10 and 0.14 for composites with a random and a unidirectional fibre orientation, respectively). The difference in stiffness between plant and glass fibres is partly equalized in composites with a random fibre orientation, and therefore, the threshold V_f is slightly lower for these composites. Likewise, the reduction in component weight is most pronounced for composites with a random fibre orientation.

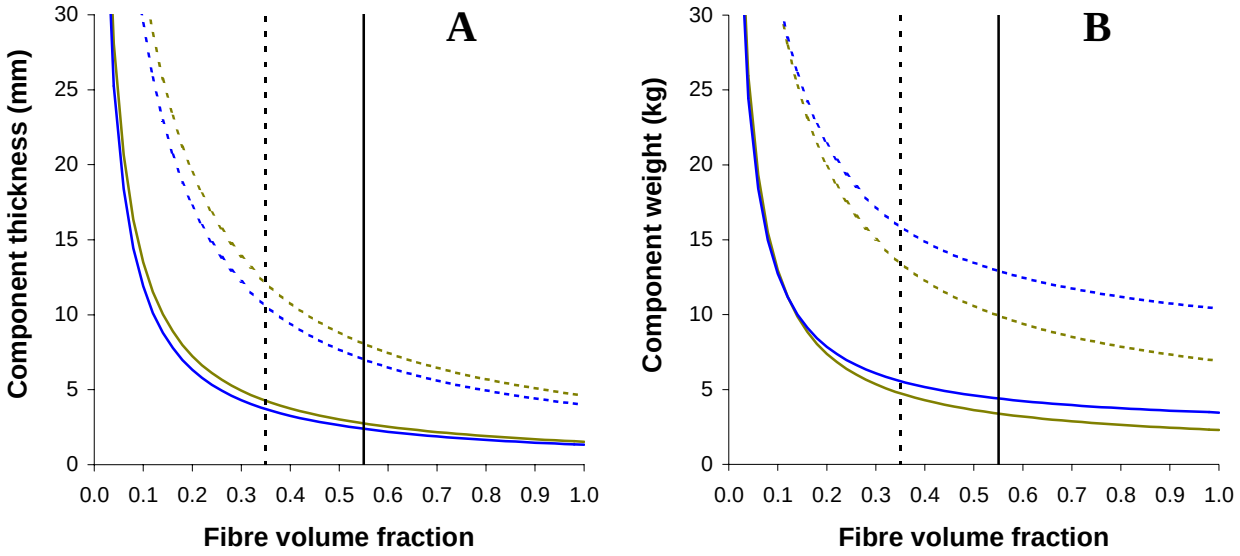

FIGURE 2.18. *The required (**A**) thickness and (**B**) weight as a function of V_f for a composite component with a predetermined compliance. Shown are composites based on plant fibres (green lines) and glass fibres (blue lines), and with random (dotted lines) and unidirectional (full lines) fibre orientation. Vertical lines indicate the maximum obtainable V_f of plant fibre composites with random (dotted line) and unidirectional (full line) fibre orientation. The calculations are based on square composite components (1x1 m^2) with a polypropylene matrix, and with a fixed compliance of 0.01 m/GN. The applied densities are 0.9, 1.5, and 2.6 g/cm^3 for polypropylene, plant fibres and glass fibres, respectively. Likewise, the applied values of stiffness are 1, 65, and 75 GPa. Composite stiffness is estimated by the "rule-of-mixtures", and a fibre orientation factor of 0.33 is used to estimate stiffness of composites with a random fibre orientation (Lilholt and Bjerre 1997).*

The ratio between material stiffness and material density (E/ρ) is an appropriate index for comparison of component weight between types of materials, and this is actually used as a materials selection criteria for components loaded in pure tension (Ashby 1997). The index is denoted the *specific stiffness*, and should be maximised in order to minimize component weight. Figure 2.19A is in principle analogous to Figure 2.18B, but now the specific stiffness of the composites is shown as a function of V_f. Thus, findings from Figure 2.19A are similar to the ones given above; i.e. for V_f beyond about 0.14, plant fibre composites are superior to glass fibre composites with respect to component weight. However, the applied plant fibre stiffness of 65 MPa is a maximum value, and a lower stiffness is indeed more likely to be representative for plant fibres. If a plant fibre stiffness of 50 GPa is used to calculate the specific stiffness of the composites, then Figure 2.19B shows that the situation is notably changed. Below a threshold V_f of about 0.55, glass fibre based composite components would then possess the lowest weight (i.e. the highest specific stiffness). However, as specified in the figure, the maximum obtainable V_f of aligned plant fibre composites is in fact about 0.55 (see Section 4.2). It can be recognized that the threshold V_f is increased when the plant fibre stiffness is decreased. The relationship between these two parameters is shown in Figure 2.20. The figure demonstrates that if plant fibres should be able to compete with glass fibres in aligned composite components loaded in pure tension, the lower limit of plant fibre stiffness is about 50 GPa. However, in composite components with a random fibre orientation, the lower limit of plant fibre stiffness is about 55 GPa. Thus, this forms another argument for the alignment of plant fibres.

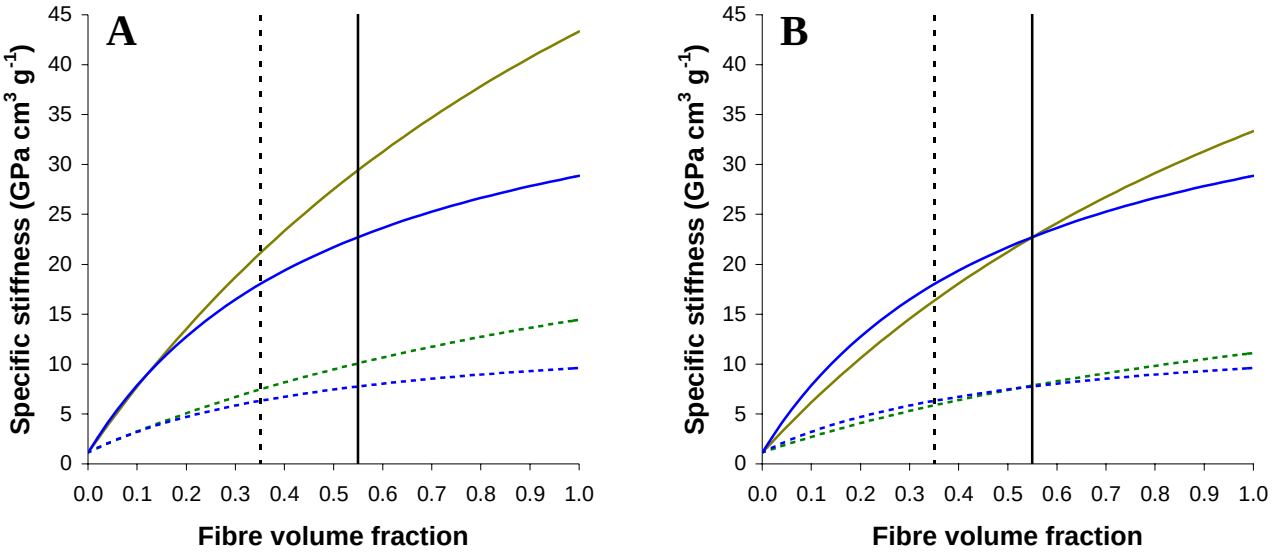

FIGURE 2.19. *Composite specific stiffness for pure tension (E/ρ) as a function of V_f. The applied plant fibre stiffness is 65 GPa in (**A**) and 50 GPa in (**B**). See more details in Figure 2.18.*

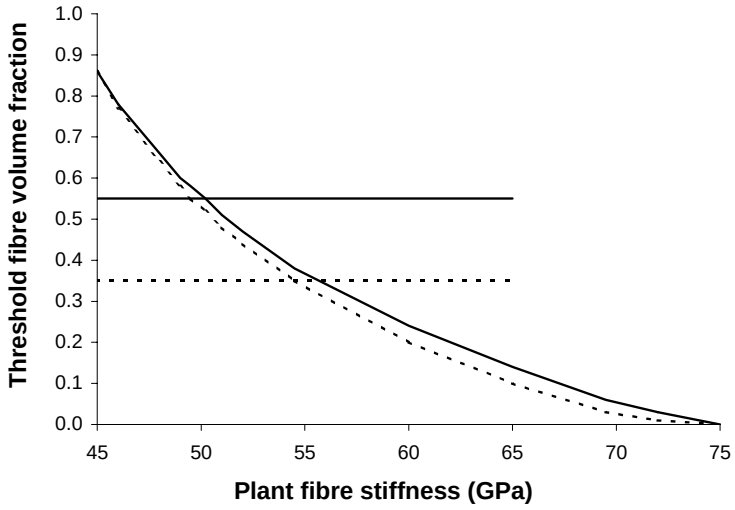

FIGURE 2.20. *Relationship between plant fibre stiffness and threshold V_f of composites with random (dotted line) and unidirectional (full line) fibre orientation. Horizontal lines are the maximum obtainable V_f in composites with the two fibre orientations. See more details in Figure 2.18.*

When loading of a component is changed from pure tension to bending, specific stiffness is adjusted to apply to the different loading mode by adding an exponent of 1/3 to the material stiffness. Thus, the index $E^{1/3}/\rho$ is then an appropriate criterion for a weight based materials selection. See Ashby (1997) for a more comprehensive interpretation of the adaptation of specific stiffness (and specific strength) to various loading modes and component shapes. Figure 2.21 is similar to Figure 2.19, but now the specific stiffness for bending is shown. It can be seen that when a component is loaded by bending, a plant fibre based composite component would possess the lowest weight, and this is true even if plant fibre stiffness is somewhat reduced.

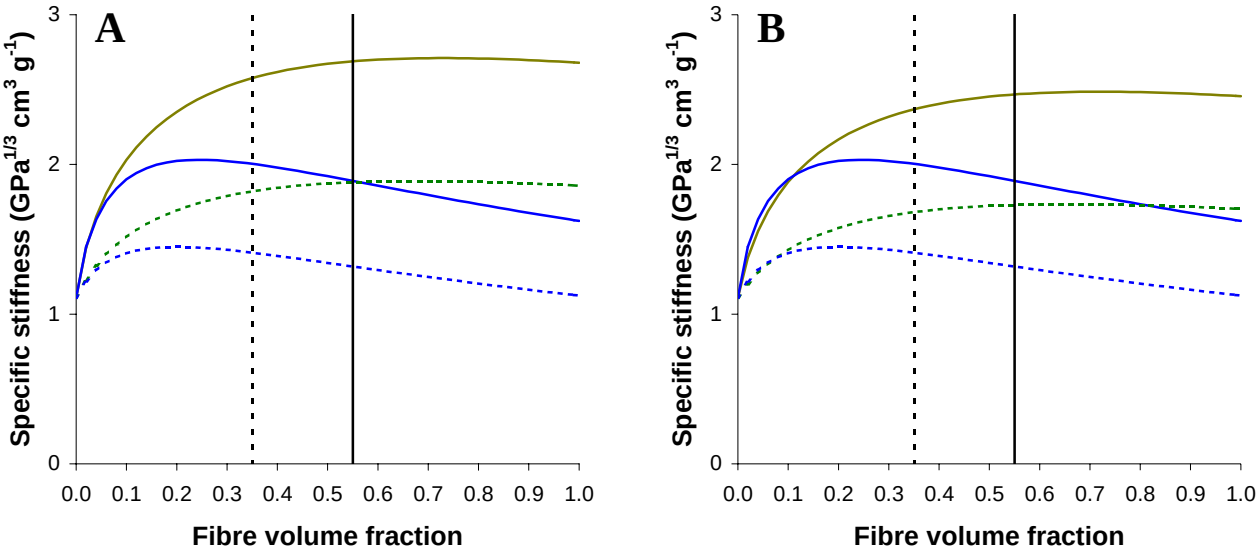

FIGURE 2.21. *Composite specific stiffness for bending ($E^{1/3}/\rho$) as a function of V_f. The applied plant fibre stiffness is 65 GPa in (**A**) and 50 GPa in (**B**). See more details in Figure 2.18.*

2.5.4 Current applications

In Europe, plant fibre composites are mainly used by the automotive industry (Ellison and McNaught 2000, Karus et al. 2002). The applied fibre semi-products are raw fibres and non-woven mats, and therefore, the composites possess moderate mechanical properties (see Table 2.7, p. 30). This makes them nevertheless well qualified to be used as non-structural components. Because of the high sensitivity of plant fibres towards water exposure, mostly interior components are made of plant fibre composites; e.g. door liners (Figure 2.22), boot liners and parcel shelves. Recently, plant fibres have also been used in exterior composite components; the engine and transmission covers of a Mercedes-Benz Travego coach (Evans et al. 2002). In 2002, the total consumption of plant fibres was about 17,000 tonnes, and the average amount of fibres per vehicle was 10-15 kg. These numbers are anticipated to increase (Karus et al. 2002). In the remaining western world, the use of non-structural composite components based on plant fibres is considerable more widespread, and wood fibres are by far the preferred fibre type. In the US, wood fibres account for about 7 % of the total amount of fillers and fibres used in composite materials, and the market is fast growing (Clemons 2000). The main applications are building components, such as deckings, windows profiles and floorings, but also products like pallets, flowerpots and office accessories are increasingly being made of plant fibre based composite materials. This development in the use of plant fibres is likely to be mirrored by Europe in the coming years (Bledzki et al. 2002).

FIGURE 2.22. *A side door liner of an Audi A2 based on a plant fibre composite material. From N-fibrebase (other examples of applications can be seen in this internet database).*

In most of the current applications of plant fibre composites, the fibre reinforcement effect is of minor importance. The fibres are not aligned and the good fibre tensile properties are therefore not efficiently utilized. Only one example has been found of strong plant fibre composites used in load

bearing applications. In India, houses, grain silos and fishing boats have been fabricated with the use of aligned jute fibre composites (Mohanty and Misra 1995).

The industrial use of plant fibres is generally driven by reductions in cost, but also the issue of environmental awareness has become important. In Europe, the EU "end of life vehicle" directive imposes that 85 % by weight of all vehicle components should be recyclable by 2006, and 95 % by 2015. In relation to plant fibre composites, the term "recyclable" is however somewhat unresolved (Peijs 2002). Plant fibres are fully recyclable by combustion, as well as being fully biodegradable, but the same cannot be implied for the remaining synthetic polymeric matrix and chemical additives. Moreover, as a material type, the recyclability (or reuseability) of composites is a field where only little practical experience has been accumulated, and as such it is inferior to other types of materials; e.g. metals and pure plastics. Glass fibre composites with a thermoplastic matrix can be recycled by remoulding used parts, but in the case of plant fibre composites, this has been shown to severely deteriorate the mechanical properties because of the repeated thermal exposure (Reussmann et al. 1999). Even though the current industrially applied plant fibre composites are not strictly recyclable, they form nevertheless a foundation for a future increasing use of environmental friendly materials.

3 MATERIALS AND METHODS

3.1 MATERIALS

Specifications of the four different types of textile plant fibre yarns applied in this study for composite reinforcement are shown in Table 3.1. He47 and He53 are two batches of the same hemp yarn type, but bought with a time interval of about two years. He91 is the only yarn type composed of two filaments of fibres that are twisted around each other. All yarn batches consisted of several bobbins of yarn. According to the supplier the yarns were spun by ring spinning. They were wet spun, as opposed to dry spun. This means that prior to spinning, the fibre filament is soaked in hot water to soften the fibres, which makes the yarn more regular with less fibres deviating from the overall fibre orientation in the yarn. Another commonly applied method to increase yarn regularity is to add a small amount of lubricating agents (i.e. oils) to the fibres prior to the drafting process. However, whether this was also the case for these yarns could not be confirmed by the supplier. Succeeding the spinning process the yarns were boiled in water to release the fibre tension generated during spinning making them more flexible. The yarns had not been paraffined, i.e. a process where a yarn is coated with wax to improve any subsequent dyeing processes.

TABLE 3.1. *Specifications of the applied types of plant fibre yarns. All yarn types were supplied by Linificio e Canapificio Nazionale (I).*

Yarn type	Product name	Filament no	Linear density (tex)		Abbreviation
			Specified	Measured	
Hemp	Imperial	1	50	47	He47
Hemp	Imperial	1	50	53	He53
Hemp	Imperial	2	100	91	He91
Flax	Smeraldo	1	63	64	Fl64

Specifications of the applied six thermoplastic matrix types are shown in Tables 3.2 and 3.3. The PET was a modified type with a lower T_m, and probably also a lower T_g, than the traditional PET. The exact T_m and T_g for the modified PET are not known, and the values in Table 3.3 are related to the traditional PET. The maleic anhydride level of MAPP was specified by the supplier to be 0.2 w%.

TABLE 3.2. *Specifications of the applied thermoplastic matrix types.*

Matrix type	Supplier and product name	Product type	Abbreviation
Polyethylene terephthalate	Trevira Neckelmann (DK)	Filament yarn	PET
Polyethylene (low-density)	Trevira Neckelmann (DK)	Filament yarn	PE
Polypropylene	Trevira Neckelmann (DK)	Filament yarn	PP
Polypropylene	Hoechst (D); Trespaphan NNA	Foils	PP^H
Polypropylene	Dow (UK); H710-05	Foils*	PP^D
Maleated polypropylene	Uniroyal Chemical (UK); Polybond 3002	Foils*	MAPP

* *Prior to the experiments the foils were extruded from granulates.*

TABLE 3.3. *Specifications of the applied thermoplastic matrix types. Density, linear density and thickness are measured in this study. Melting point (T_m) and glass transition temperature (T_g) are refereed from Muzzy (2000), except T_m of MAPP, which is specified by the supplier.*

Matrix type	Density (g/cm^3)	Linear density (tex)	Thickness (mm)	T_m (°C)	T_g (°C)
PET	1.34	56		250	80
PE	0.97	28		120	–90
PP	0.91	90		165	–20
PP^H	0.91		0.03	165	–20
PP^D	0.91		0.15	165	–20
MAPP	0.91		0.15	165	-

3.2 METHODS – COMPOSITE FABRICATION

The fabrication route of the aligned plant fibre yarn composites is depicted in Figure 3.1. The yarn was aligned by filament-winding (see experimental set-up in Figure 3.2). With a custom-built winding-machine the yarn was wound on to a metal frame (400x400 mm^2) with small sideward movement per rotation (about 0.7 mm/rotation) producing yarn assemblies with a high degree of alignment and controlled thickness. Two techniques of fibre/matrix mixing were applied: film-stacking and commingled filament-winding. In film-stacking, thermoplastic foils were stacked in between layers of aligned yarn assemblies. In commingled filament-winding, thermoplastic filament yarn was concurrently wound together with plant fibre yarn. Advantages and disadvantages of the two fibre/matrix mixing techniques are presented in Subsection 4.5.1.

The fibre/matrix assemblies were processed into composite laminates by a specially designed compression moulding system, which previously has been described by Andersen (1997). It

consists of three units: (i) a loading unit, (ii) a heating unit, and (iii) a press unit. The fibre/matrix assembly is automatically and rapidly conveyed between the units. After placement of the assembly in the loading unit it is conveyed to the heating unit. In this unit the assembly is contact heated under vacuum. The assembly is subsequently conveyed to the press unit where it is consolidated by compression at high pressure. Composite processing conditions are accurately controlled: e.g. time and temperature in the heating and press units, and the consolidation pressure. The applied conditions are given in Figure 3.1. In addition to the different combinations of materials, the variable parameters in composite fabrication were the fibre weight fraction (0-0.7) and the temperature in the heating unit (180, 200 and 220 °C). One advantage of the applied method is the established vacuum condition during heating of the fibre/matrix assembly, which tends to remove water vapour (i.e. more efficient drying of the fibres) and limit oxidative chemical reactions. The latter effect might reduce the potential thermal degradation of the plant fibres. The rectangular area (length x width) of the fabricated composite laminates was 300x260 mm^2 with a variable thickness (1.9-2.6 mm).

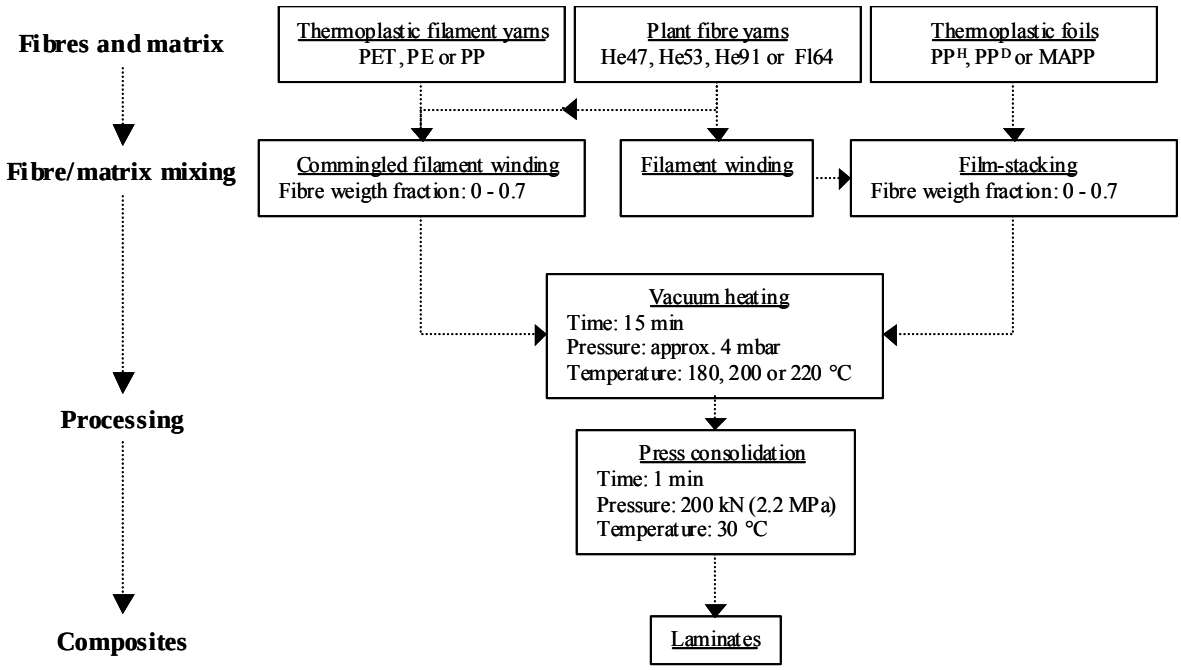

FIGURE 3.1. *Diagram showing the applied fabrication route of composite laminates.*

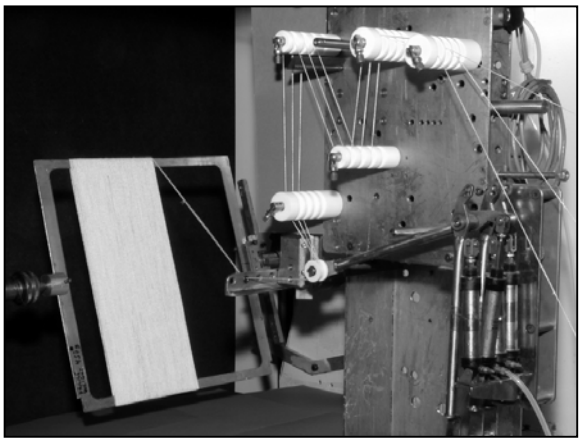

FIGURE 3.2. *Experimental set-up for filament-winding of plant fibre yarn. Note that this is also the set-up used for commingled filament-winding.*

3.3 METHODS – TESTING

Detailed descriptions and specifications are given for the applied testing methods. However, for methods described elsewhere in this thesis, only short explanatory descriptions are presented in this section. No information is given on the types of materials actually tested by the methods (i.e. types of plant fibre yarns, thermoplastics and composites), but this can be seen from the presented results in Chapter 4.

3.3.1 Plant fibre yarn characteristics

The effect of composite processing conditions on yarn characteristics was included in the investigations. Aligned assemblies of yarn, without any thermoplastic filaments, were processed by vacuum heating (180, 200 or 220 °C; 15 min) and press consolidation (2.2 MPa, 30 °C; 1 min) (see Section 3.2). These yarn samples will be identified by the actual temperature used in vacuum heating (180, 200 or 220 °C), and will be denoted *processed yarn*.

Fibre chemical composition

The proportional mass distribution of cellulose, hemicellulose and lignin was determined by a method of Goering and van Soest (1970). The yarn fibres were grounded in a Whiley knife-mill and passed through a 1 mm sieve, after which their dry mass was determined by oven-drying (103 ± 2 °C; at least 18 hours). Subsequently, the chemical composition was gravimetrically determined (in weight percentage of dry mass; w%) by sequential degradation and/or extraction of the cell wall constituents: (i) non cell wall materials (i.e. ash and pectins) were degraded by boiling the fibres in a neutral detergent agent, (ii) hemicellulose was degraded by boiling the fibres in an acid detergent

agent, (iii) lignin was degraded by oxidation with potassium permanganate, and (iv) cellulose was degraded by 72 w% sulphuric acid.

The content of surface lipids was determined by extracting dry yarn fibre samples with a mixture of toluene, acetone and ethanol (4:1:1 by volume) in a Soxhlet apparatus for 5 hours. The solvent mixture was evaporated and the weight of the residual part was determined.

Fibre density

The dry fibre density (g/cm^3) was determined by pycnometry (Pratten 1981, ASTM D792). The method consists in gravimetric measurements of a small bottle (25 ml), called a pycnometer, containing a sample of dry fibres and/or liquid water as displacement medium. The yarn fibre sample (about 1 g) was dried in a vacuum oven (0.9 mbar; 20 °C) for at least 18 hours. Water was added to the pycnometer containing the fibre sample under vacuum conditions. See more details in Appendix A. See considerations of absolute and apparent fibre density in Subsection 4.1.2.

Yarn linear density

The dry yarn linear density (tex; g/1000 m) was determined from the dry weights of 10 m yarn lengths. The yarn samples were dried in a vacuum oven (0.9 mbar; 20 °C) for at least 18 hours. In addition, the moist yarn linear density was determined for tensile tested yarn samples (see below). The weight of these yarn samples was measured in a climate room with conditions: 65 ± 5 % RH and 20 ± 1°C.

Yarn structure

The external yarn structure was qualitatively assessed from environmental scanning electron microscope (ESEM) images. Fibre twisting angle and yarn diameter were measured from optical microscope (OM) images. To test for any interrelations between the two parameters they were measured pair wise on single locations along the yarn.

Fibre size distribution

Fibre cross-sectional areas were measured from OM images of polished composite cross-sections. The measurements were performed manually by the aid of an image analysis software (Leica IM500 ver. 1.2 from Leica Microsystems AG).

Fibre length distribution

It was attempted to determine the fibre length distribution by disentangling the yarns and removing single fibres. However, the fibres are well integrated in the yarn structure and it proved impossible

to avoid fibre breakage. Thus, this parameter is not determined, and instead the fibre lengths of the yarns are assumed comparable to the fibre lengths reported in Table 2.1 (p. 6).

Fibre water sorption

Water sorption of the yarn fibres was measured in a specially designed climate chamber (Strømdahl 2000) where the humidity was accurately controlled (± 0.1 % RH), and where it was possible to weigh a sample without removing it from the controlled environment. All experiments were performed isothermally at a temperature of 20 ± 1 °C. Equation (2.2) (p. 13) was applied to calculate the equilibrium water content (u_{RH} or U_{RH}; %) of a yarn sample (about 10 g) at a given relative humidity (RH) (e.g. U_{65} is the equilibrium water content at 65 % RH):

$$u_{RH} = \frac{U_{RH}}{100} = \frac{m_{RH} - m_0}{m_0}$$

The dry mass was determined by oven drying (103 ± 2 °C; at least 18 hours). The applied criterion to assess whether a sample had reached equilibrium was that the mass change between two consecutive weighings separated by at least 24 hours was less than 0.02 %.

The complete sorption isotherm of a few yarn fibre samples were determined by changing the humidity in steps between 4 and 95 % RH; first in an ascending sequence (4, 15, 35, 50, 65, 80, 85, 90, 95) and then in a descending sequence (95, 80, 65, 35). At each humidity the equilibrium fibre mass was noted. In addition, an experiment was carried out to determine the water sorption capacity of (i) the different yarn types and (ii) the processed yarn. In this experiment the equilibrium water content was determined at three humidities in an ascending sequence: 35, 65 and 85 % RH. Finally, for a single yarn fibre sample, the change in water content between 65 and 85 % RH was studied by weighing the sample at small time intervals until equilibrium was reached at 85 % RH.

Yarn tensile properties

The yarn tensile properties were measured with an Instron testing machine with settings: load cell 10 kN, cross-head speed 2 mm/min and sampling rate 20 data points/s. To ensure that the yarn was sufficiently clamped and concurrently not damaged, it was clamped between two leather pieces (to increase friction) with a controlled low pressure. The gauge length was 3 mm. Conditions in the testing room were 65 ± 5 % RH and 20 ± 1 °C. However, to study the effect of a changed fibre water content, the humidity in the testing room was changed to 35 ± 5 or 85 ± 5 % RH. Before testing, the yarn fibres were allowed at least an 18 hours period of time to reach equilibrium.

The cross-sectional area used to convert load into stress was calculated from the fibre density and the yarn linear density. However, the determined fibre density corresponds to dry condition ($\rho_{f\,0}$), and the linear density of the tested yarn lengths was determined at 65 % RH (tex_{65}). Therefore, both the determined fibre density and the determined yarn linear density were adjusted for the fibre water content at the humidity condition at testing (u_{RH}):

$$\rho_{f\,RH} = \frac{1 + u_{RH}}{1/\rho_{f\,0} + u_{RH}/\rho_w}$$

$$tex_{RH} = \frac{tex_{65}\,(1 + u_{RH})}{(1 + u_{65})} \qquad (3.1)$$

See Subsection 2.2.3 for details on the assumptions made to interrelate fibre density and fibre water content (equation (2.3), p. 19). Finally, the yarn fibre cross-section (A_{RH}; m^2) at the humidity condition at testing was determined:

$$A_{RH} = \frac{tex_{RH}}{\rho_{f\,RH}}\ 10^{-9} \qquad (3.2)$$

While fibre density assumingly is constant along the yarn axis, yarn linear density is not, and therefore it was specifically determined for each of the tested yarn lengths (clamp length plus gauge length = 14.8 mm) by the use of a high-precision weight (± 0.00001 g) (Cahn DCA 322). By applying individually values of yarn linear density, instead of an overall mean value, the scatter of the measurements was reduced considerable; e.g. the coefficient of variation for yarn ultimate stress decreased from 25 to 15 %.

The results from yarn tensile tests showed that the initial part of the load-displacement curve was not linear, but it was slowly increasing in slope until it finally became linear (Figure 3.3A) (see Subsection 4.1.7 for an explanation). The length of the non-linear part was highly variable between the tested yarn samples (0.02-0.15 mm), and this increased the scatter of the determined stress-strain curves within the same yarn type. Thus, initiatives were taken to set off this difference between samples. By linear regression, the linear part of a curve was extended to the axis of displacement and as such this represents the apparent initial linear part (Figure 3.3B). The point of intercept was interpreted as a gauge length addition (Δl) [1]. Subsequently, strain (ε) was calculated:

$$\varepsilon = \frac{x - \Delta l}{l + \Delta l} \qquad (3.3)$$

where x is displacement data and l is gauge length. For each stress-strain curve the apparent stiffness (the slope of the apparent initial linear part; GPa), the ultimate stress (MPa), and the strain at ultimate stress were determined.

1. More correctly Δl should not be added to the gauge length in the denominator of the equation. The situation was however misinterpreted, which means that the reported yarn properties need to be slightly adjusted by a factor of about 1.02 (i.e. lower stiffness and larger strain at ultimate stress). The results are used on a pure comparative basis, and therefore this small deviation from the correct properties does not interfere with any conclusions.

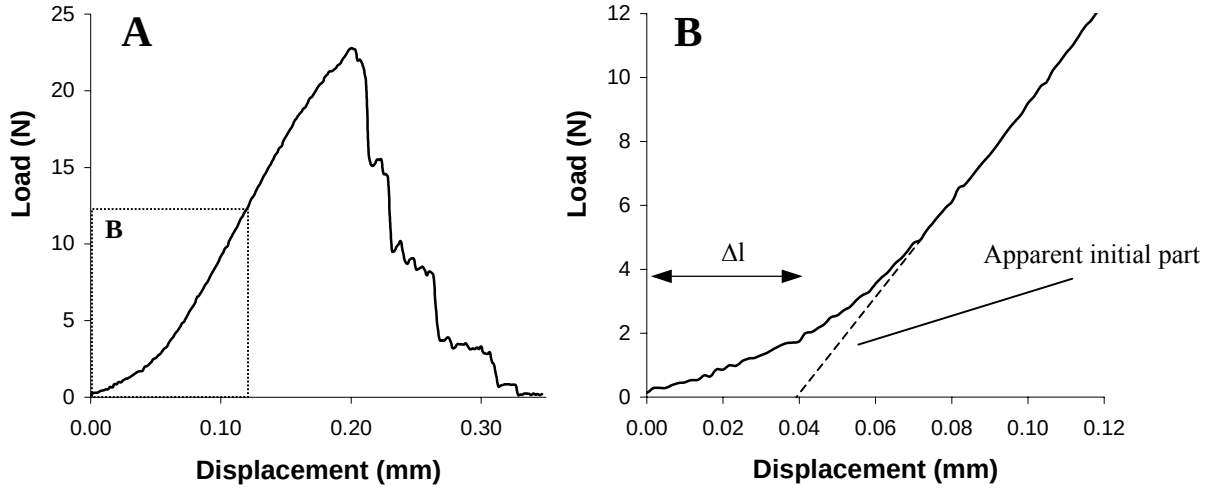

FIGURE 3.3. *Example of a load-displacement curve. (**A**) is the complete curve and (**B**) is a close-up of the initial non-linear part.*

3.3.2 Matrix properties

Pure thermoplastic matrix laminates were fabricated by the method also used for composite laminates. The process temperature was 200 °C for all fabricated thermoplastic laminates.

Rheological properties

The viscosity of the thermoplastics was measured with a rotation rheometer (Rheologica StressTech) using circular samples (diameter 20 mm). The rheometer was a parallel-plate viscometer where a couple (N m) was applied to one plate and its rate of rotation (radians/s) was measured at steady state. The shear rate (1/s) and the viscosity (Pa s) of the sample positioned between the two plates were calculated from sample dimensions, the couple and the rate of rotation (Barnes et al. 1996). The applied stress was increased stepwise in the range 10-5000 Pa. Viscosity as a function of shear rate was measured isothermally at the three temperatures: 180, 200 and 220 °C.

Water sorption

These investigations were performed along with the measurements of composite water sorption (see Subsection 3.3.5).

Tensile properties

An Instron testing machine was used with settings: load cell 5 kN, crosshead speed 2 mm/min and sampling rate 5 data points/s. The thermoplastic laminates were cut out into dumbbell shaped test specimens (180x25 mm^2 with gauge section 30x15 mm^2). Before testing, the specimens were conditioned in a climate cabinet at 65 ± 1 % RH and 20 ± 1 °C. However, to study the effect of

changed water content some specimens were conditioned at low humidity (< 10 % RH; in a closed container with silicate gel), and some specimens were conditioned at high humidity (> 99 % RH; in a closed container with a water bath). The specimens were conditioned until equilibrium. All handling of the conditioned specimens outside the controlled climate was carried out within 10 min, which was demonstrated in a preliminary study to cause only very small weight changes. The gauge section dimensions of the conditioned specimens were determined with a micrometer screw. Two extensometers were used to measure strain in the axial and in the transverse direction to determine Poisson's ratio. Stiffness (GPa), ultimate stress (MPa), and strain at ultimate stress were determined from the measured stress-strain curves. Poisson's ratio and stiffness were determined from linear regression between axial strain 0.0005 and 0.0020.

3.3.3 Compaction of plant fibre assemblies

The compaction behaviour of plant fibre assemblies was assessed from the relationship between fibre volume fraction and compaction pressure. This was measured with an Instron testing machine (see experimental set-up in Figure 3.4). The fibre volume fraction was calculated as the ratio between the theoretical thickness of the fully compacted solid fibre assembly and the distance between the press platens. The press area was 180x140 mm^2, which gave a maximum compaction pressure of about 4 MPa. Two different compaction tests were performed: (i) single compaction, where the fibre assembly was loaded until maximum pressure a single time, and (ii) multiple compaction, where the fibre assembly was loaded-unloaded between zero and maximum pressure in four succeeding compaction cycles. Aligned assemblies of plant fibre yarn were made by filament-winding. The investigations included also plant fibre assemblies with a random fibre orientation: non-woven mats of hemp, flax and jute. Moreover, for means of comparison the compaction behaviour of glass fibre assemblies was measured. See more details in Paper III.

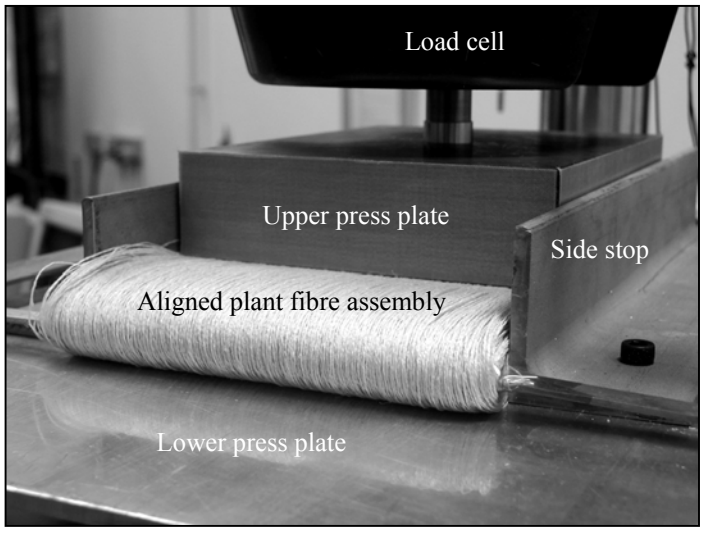

FIGURE 3.4. *Experimental set-up for compaction of fibre assemblies. The upper press plate was fixed, whereas the lower press plate moved upwards.*

3.3.4 Composite volumetric composition

Small samples (15x15 mm^2) were cut out from the composite laminates and composite density was measured by the buoyancy method (ASTM D792). The fibre weight fraction (W_f) was determined by chemically dissolving the thermoplastic matrix: PET was dissolved by hexafluoro-2-propanol, and PE, PP and MAPP were dissolved by xylene. However, when commingled filament-winding was used for fibre/matrix mixing W_f was also determined by the equation:

$$W_f = \frac{no_f \ tex_f}{no_f \ tex_f + no_m \ tex_m} \tag{3.4}$$

where no is number of yarn threads in the winding process and the subscript m denotes matrix. Based on W_f and the measured densities of composite, fibres and matrix, the equations (4.41)-(4.43) (p. 113-114) were used to calculate volume fractions of fibres, matrix and porosity.

3.3.5 Composite water sorption

Composite laminates were cut out into square standard samples with nominal side lengths of 15 mm (Type A, Figure 3.5). The four sides at the edges of the samples were carefully grinded to remove any loose attached material fragments, and to improve the measuring accuracy of sample length and width. The samples were placed in pre-weighed bags (60x170 mm^2) made of commercial PET fabric with a pore size of 73 μm (Polymon 07-73/40; Udsen & Co, DK). The bags contained small pockets for the samples to prevent any contact between samples.

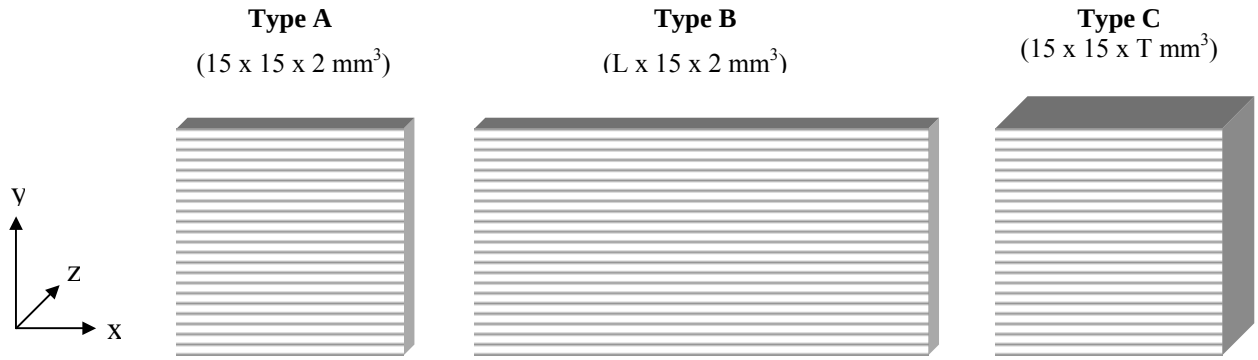

FIGURE 3.5. *The three types of composite samples used for measurements of water sorption. Samples of types B and C have variable lengths (L) and thicknesses (T), respectively. The width (W) was 15 mm for all samples. The lines at the sample surfaces identify the direction of the aligned plant fibre yarn.*

The experimental procedure was to condition the bags with the samples at various levels of ambient relative humidities. Each bag contained 5 samples from a single laminate. At regularly time intervals (1-7 days) the bags with the samples were weighed until they reached equilibrium, and then the mass and dimensions of the single samples were measured. The applied criterion for an equilibrium condition was that the weight change between two consecutive weighings separated by at least 24 h was less than 0.01 %. The precision of the weighing measurements was ± 0.0001 g. Sample dimensions were measured with a micrometer screw (± 0.001 mm). Special markers made on the surface of the samples ensured that the dimensions were measured on exact locations (Figure 3.6). On each sample, 2 locations were assigned to measurements of each of the three dimensions (length, width and thickness). To further reduce the scatter of the measurements, the equilibrium mass and dimensions of single samples were measured 2 times with an interval of a few days.

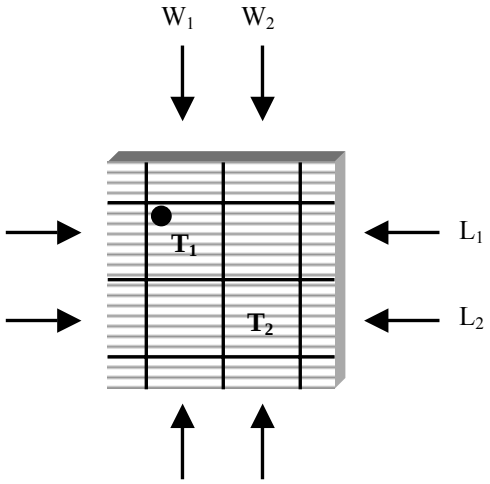

FIGURE 3.6. *The markers (black drawings) made on the surface of a standard laminate sample (type A), which identified the two locations of the measured sample dimensions: length (L), width (W) and thickness (T).*

The measurements of sample dimensions contained four levels, which are represented by four indexes:

i = 1, 2, 3, ... (the experimental levels of ambient relative humidity)
j = 1, 2, 3, 4 and 5 (the five samples in a bag)
k = 1 and 2 (the two locations within a sample for measurements of a given dimension)
l = 1 and 2 (the two repeated measurements in time)

The procedure of data processing to calculate the percentage change in sample dimensions was as follows. Initially, the mean dimension (D; mm, which represents L, W and T) was calculated for the two repeated measurements in time:

$$D_{(i,j,k)} = \frac{D_{(i,j,k,1)} + D_{(i,j,k,2)}}{2} \quad \text{for all values of i, j and k} \tag{3.5}$$

The mean dimensional change between one level of ambient humidity to another was calculated within the single samples, and the grand mean dimensional change (S; %) was calculated for all samples:

$$S_i = 100 \frac{\sum_j \sum_k \frac{D_{(i,j,k)} - D_{(i^*,j,k)}}{D_{(i^*,j,k)}}}{5 \cdot 2} \quad \text{for all values of i, where } i^* \text{ is fixed} \tag{3.6}$$

where i* is the level of humidity used as the reference condition. The two equations were used for each of the three measured sample dimensions, length, width and thickness, and the calculated percentage changes are denoted $S_{x\,RH}$, $S_{y\,RH}$ and $S_{z\,RH}$, respectively, where RH is ambient humidity. As an example, $S_{x\,85}$ is the percentage change in sample length when the ambient humidity is changed from a given reference condition to 85 % RH. The same procedure (but without the index k) was applied to calculate the percentage change in sample mass between one level of humidity to another. The change in sample mass is named the relative water content and is denoted U^*_{RH}.

The intended three levels of humidities were 35, 65 and 85 % RH. The two latter conditions were acceptably reached in climate rooms with a source of water-saturated air controlled to be either on or off depending on the set point. The humidities in the two rooms were measured to be 65 ± 1 and 85 ± 1 % RH. A smaller chamber containing a saturated solution of magnesium chloride was used for the lower humidity level. The tabulated humidity of the salt solution is 33.1 % RH, and the humidity in the chamber was measured to be 33 ± 1 % RH. The humidity in the chamber was slightly below the planned 35 % RH, but this small difference is negligible, and the humidity will subsequently be specified as being equal to 35 % RH. The conditioning temperature was not

controlled, but it was measured in the ranges 18-20, 23-26 and 21-23 °C for the three levels of humidities, respectively. The air in the conditioning climates was circulated by a ventilator.

A preliminary study showed that the samples required long time (several months) to reach equilibrium at a given level of ambient humidity. Therefore, a special experimental design was adopted to reduce the time span of the investigations (Figure 3.7). For each laminate, 10 samples were placed in two bags (e.g. bag no 1d and 1a from laminate no 1), with 5 samples in each. Initially, all bags were conditioned at 65 % RH until they reached equilibrium, and this humidity level was the applied reference condition. Since the starting point of the fabricated composites corresponds to a dry condition, the equilibrium at 65 % RH was reached by water adsorption. Then, half the bags (e.g. bag no 1d) were conditioned at 35 % RH (desorption), and half the bags (e.g. bag no 1a) were conditioned at 85 % RH (adsorption). Finally, all bags were oven-dried (50 °C) (desorption). A preliminary attempt to dry composite samples with a PET matrix at 65 °C showed that this severely distorted the samples. The explanation is most likely that 65 °C is too close to the glass transition temperature of about 80 °C for PET. Thus, any internal stresses in PET were released and the samples were distorted. Subsequently, a lower drying temperature of 50 °C was applied, and the samples were not distorted.

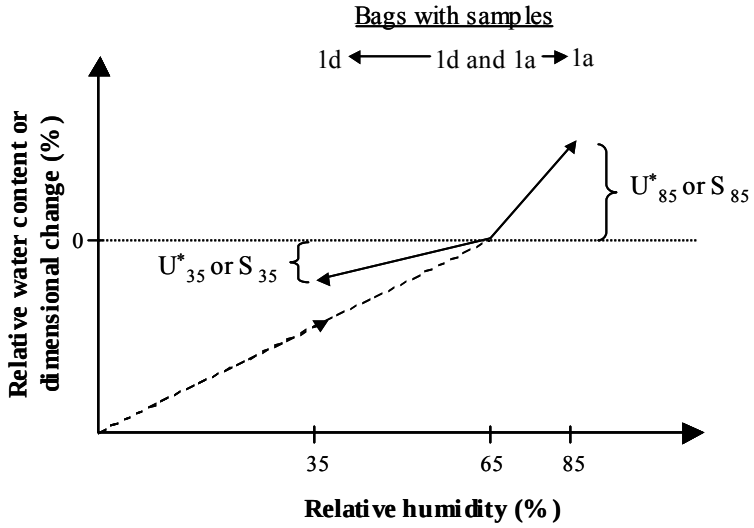

FIGURE 3.7. *The principles in the experimental design. See text for explanation.*

The experiment included also investigations of the difference in water diffusion in the three laminate directions. This was assessed from laminate samples with variable lengths (30, 60, 90 and 240 mm) and variable thicknesses (4, 6, 10 and 15 mm) (types B and C in Figure 3.5), but with the same width (15 mm). The samples with variable thicknesses were made by exposing stacks of standard laminate samples (15x15x2 mm^3) to an elevated temperature (about 100 °C) and a

moderate compression in the thickness direction. In this process, the single samples were effectively attached to each other by the aid of the thermoplastic matrix. Moreover, 4 out of 6 sides of three cubic samples (15x15x15 mm^3) were sealed. Thus, water diffusion was only allowed in one direction (length, width or thickness). The sample sides were sealed with thin (50 μm) brass foils. The foils were attached to the sides with bicomponent epoxy glue (Araldit®). Only the process of water adsorption (65 to 85 % RH) was investigated for the samples with variable lengths and thicknesses, and for the cubic samples with sealed sides.

All measurements of sample mass and dimensions were performed in a room with uncontrolled conditions, and this represents a potential source of error. However a preliminary study showed that when a composite sample in equilibrium at 85 % RH was moved to the measuring room with a humidity of about 50 % RH, the time-dependent decrease in sample mass was indeed very slow; after 30 min the mass was only decreased by about 0.04 %. However, two provisions were made to impede these changes in sample mass and dimensions: (i) the samples were kept in closed plastic boxes, and (ii) the measurements were performed within 10 min.

Finally, the experiment included also composite laminate samples of type A with polished cross-sections. These samples were conditioned along with the other samples, and cross-sectional OM images were obtained at equilibrium. A system was adopted to be able to localise the same cross-sectional area of a sample conditioned at different humidities. Thus, the images were intended to provide information of the microscale dimensional changes of the composites, as well as other water related changes in the internal structure (e.g. cracks).

3.3.6 Composite tensile properties

The composite laminates were cut out into dumbbell shaped test specimens (180x25 mm^2 with gauge section 30x15 mm^2). Prior to testing the specimens were conditioned in a climate cabinet at 65 ± 1 % RH and 20 ± 1 °C until equilibrium. All handling of the conditioned specimens outside the controlled climate was carried out within 30 min, which was demonstrated in a preliminary study to cause only very small weight changes. The gauge section dimensions of the conditioned specimens were determined with a micrometer screw. Tensile tests were performed on an Instron testing machine with settings: load cell 25 kN, crosshead speed 2 mm/min and sampling rate 5 data points/s. Axial strain was measured with two extensometers centred on each side of the specimens. Shown in Figure 3.8 is a tensile specimen mounted for testing. Stiffness (GPa, linear regression between axial strain 0.0001 and 0.0010), ultimate stress (MPa) and strain at ultimate stress were determined from the measured stress-strain curves.

Two variable parameters were included in the above standard procedure of composite tensile testing: testing direction and composite water content. The effect of a changed testing direction was studied by cutting out the tensile specimens with different angles to the yarn axis. The effect of a changed composite water content was studied by re-conditioning some of the tensile specimens at 35 ± 1 or 85 ± 1 % RH. It should be noted that originally in this study, the tensile specimens were not conditioned in a controlled climate before testing. After fabrication, these specimens were placed in plastic bags for variable periods of time, and the conditioning humidity was therefore uncontrolled. The water content of these specimens at testing was presumable low since the initial dry condition of the fabricated laminates was more or less preserved.

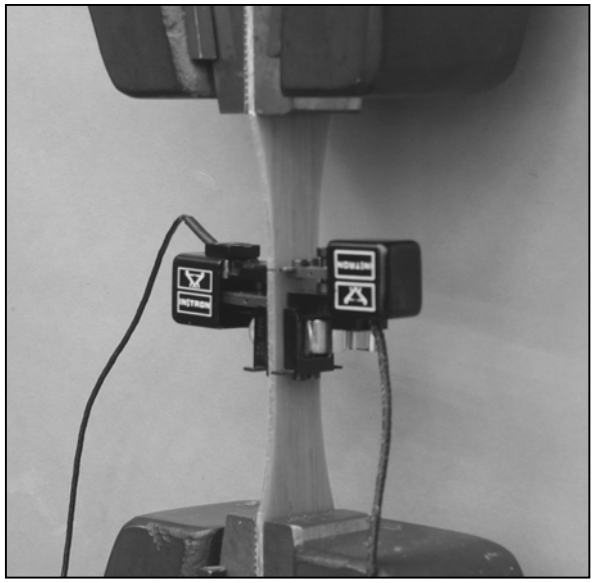

FIGURE 3.8. *Tensile specimen mounted for testing with two extensometers centred at the gauge section.*

4 RESULTS AND DISCUSSION

4.1 PLANT FIBRE YARN CHARACTERISTICS

In relation to the use of plant fibre yarns as composite reinforcement a number of yarn characteristics were investigated:

- Fibre chemical composition
- Fibre density
- Yarn linear density
- Yarn structure
- Fibre size distribution
- Fibre water sorption
- Yarn tensile properties

4.1.1 Fibre chemical composition

The chemical analysis showed that the hemp yarn fibres consist primarily of cellulose (about 90 w%), whereas hemicellulose and lignin represent a smaller fraction (about 10 w%). The content of inorganic materials and non cell wall materials (e.g. pectins) are negligible. The results for the three hemp yarn types (He47, He53 and He91) are presented in Table 4.1. He47 contains 89 w% cellulose and 9 w% hemicellulose. He53 and He91 have an identical chemical composition with 91 w% cellulose and 7 w% hemicellulose. Thus, He47 contains slightly less cellulose, and slightly more hemicellulose than He53 and He91.

Using a similar chemical analysis as the one used in this study, the cellulose content in raw hemp fibres has been determined to be about 60 w% (Thygesen et al. 2002), which is consistent with values in the range 60-80 w% reported elsewhere (Lilholt and Lawther 2000, Bledzki et al. 2002). The explanation for the relative high cellulose content measured in this study can only be speculative since no information has been given by the supplier on fibre treatments. However, it seems plausible that the fibres have been treated chemically to further separate the retted fibre bundles into single fibres. One type of chemical treatment is alkalisation, which is an alkali treatment typically used for textile flax fibres (Perry 1985). This treatment removes, not only the substances that cement the fibres together (i.e. pectins) (Wang et al. 2003), but fractions of cell wall constituents are removed as well (Gassan and Bledzki 1999a). If equal amounts of the various cell wall constituents are removed, this will result in proportionally larger cellulose content. This explanation is supported by observations of hemp yarn cross-sections, such as in Figure 4.5 (p. 62), showing that relative few fibres are grouped in bundles.

The effect of composite process conditions is also shown in Table 4.1. For both He47 and He53, the processed yarn fibres have a slightly larger content of cellulose and a slightly lower content of hemicellulose. This can be explained in two ways: (i) equal amounts of cellulose and hemicellulose are degraded by the thermal stress induced during processing, or (ii) hemicellulose is predominantly degraded. The latter explanation is most likely since the thermal stability of cell wall chemical constituents is known to increase in order of: hemicellulose, cellulose and lignin (Gassan and Bledzki 2001).

TABLE 4.1. *Fibre chemical composition of the three types of hemp yarn. Sample size is 2 or 4.*

Yarn type	Process conditions	Chemical composition (w%)		
		Cellulose	Hemicellulose	Lignin
He47	None	89	9	2
	200 °C	90	8	2
He53	None	91	7	2
	220 °C	92	5	3
He91	None	91	7	2

A common method to improve yarn regularity is to add a small amount of lubricating agents (i.e. oils) to the fibres before the drafting process. For jute fibres, which have a low natural content of fats and waxes, mineral oil as an emulsion in water is typically added to the fibres in amounts ranging between 0.8 and 5.0 w% (Stout 1988). Table 4.2 presents the results of the chemical analysis of surface lipids. He47 contains about 1.1 w% surface lipids, whereas He53 and He91 contain about 0.7 and 0.6 w%, respectively. The chemical composition of the extracted lipid fraction was not determined, and it can therefore not be established to what extent it was made of an added lubricating oil, in relation to natural occurring fats and waxes. The difference in the lipid content between the three hemp yarn types was supported by observations of the processed yarns: He47 was adopting a very "burned" appearance and became less flexible, whereas He53 and He91 were practically unaffected. Table 4.2 shows the effect of composite process conditions on the lipid content in He47. The lipid content in the processed yarn is reduced to about 0.9 w% with a process temperature of 200 °C, and it is furthermore reduced to about 0.7 w% at 220 °C. Thus, the results indicate that the surface lipids are either degraded or transformed into other chemical compounds as an effect of thermal stress.

TABLE 4.2. *Content of surface lipids in the three types of hemp yarn.*

Yarn type	Process conditions	Content of surface lipids (w%)
	None	1.08
He47	200 °C	0.93
	220 °C	0.70
He53	None	0.66
He91	None	0.61

4.1.2 Fibre density

Accurate determinations of fibre, matrix and composite density are crucial when volume fractions in composites are to be calculated (see Subsection 4.5.5). However, whereas the density of matrix and composite samples readily can be determined because of their massive and solid forms, the density of the delicate and porous fibres is far more problematic to determine accurately. A number of methods for density determinations of small samples have been reviewed by Pratten (1981). Pycnometry was the method employed in this study. Liquid water was selected as the displacement medium to ensure that the hydrophilic plant fibres were perfectly surrounded by the medium. However, the hygroscopic nature of the fibres entails some implications for the applied method:

- The fibre dimensions are increased when water enters into the submerged fibres and becomes hydrogen bound to the various chemical constituents of the cell wall. It must therefore be considered whether this swelling action interferes with the determined fibre density. In the case where bound water density is equal to liquid water density, it can be recognized that the determined fibre density is unaffected by fibre swelling. However, results obtained by Weatherwax and Tarkow (1968) in a study of wood fibres showed that owing to bonding forces, bound water is compressed relative to liquid water. Bound water density was approximated to be about 1.017 g/cm^3. In Appendix A it is estimated that this slightly larger density of bound water will only slightly change the determined fibre density. However, if this issue is to be investigated furthermore, a potential method for the determination of bound water density is presented in Appendix B.
- If the central lumen of the submerged fibres is filled with water, it means that the determined fibre density is the absolute density of the fibre solid matter (i.e. the cell wall) as opposed to the apparent density that includes the central lumen. The luminar dimensions of the hemp fibres in this study are found to be small (see Subsection 4.1.4), and the two fibre densities are therefore just about identical. But for other types of plant fibres with larger luminar dimensions, e.g. jute (Lilholt and Bjerre 1997) and sisal (Perry 1985), the apparent density is notably smaller than the absolute density. To detect whether the lumen of the submerged fibres is filled with water is not

a simple task. The following considerations are based on Siau (1995). If the cell wall contains no openings to the outside environment, the water in the form of bound water is limited to progress across the cell wall by diffusion. Eventually this will increase the water vapour pressure in the lumen towards saturation, i.e. humidity in the lumen approaches 100 % RH. If the lumen contains cavities with small dimensions (diameter < 1 μm), the bound water can be thought to form minute water surfaces, and water vapour will condense into these cavities by capillary water sorption (see Subsection 2.2.1). However, the entire lumen is unlikely to be filled with liquid water by this mechanism. In contrast, if the cell wall contains openings, such as the pits found in wood fibres, liquid water will be able to fill out the lumen. At present, no information on the existence of pits in the cell wall of non-wood plant fibres has been found. In some studies on plant fibre composites it has been reported that the matrix apparently is deposited in the lumen of the fibres (Lilholt and Bjerre 1997, Cichocki and Thomason 2002), and this might indicate that the cell wall of at least some plant fibres contains pits. This is furthermore supported by the relative high fibre densities determined in this study (see below), which suggest that liquid water is able to fill out the small lumen in these fibres.

- When dry plant fibres are exposed to ambient humidity, their weights are rapidly increased because of water adsorption. Thus, the weight of the pycnometer containing the dry fibre sample is critical in relation to the determined fibre density (see Appendix A). Figure 4.1A shows the water content of a hemp yarn sample as a function of time after the dry sample was exposed to ambient humidity (about 65 % RH). The time until the sample reaches an equilibrium water content of approximately 7 % is about 20 min. However, the water content is rapidly increased within the first few minutes, and after only 3 min it is about 4 %. It can be shown that the determined fibre density underestimates the correct fibre density if the weight of the dry fibre sample is overestimated. Figure 4.1B demonstrates how the determined density and the correct density deviate from each other for different water contents of the "dry" fibres. If the correct fibre density is 1.55 g/cm^3 and the weight of the dry fibres is overestimated by 4 %, the figure shows that the determined density is only 1.52 g/cm^3. Consequently, the applied weighing procedure has to be fast to approach the true dry fibre weight, and maybe more importantly, it has to be reproducible to minimize the variation of results between repeated analyses. Alternatively, the dry weight of a fibre sample can be approximated from measurements of sample weight as a function of time after the sample is exposed to ambient humidity. By fitting a suitable mathematical function (e.g. a power-law relationship) to the data points, the dry sample weight at zero time can be approximated by extrapolation.

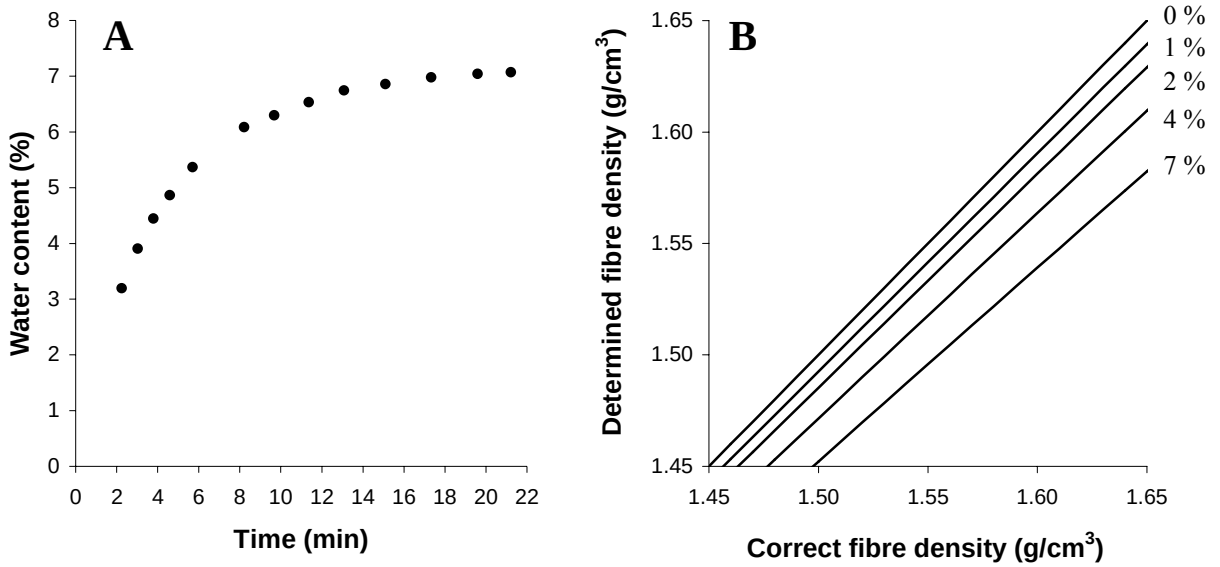

FIGURE 4.1. *(**A**) shows the water content of a "dry" hemp yarn sample (He53) measured as a function of time after being exposed to ambient humidity (about 65 % RH). The dry weight of the sample has been adjusted to give an equilibrium water content of about 7 %. (**B**) shows the determined dry fibre density as a function of the correct dry fibre density for different levels of water content of the "dry" fibres.*

The applied method to determine dry fibre density has been continuously improved during this study with respect to weighing procedure, control of temperature and accuracy in the gravimetric measurements. Consequently, it is believed that the fibre densities determined by the current improved method are closely reflecting the correct densities. This implies that some the fibre densities reported in Papers I-III need to be slightly adjusted, however this will only slightly change the presented results. Table 4.3 shows the latest results for dry fibre densities of He47 and He53. The densities were determined in three experimental analyses separated in time. Each analysis consisted of four fibre samples: two samples of He47 and two samples of He53. It can be seen that the scatter in the determined fibre densities is relatively small both within and between the analyses. Moreover, the results clearly indicate a small difference in fibre density between He47 and He53 with grand means 1.58 and 1.60 g/cm^3, respectively. To underline the robustness of the method, the difference in fibre density is also expected since He47 contains slightly less cellulose and slightly more surface lipids than He53 (see Subsection 4.1.1). The fibre density (mean ± stdv., n=6) of He91 and Fl64 was determined to be 1.59 ± 0.01 and 1.56 ± 0.01 g/cm^3, respectively.

TABLE 4.3. *Dry fibre absolute densities of He47 and He53 determined at three analyses separated in time.*

Analysis no	Fibre density (g/cm^3)	
	He47	**He53**
1	1.586	1.609
	1.587	1.613
2	1.581	1.578
	1.579	1.598
3	1.583	1.599
	1.567	1.592
Mean	**1.581**	**1.598**
Stdv.	**0.007**	**0.013**

The determined fibre densities are relative high compared with the typical reported densities of plant fibres varying between 1.2 and 1.5 g/cm^3 (e.g. Lilholt and Lawther 2000, Bledzki et al. 2002). However, in many cases it is not stated whether the reported fibre density corresponds to an absolute or an apparent density, and moreover, in most studies the fibre density is not determined but is simply refereed from other studies. The high fibre densities determined in this study can be justified by some quantitative considerations of how the various cell wall constituents contribute to the fibre density. The cellulose content of the hemp yarn fibres is about 90 w% and the remaining 10 w% consists of hemicellulose and lignin. In a study by Thygesen et al. (2002) on raw hemp fibres, the cellulose crystallinity is measured to be 70 %. In Appendix C the density of crystalline cellulose is estimated to be 1.64 g/cm^3. The densities of hemicellulose, lignin and amorphous cellulose have not been found in the literature, but are conservatively all assumed to be 1.40 g/cm^3. From these numbers, the density of cellulose is calculated to be 1.57 g/cm^3 (= 0.7·1.64 g/cm^3 + 0.3·1.40 g/cm^3), and subsequently the fibre density is 1.55 g/cm^3 (= 0.9·1.57 g/cm^3 + 0.1·1.40 g/cm^3). More correctly the w% should be changed into v%, but this will only slightly change the result. Thus, for fibres with high content of cellulose (and high degree of crystallinity), the fibre density is approaching the maximum obtainable density of 1.64 g/cm^3 for cellulose-based fibres.

4.1.3 Yarn linear density

This is the typical parameter used by the textile industry to specify yarn fineness. It defines mass per length of the yarn, and is therefore an indirect measure of the cross-sectional fibre area. This is important when yarn fibres are to be impregnated with a high-viscous thermoplastic matrix. Generally, it can be stated that the higher the linear density, the longer the flowing distance from the periphery to the centre of the yarn (assuming equal fibre density). Yarn linear density is however not constant along the yarn, but varies as a function of the number of fibres at a given cross-section.

Table 4.4 shows results from the determinations of yarn linear density using different measuring lengths. The variation in yarn linear density is large at small measuring lengths, but the variation is decreased when the measuring length is increased. The large mean linear density of about 62 g/1000 m for He53 at a measuring length of 0.015 m presumable reflects that a larger sample size is required to approach the expected mean linear density of about 53 g/1000 m. Thus, the short-range variability in linear density is a useful indication of yarn regularity, which also is employed by the textile industry to assess yarn quality (Stout 1988).

TABLE 4.4. *Yarn linear density (g/1000 m) determined with different measuring lengths. The linear densities correspond to a dry condition. Data are mean ± stdv. Sample sizes (n) are given in brackets.*

Yarn type	Measuring length (m)		
	0.015* (n=70)	**0.132* (n=10)**	**10 (n=10)**
He47	44.4 ± 12.5	-	46.5 ± 1.1
He53	62.3 ± 21.4	53.5 ± 9.0	52.9 ± 2.5
He91	87.0 ± 16.1	-	90.8 ± 2.7
Fl64	-	-	63.8 ± 1.2

** These results were obtained as part of the tensile testing of yarns (see Subsection 3.3.6).*

4.1.4 Yarn structure

The ESEM images in Figure 4.2 show that the overall structure of the hemp yarns can be described as numerous individual fibres that are twisted with a right-handed angle to the yarn axis (a so-called Z-twist). The two filaments in He91 are twisted with a left-handed angle (a so-called S-twist). In textile yarns consisting of two filaments, the filaments are twisted in the opposite direction to the fibres to make the yarn more bulky, but with a lower breaking load (Munksgaard 1961). In addition to this simple depiction of the yarn structure a number of irregularities can be observed on the images: (i) the fibres are not homogenous entities, but are varying in widths, (ii) the inclination angle is varying slightly for groups of fibres, and (iii) the fibres are not smooth cables but contain some irregular surface structures.

The results from the concomitant measurements of fibre twisting angle and yarn diameter of He47 and He53 are presented in Figure 4.3. The figure demonstrates a considerable spread of data for both parameters. The mean ± stdv. for the twisting angle is 15.1 ± 0.4° and 15.9 ± 0.4° for He47 and He53, respectively. The mean ± stdv. for the yarn diameter is 242 ± 5 μm and 221 ± 5 μm for He47 and He53, respectively.

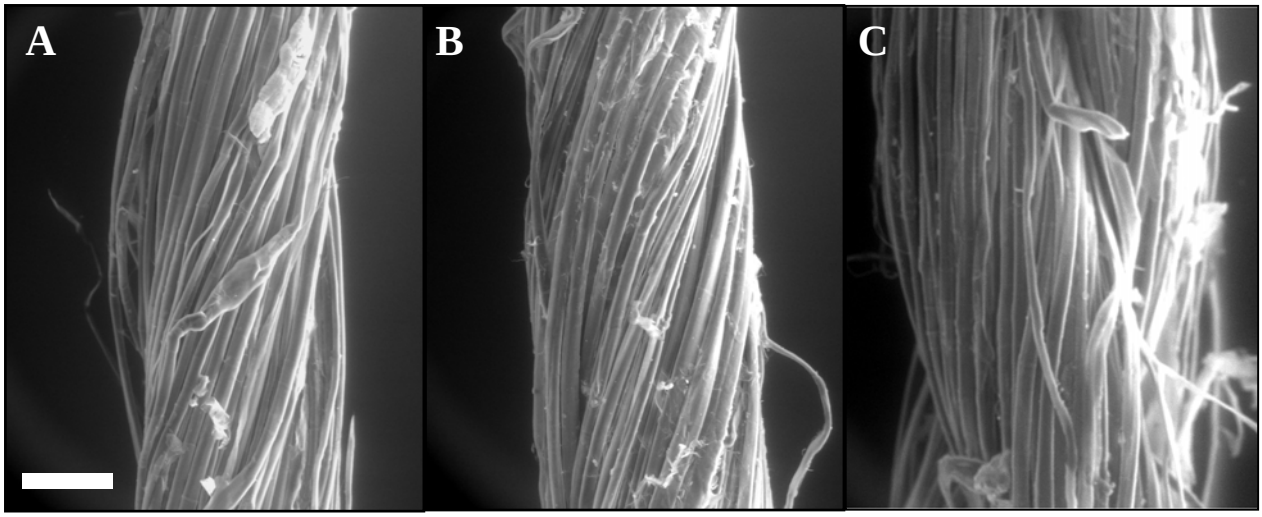

FIGURE 4.2. *ESEM images of the three types of hemp yarn: (**A**) He47, (**B**) He53 and (**C**) He91. Scale bar is 100 μm.*

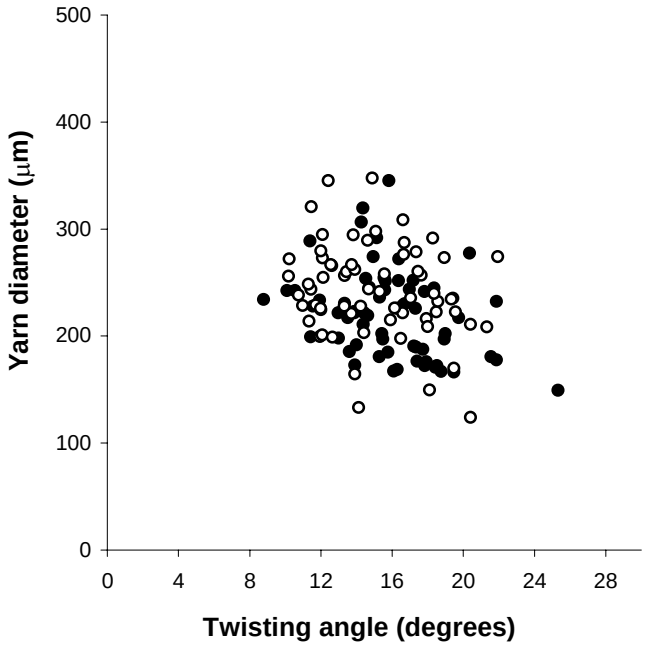

FIGURE 4.3. *The results from the concomitant measurements of twisting angle and yarn diameter of He47 (o) and He53 (•). Sample size is 65 for each yarn type.*

The twisted helical structure of plant fibre yarns is an important characteristic in the perspective of composite reinforcement, as opposed to the normally un-twisted rovings of synthetic fibres. Because of the twisted structure, the fibre orientation in aligned plant fibre yarn composites is not perfectly unidirectional, but can be denoted quasi-unidirectional with a fibre orientation given by the twisting angle. However, the actual twisting arrangement in plant fibre yarns depends on the

applied spinning method. For ring spun yarns the twisting angle is decreasing from the outside inwards (Figure 4.4) (Klein 1998). In Appendix D a model is presented to estimate the mean fibre angle of a ring spun yarn. The model predicts that the mean fibre angle is independent of the yarn diameter, but is solely a function of the fibre angle at the yarn surface. For surface fibre angles below 40°, the mean fibre angle is approximately related to the surface fibre angle by a factor 0.7. Thus, the mean fibre angle of He47 and He53 is about 11° and the fibre orientation in such quasi-unidirectional hemp yarn composites can therefore be stated to be ± 11°.

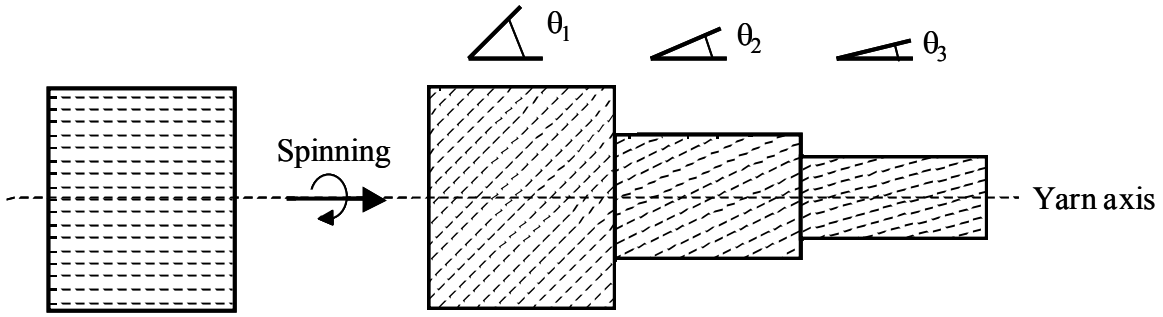

FIGURE 4.4. *The effect of spinning on the twisted helical structure of a ring spun yarn. Modified from Klein (1998).*

The internal yarn structure can be assessed from cross-sectional observations. Figure 4.5 shows a representative cross-section of He53 (see also Figure 1 in Paper I). It demonstrates that (i) the yarn cross-section is approximately circular, (ii) the spatial fibre distribution is practically uniform, (iii) the fibres have variable sizes and variable non-circular polygonal cross-sections, and (iv) only a small part of the fibres are grouped in bundles. From a composite reinforcement point of view, the latter finding is beneficial since a large fibre surface area is available for efficient impregnation and for efficient stress transfer between fibres and matrix. The twisting arrangement of the fibres cannot be interpreted from the yarn cross-section, although for a bundle of circular fibres this would result in elliptic fibre cross-sections. The non-circular fibre cross-sections and the low twisting angle presumably obstruct any sign of twist.

As can be seen in Figure 4.5 and Figure 1 in Paper I, the luminar dimensions of the hemp yarn fibres are very small, and for some of the fibres the lumen cannot even be identified. The same small luminar dimensions were observed for the flax yarn fibres (see Figure 1 in Paper II). An attempt to quantify the general magnitude of the luminar dimensions showed that the sizes were in the range 0-5 % of the fibre cross-sectional area. The luminar dimensions are assessed from composite cross-sections, and the possible effect of composite process conditions must therefore be considered (e.g. lumen collapse). However, cross-sectional observations of hemp yarn/epoxy composites, which were processed by low temperature and low pressure, showed the same small

luminar dimensions, and this point towards that the luminar dimensions are not changed by composite process conditions.

FIGURE 4.5. *OM image showing an example of a hemp yarn cross-section (He53). Matrix is PET. Scale bar is 100 μm.*

4.1.5 Fibre size distribution

Because of the measured variation in yarn linear density, it can be expected that the total fibre cross-sectional area varies considerably along the yarn axis. The total fibre cross-sectional area was measured to vary between 12,000 and 42,000 μm^2 in 18 hemp yarn cross-sections (He47 and He53). Figure 4.6A shows that nearly identical linear relationships are established for He53 and He47 when the total fibre cross-sectional area is plotted as a function of the number of fibres. This indicates that the mean fibre size does not change along the yarn axis, and that it is just about identical for the two yarn types. In Figure 4.6B, based on the underlying data of Figure 4.6A, the cumulative frequency distribution of fibre size is presented for He47 and He53. This shows the large span of fibre sizes and moreover, it verifies the small difference in fibre size distribution between the two yarn types as indicated in Figure 4.6A. Thus, the size of the fibres in He47 is generally smaller than the fibres in He53 with means of 128 and 140 μm^2, respectively (which correspond to the slopes of the regression lines in Figure 4.6A). From the determined yarn linear densities and fibre densities of He47 and He53, the mean total fibre cross-sectional area is calculated to be about 30,000 and 33,000 μm^2, respectively. Subsequently, the mean number of fibres in yarn cross-sections of He47 and He53 is calculated to be 234 and 236 fibres, respectively.

Overall, the results show that the fibre size distribution does not change along the yarn axis, and that it is nearly identical for He47 and He53, which are two batches of the same hemp yarn type, but

bought with a time interval of two years. This indicate that the processes of fibre manipulations during yarn production are impressing well controlled within a single yarn batch, and moreover, the processes can be accurately repeated in the production of two yarn batches separated in time.

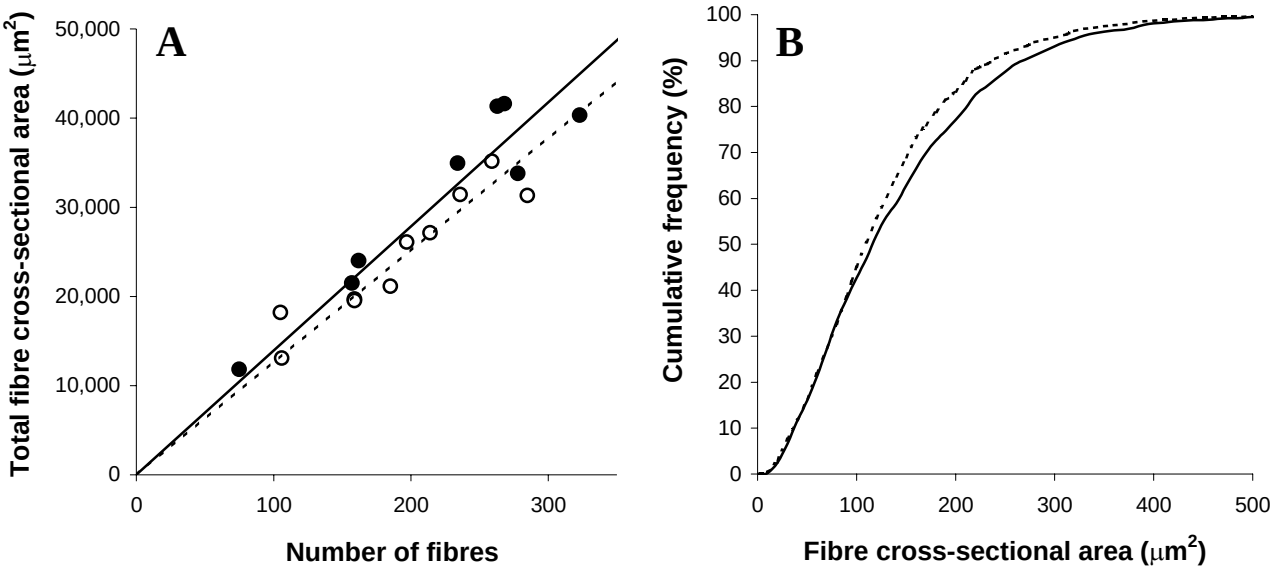

FIGURE 4.6. *(**A**) shows the relationship between the total fibre cross-sectional area and the number of fibres in yarn cross-sections of He47 (o) and He53 (•). Lines are regression lines for He47 (dotted; y=126x, R^2=0.85) and He53 (full; y=139x, R^2=0.89). (**B**) is based on data in (**A**) and shows the cumulative frequency distribution of fibre cross-sectional area of He47 (dotted line; n=1746) and He53 (full line; n=1919).*

4.1.6 Fibre water sorption

The water sorption capacity of hemp yarn fibres can be seen from the adsorption isotherm in Figure 4.7. Included in the figure are previously reported adsorption isotherms for wood fibres and raw hemp fibres (Strømdahl 2000). The sorption isotherms are characterised by sigmoidal curves where the equilibrium water content changes most radically in the region of low humidities (0-15 % RH) and in the region of high humidities (65-100 % RH). However, the sorption isotherm of the hemp yarn fibres is shifted downwards with respect to the sorption isotherms of wood and raw hemp fibres, and moreover, the difference is increased with the humidity. The water content at 95 % RH for wood and raw hemp fibres is about 35 %, whereas it only is about 15 % for hemp yarn fibres. This point towards that some of the processes applied during yarn production dramatically reduces the water sorption capacity of the hemp yarn fibres. One possibility is alkalisation, which presumable has been used to improve the separation of fibre bundles into single fibres, but as a side effect the content of hemicellulose is decreased (see Subsection 4.1.1). Thus, since hemicellulose is the cell wall constituent with the largest sorption capacity, alkalisation might (partly) explain the

reduced water sorption capacity of the hemp yarn fibres. The lower sorption capacity is beneficial from a composite point of view: i.e. improved dimensional stability.

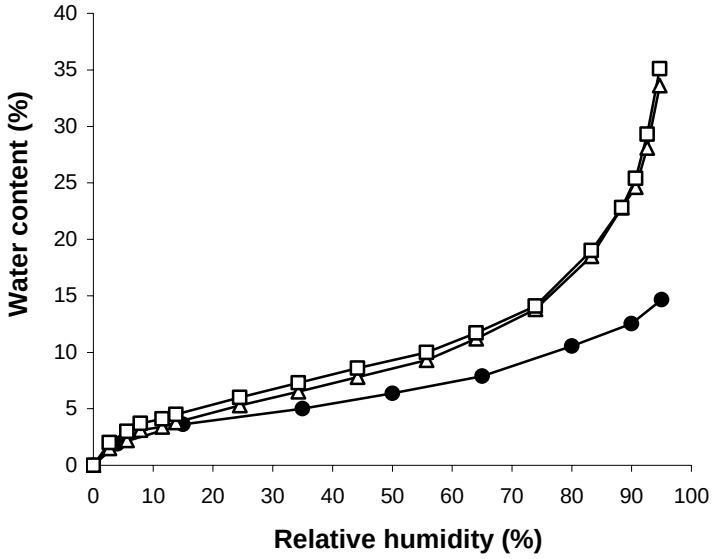

FIGURE 4.7. *Adsorption isotherms for hemp yarn fibres (He53;●), wood fibres (spruce; Δ) and raw hemp fibres (□). Data for wood fibres and raw hemp fibres are from Strømdahl (2000).*

Shown in Figure 4.8 is the adsorption isotherm and part of the desorption isotherm for two samples of hemp yarn fibres (unprocessed He53 and He53 processed at 200 °C). The dissimilarity between isotherms of adsorption and desorption demonstrates that water sorption in hemp yarn fibres exhibits hysteresis, which is a well-known phenomenon in wood fibres (Skaar 1988). The mean ratio between adsorption and desorption at 35, 65 and 80 % RH is 0.90 for the unprocessed fibres, and 0.84 for the processed fibres. The figure shows also that the sorption isotherms for the processed fibres are shifted downwards (see below).

Table 4.5 presents the measured water contents of He47, He53 and He91 at 35, 65 and 85 % RH. The water contents at 85 % RH are 12.2, 11.0 and 11.4 % for the three hemp yarn types, respectively. Generally, the water sorption capacity of He47 is slightly larger than He53 and He91, which in turn are nearly identical. The hemicellulose content of He47 is measured to be about 2 w% larger than He53 and He91 (see Table 4.1, p. 54) and this validates the larger water contents of He47. Table 4.5 shows also that the water sorption capacity of the hemp yarn fibres is reduced as an effect of composite process conditions, and that it is consistently reduced when the process temperature is increased. The water content of He47 at 85 % RH is reduced to 11.6 % at 180 °C, and is furthermore reduced to 10.8 % at 220 °C. The reduced water sorption capacity of the processed hemp yarn fibres can be related to their lower content of hemicellulose (see Table 4.1, p. 54), which is caused by thermal degradation.

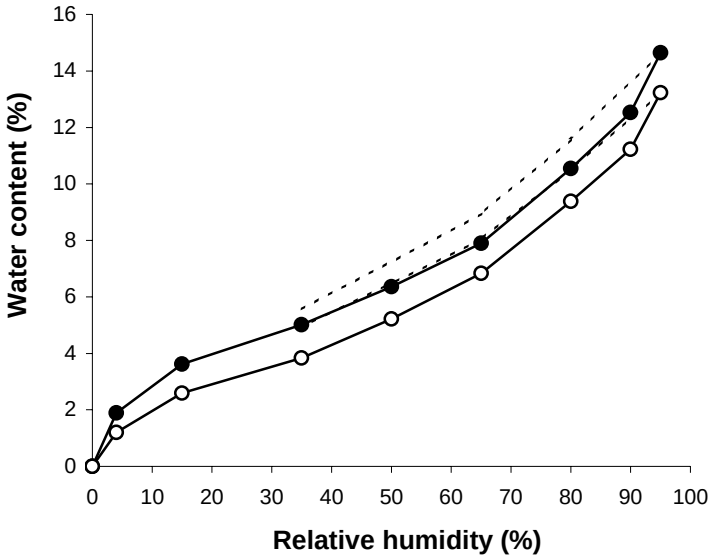

FIGURE 4.8. *Sorption isotherms for unprocessed hemp yarn fibres (He53; •) and hemp yarn fibres processed at 200 °C (He53;* o*). Full lines are adsorption isotherms and dotted lines are part of the desorption isotherms.*

TABLE 4.5. *Equilibrium water content (%) of the three hemp yarn types at three relative humidities. Shown is also the water content of processed hemp yarn samples.*

Yarn type	Process conditions	Relative humidity (%) 35	65	85
He47	None	5.5	8.0	12.2
	180 °C	4.8	7.7	11.6
	200 °C	4.4	7.4	11.4
	220 °C	4.0	6.9	10.8
He53	None	4.7	7.1	11.0
	200 °C	4.2	6.1	9.8
He91	None	5.0	7.4	11.4
	200 °C	4.0	6.7	10.4
	220 °C	4.2	6.7	10.5

4.1.7 Yarn tensile properties

Tensile testing of yarns is widely employed by the textile industry as a way of controlling yarn quality. The testing is an integrated part in the process of yarn production, and is performed routinely on automatic tensile testing instruments. From a textile point of view, the two most important yarn tensile properties are breaking load (N/tex) and breaking elongation (%) (Furter 1985). These properties are measured with relative large gauge lengths (standard is 250 or 500 mm; ASTM D2256, ISO 2062), and they reflect therefore long-range yarn behaviour where fibre-fibre friction is an essential factor. However, with the objective of composite reinforcement, measurements of short-range yarn behaviour are more important in order to approximate fibre properties rather than fibre-fibre frictional forces. This requires a small gauge length to ascertain that the main part of fibres is extending continuously along the tested yarn sample. The length of raw hemp fibres has been reported to be in the range 5-55 mm with a mean of 25 mm (Bledzki et al. 2002). A gauge length of 3 mm was selected in this study to measure the tensile properties of hemp yarn.

As noted in Subsection 3.3.1, the yarn samples were subjected to different process temperatures and conditioned at different humidities before testing. These results will be presented in the relevant subsections on composite tensile properties. However, in this subsection, Figure 4.9 shows the determined stress-strain curves of He47, He53 and He91, which were unprocessed and conditioned at 65 % RH. Despite the large spread, the curves seem to be divided into three groups represented by the three yarn types. This is verified from the determined tensile properties presented in Table 4.6. Generally, He47 has larger apparent stiffness, larger ultimate stress, and lower strain at ultimate stress than He53 and He91, which in turn have more similar tensile properties. The difference in tensile properties between the yarn types might be explained by the measured slightly lower twisting angle of He47 as compared to He53, which point towards improved tensile properties of He47. However, other explanations must also be considered: e.g. differences in microfibril angle, cellulose crystallinity and fibre length distribution. It is worth noting that the absolute breaking load of He47 and He53 are nearly identical with means 19.5 and 19.4 N, respectively. As mentioned above, He47 and He53 are two batches of the same yarn type, but bought with a time interval of two years. Thus, it is tempting to propose that the difference in fibre tensile properties between the two yarn batches has been noticed by the supplier, and consequently the yarn linear densities have been adjusted to obtain an identical absolute breaking load.

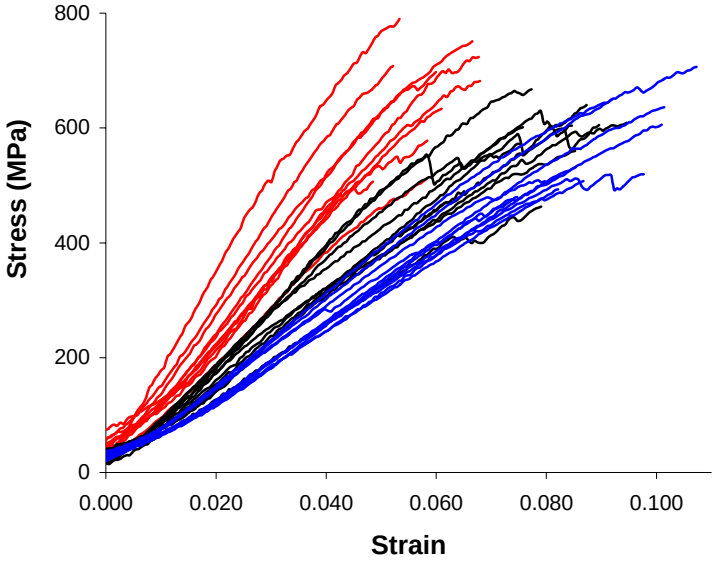

FIGURE 4.9. *Stress-strain curves of He47 (red lines), He53 (black lines) and He91 (blue lines). The yarn samples were unprocessed and conditioned at 65 % RH before testing. Sample size is 10 for each yarn type.*

TABLE 4.6. *Yarn tensile properties. Data are means ± stdv. (n=10). Yarn samples were unprocessed and conditioned at 65 % RH before testing.*

Yarn type	Stiffness* (GPa)	Ultimate stress (MPa)	Strain at ultimate stress*
He47	13.2 ± 2.1	658 ± 98	0.059 ± 0.007
He53	9.3 ± 1.3	581 ± 63	0.081 ± 0.009
He91	7.2 ± 0.5	575 ± 77	0.093 ± 0.009

* *The results need to be adjusted by a factor of about 1.02 (see Subsection 3.3.1).*

According to Table 4.6, the apparent stiffness of the hemp yarns is in the range 7-13 GPa, and this is much below the reported stiffness of single hemp fibres, which is in the range 30-60 GPa (Lilholt and Lawther 2000). The ultimate stress of the hemp yarns is in the range 580-660 MPa, and this is however within the range of 350-800 MPa for ultimate stress reported for single hemp fibres (Lilholt and Lawther 2000).

Several models have been developed to predict the mechanical behaviour of plant fibre yarns (Zeidman and Sawhney 2002, and references cited herein), but these models have mostly been concerned with long-range yarn behaviour. As noted in Subsection 3.3.1, the initial part of the measured load-displacement curves is characterised by a slowly increasing slope towards a linear region (see Figure 3.3, p. 44). The same phenomenon has been observed for wool yarn (Carnaby and Grosberg 1976) and aramid yarns (Creasy 2000), but most often this is not shown because the

yarn is pre-tensioned before testing (Furter 1985). The initial region of non-linearity can be explained by the loose and twisted arrangement of fibres in the yarn. This means that only a minor fibre fraction at the yarn centre is strained at the onset of a tensile test, whereas the remaining fibres are free to move inwards before tensile strain is developed (Carnaby and Grosberg 1976). Thus, a given yarn displacement is required before all fibres are strained and the linear region of the load-displacement curve is approached, at which the apparent yarn stiffness is determined. Accordingly, the fibres are strained differently during a tensile test. For a bundle of fibres that are strained uniformly it can be shown theoretically by Weibull analysis that the ultimate stress of the bundle is below the mean fibre ultimate stress (Lilholt 2002), and this has been experimentally verified for flax fibres (Bos et al. 2002, Romhány et al. 2003). Moreover, in a study by Creasy (2000) it has been shown that for a bundle of fibres that are strained non-uniformly, not only the ultimate stress, but also the stiffness of the bundle is markedly reduced in comparison to the mean fibre stiffness. These considerations are based on bundles of untwisted fibres. The twisted fibre arrangement in a plant fibre yarn means that the fibres are inclined with an angle to the yarn axis, and this will furthermore reduce yarn tensile properties in relation to fibre tensile properties. At present no attempt has been made to predict fibre properties from yarn properties, and the results on yarn tensile properties can therefore only be used on a comparative basis.

4.2 COMPACTION OF PLANT FIBRE ASSEMBLIES

When composites are fabricated by compression moulding, the compactibility of the fibre assembly sets the limits of the reinforcement efficiency. In the literature several studies have addressed the derivation of suitable models for compaction (e.g. Gutowski et al. 1987, Simácek and Karbhari 1996, Toll 1998, Lomov and Verpoest 2000, Beil and Roberts 2002). Many of these are modifications of a power-law relationship first proposed by van Wyk (1946) based on three-dimensional randomly oriented fibre assemblies:

$$P = K\ E_f \left(V_f^3 - V_{f+}^3 \right) \tag{4.1}$$

where P is compaction pressure, V_f is fibre volume fraction of the compacted assembly, V_{f+} is fibre volume fraction of the uncompacted assembly, E_f is fibre stiffness and K is an empirical parameter that accounts for fibre geometry, fibre orientation and other fibre characteristics. In general, although the various models offer an acceptable fit to the experimental data, at least one adjustable parameter must be approximated. With plant fibre assemblies, the large variation in the parameters normally assigned to the compaction mechanisms (e.g. fibre orientation, fibre aspect ratio and fibre stiffness) and the difficulties of their determinations, makes compactibility less straightforward to

predict as compared to assemblies of synthetic fibres. Moreover, the critical assumption of the fibres being uniformly packed employed in many theoretical models is certainly more questionable in plant fibre assemblies. Thus, the compactibility of any given type of plant fibre assembly is expectedly unique, and needs to be documented in order to determine the maximum V_f at a given consolidation pressure applied for composite fabrication (see Section 4.3).

The following work on the compactibility of plant fibre assemblies is a summary of the work presented in Paper III, however some additional experimental results are included in this presentation.

Figure 4.10 shows the compaction behaviour of a range of fibre assemblies, differing in fibre type (glass, hemp, flax and jute) and fibre orientation (unidirectional; UD, and random; RD). In the case of UD assemblies, glass fibres are compacted considerably more than flax fibres (Fl64), which in turn are compacted slightly more than hemp fibres (He53). This is numerically exemplified at 2.2 MPa, where V_f is 0.71, 0.56 and 0.54[2] for glass, flax and hemp, respectively. Compared with the UD assemblies, the curves for the RD assemblies are shifted downwards. At a given compaction pressure, the compactibility is decreased for the RD assemblies in the order: glass, flax, hemp, jute. This is numerically exemplified at 2.2 MPa, where V_f is 0.52, 0.38, 0.35 and 0.28 for the four fibre types, respectively.

As expected from common sense of packing, the results in Figure 4.10 show that compactibility is positively correlated with the fibre alignment. However, the effect of fibre type, the glass fibres being easier to compact than the plant fibres, requires some more explanation. The UD glass fibre assembly is essentially unidirectional since it is made of rovings with continuous and parallel fibres. In contrast, the UD plant fibre assemblies are made of yarns with discontinuous and twisted fibres, which reduce the degree of fibre alignment and the compactibility is therefore lowered. The same explanation could be given for the RD assemblies. This implies that the fibre orientation in the RD jute assembly, which shows the lowest compactibility, is close to random, whereas it is less random in the RD glass assembly. However, results in Paper III show identical compaction behaviour of RD hemp yarn assemblies made manually, and therefore probably with highly variable fibre orientations. This point towards that differences in fibre orientation cannot explain the different compaction behaviour of the RD assemblies. The influence of fibre length distribution on the compaction behaviour can probably also be ignored. The high fibre aspect ratio, even for relative short fibres, means that a large number of contact points occur per fibre, which makes the exact fibre length less important (Toll 1998). Another possible parameter is the degree of fibre separation in the assemblies. Based on micro mechanical considerations it has been demonstrated by Toll (1998) that compactibility is increased with the degree of fibre separation; i.e. the compactibility is

2. The determined V_f of 0.54 for He53 is based on a fibre density of 1.56 g/cm^3. However, as can be seen in Table 4.3, the density should be 1.60 g/cm^3, and this will change V_f to 0.52.

largest for assemblies where the fibres are well separated from each other. In fact, cross-sectional observations of the RD fibre assemblies in this study indicated a difference in the degree of fibre separation: the highly separated glass fibres at one extreme and the jute fibres clustered together in larger bundles at the other (see Figure 4 in Paper III). The apparent positive effect of fibre separation on the maximum obtainable V_f in composites underlines the importance of the process applied to separate plant fibre bundles into individual fibres.

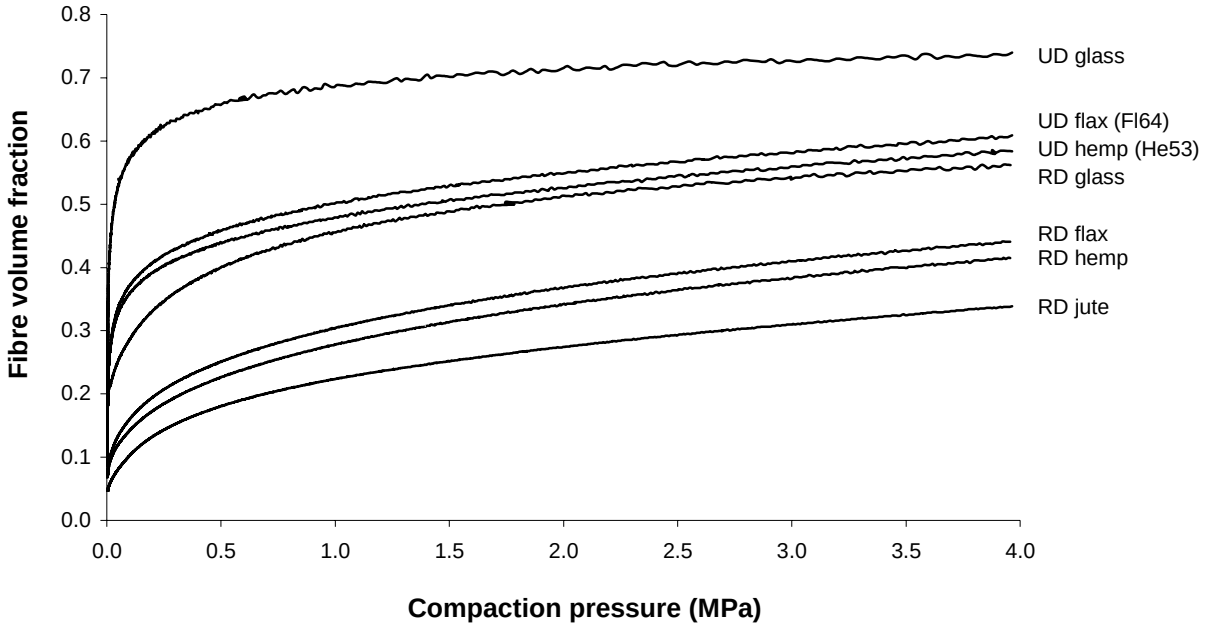

FIGURE 4.10. *Results from single compaction test of different types of fibre assemblies. UD is unidirectional assemblies made from fibre yarns or rovings, and RD is randomly oriented assemblies made from non-woven mats.*

Quantitative measures of the shape of the curves in Figure 4.10 were obtained by fitting a power-law function to the curves:

$$V_f = a\, P^b \tag{4.2}$$

where *a* and *b* are two adjustable fitting parameters. The equation is analogous to equation (4.1), but with the compaction pressure as the independent variable. Presented in Figure 4.11 are the determined fitting parameters for the curves in Figure 4.10. This demonstrates that (i) *a* is reflecting the vertical positions of the curves, and (ii) *b* is inversely related to how fast the curves approach their asymptotic V_f (i.e. the asymptotic V_f is rapidly approached when *b* is small). Thus, the two fitting parameters are valuable measures to assess the compactibility of a fibre assembly. Optimally, a high value of *a* and a low value of *b* should be aimed for in order to obtain a large V_f at a given compaction pressure.

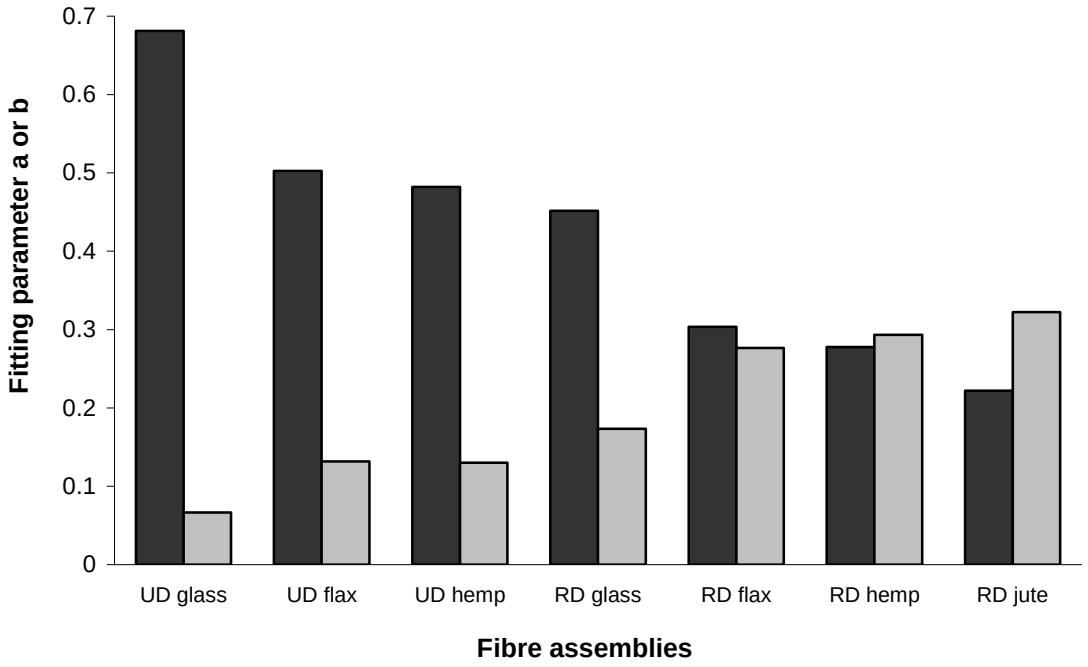

FIGURE 4.11. *The determined fitting parameters of the compaction curves shown in Figure 4.10: a (black columns) and b (grey columns).*

A number of factors can be suspected to improve the compactibility of a fibre assembly, such as compaction speed, multiple compaction and fibre lubrication. Based on tests of UD hemp fibre assemblies, Table 4.7 shows how the determined fitting parameters are affected by these three factors. It can be recognized that the compactibility is more or less unaffected by compaction speed and fibre lubrication. However, if the fibre assembly is compacted in successive cycles, the fitting parameters are changed considerable; *a* is increased and *b* is decreased with the cycle number (see also compaction curves in Figure 5 in Paper III). The effect is most pronounced at the second compaction cycle where after the effect is diminishing. Similar results are shown in a study by Gutowski et al. (1987) on UD carbon fibre assemblies. Thus, it is indicated that if a fibre assembly is pre-compacted prior to composite fabrication, the maximum obtainable V_f can be increased.

TABLE 4.7. *The determined fitting parameters a and b as an effect of different compaction factors. The results are based on tests of UD hemp fibre assemblies (He53).*

Compaction factor	a	b
Compaction speed		
0.5 mm/min	0.484	0.141
2 mm/min	0.482	0.130
10 mm/min	0.484	0.139
Multiple compaction		
1st cycle	0.482	0.130
2nd cycle	0.520	0.082
3rd cycle	0.532	0.072
4th cycle	0.539	0.067
Lubrication*		
None	0.482	0.130
Oil	0.489	0.130
Water	0.484	0.150

** The assemblies were impregnated with an excess of oil or water before testing.*

4.3 COMPOSITE VOLUMETRIC INTERACTION

Most studies on plant fibre composites have primarily focused on the fibre and matrix part of the composites, and ignored the existence of the third part, the porosity. Porosity, which is identified as air-filled cavities inside an otherwise continuous material, is an unavoidable part in all composite materials caused by the mixing and consolidation of two discrete material parts. With synthetic fibre composites considerable knowledge has been built up over the years in order to control and optimise the fabrication process, and consequently the porosity content is normally relative low (<2 %) (Lystrup 1998). However, in the case of plant fibre composites, the less-developed fabrication techniques and the porous structure of the fibres cause the porosity part to make a noteworthy contribution to the overall composite volume (Lilholt et al. 1999).

The following improved model of composite volumetric interaction is based on similar models presented in Andersen and Lilholt (1999) and Paper II.

Composite V_f can be calculated from the ideal fibre volume fraction with no porosity (V_{f*}) and the actual porosity content (V_p) (see derivation of equations in Paper II):

$$V_f = V_{f*}\left(1 - V_p\right) \quad ; \quad V_{f*} = \frac{\dfrac{W_f}{\rho_f}}{\dfrac{W_f}{\rho_f} + \dfrac{W_m}{\rho_m}} \qquad (4.3)\ ;\ (4.4)$$

Figure 4.12 shows V_{f*} and V_{m*} (=1- V_{f*}) as a function of W_f, in addition to the measured volume fractions of He53/PET composites processed at 200 and 220 °C. Since the composites contain some porosity it is anticipated that the ideal curves does not fit the experimental data, but overestimate both the experimental fibre and matrix volume fractions. This is in particular true for large values of W_f. To improve the predictions of composite volume fractions, the porosity content needs to be taken into account.

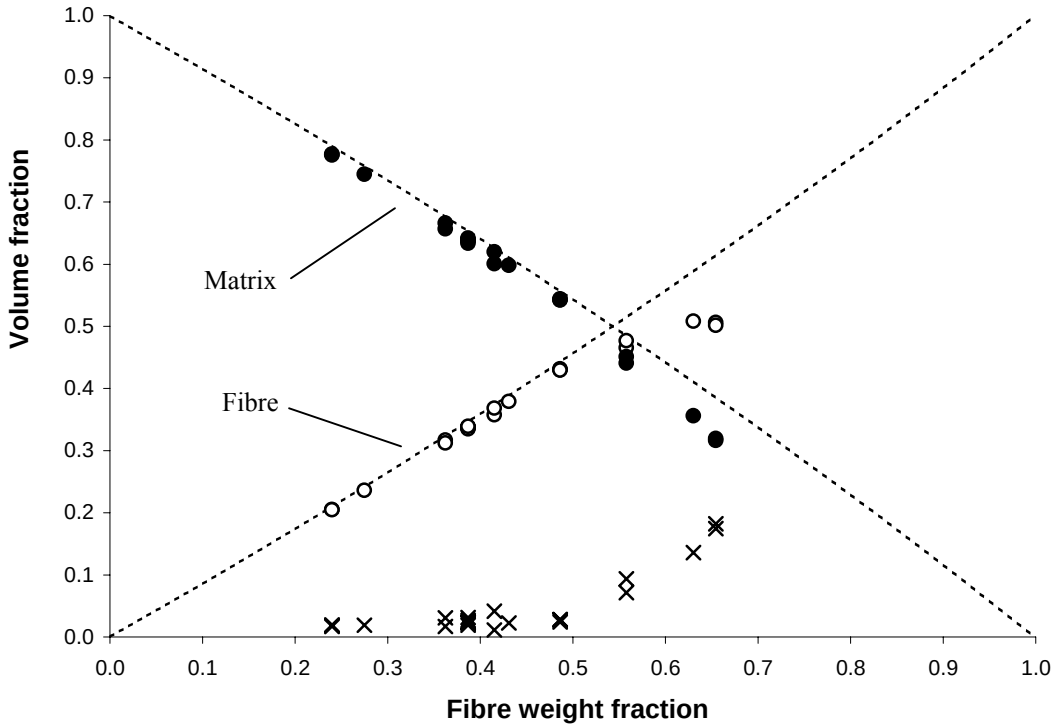

FIGURE 4.12. *Volumetric interaction in He53/PET composites. The dotted lines are the ideal volume fractions with no porosity, and the symbols are measured volume fractions of fibres (o), matrix (•) and porosity (x). A fibre density of 1.60 g/cm^3 and a matrix density of 1.34 g/cm^3 were used to calculate the ideal volume fractions.*

The porosity content is assumed to be the summation of three independent porosity components. In the first component, denoted $V_{p\ (1)}$, the porosities are located at the fibre/matrix interface as an

effect of incomplete wetting of the fibres. The porosities in the second component, denoted $V_{p\,(2)}$, are caused by the central air-filled lumen in plant fibres. In the third component, denoted $V_{p\,(3)}$, the porosities are assigned to the incomplete compaction of the fibres beyond the maximum obtainable V_f (see Section 4.2).

The magnitude of $V_{p\,(1)}$ can be estimated by presuming that the fibres are circular, and that the gaps at the fibre/matrix interface are deposited as rings that surround the fibres [3]:

$$V_{p(1)} = V_{f^*} \frac{\pi (r+w)^2 - \pi r^2}{\pi r^2} = V_{f^*} \frac{(r+w)^2 - r^2}{r^2} \tag{4.5}$$

where r is fibre radius and w is width of the air-filled ring around the fibres.

$V_{p\,(2)}$ can be estimated from the lumen volume fraction (V_L); i.e. the ratio between the area of the central lumen and the fibre cross-sectional area [3]:

$$V_{p(2)} = V_{f^*} V_L \tag{4.6}$$

The third porosity component, $V_{p\,(3)}$, is controlled by the maximum obtainable V_f at the compaction pressure applied for composite fabrication ($V_{f\,(max)}$). Since V_f never exceeds this limit, equation (4.3) can be rearranged to estimate $V_{p\,(3)}$:

$$V_{f\,(max)} = V_{f^*} (1 - V_{p\,(3)}) \qquad \Rightarrow \qquad V_{p\,(3)} = \frac{V_{f^*} - V_{f\,(max)}}{V_{f^*}} \tag{4.7}$$

According to the three above equations knowledge is required of four parameters: r, w, V_L and $V_{f\,(max)}$, in order to predict the porosity content of the He53/PET composites shown in Figure 4.12. The mean fibre cross-sectional area in He53 is measured to be 140 μm^2, which gives a radius (r) of 6.7 μm, assuming that the fibres are circular. The width of the gaps at the fibre/matrix interface (w) can be interpreted from Figure 4.13, which is a high-magnification SEM image of hemp yarn fibres embedded in a PP matrix. It verifies that due to the poor fibre/matrix compatibility there are some irregular deposited gaps at the fibre/matrix interface. Based on digital magnification of the interfacial gaps, the mean width is estimated to be 0.15 μm. It should be noted that the gaps might be smaller when the fibres are embedded in a PET matrix (see Subsection 4.5.4). The luminar dimensions of the hemp yarn fibres are small, and the lumen volume fraction (V_L) is determined to be in the range 0.00-0.05. Accordingly, the mean lumen volume fraction is assumed to be 0.025. The consolidation pressure applied for composite fabrication is 2.2 MPa, and in Section 4.2 it is shown that this corresponds to a maximum obtainable fibre volume fraction ($V_{f\,(max)}$) of about 0.52

3. More correctly, the equations for $V_{p\,(1)}$ and $V_{p\,(2)}$ should include the factor $(1-V_p)$. However, in the case of a small magnitude of V_p this can be neglected. The model of volumetric interaction in composites has been furthermore developed, and a paper is in preparation to be submitted in Composites Science and Technology.

for He53. Figure 4.14 shows the three predicted porosity components as a function of W_f, in addition to the experimental porosity data.

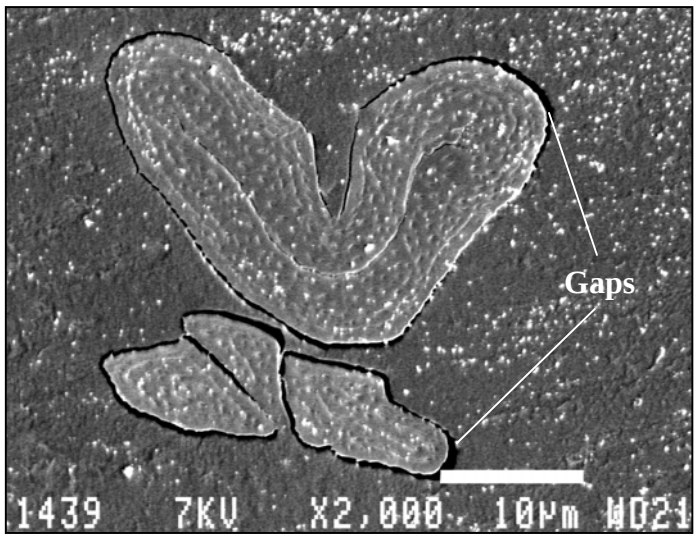

FIGURE 4.13. *SEM image of four hemp yarn fibres embedded in a PP matrix. Scale bar is 10 µm. The white dots are not part of the composite material, but are probably impurities induced during the polishing process.*

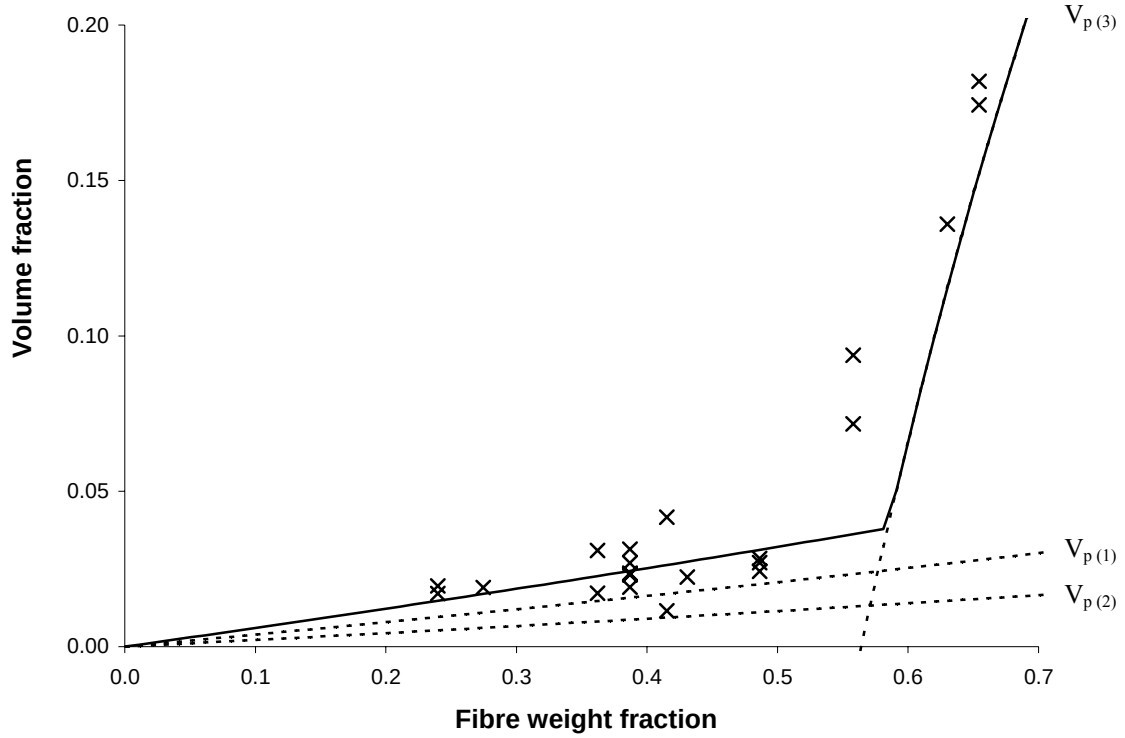

FIGURE 4.14. *Enlargement of Figure 4.12 showing the experimental data of porosity. The dotted lines are the predicted three porosity components. The full line is the predicted total porosity. Note that the predicted lines are not straight lines.*

As can be recognized from the above considerations, V_p is given by the summation of $V_{p\,(1)}$ and $V_{p\,(2)}$ when V_f is below $V_{f\,(max)}$. However, V_p is given by $V_{p\,(3)}$ when V_f is equal to $V_{f\,(max)}$. Subsequently, the complete model is described by the equations:

for $V_f < V_{f\,(max)}$

$$V_p = \frac{V_{f*}\left((r+w)^2 - r^2\right)}{r^2} + V_{f*}\,V_L \qquad ; \qquad V_f = V_{f*}\left(1 - V_p\right) \qquad (4.8)\ ;\ (4.3)$$

else

$$V_p = \frac{V_{f*} - V_{f\,(max)}}{V_{f*}} \qquad ; \qquad V_f = V_{f\,(max)} \qquad (4.9)\ ;\ (4.10)$$

Shown in Figure 4.15 are the predicted volume fractions of the He53/PET composites. The figure shows a fairly good agreement between the predicted and the experimental volume fractions. Thus, the model is a suitable tool for the prediction of composite volumetric interaction. However, more documentation is required to verify its usefulness in other types of plant fibre composites differing in fibre/matrix compatibility, fibre luminar dimensions and compactibility of the fibre assembly.

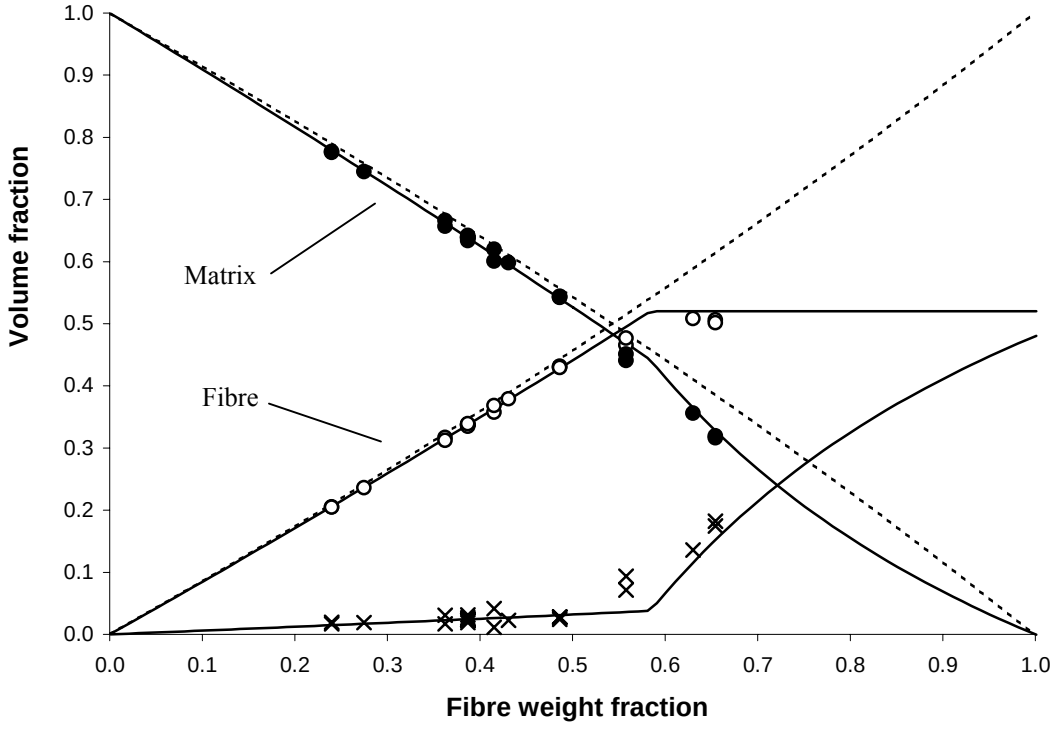

FIGURE 4.15. *Volumetric interaction in He53/PET composites. The full lines are the predicted volume fractions of fibre, matrix and porosity. See Figures 4.12 and 4.14 for more details.*

4.4 COMPOSITE WATER SORPTION

Thorough knowledge of water sorption in composites is the basis for an assessment of the water related dimensional stability of composites. Moreover, it is important with respect to the many properties of composites that are affected by water sorption: e.g. mechanical properties (see Subsection 4.5.7), electrical properties and thermal properties. As opposed to plant fibre composites, the mechanisms of water sorption in synthetic fibre composites (e.g. glass/epoxy) are well documented (see review in Weitsman 2000). The water sorption capacity of these composites is typically low and is mainly confined to the matrix. However, in plant fibre composites, the water sorption capacity is large and is mainly confined to the fibres. Thus, the existing knowledge of composite water sorption does not necessarily apply to plant fibre composites.

A practical perspective is adopted in the investigations of composite water sorption. The use of materials is normally limited to a given range of ambient conditions, and the change in material properties within this range is expressed in relation to a common reference condition. The selected reference humidity condition in this study is 65 % RH, which also is the reference humidity used for wood (Kollmann and Côté 1984). The span of ambient humidities varies geographically, but a range of 35-85 % RH is assumed to be typical for most European climates. The two extreme conditions in this range (35 and 85 % RH) are used to assess the typical span of water sorption in plant fibre composites, with respect to the reference condition (65 % RH).

Table 4.8 shows specifications of the composite laminates used in the investigations of water sorption. Only a single type of hemp yarn is applied (He53). The two central parameters are W_f (or V_f) and matrix type. W_f varies in the range 0.24-0.49 for the PET matrix composites. Matrix type varies between PET, PE and PP for composites with a W_f of about 0.45 (but with different V_f). The investigations include also pure matrix laminates (W_f=0). It should be noted that the investigations are still on going, and some results are therefore yet to come.

TABLE 4.8. *Physical properties of the composite and pure matrix laminates used in the investigations of water sorption. The laminates were fabricated by commingled filament-winding and a process temperature of 200 °C.*

Yarn type	Matrix type	W_f	V_f	V_p	Sample type*
He53	PET	0	0		A
		0.240	0.205	0.020	A
		0.387	0.339	0.019	A B C
		0.431	0.379	0.022	A
		0.486	0.430	0.028	A
	PE	0	0		A
		0.448	0.317	0.038	A
	PP	0	0		A
		0.469	0.328	0.018	A

* *See Subsection 3.3.5 (Figure 3.5, p. 47).*

4.4.1 Water adsorption behaviour

If sorption of water into a solid material is strictly driven by the gradient of water concentration (i.e. relative humidity) between the surroundings and inside the material, the degree of water saturation as a function of time can be described by the Fickian diffusion model:

$$\frac{U_{RH}(t)}{U_{RH}} = 1 - \frac{8}{\pi^2} \sum_{i=0}^{\infty} \frac{1}{(2i+1)^2} \exp\left(- \frac{(2i+1)^2 \pi^2 D t}{(2d)^2} \right) \tag{4.11}$$

where $U_{RH}(t)$ is the unsaturated water content as a function of time, and U_{RH} is the saturated water content in equilibrium with the surrounding humidity. D is the diffusion coefficient (m^2/s) and d is the diffusion distance (m). The diffusion coefficient in the model applies only to a given humidity gradient, and it is a mean value in space and time. The model assumes that water diffusion occurs only in a single direction. Thus, it is typically applied to predict the water sorption behaviour of plane materials sheets with a low ratio between the thickness dimension and the planar dimensions (length and width). Water sorption is then governed by diffusion in the thickness direction and 2d is equal to the sheet thickness.

In the case of spherical materials (such as fibres), water is sorped from the entire circumference in a radial direction. Thus, equation (4.11) does not apply to plant fibres. Instead, a modified model has previously been proposed to account for the different diffusion path in spherical materials, and this model can be used to predict the water sorption behaviour of plant fibres (Marcovich et al. 1999):

$$\frac{U_{RH}(t)}{U_{RH}} = 1 - \frac{6}{\pi^2} \sum_{i=1}^{\infty} \frac{1}{i^2} \exp\left(-\frac{i^2 \pi^2 D t}{r^2}\right) \tag{4.12}$$

where r is fibre radius (m).

The diffusion coefficient is typically the only unknown parameter in the two above equations, and it can therefore be adjusted to fit the model to the experimental data. In equation (4.11), the diffusion coefficient can however be directly estimated by plotting $U_{RH}(t)$ as a function of $t^{0.5}$, and by choosing two values of $U_{RH}(t)$ corresponding to two values of $t^{0.5}$ in the initial linear region (Tsai and Hahn 1980):

$$D = \frac{\pi}{16} \left(\frac{U(t_2) - U(t_1)}{\sqrt{t_2} - \sqrt{t_1}}\right)^2 \frac{(2d)^2}{U_{RH}^{\ 2}} \tag{4.13}$$

The halftime to saturation (t½) can then be calculated (Tsai and Hahn 1980):

$$t_{½} = \frac{(2d)^2}{\pi^2 D} \ln \frac{16}{\pi^2} \tag{4.14}$$

As mentioned in Subsection 3.3.5 the water adsorption behaviour was investigated by conditioning the laminate samples at 65 % RH and then they were allowed to reach equilibrium at 85 % RH. The *relative water content* was calculated with respect to the sample mass at 65 % RH:

$$U^*_{85}(t) = 100 \frac{m_{85}(t) - m_{65}}{m_{65}} \quad \text{at non-equilibrium} \tag{4.15}$$

$$U^*_{85} = 100 \frac{m_{85} - m_{65}}{m_{65}} \quad \text{at equilibrium} \tag{4.16}$$

where the asterisk specifies that the water content is not calculated with respect to a dry condition.

Figure 4.16 shows the water adsorption behaviour of a fibre sample (He53), a matrix sample (PET) and a composite sample (He53/PET). The hemp fibres rapidly reach a large U^*_{85} of about 3.5 %, whereas PET slowly reach a low U^*_{85} of about 0.3 %. U^*_{85} for the composite is about 1.3 %. Equations (4.11) and (4.12) were used to model the water adsorption behaviour, and diffusion coefficients of about 0.0004, 0.41 and 0.22 10^{-12} m^2/s were estimated for He53, PET and composite, respectively. The halftime to saturation was estimated to be about 1, 143 and 295 hours for the three samples, respectively.

It is evident from Figure 4.16 that the experimental data deviate to some extends from the Fickian diffusion model (see considerations below), and the calculated constants might therefore not reflect the true process of water adsorption. Nevertheless, the results show that even though D_f is below D_m and D_c by a factor 10^{-3} water is rapidly adsorped by the hemp fibres. This can be justified by the much smaller diffusion distance for the fibres with a mean radius of about 7 10^{-6} m, whereas the diffusion distance for the laminates in the thickness direction is about 1 10^{-3} m. It has been proposed that water diffusion in polar systems, such as the cell wall of plant fibres, is delayed by the hydrogen bonding of the water molecules (Marcovich et al. 1999), and this might explain the low D_f. In a study by Marcovich et al. (1999), the diffusion coefficients of wood fibres, polyester and wood fibre/polyester composites were found to be about 0.0027, 1.51 and 0.55 10^{-12} m^2/s, respectively. The applied humidity gradient was 60 % RH (0 to 60 % RH). Obviously, the reported diffusion coefficients cannot be directly compared with the results in this study, but they nevertheless show the same relation between plant fibres, matrix and composites, i.e. $D_f << D_c < D_m$. It has previously been attempted to predict D_c from D_f and D_m by the use of simple mixture models, but generally D_c was not very well predicted by the models (Marcovich et al. 1999, Alvarez et al. 2004).

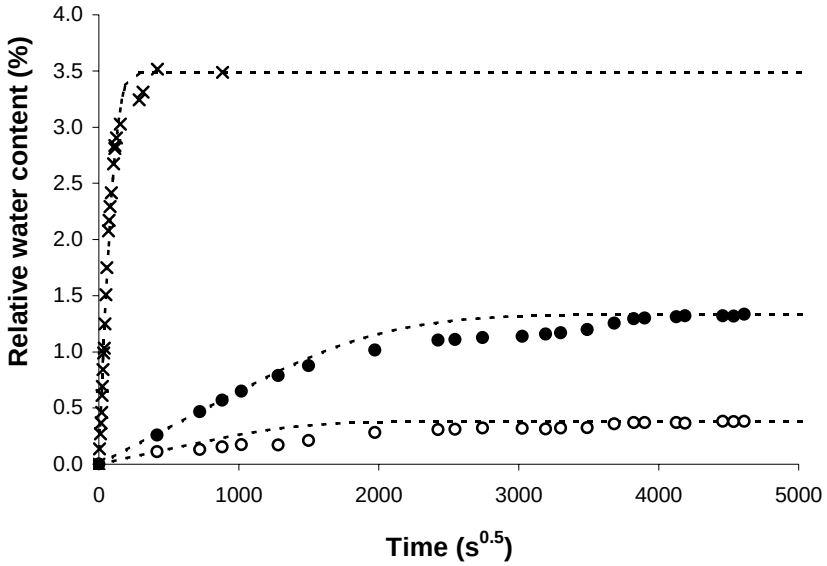

FIGURE 4.16. *Relative water content as a function of time for He53 (x), PET (o) and He53/PET composite (•). The humidity gradient is 20 % RH (65 to 85 % RH). He53 was processed at 200 °C prior to the experiment. The data for PET correspond to a bag with 5 laminate samples of type A. The data for He53/PET correspond to a single laminate sample of type B with length 240 mm and W_f 0.39. The dotted lines are the water adsorption behaviour predicted by the Fickian diffusion model.*

It was intended to investigate how the water adsorption behaviour of the composites is affected by changes in W_f and matrix type (see Table 4.8, p. 78). The laminate samples for these studies were of type A (15x15x2 mm^3), and they were weighed directly in the bags in which they were

conditioned. Unfortunately, the analysis of the results showed that the water content of the bags themselves was rapidly changed when they were moved to the weighing room with uncontrolled humidity conditions. The small but inconsistent weight changes of the bags were a notable source of error in the measurements. Moreover, the relative small length and width dimensions of the samples means that water diffusion in these two directions cannot be neglected (see below), and the one-dimensional Fickian diffusion model can therefore not be applied to estimate the diffusion coefficients. Anyway, without further comments, the results are shown in Figure 4.17 to substantiate the performed work.

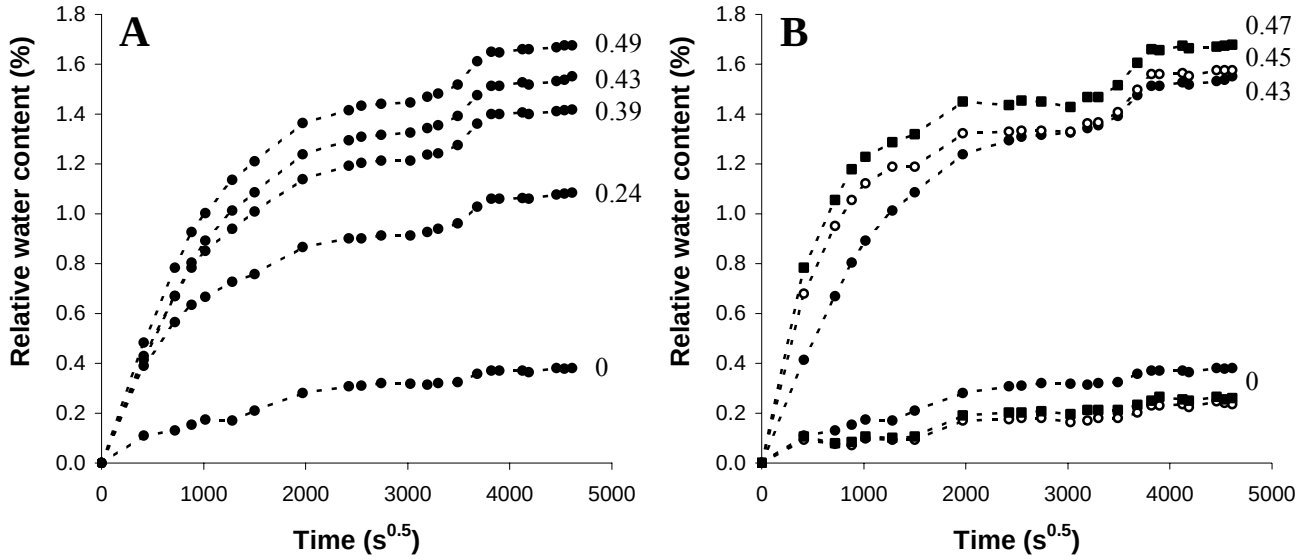

FIGURE 4.17. *Relative water content as a function of time for He53 composite samples. (**A**) shows results for PET matrix composites with different W_f, and (**B**) shows results for PET (•), PE (o) and PP (■) matrix composites with a W_f of about 0.45, in addition to results for pure matrix laminates. The shown values in the figures are composite W_f. The humidity gradient is 20 % RH (65 to 85 % RH). Sample dimensions are 15x15x2 mm^3.*

Water diffusion in the aligned hemp yarn composites is expectedly not isotropic, but different diffusion coefficients must exist in at least two directions within the composites, i.e. along the fibres (D_x) and transverse to the fibres ($D_y = D_z$). In the case of wood fibres, it has been shown that the diffusion coefficient along a fibre is two to three times larger than the coefficient in the transverse direction (Siau 1995). Moreover, the aligned arrangement of the fibres in the composites means that the diffusion path is different in the two directions. It can be stated that diffusion occurs in parallel in the axial direction, whereas it occurs in series in the transverse direction (Figure 4.18). By this simple model, it follows that D_x is larger than D_y (and D_z) since the diffusion coefficient of the fibre and matrix part is different from each other.

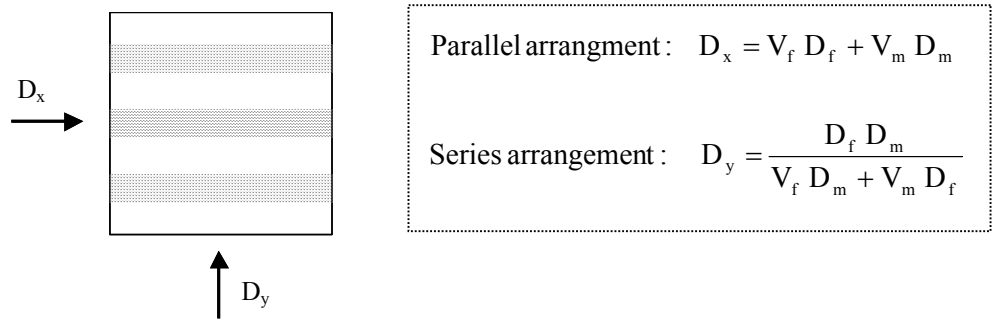

FIGURE 4.18. *Two-dimensional representation of the water diffusion path in the axial and transverse direction of the aligned hemp yarn composites.*

The water adsorption behaviour in the three directions of the composites, length (x), width (y) and thickness (z), was measured by sealing 4 out of 6 sides of cubic composite samples, i.e. water diffusion was allowed in only one direction. Figure 4.19 shows the water adsorption behaviour of these samples. Diffusion in the length direction is as expected faster than in the two transverse directions. Results are not yet available to show how and when the equilibrium relative water content is reached in the two transverse directions, but the current results reveal that water diffusion is not transverse isotropic. Initially, water diffusion in the thickness direction is slower than in the width direction, however the diffusion rate in the thickness direction increases as a function of time. In contrast, the diffusion rate in the width direction is gradually decreasing with time, which is in agreement with the Fickian diffusion model.

The unexpected difference in the water adsorption behaviour in the two transverse directions might be explained by the existence of internal stresses. It is likely that compression moulding of the composites generates internal compression stresses in the thickness direction, and tension stresses in the plane directions. This is supported by the results shown in Subsection 4.4.3 on the dimensional changes of the composites. It is hypothesised that the internal compression stresses in the thickness direction initially slow down the rate of water diffusion. However, the time-dependent and water related relaxation of the compression stresses means that the diffusion rate in the thickness direction is increased with time.

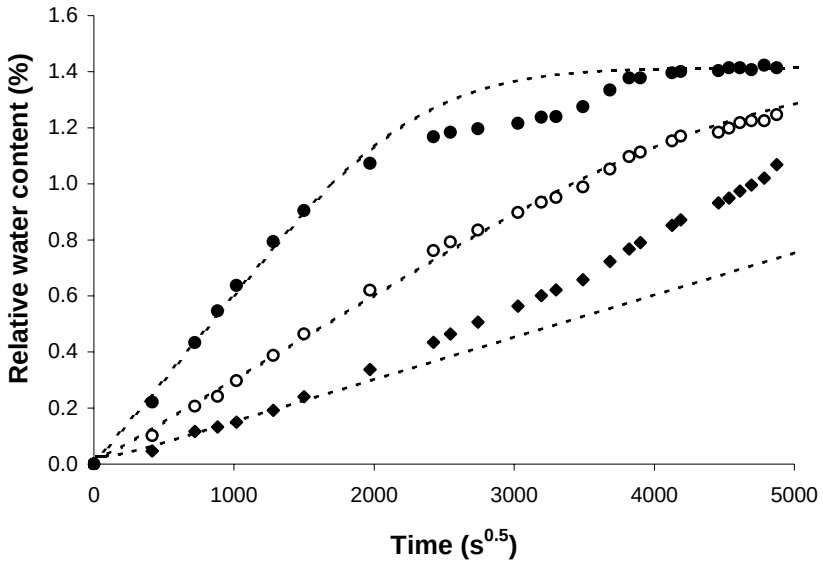

FIGURE 4.19. *Relative water content as a function of time for three cubic samples of He53/PET composites with dimensions 15x15x15 mm^3 and a W_f of 0.39. The humidity gradient is 20 % RH (65 to 85 % RH). Water diffusion was allowed in only one direction for each sample: length (•), width (o) and thickness (♦). The dotted lines are the water adsorption behaviour predicted by the Fickian diffusion model.*

In the Fickian diffusion model shown in equation (4.11) it is assumed that water diffusion occurs primarily in one direction, and that diffusion in other directions can be neglected. The verification of this assumption requires that for any two directions, the ratio of diffusion coefficients must be considered in relation to the ratio of sample dimensions. Based on the results in Figure 4.19, the directional diffusion coefficients are estimated to be 8.25, 2.16 and 0.56 10^{-12} m^2/s for D_x, D_y and D_z, respectively. D_z is estimated for the initial linear region according to the Fickian diffusion curve in the figure. U^*_{85} is assumed to be 1.4 % for all three directions. The ratio between D_x and D_z is about 14. This ratio governs the required minimum ratio between laminate length (L) and thickness (T) in order to neglect diffusion in the length direction. In Siau (1995) it is stated that water diffusion in a given direction can be neglected if its contribution to the water content is less than 10 %. With a D_x/D_z ratio of 14 the corresponding minimum L/T ratio is 30 (Siau 1995). Accordingly, for laminates with a thickness of 2 mm, the required minimum length is 60 mm in order to neglect diffusion in the length direction.

Since estimates are available for the three directional diffusion coefficients, the water adsorption behaviour can in principle be predicted for laminate samples with any combination of dimensions. One approach is to use the three-dimensional version of the Fickian diffusion model, which is presented in Blikstad et al. (1988). Another more illustrative approach will however be presented to demonstrate the relative importance of D_x, D_y and D_z in laminate samples with different dimensions. The degree of water saturation as calculated by equation (4.11) is denoted E

(=$U_{RH}(t)/U_{RH}$). Accordingly, E_x is the degree of water saturation as a result of water diffusion in the length direction, and $(1-E_x)$ is the additional fraction required to reach the equilibrium water content. The latter quantity is reduced by the contribution from diffusion in the two other directions. It can be shown that the remaining fractional water content for the sample (1-E) is given by the product of the corresponding values in the three directions (Siau 1995):

$$(1-E)=(1-E_x)(1-E_y)(1-E_z) \tag{4.17}$$

For a sample with given dimensions, equation (4.11) is used to calculate $(1-E_x)$, $(1-E_y)$ and $(1-E_z)$ as a function of time, and subsequently (1-E) is calculated by equation (4.17).

Figure 4.20A shows how water diffusion in the three directions is contributing to the degree of water saturation in a composite sample with dimensions 240x15x2 mm^3 (LxWxT). Even though D_z is lower than D_x and D_y, the relative small sample thickness of 2 mm means that E_z is the dominant diffusion component. E_x can be neglected because of the large sample length of 240 mm. However, the predicted E overestimates the experimental data, which indicates that the applied values of D_y and D_z are too large. If D_z is reduced from 0.56 to 0.08 10^{-12} m^2/s, then Figure 4.20B shows that the experimental data are well predicted.

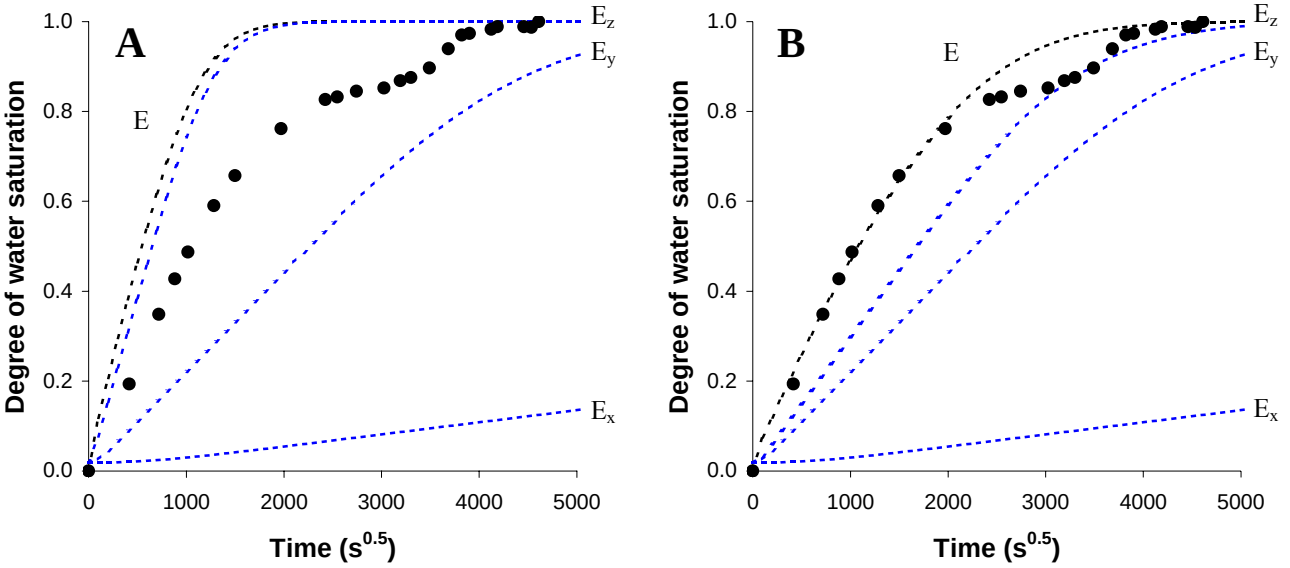

FIGURE 4.20. *The degree of water saturation as a function of time for a He53/PET composite sample with dimensions 240x15x2 mm^3 and a W_f of 0.39. The humidity gradient is 20 % RH (65 to 85 % RH). The symbols (•) are experimental data. The dotted lines are the degree of water saturation predicted by the Fickian diffusion model. The applied values of D_x, D_y and D_z are 8.25, 2.16 and 0.56 10^{-12} m^2/s in (**A**), whereas D_z is changed to 0.08 10^{-12} m^2/s in (**B**).*

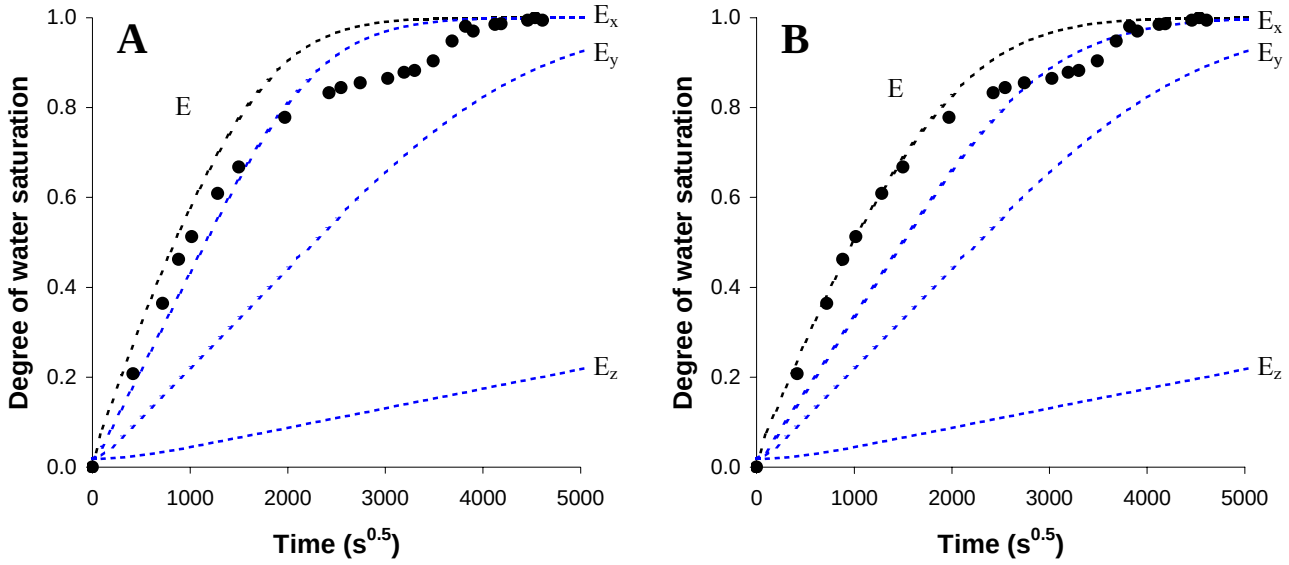

FIGURE 4.21. *The degree of water saturation as a function of time for a He53/PET composite sample with dimensions 15x15x15 mm^3 and a W_f of 0.39. The applied values of D_x, D_y and D_z are 8.25, 2.16 and 0.08 10^{-12} m^2/s in (**A**), whereas D_x is changed to 4.95 10^{-12} m^2/s in (**B**). See Figure 4.20 for more details.*

Based on a composite sample with dimensions 15x15x15 mm^3, Figure 4.21A shows that E_x is the dominating diffusion component since D_x is the largest diffusion coefficient, and since the diffusion distance is the same in all three directions. In this case, E_z can be neglected. However, the experimental data are slightly overestimated by the predictions. Figure 4.21B shows that the predictions of the experimental data are improved if D_x is reduced from 8.25 to 4.95 10^{-12} m^2/s.

According to the above considerations, the adjusted values of D_x and D_z are 4.95 and 0.08 10^{-12} m^2/s, respectively, whereas D_y is unchanged at 2.16 10^{-12} m^2/s. When these diffusion coefficients are used the water adsorption behaviour is found to be well predicted for other samples with different L/T ratios. Figure 4.22 shows two representative examples.

As can be seen in Figures 4.20-4.22, the water adsorption behaviour of the composite samples is in fact not very different from each other, irrespective of their actual dimensions. Thus, to provide more support for the presented model, samples are required with dimensions that would lead to very different water adsorption behaviours, e.g. 100x100x4, 100x4x10 and 4x100x10 mm^3. This would also provide the necessary information in order to adjust D_y.

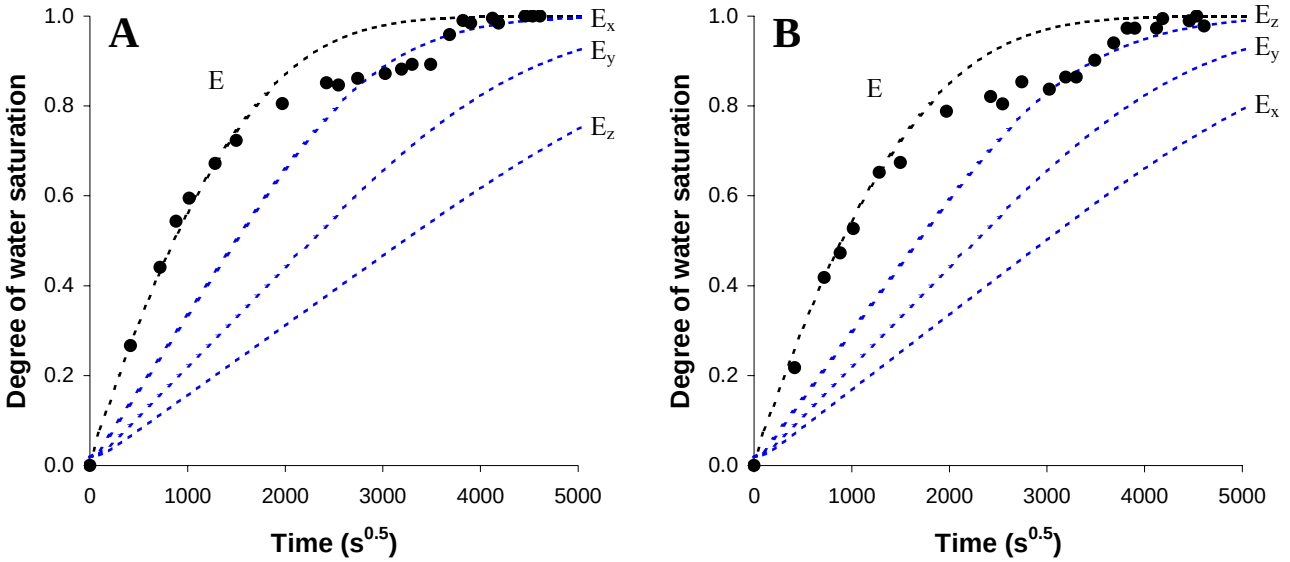

FIGURE 4.22. *The degree of water saturation as a function of time for He53/PET composite samples with dimensions (**A**) 15x15x4 and (**B**) 30x15x2 mm³. Composite W_f is 0.39. The applied values of D_x, D_y and D_z are 4.95, 2.16 and 0.08 10^{-12} m^2/s. See Figure 4.20 for more details.*

As shown in Figure 4.19 (p. 83), water diffusion in the length direction is at first well predicted by the Fickian diffusion model, and seems to approach an apparent U^*_{85} of about 1.2 %. However, the relative water content starts to increase and reaches a larger U^*_{85} of about 1.4 %. This two-stage diffusion behaviour was in fact observed for all tested samples independent of dimensions, W_f and matrix type (see Figures 4.16-4.17 and Figures 4.20-4.22). The humidity in the conditioning room was frequently measured to be constant at about 85 % RH, and the observed deviations are therefore not caused by changes in the surrounding humidity. This is furthermore supported by the stable and expected rate of water diffusion in the width direction of the composites (Figure 4.19, p. 83). In the literature several examples of a similar two-stage diffusion behaviour have previously been reported for plant fibre composites (Riccieri et al. 1999), synthetic fibre composites (Zhou and Lucas 1995) and pure thermosettings (Barton and Pritchard 1994) (see also examples in review by Weitsman 2000). Two models have been proposed to account for the observed non-Fickian diffusion. In one model, it is hypothesised that water diffuses into the composites in two phases: a free diffusion phase and a combined diffusion phase (Bonniau and Bunsell 1984). In the latter phase, the water molecules are combined with matrix or fibres, and the diffusitivity in this phase is therefore restrained. In another model, the deviation from Fickian diffusion is assigned to the viscoelastic mechanical response of the matrix (Cai and Weitsman 1994). It is hypothesised that the diffusion process is governed by time-dependent humidity boundary conditions even though the ambient humidity is constant. In both models, mathematical equations have been developed and are shown to be in good agreement with the experimental data. However, there seems to be a lack of

experimental data to verify the underlying hypotheses. At present, the observed deviation from Fickian diffusion in this study has not been analysed further.

4.4.2 Equilibrium water content

The relative water content of the hemp yarn composites can be calculated from the relative water content of the fibre and matrix parts ($U^*_{f\,RH}$ and $U^*_{m\,RH}$) by a simple mixture model:

$$U^*_{RH} = W_f \; U^*_{f\,RH} + (1 - W_f)\, U^*_{m\,RH} \tag{4.18}$$

This requires however that the fibre and matrix water sorption capacities are unchanged in the composites. It is known that the water sorption capacity of plant fibres is affected by mechanical stress (see Subsection 2.2.2). It is reduced by compression stress, and increased by tension stress. Accordingly, the sorption capacity of the hemp fibres in the composites might be reduced if they are restrained from swelling by the surrounding PET matrix. The relative water content of He53 is determined to be -1.78 and 3.47 % at 35 and 85 % RH, respectively. These values correspond to the water contents shown in Table 4.5 (p. 65) for He53 processed at 200 °C (but calculated with respect to a dry reference condition). The relative water contents of PET are given in Tables 4.9 and 4.10 (p. 89). Based on equation (4.18), Figure 4.23 shows the predicted relative water content of He53/PET composites as a function of W_f. Shown are also the measured relative water contents of the composites. The experimental data are slightly overestimated at both 35 and 85 % RH, but they are nevertheless linearly related to W_f. By adjusting the relative water contents of He53 to be –1.57 and 3.05 %, it is shown in the figure that the experimental data are then very well predicted. The required adjustment of the relative water content of He53 at 85 % RH is larger than the adjustment at 35 % RH (3.47 to 3.05 % and –1.78 to –1.57 %, respectively). Thus, it is indicated that the water sorption capacity of the hemp fibres in the composites is reduced when water is adsorped; i.e. the fibres are restrained from swelling. Other studies have also shown that the mixture model tends to overestimate the water content in plant fibre composites (Marcovich et al. 1999, Alvarez et al. 2004). However, in Subsection 2.2.2 it is noted that the water content of plant fibres is affected by the history of humidity exposures. Since it is unlikely that fibres inside and outside the composites have been exposed to the exact same history of humidities, this might also explain the observed deviations from the mixture model. Thus, without further documentation, the restraining effect of the matrix cannot readily be verified.

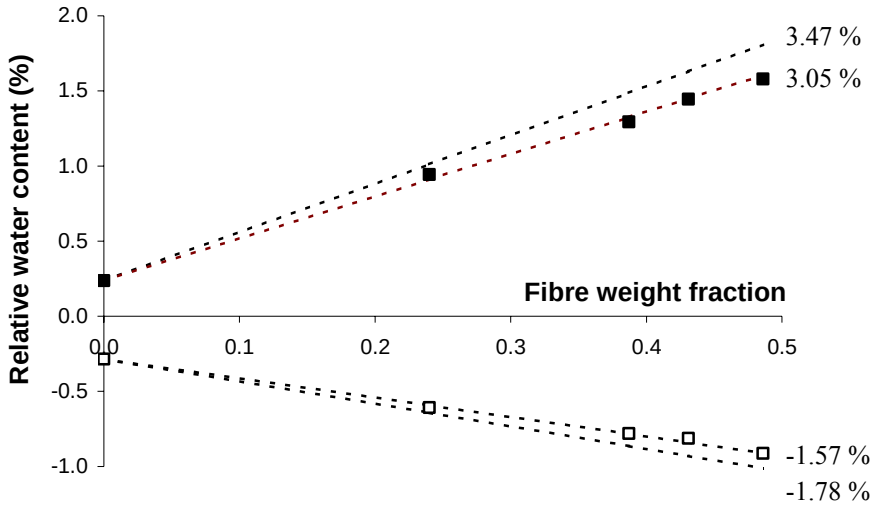

FIGURE 4.23. *Relative water content at 35 % RH (empty symbols) and 85 % RH (filled symbols) of He53/PET composite samples as a function of W_f. The dotted lines are the relative water content of the composites predicted by equation (4.18). The numbers are the relative water contents of He53.*

4.4.3 Water related dimensional stability

Appendix E presents a complete collection of the measured absolute equilibrium mass and dimensions of the laminate samples of type A. All samples were conditioned at 65 % RH (reference humidity), and then they were either conditioned at 35 % RH or at 85 % RH. The dimensional swelling or shrinkage in the three directions ($S_{x\,RH}$, $S_{y\,RH}$ and $S_{z\,RH}$) were calculated from the absolute sample dimensions (L, W and T):

$$S_{x\,RH} = 100\,\frac{L_{RH} - L_{65}}{L_{65}} \;;\; S_{y\,RH} = 100\,\frac{W_{RH} - W_{65}}{W_{65}} \;;\; S_{z\,RH} = 100\,\frac{T_{RH} - T_{65}}{T_{65}} \qquad (4.19)\,;\,(4.20)\,;\,(4.21)$$

where the subscript RH is either 35 or 85 % RH. The calculated dimensional changes of the samples are presented in Table 4.9 (from 65 to 35 % RH) and Table 4.10 (from 65 to 85 % RH). The results in the two tables are graphically depicted in Figures 4.24-4.26.

Based on results of He53/PET composite laminates, it is shown in Figure 4.24 that the dimensional changes in the width and thickness directions are approximately linearly increased with W_f at both 35 and 85 % RH, and that the dimensional changes in the length direction are small and unaffected by W_f. However, the figure points out two interesting characteristics: (i) the dimensional changes in the length direction are negative at 85 % RH; i.e. the composites shrink in the length direction, and (ii) the dimensional changes in the width and thickness directions are not identical.

TABLE 4.9. *Relative water content (U^*_{35}) and dimensional swelling/shrinkage ($S_{x\ 35}$, $S_{y\ 35}$ and $S_{z\ 35}$) of laminate samples in equilibrium at 35 % RH. Shown is also the sample density at 65 % RH, which is calculated from the measured absolute mass and dimensions of the samples.*

Yarn type	Matrix type	W_f	ρ_{65} (g/cm^3)	U^*_{35} (%)	$S_{x\ 35}$ (%)	$S_{y\ 35}$ (%)	$S_{z\ 35}$ (%)
He53	PET	0	1.287 ± 0.007	– 0.28	– 0.14	– 0.15	– 0.28
		0.240	1.330 ± 0.002	– 0.61	– 0.04	– 0.31	– 0.44
		0.387	1.357 ± 0.011	– 0.78	+ 0.03	– 0.40	– 0.47
		0.431	1.352 ± 0.012	– 0.81	– 0.02	– 0.46	– 0.57
		0.486	1.361 ± 0.007	– 0.91	– 0.02	– 0.54	– 0.69
	PE	0	0.925 ± 0.007	– 0.09	– 0.11	– 0.08	– 0.02
		0.448	1.095 ± 0.005	– 0.85	– 0.01	– 0.43	– 0.60
	PP	0	0.885 ± 0.002	– 0.09	– 0.07	– 0.13	– 0.15
		0.469	1.078 ± 0.007	– 0.92	– 0.01	– 0.47	– 0.51

TABLE 4.10. *Relative water content (U^*_{85}) and dimensional swelling/shrinkage ($S_{x\ 85}$, $S_{y\ 85}$ and $S_{z\ 85}$) of laminate samples in equilibrium at 85 % RH. Shown is also the sample density at 65 % RH, which is calculated from the measured absolute mass and dimensions of the samples.*

Yarn type	Matrix type	W_f	ρ_{65} (g/cm^3)	U^*_{85} (%)	$S_{x\ 85}$ (%)	$S_{y\ 85}$ (%)	$S_{z\ 85}$ (%)
He53	PET	0	1.291 ± 0.005	+ 0.24	– 0.07	– 0.06	– 0.07
		0.240	1.325 ± 0.009	+ 0.94	– 0.08	+ 0.39	+ 0.42
		0.387	1.348 ± 0.008	+ 1.29	– 0.09	+ 0.68	+ 0.62
		0.431	1.353 ± 0.012	+ 1.45	– 0.09	+ 0.81	+ 0.86
		0.486	1.370 ± 0.006	+ 1.58	– 0.07	+ 0.91	+ 1.12
	PE	0	0.922 ± 0.006	+ 0.05	– 0.05	– 0.05	– 0.07
		0.448	1.098 ± 0.003	+ 1.41	– 0.14	+ 0.59	+ 0.71
	PP	0	0.884 ± 0.003	+ 0.10	– 0.03	– 0.10	+ 0.004
		0.469	1.082 ± 0.009	+ 1.50	+ 0.03	+ 0.64	+ 0.89

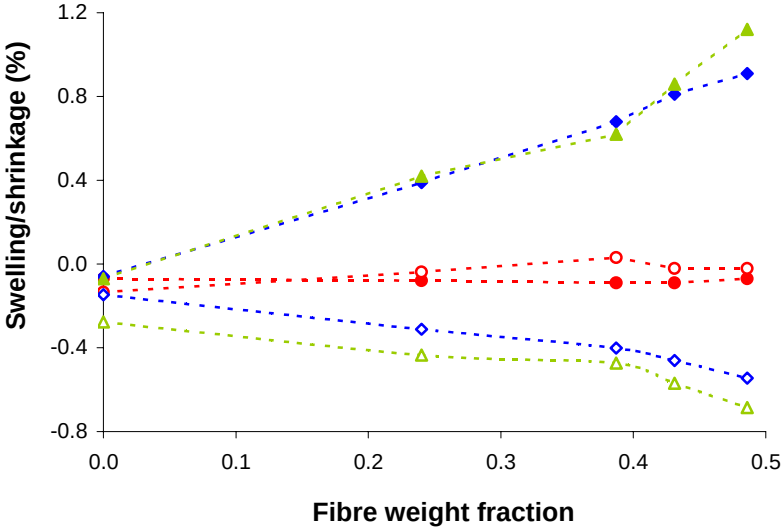

FIGURE 4.24. *Swelling/shrinkage of He53/PET composite samples as a function of W_f at 35 % RH (empty symbols) and at 85 % RH (filled symbols) in the length (o; red), width (◇; blue) and thickness (Δ; green) direction.*

Since hemp fibres swell and shrink mainly in the transverse directions, the observed small dimensional changes in the length direction of the composites are expected, but the consistent shrinkage in the length direction at 85 % RH is unexpected. This phenomenon can however be explained by Figure 4.25, which shows the dimensional changes of pure matrix samples (PET, PE and PP). It reveal that the dimensional changes at 85 % RH are negative for all three matrix types (except for PP in the thickness direction). Thus, the matrix shrinks when water is adsorped, and this explains the shrinkage in the length direction of the composites at 85 % RH.

The shrinkage of the matrix points to the existence of a mechanism that works against the swelling effect of water adsorption. It can be hypothesised that the adsorped water molecules tend to bring the polymer chains in the thermoplastics closer together by intermolecular hydrogen bonding. This implies however that the pure matrix samples are supposed to swell as an effect of water desorption, and this cannot be observed in Figure 4.25. Furthermore, the matrix types PP and PE contain no potential sites for hydrogen bonding (see Figure 4.36, p. 107). Instead, another mechanism is proposed to account for the shrinkage of the thermoplastics at 85 % RH. As already noted, it is likely that compression moulding generates internal stresses in the fabricated laminates. Compression stresses are generated in the thickness direction, and tension stresses are generated in the plane directions. When water is adsorped, the mobility of the thermoplastic polymer chains is increased, and the internal stresses are released. This might explain that pure matrix samples shrink in the length and width directions at 85 % RH. Likewise, the samples are supposed to swell in the thickness direction, but this is only true for PP as shown in Figure 4.25C. However, as can be seen

in Appendix E, the differences in mean thickness of the pure matrix samples between 65 and 85 % RH are indeed very small (i.e. a few micrometers), which means that the calculated percentage changes in thickness of the pure matrix samples are less trustworthy.

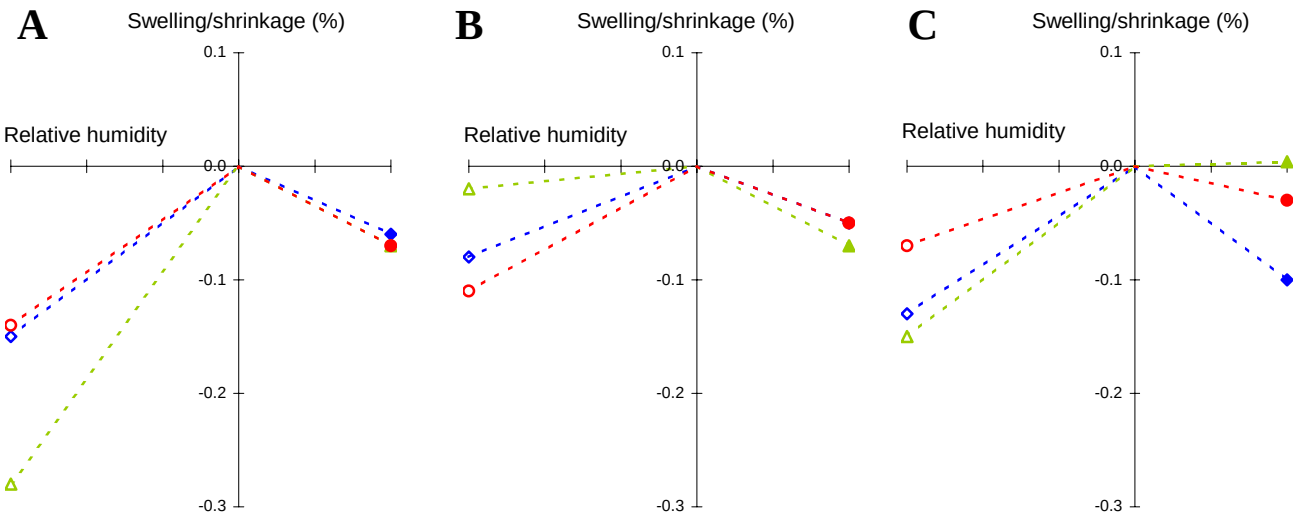

FIGURE 4.25. *Swelling/shrinkage in the length (○; red), width (◇; blue) and thickness (Δ; green) directions of pure matrix samples conditioned at two humidities: 35 % RH (empty symbols) and 85 % RH (filled symbols). The reference humidity is 65 % RH, which corresponds to the origin of the x-axis. The matrix types are (**A**) PET, (**B**) PE and (**C**) PP.*

Figures 4.24 and 4.26 show that the dimensional changes of the aligned hemp yarn composites are not transverse isotropic. Generally, the composites swell more in the thickness direction than in the width direction at 85 % RH. Likewise, the composites shrink more in the thickness than in the width direction at 35 % RH. The same phenomenon has been shown in a study by Lu et al. (2003) on aligned sisal fibre composites submerged in water. The different internal stresses in the width and thickness direction of the composites might serve to explain the transverse anisotropic dimensional changes. However, at present the results have not been analysed further to explain the phenomenon in more details.

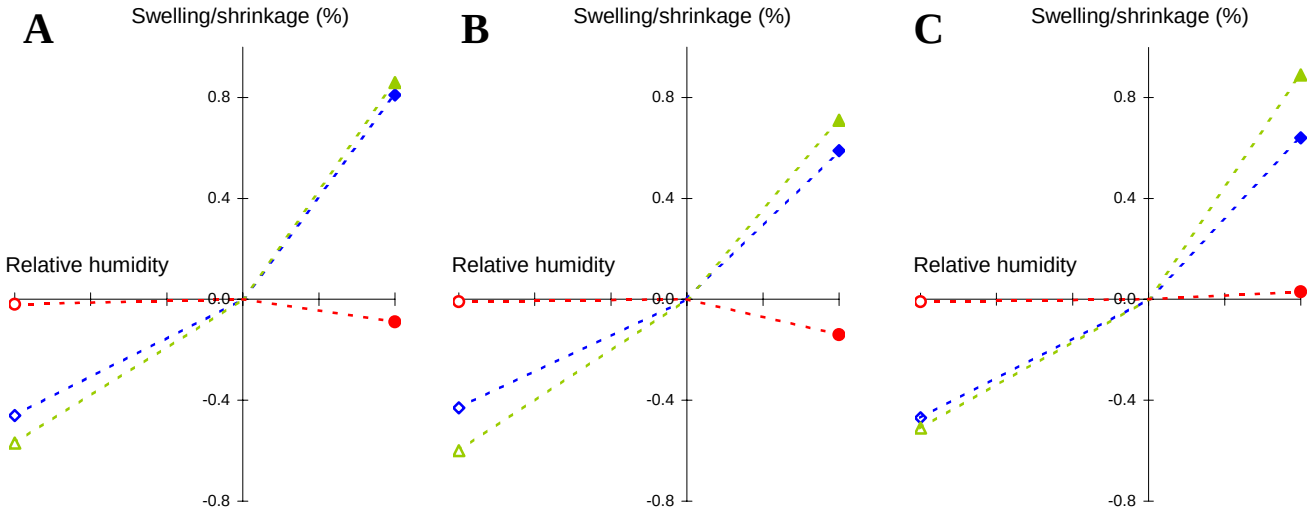

FIGURE 4.26. *Swelling/shrinkage in the length (○; red), width (◇; blue) and thickness (Δ; green) directions of composite samples conditioned at two humidities: 35 % RH (empty symbols) and 85 % RH (filled symbols). The reference humidity is 65 % RH, which corresponds to the origin of the x-axis. The matrix types are (**A**) PET, (**B**) PE and (**C**) PP, and the yarn type is He53 with a W_f of about 0.45.*

4.4.4 Hygroexpansion coefficients

The numerical relation between the relative water content and the dimensional swelling/shrinkage is generally assumed to be linear. The interrelating constants are denoted hygroexpansion coefficients (β_x, β_y and β_z):

$$S_{x\,RH} = \beta_x\, U^*_{RH} \quad ; \quad S_{y\,RH} = \beta_y\, U^*_{RH} \quad ; \quad S_{z\,RH} = \beta_z\, U^*_{RH} \qquad (4.22)\ ;\ (4.23)\ ;\ (4.24)$$

The linearity is based on two assumptions: (i) the density of sorped water is equal to the density of liquid water, and (ii) the volumetric swelling/shrinkage ($S_{v\,RH}$) is directly proportional to the volume of sorped water (see considerations in Subsection 2.2.3). It can then be shown that the volumetric hygroexpansion coefficient (β_v) is equal to the density of the samples at 65 % RH (ρ_{65}):

$$\beta_v = \frac{S_{v\,RH}}{U^*_{RH}} = \frac{\dfrac{v_{RH} - v_{65}}{v_{65}}}{\dfrac{m_{RH} - m_{65}}{m_{65}}} = \frac{m_{65}}{v_{65}} \frac{v_{RH} - v_{65}}{m_{RH} - m_{65}} = \rho_{65} \frac{v_w}{m_w} = \rho_{65} \frac{1}{\rho_w} \approx \rho_{65} \qquad (4.25)$$

where the subscript w is sorped water, and the subscript RH is either 35 or 85 % RH.

Since $S_{v\,RH}$ can be approximated by summation of the three dimensional changes, it follows that β_v (and ρ_{65}) can be approximated by summation of the three directional hygroexpansion coefficients:

$$S_{v\,RH} \approx S_{x\,RH} + S_{y\,RH} + S_{z\,RH} \quad \Rightarrow \quad \beta_v \approx \beta_x + \beta_y + \beta_z \qquad (4.26)$$

Subsequently, if the thermoplastic matrices are assumed to be isotropic then their dimensional stability can be assessed from their relative water content and their density at 65 % RH:

$$S_{x\,RH} = \tfrac{1}{3}\,\rho_{65}\,U^{*}_{RH} \quad ; \quad S_{y\,RH} = \tfrac{1}{3}\,\rho_{65}\,U^{*}_{RH} \quad ; \quad S_{z\,RH} = \tfrac{1}{3}\,\rho_{65}\,U^{*}_{RH} \qquad (4.27)\ ;\ (4.28)\ ;\ (4.29)$$

Likewise, the dimensional stability can be assessed for the aligned hemp yarn composites if they are assumed to be transverse isotropic with negligible dimensional changes in the length direction:

$$S_{x\,RH} = 0 \quad ; \quad S_{y\,RH} = \tfrac{1}{2}\,\rho_{65}\,U^{*}_{RH} \quad ; \quad S_{z\,RH} = \tfrac{1}{2}\,\rho_{65}\,U^{*}_{RH} \qquad (4.30)\ ;\ (4.31)\ ;\ (4.32)$$

Based on the results in Tables 4.9 and 4.10 (p. 89), the equations (4.22)-(4.24) were used to calculate the directional hygroexpansion coefficients (β_x, β_y and β_z) of the samples conditioned at 35 and 85 % RH. Strictly speaking, the term hygroexpansion coefficient is less appropriate in the case of shrinkage, but it will nevertheless be used to specify both swelling and shrinkage. Equation (4.26) was used to calculate the volumetric hygroexpansion coefficients (β_v) at 35 and 85 % RH.

The calculated hygroexpansion coefficients for He53/PET composite samples are shown in Figure 4.27 as a function of W_f. Also shown in the figure is the mean density of the samples at 65 % RH (ρ_{65}) (see Tables 4.9 and 4.10, p. 89), as well as the mean density divided by 2 ($\rho_{65}/2$). Figure 4.27A shows that for composite samples conditioned at 35 % RH, the hygroexpansion coefficients are relatively unaffected by W_f, and moreover, they are in fairly good agreement with the predictions: β_v is nearly equal to ρ_{65}, β_y and β_z are nearly equal to $\rho_{65}/2$, and β_x is nearly zero. In contrast, Figure 4.27B shows that the hygroexpansion coefficients for composite samples conditioned at 85 % RH are increasing with W_f, and only approach the predictions at the largest W_f. Knowing that the PET matrix shrinks as an effect of water adsorption (see Subsection 4.4.3), the low hygroexpansion coefficients of the composite samples at 85 % RH are expected. Moreover, it seems likely that when W_f is increased, the influence of the matrix is diminished, and consequently the hygroexpansion coefficients are increased towards the predictions.

The hygroexpansion coefficients of the pure PET samples are also shown in Figure 4.27 (at W_f=0). According to the predictions, β_v should be equal to ρ_{65}, and β_x, β_y and β_z should be equal to $\rho_{65}/3$. However, at 35 % RH the hygroexpansion coefficients are larger than the predictions, i.e. PET shrinks more than can be expected from the volume of desorped water. At 85 % RH the hygroexpansion coefficients are lower than the predictions, i.e. PET swells less than can be expected from the volume of adsorped water. These two findings might be assigned to the internal stresses in PET, which might enhance shrinkage and restrain swelling. The internal stress induced shrinkage of PET at 35 % RH is apparently less dominating in the composites, since the

hygroexpansion coefficients of the composite samples at 35 % RH is close to the predictions. However, it can be anticipated that for composites with low values of W_f, the hygroexpansion coefficients at 35 % RH would be larger than the predictions.

Overall, it can be concluded that for large values of W_f, the dimensional changes of aligned hemp yarn composites are fairly well predicted in the humidity range 35-85 % RH. The predictions are based on the relative water content and the density of the composites.

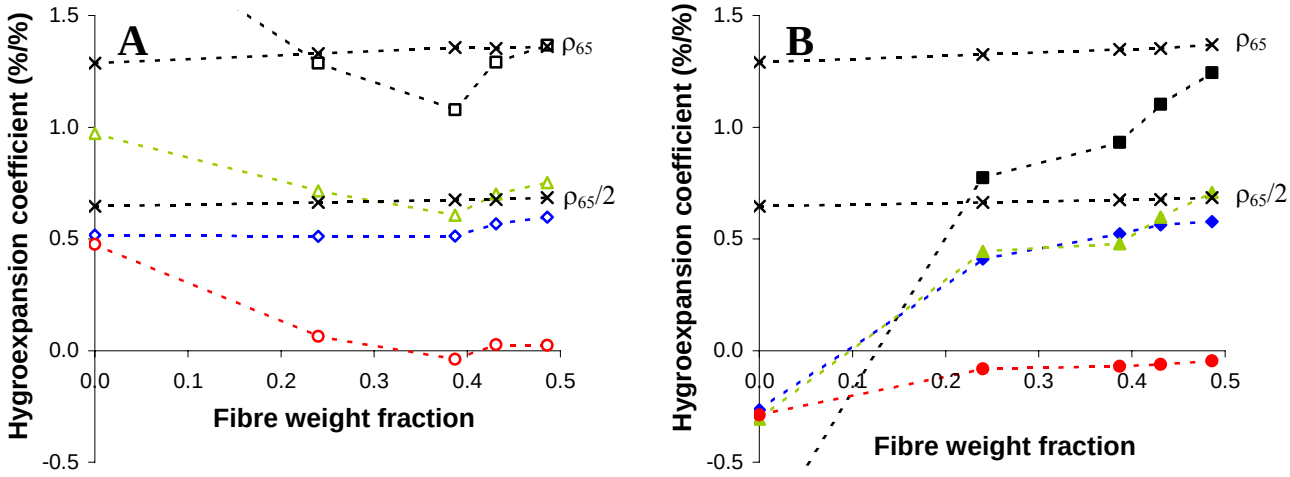

FIGURE 4.27. *Hygroexpansion coefficients of He53/PET composites as a function of W_f at (**A**) 35 % RH (empty symbols) and at (**B**) 85 % RH (filled symbols). The symbols are β_v (□; black), β_x (o; red), β_y (◇; blue) and β_z (Δ; green). β_v for pure PET samples at 35 and 85 % RH are not shown in the figures, but are 1.96 and –0.86 %/%, respectively.*

4.4.5 Microstructural changes

The difference in water sorption capacity between the hemp fibres and the thermoplastic matrix are likely to induce cracks inside the composites when water is sorped. In the case of carbon fibre/epoxy composites, it has previously been shown that interfacial cracks are developed when composite samples are submerged in water (Zhou and Lucas 1995). Even though the water exposure in this study is less severe, the obtained cross-sectional images of composite samples reveal that cracks are generated in samples conditioned at 85 % RH. In contrast, no cracks are observed in samples conditioned at 35 and 65 % RH. Figure 4.28 shows cross-sectional images of a He53/PP composite sample in equilibrium at 65 and 85 % RH. The same cross-sectional area is shown for the two humidities, and the figure demonstrates that cracks have been developed at 85 % RH. Likewise, cracks are also observed in PET and PE matrix composites conditioned at 85 % RH. The cracks are localised within the yarn fibre bundles where they propagate along the periphery of the fibres, i.e. interfacial cracks. No cracks are observed in the matrix rich areas. At present, no attempt has been made to quantify the cracks with respect to size and number. Originally, the

cross-sectional images were intended to provide information of the microscale dimensional changes (e.g. changes in cross-sectional area of the fibres) in composites conditioned at different humidities. However, this is not possible due to the small dimensional changes and the low magnification of the images. Cross-sectional images of dry composite samples are not yet available, but because of the larger humidity difference (i.e. 85 to 0 % RH) these images might provide interesting information of microscale dimensional changes.

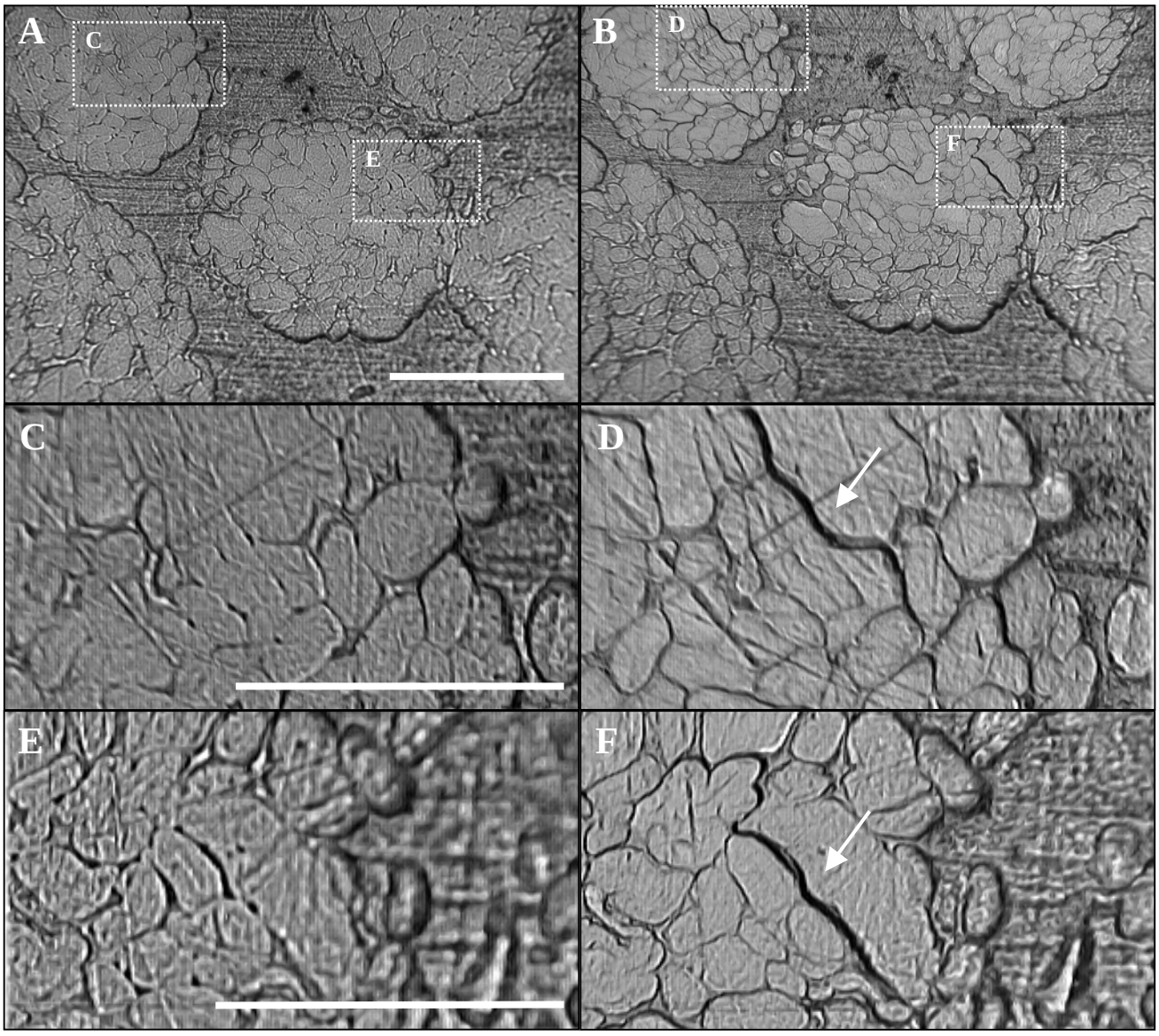

FIGURE 4.28. *OM images of the same cross-sectional area of a He53/PP composite sample in equilibrium at (**A**) 65 % RH and (**B**) 85 % RH. (**C**)-(**F**) shows enlargements of the regions specified in (**A**) and (**B**). Interfacial cracks in (**D**) and (**F**) are identified by arrows. Scale bars are 200 μm in (**A**) and (**B**), 100 μm in (**C**) and (**D**), and 100 μm in (**E**) and (**F**).*

4.5 COMPOSITE TENSILE PROPERTIES

The measurements of tensile properties of aligned plant fibre yarn composites include a number of parameters:

Parameter	Variables
Fibre/matrix mixing	Film-stacking, Commingled filament-winding
Testing direction	0°, 10°, 20°, 30°, 45°, 60°, 90°
Yarn type	He47, He53, He91, Fl64
Matrix type	PET, PE, PP, MAPP
Fibre volume fraction	0.2-0.3, 0.3-0.4, 0.4-0.5, 0.5-0.6
Process temperature (°C)	180, 190, 200, 210, 220
Conditioning humidity (% RH)	35, 65, 85, Uncontrolled

Appendix F shows the possible combinations of these parameters and their variables, and the combinations that were actually tested are identified. A total sum of 59 laminates were fabricated and tested, and a complete list of the results is given in Appendix G. In the following subsections these results will be discussed in relation to the different experimental parameters.

4.5.1 Fibre/matrix mixing

When composites are fabricated by compression moulding it requires that the fibre and the thermoplastic matrix parts are appropriately mixed before they are processed into composites by heat and pressure. Such fibre/matrix mixing can be made by film-stacking where thermoplastic films are stacked in between layers of fibres, which is a technique well suited for non-woven fibre mats (Andersen and Plackett 2002). However, in the case of plant fibre yarns, fibre/matrix mixing can as well be made by commingled filament-winding where plant fibre yarn and thermoplastic filament yarn are wound concurrently.

In the beginning of this study film-stacking was the applied fibre/matrix mixing technique, however for a number of reasons it was found to be less optimal:

- A number of thin fibre assemblies are required to ensure that the flowing distance of the matrix is short enough to impregnate all fibres (Figure 4.29A). Since the aligned assemblies of plant fibre yarn are made by filament-winding, which is a relative time-consuming process, the number of assemblies is critical. Moreover, the arrangement of the stack of fibre and matrix layers is too a time-consuming process.
- Composite cross-sections show that the spatial distribution of fibres and matrix is clearly non-uniform with regions of pure matrix at the borders and between layers of fibre assemblies (Figure 4.30A). This complicates any succeeding analyses and modelling of composite properties.

- The minimum obtainable composite V_f is about 0.40. With a lower V_f, the flow of the matrix into the fibre assemblies introduces lateral yarn displacements.

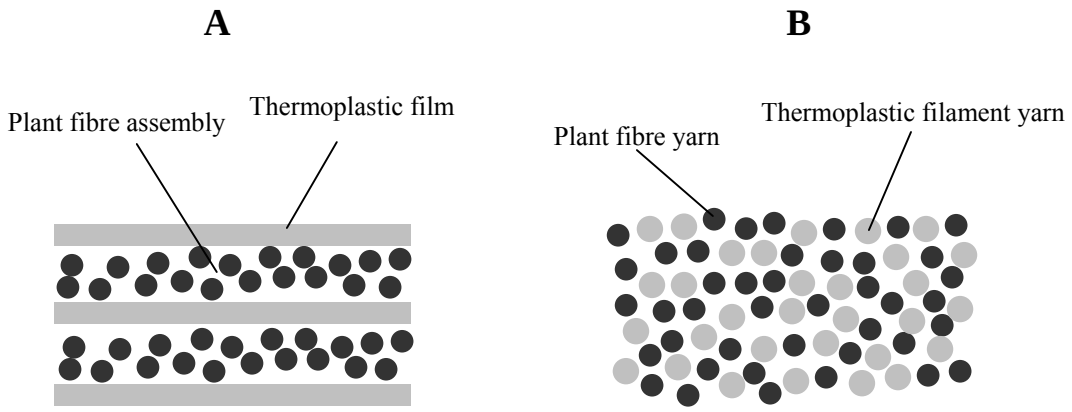

FIGURE 4.29. *Cross-sections of a fibre/matrix assembly mixed by (**A**) film-stacking and (**B**) commingled filament-winding.*

Commingled filament-winding was found to be a much more optimal approach for fibre/matrix mixing:

- The intimate mixing of fibres and matrix effectively reduces the impregnation distance of the matrix (Figure 4.29B) (see theoretical considerations in Svensson et al. 1998). Moreover, the fibre/matrix assembly is made in a single operation, which makes this technique less time-consuming.
- The spatial distribution of fibres in composite cross-sections is nearly uniform with no matrix-rich regions (Figure 4.30B, p. 98 and Figure 4.40, p. 112).
- There is no lower limit of composite V_f.

The change from film-stacking to commingled filament-winding was made because of the reasons mentioned above. Thus, it was not planned to compare tensile properties of composites fabricated by the two fibre/matrix mixing techniques. In fact none of the investigated parametric combinations presented in Appendix F is fully identical for composites fabricated by the two techniques. However, as can be seen from the results presented in the following subsections, no obvious difference in tensile properties can be observed. Only the porosity is slightly larger for composites fabricated by film-stacking, which also is expected due to the longer impregnation distance.

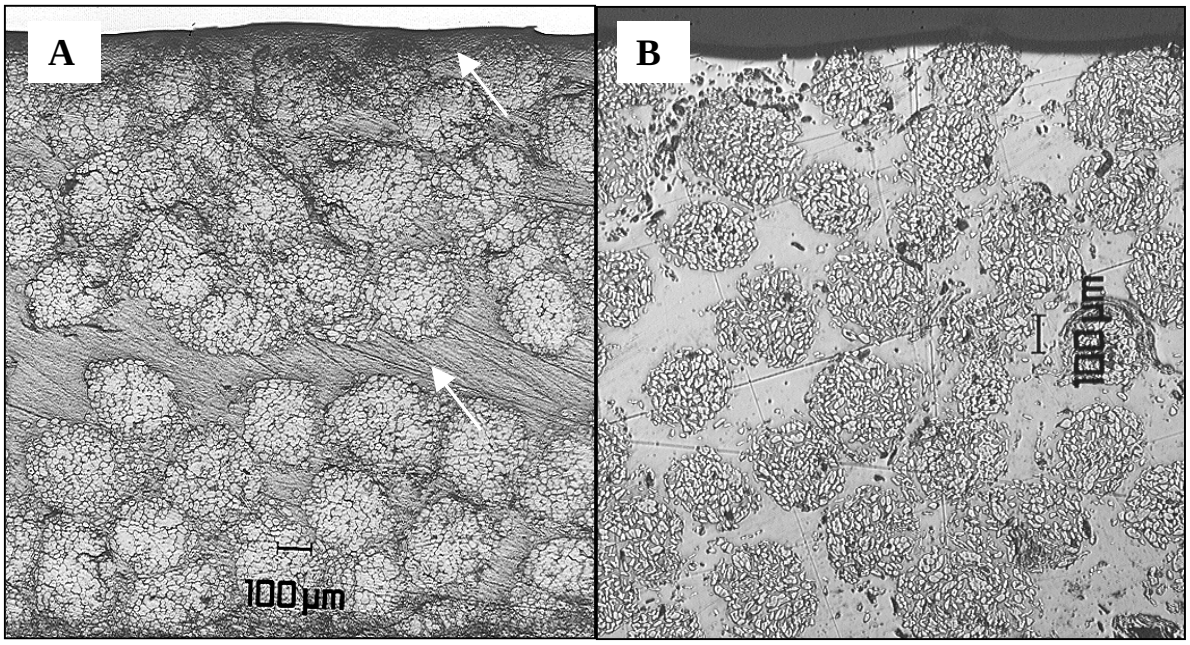

FIGURE 4.30. *Examples of cross-sections of composites fabricated by (**A**) film-stacking and (**B**) commingled filament-winding. (**A**) is a Fl64/PP composite with a V_f of 0.51 and (**B**) is a He53/PET composite with a V_f of 0.43. Arrows in (**A**) shows the matrix-rich regions at the border and between two fibre layers.*

4.5.2 Testing direction

The previously reported tensile properties of aligned plant fibre composites are mostly based on tests in the axial direction (i.e. the fibre direction). These tests are appropriate in order to analyse fibre properties in relation to composite properties. However, to characterise properties of the composite material as a whole requires tests in off-axis directions as well. In a larger perspective, if aligned plant fibre composites are to be used for structural applications, off-axis properties are fundamental to predict the response to loads in any given direction (e.g. by laminate theory, see Hull and Clyne 1996). In the literature only three studies of aligned plant fibre composites have been found that include off-axis properties: (i) a study of jute/polyester composites tested in the directions 0, 45 and 90° (Kumar 1986), (ii) a study of flax/epoxy composites tested in the directions 0 and 90° (Van de Weyenberg et al. 2003), and (iii) a study of jute/epoxy composites tested in the direction 0, 10, 17, 25, 37, 50, 63 and 80° (Cichocki and Thomason 2002). In the latter study, composite stiffness was measured by dynamic mechanical analysis, and micro-mechanical models were applied to determine the elastic constants of both composites and fibres.

To measure off-axis tensile properties, in addition to axial tensile properties, requires that the applied method of composite fabrication is highly controllable in order to fabricate a number of identical composite laminates. In most studies of aligned plant fibre composites the fibres are aligned manually by hand lay-up (e.g. White and Ansell 1983, Kalaprasad 1997, Hepworth et al.

2000). This is a time-consuming process, which restricts the number of fabricated laminates, and moreover it makes it difficult to obtain identical V_f and identical degree of fibre alignment between laminates. In contrast, this can be achieved by commingled filament-winding of plant fibre yarn, where a number of laminates readily are made with identical V_f (see below) and a degree of fibre alignment given by the twisted fibre arrangement in the yarn.

In this study, all composite laminates were routinely tested in the axial direction (0°) and in the transverse direction (90°). However, for He53/PET composites processed at 200 °C and conditioned at 65% RH, four more laminates were fabricated to measure the intermediate off-axis properties. V_f and V_p of all five laminates are almost identical with means ± stdv. of 0.337 ± 0.001 and 0.025 ± 0.003, respectively. Figure 4.31A shows an image of the tensile specimens with the yarn axis inclined at different angles to the testing direction. The yarn axis can clearly be identified from the surface texture of the specimens, and the inclination angles correspond fairly well with the superimposed angles in the figure. The stress-strain curves in Figure 4.31B give a firsthand impression of how the tensile properties consecutively are declining when the yarn angle is increased. Figures 4.32 and 4.33 show the determined composite stiffness and ultimate stress as a function of yarn angle, in addition to theoretical predictions.

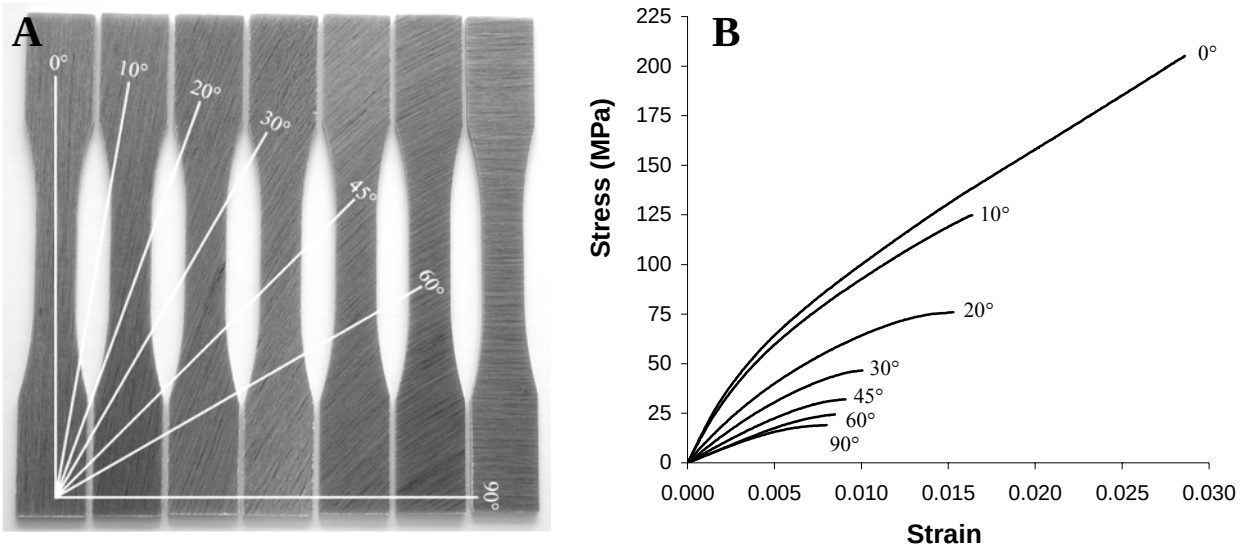

FIGURE 4.31. *Shown in (**A**) are examples of He53/PET tensile specimens with the yarn axis inclined at various angles to the testing direction. Shown in (**B**) are representative stress-strain curves.*

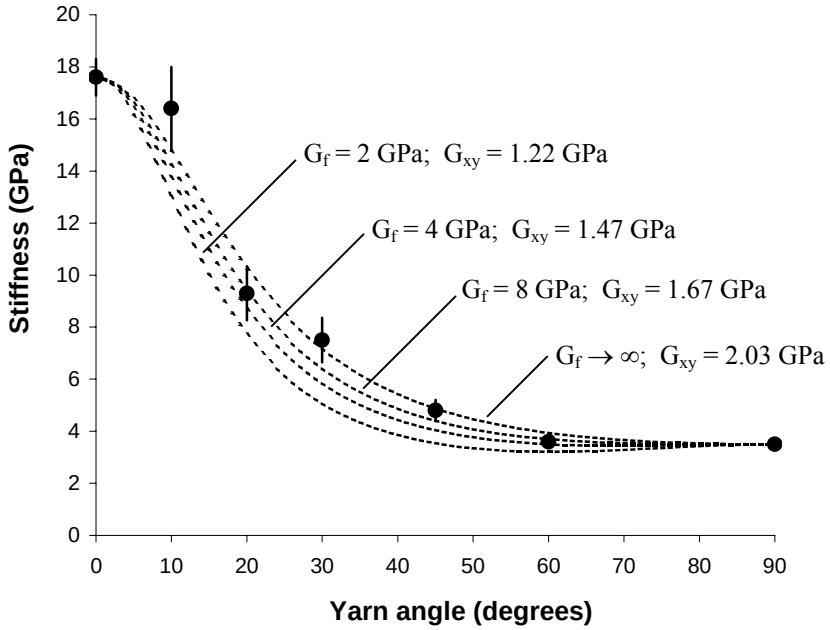

FIGURE 4.32. *Stiffness of He53/PET composites with the yarn axis inclined at different angles to the testing direction. Data points are means of experimental results and vertical bars are standard deviations (n=6). Dotted lines are theoretical predictions. See text for more details.*

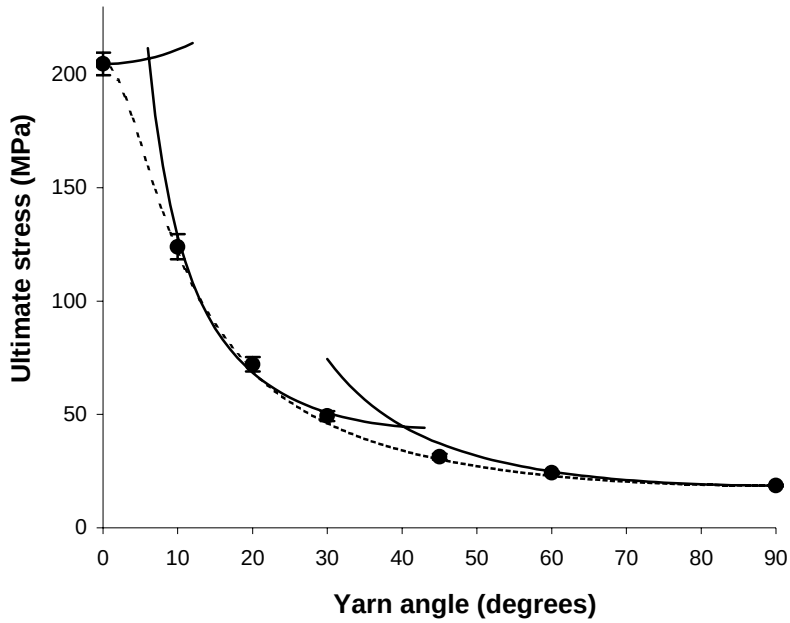

FIGURE 4.33. *Ultimate stress of He53/PET composites with the yarn axis inclined at different angles to the testing direction. Data points are means of experimental results and vertical bars are standard deviations (n=6). The full lines are ultimate stress predicted from the maximum stress theory with a shear stress of 22 MPa. The dotted line is ultimate stress predicted from the Tsai-Hill criterion with a shear stress of 26 MPa.*

The following theoretical considerations are based on Harris (1980) and Hull and Clyne (1996). If the tensile properties of aligned hemp yarn composites are assumed to be orthotropic, and that a state of plane stress is assumed, the tensile stiffness at a given angle to the yarn axis (E_θ) can be estimated by the equation:

$$\frac{1}{E_\theta} = \frac{\cos^4\theta}{E_x} + \frac{\sin^4\theta}{E_y} + \sin^2\theta\cos^2\theta\left(\frac{1}{G_{xy}} - \frac{2\nu_{xy}}{E_x}\right) \tag{4.33}$$

where G is composite shear stiffness, ν is composite Poisson's ratio and the subscripts x and y are material axes, where x is axial direction and y is transverse direction, respectively. The two unknown constants in the equation are G_{xy} and ν_{xy}. The partial contributions of the fibre and matrix shear stiffness (G_f and G_m) to G_{xy} can be estimated by the semi-empirical Halpin and Tsai expression:

$$G_{xy} = \frac{G_m(1+\xi\,\eta\,V_f)}{(1-\eta\,V_f)} \qquad \text{where} \quad \eta = \frac{\frac{G_f}{G_m}-1}{\frac{G_f}{G_m}+\xi} \tag{4.34}$$

where ξ is an adjustable parameter assumed to be equal to 1 (Hull and Clyne 1996). If the tensile properties of the matrix are assumed to be isotropic, G_m can be estimated by the equation:

$$G_m = \frac{E_m}{2(1+\nu_m)} \tag{4.35}$$

Tensile stiffness (E_m) and Poisson's ratio (ν_m) for pure PET laminates are measured to be 2.7 GPa and 0.4, respectively (Table 4.15, p. 108). Accordingly, G_m is calculated by equation (4.35) to be 1.0 GPa. When G_m is known, G_{xy} can be calculated for various values of G_f by equation (4.34). In Cichocki and Thomason (2002) it is shown that ν_{xy} is about 0.1 below ν_m, and therefore ν_{xy} is assumed to be 0.3. Subsequently, E_θ can be calculated for various values of G_f by equation (4.33), and this is shown in Figure 4.32. The prediction of the experimental E_θ is improved when G_f is increased above 2 GPa. Moreover, G_{xy} is approaching 2.0 GPa (≈1.34/0.66, see equation (4.34)) when G_f is increased towards infinity. An exact value of G_f can not be found from these quantitative considerations, but G_f is at least 8 GPa according the to fitting lines in Figure 4.32. Thus, it can be stated that G_f is larger than both G_m and G_{xy}. The shear stiffness of the composites is therefore predominantly governed by the shear stiffness of the matrix, and this has also been shown to be the case for unidirectional glass/epoxy composites (Hull and Clyne 1996). In Cichocki and Thomason (2002), based on jute/epoxy composites, G_{xy} and G_f were estimated to be 1.7 and 4.7 GPa, respectively. In Gassan et al (2001), G_f is reported to be 4.4 GPa for cellulose. In Page et

al. (1977), G_f is reported to be 7 GPa for wood fibres. Generally, these results are comparable to the results obtained in this study.

The prediction of ultimate stress at a given angle to the yarn axis (σ_θ) is made by two models: the maximum stress theory and the Tsai-Hill criterion. The maximum stress theory characterises three modes of failure, which are defined by three equations:

$$\sigma_\theta = \frac{\sigma_x}{\cos^2\theta} \quad \text{(for failure controlled by tensile fracture of fibres)}$$

$$\sigma_\theta = \frac{\tau_{xy}}{\sin\theta\,\cos\theta} \quad \text{(for failure controlled by shear parallel with fibres)} \qquad (4.36)$$

$$\sigma_\theta = \frac{\sigma_y}{\sin^2\theta} \quad \text{(for tensile failure normal to fibres)}$$

where τ is shear stress. The Tsai-Hill criterion is defined by the equation:

$$\frac{1}{\sigma_\theta^{\,2}} = \frac{\cos^2\theta\left(\cos^2\theta - \sin^2\theta\right)}{\sigma_x^{\,2}} + \frac{\sin^4\theta}{\sigma_y^{\,2}} + \frac{\cos^2\theta\,\sin^2\theta}{\tau_{xy}^{\,2}} \qquad (4.37)$$

The two model were fitted to the experimental data in Figure 4.33, and τ_{xy} was estimated to be 22 and 26 MPa, respectively. The shear stress of the isotropic PET matrix (τ_m) can be estimated by the equation:

$$\tau_m = 0.5\,\sigma_{m*} \qquad (4.38)$$

where σ_{m*} is the stress of the PET matrix at the point of composite failure. Figure 4.31B shows that composite failure strain is decreasing with the yarn angle. The mean failure strain is 0.014. From the measured stress-strain curves of pure PET laminates, the stress at strain 0.014 is determined to be about 36 MPa (see Figure 4.37A, p. 109). Subsequently, τ_m is estimated by equation (4.38) to be 18 MPa, which is just below the predicted composite shear stresses of 22 and 26 MPa. Thus, as for shear stiffness, it is indicated that the shear stress of the composites are closely correlated with the shear stress of matrix.

The objective of the above quantitative analysis is to form a basis for future studies of off-axis properties of aligned plant fibre yarn composites. Optimally, a number of parameters can be added to the investigations, such as V_f, V_p and fibre/matrix interface properties.

4.5.3 Yarn type

A literature survey was performed on the previously reported tensile properties of aligned plant fibre composites. A number of different plant fibre types have been applied (e.g. hemp, flax jute and sisal), and they have typically been combined with the two thermosetting matrix types: epoxy and polyester. The reported stiffness and ultimate stress of the composites are shown in Table 4.11. The properties are quite diverse with no consistent effect of either fibre type or composite V_f. This is anticipated since the measured properties probably are biased by the actual procedure of fibre alignment, composite fabrication and testing. Moreover, the method to estimate composite V_f varies between the studies (see Subsection 4.5.5), and this complicates the comparison of tensile properties.

TABLE 4.11. *Outcome of literature survey on the tensile properties of aligned plant fibre composites. If not otherwise noted the fibres are raw fibres (i.e. non-textile fibres).*

Fibre type	Matrix type	V_f	Stiffness (GPa)	Ultimate stress (MPa)	Reference
Wheat straw	Polyester	0.37	5	-	White and Ansell (1983)
Pineapple	Polyester	0.21	-	45	Mishra et al. (2003)
Hemp	Epoxy	0.20	8	90	Hepworth et al. (2000)
Sunhemp	Polyester	0.30	13	125	Sanadi et al. (1986)
Flax	Epoxy	0.26	7	105	Hepworth et al. (2000)
Flax	**Epoxy**	**0.21**	**22**	**195**	**Oksman (2001)**
Flax	Cell. diacetate	0.35	-	180	Bos et al. (1997)
Flax*	Epoxy	0.40	25	140	Van de Weyenberg et al. (2003)
Jute*	Epoxy	0.33	15	100	Shah and Lakkad (1981)
Jute*	Polyester	0.40	8	150	Sridhar et al. (1984)
Jute*	**Polyester**	**0.31**	**20**	**170**	**Roe and Ansell (1985)**
Jute*	Epoxy	0.30	17	120	Kumar (1986)
Jute*	Epoxy	0.30	14	-	Cichocki and Thomason (2002)
Jute*	PP	0.28	12	120	Karmaker and Hinrichsen (1991)
Sisal	PE	0.22	1	30	Kalaprasad et al. (1997)
Sisal	**Epoxy**	**0.35**	**15**	**180**	**Oksman et al. (2002)**
Sisal	Epoxy	0.30	9	200	Rong et al. (2001)
Sisal	Polyester	0.21	-	70	Mishra et al. (2003)

* *Textile yarn*

The results in this study on tensile properties of composites with different yarn types are presented in Tables 4.12 and 4.13. It should be noted that composite parameters are different in the two tables, and the results cannot be directly compared between the tables. Table 4.13 shows that for hemp yarn composites with V_f in the range 0.30-0.34, stiffness is in the range 16-20 GPa and ultimate stress is in the range 190-220 MPa. These properties are superior to most of the previously reported properties of aligned plant fibre composites (Table 4.11). However, they are comparable to the results of a few studies such as Roe and Ansell (1985), Oksman (2001) and Oksman et al. (2002) (marked in bold in Table 4.11). In particular, the study of Oksman (2001) is noteworthy. A stiffness of 22 GPa and an ultimate stress of 195 MPa are reported for flax/epoxy composites with a V_f of only 0.21. The flax fibres were retted and extracted by a biotechnical process using enzymes and microbial cultures, and this might explain their good tensile properties.

TABLE 4.12. *Axial tensile properties of composites with different yarn types. Data are means ± stdv. (n=5). The composites were fabricated by film-stacking and a process temperature of 190 °C, and the conditioning humidity was uncontrolled. In brackets are given the estimated fibre properties as calculated by equations (4.53) and (4.54).*

Yarn type	Matrix type	V_f	V_p	Stiffness (GPa)	Ultimate stress (MPa)	Strain at ultimate stress
He53	PP^D	0.415	0.057	21.1 ± 0.9 (54.8)	215 ± 8 (553)	0.022 ± 0.001
He91	PP^H	0.474	0.060	22.8 ± 1.7 (52.5)	233 ± 14 (532)	0.023 ± 0.002
Fl64	PP^H	0.420	0.044	26.9 ± 1.4 (67.6)	251 ± 8 (629)	0.015 ± 0.001

TABLE 4.13. *Axial tensile properties of composites with different yarn types. Data are means ± stdv. (n=6). The composites were fabricated by commingled filament-winding and a process temperature of 200 °C, and they were conditioned at 65 % RH before testing. In brackets are given the estimated fibre properties as calculated by equations (4.53) and (4.54).*

Yarn type	Matrix type	V_f	V_p	Stiffness (GPa)	Ultimate stress (MPa)	Strain at ultimate stress
He47	PET	0.313	0.028	20.1 ± 0.6 (62.0)	221 ± 5 (646)	0.018 ± 0.0004
He53	PET	0.335	0.031	17.6 ± 0.7 (50.6)	205 ± 5 (533)	0.029 ± 0.002
He91	PET	0.302	0.035	16.1 ± 0.4 (51.0)	187 ± 8 (533)	0.024 ± 0.001

The reinforcement efficiency of the four different yarn types used in this study (He47, He53, He91 and Fl64) can be estimated by equations (4.53) and (4.54) (p. 117), which calculate fibre tensile properties from composite tensile properties. These fibre estimates are also shown in Tables 4.12 and 4.13. The two yarn types with the largest reinforcement efficiency are Fl64 and He47. The fibre stiffness is 68 and 62 GPa, and the fibre ultimate stress is 629 and 646 MPa, for the two yarn types, respectively. In contrast, the estimated fibre properties of He53 and He91 are clearly lower, and moreover, they are nearly identical for the two yarn types in both tables. The grand mean fibre stiffness and ultimate stress for He53 and He91 are about 52 GPa and 538 MPa, respectively.

The estimated fibre properties of the three hemp yarn types (He47, He53 and He91) are well correlated with findings from the measurements of yarn tensile properties (see Table 4.6, p. 67): stiffness and ultimate stress are larger for He47 than for He53 and He91, which in turn have nearly identical tensile properties. Figure 4.34 shows stress-strain curves of yarn and composite samples based on He47, He53 and He91. The shape of the yarn curves is different between the yarn types, and this difference is reflected in the composite curves. Overall, the results show that measurements of yarn properties might be a fast and reliable method to estimate composite properties. However, the conversion between yarn and composite tensile behaviour requires more investigations in order to elucidate the underlying mechanical mechanisms.

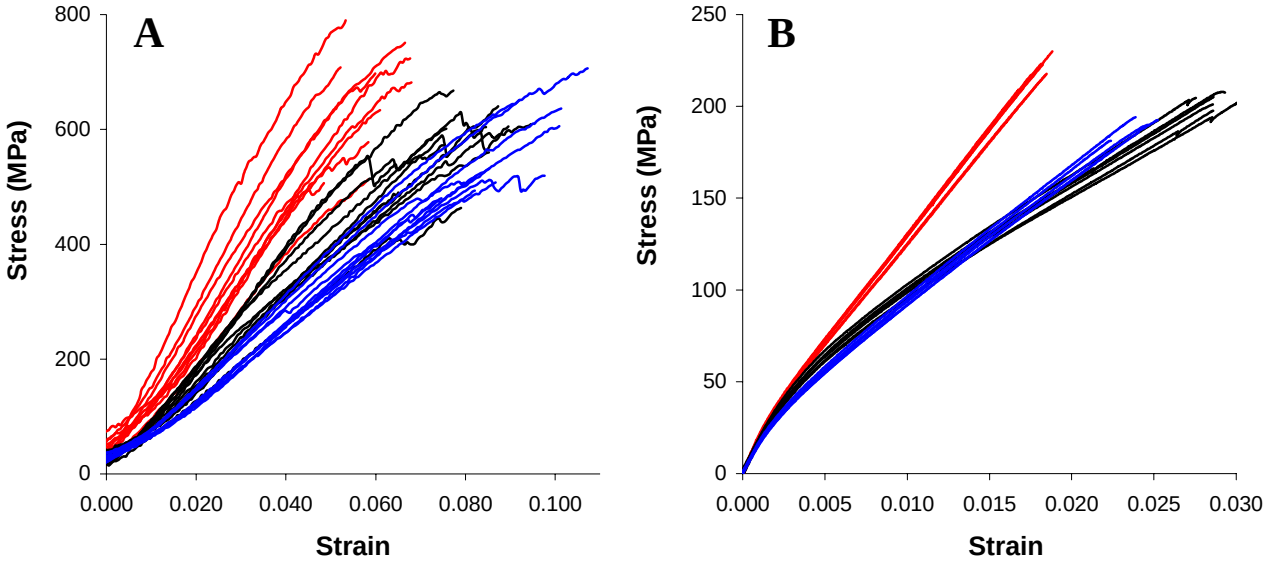

FIGURE 4.34. *Stress-strain curves of He47 (red lines), He53 (black lines) and He91 (blue lines). Shown are the results of tensile tests of (**A**) yarn samples and (**B**) composite samples tested in the axial direction. (**A**) is identical to Figure 4.9. See specifications of composites in Table 4.13.*

Table 4.14 shows the transverse tensile properties of composites with the yarn types He47, He53 and He91. The corresponding stress-strain curves are shown in Figure 4.35. The stress-strain characteristics are different between the yarn types: composite stiffness and ultimate stress are slightly lower for He47 than for He53 and He91. E.g. transverse stiffness and ultimate stress are 3.2 GPa and 15.1 MPa for the He47 composite, whereas they are 3.5 GPa and 18.8 MPa for the He53 composite. Two explanations can be given for this difference in transverse properties. The slightly lower fibre twisting angle in He47 as compared to He53 (see Subsection 4.1.4) will make the fibres contribute less to the transverse composite properties (and more to the axial composite properties, which also is observed). Another possible explanation is the larger content of surface lipids in He47 as compared to He53 and He91 (see Table 4.2, p. 55), which presumably will have a negative effect on the bonding between fibres and matrix.

TABLE 4.14. *Transverse tensile properties of composites with different yarn types. Data are means ± stdv. (n=4). See specifications of composites in Table 4.13.*

Yarn type	Matrix type	V_f	V_p	Stiffness (GPa)	Ultimate stress (MPa)	Strain at ultimate stress
He47	PET	0.313	0.028	3.2 ± 0.08	15.1 ± 0.3	0.006 ± 0.0003
He53	PET	0.335	0.031	3.5 ± 0.08	18.8 ± 0.2	0.008 ± 0.0007
He91	PET	0.302	0.035	3.5 ± 0.04	18.0 ± 0.4	0.006 ± 0.0003

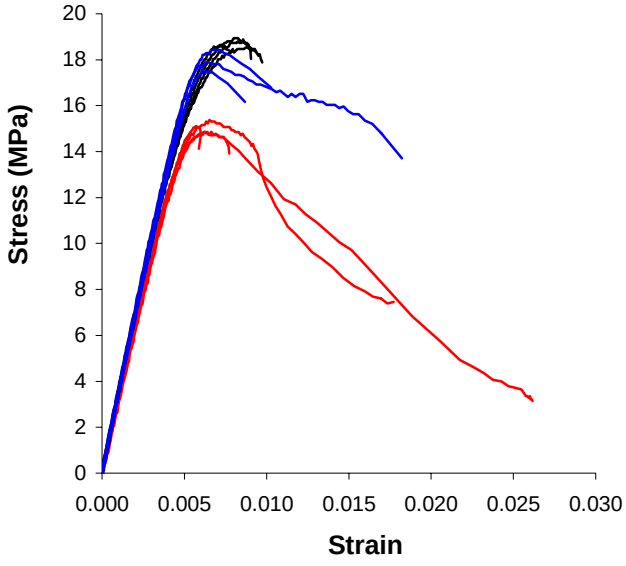

FIGURE 4.35. *Stress-strain curves for PET matrix composites tested in the transverse direction. Shown are results from composites with He47 (red lines), He53 (black lines) and He91 (blue lines). Sample size is 4 for each yarn type. See specifications of composites in Table 4.13.*

Conclusively, it can be stated that the reinforcement efficiency of the applied plant fibre yarns is fairly good in comparison to the previously reported tensile properties of aligned plant fibre composites. Moreover, it is found that yarn and composite tensile properties are closely reflecting each other, which underlines the need for a better understanding of yarn mechanical behaviour in order to estimate fibre properties (and composite properties). Finally, the results demonstrate that even if He47 and He53 are identical from a textile point of view, they are markedly different from each other in relation to composite reinforcement.

4.5.4 Matrix type

As can be observed in Table 4.11 (p. 103) only two studies of aligned plant fibre composites have used a thermoplastic matrix (Karmaker and Hinrichsen 1991, Kalaprasad et al. 1997). Nevertheless, the general trend in industrial plant fibre composites is an increasing use of thermoplastics in relation to thermosettings (Clemons 2000, Karus et al. 2002). The low polarity of thermoplastics is however a central disadvantage with respect to the compatibility between plant fibres and the thermoplastic matrix. In this study PET was used as the standard thermoplastic matrix type, and PE and PP were applied to investigate the effect of a changed fibre/matrix compatibility. The polarity of the terephthalate group in PET makes it more polar, and therefore less hydrophobic as compared to PE and PP, which consist of pure hydrocarbon chains (Figure 4.36).

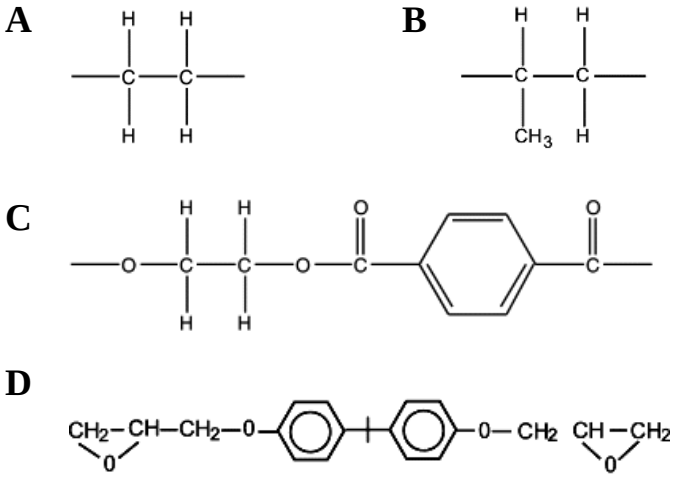

FIGURE 4.36. *Chemical structure of (**A**) PE, (**B**) PP, (**C**) PET and (**D**) epoxy (diglycidyl ether of bisphenol A). (**A**)-(**C**) are from Muzzy (2000) and (**D**) is from Varma and Gupta (2000).*

Table 4.15 presents the measured tensile properties of PET, PE and PP (pure matrix laminates). Representative stress-strain curves are shown in Figure 4.37A. Stiffness and ultimate stress of PET are 2.7 GPa and 60 MPa, respectively. Moreover, PET displays nearly no plastic deformation (strain at ultimate stress ≈ strain at failure). Thus, PET is a rather brittle thermoplastic polymer with tensile properties that are comparable to thermosetting polymers: e.g. epoxy with stiffness and ultimate stress of about 3.5 GPa and 50 MPa, respectively (Hull and Clyne 1996). The stress-strain characteristics of PE and PP are more like typical thermoplastic materials with low stiffness, low ultimate stress, and substantial plastic deformation beyond the yielding point.

TABLE 4.15. *Tensile properties of PET, PP and PE. Data are means ± stdv. (n=7). The pure matrix laminates were fabricated with a process temperature of 200 °C, and conditioned at 65 % RH before testing.*

Matrix type	Stiffness (GPa)	Ultimate stress (MPa)	Strain at ultimate stress	Strain at failure	Poisson's ratio
PET	2.7 ± 0.1	60 ± 1.2	0.028 ± 0.001	0.030 ± 0.003	0.37 ± 0.02
PE	1.1 ± 0.1	18 ± 0.3	0.131 ± 0.030	> 0.2	0.51 ± 0.02
PP	1.7 ± 0.1	28 ± 0.5	0.088 ± 0.017	> 0.2	0.41 ± 0.03

Axial tensile properties of He53 composites with the three matrix types are shown in Table 4.16. Representative stress-strain curves are shown in Figure 4.37B. Stiffness and ultimate stress are lower for the PE and PP matrix composites, as compared to the PET matrix composite. E.g. stiffness and ultimate stress are 15.4 GPa and 173 MPa for the PP matrix composite, whereas they are 17.6 GPa and 205 MPa for the PET matrix composite. This difference in tensile properties of the composites is expected from the difference in tensile properties of the matrix types. The difference in matrix properties can be equalized by estimating fibre properties from composite properties (see Subsection 4.5.5), and these estimates are also presented in Table 4.16. Fibre stiffness and ultimate stress are more or less the same irrespective of matrix type. Thus, the results point towards that the reinforcement efficiency of the fibres is unaffected by the change in fibre/matrix compatibility.

Table 4.16 presents also results on composite V_p, and shows that V_p is slightly lower for the PET matrix composite than for the PE and PP matrix composites. This correlates well with the larger fibre/matrix compatibility in the PET matrix composites.

TABLE 4.16. *Axial tensile properties of composites with different matrix types. Data are means ± stdv. (n=6). The composites were fabricated by commingled filament-winding and a process temperature of 200 ℃, and conditioned at 65 % RH before testing. In brackets are given the estimated fibre properties as calculated by equations (4.53) and (4.54).*

Matrix type	Yarn type	V_f	V_p	Stiffness (GPa)	Ultimate stress (MPa)	Strain at ultimate stress
PET		0.335	0.031	17.6 ± 0.7 (50.6)	205 ± 5 (533)	0.029 ± 0.002
PE	He53	0.319	0.034	15.8 ± 0.3 (50.7)	161 ± 3 (513)	0.027 ± 0.002
PP		0.322	0.036	15.4 ± 0.4 (47.9)	173 ± 5 (530)	0.030 ± 0.001

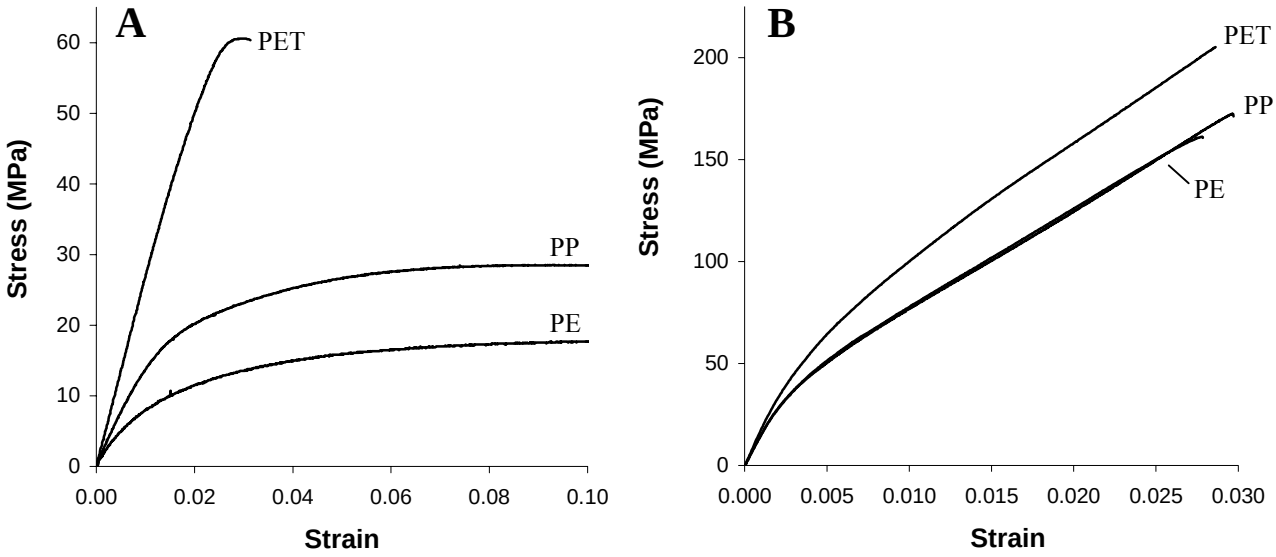

FIGURE 4.37. *Representative stress-strain curves of (**A**) pure matrix laminates and (**B**) composite laminates with different matrix types. See more specifications of laminates in Tables 4.15 and 4.16.*

The above considerations on fibre/matrix compatibility are impeded by the use of different matrix types with different tensile properties. Moreover, the assumed positive correlation between matrix polarity and fibre/matrix compatibility is related to how intimately the fibres are wetted by the matrix, and the properties of the fibre/matrix interface are therefore not changed dramatically. To improve the investigations of fibre/matrix compatibility, two matrix types are required with the same tensile properties but with markedly different compatibility for plant fibres. This was accomplished by the use of the matrix types PP^D and MAPP. Tensile properties of PP^D and MAPP were measured in a study by Andersen and Plackett (2002) to be 1.6 and 1.8 GPa for stiffness and 27.7 and 29.2 MPa for ultimate stress, respectively. Thus, PP^D and MAPP have approximately identical tensile properties, which moreover are comparable to the measured properties of PP (see Table 4.15). As noted above, the low polarity of PP means that the fibre/matrix compatibility is low. In contrast, the maleic anhydride groups in MAPP are known to form covalent bonds and

hydrogen bonds with the hydroxyl groups on the surface of plant fibres (Cantero et al. 2003a), and this have been reported to improve the tensile properties of randomly oriented plant fibre composites (Myers et al. 1991, Cantero et al. 2003b) (see also Subsection 2.5.1).

Axial and transverse tensile properties of He53/PP^D and He53/MAPP composites are shown in Table 4.17. Representative stress-strain curves are shown in Figure 4.38. Axial stiffness and ultimate stress are almost identical for PP^D and MAPP matrix composites. These findings correlate well with a study on unidirectional glass fibre composites, which also showed no difference in axial tensile properties between PP and MAPP matrix composites (Gamstedt et al. 1999). For perfectly aligned and continuous fibre composites, such as unidirectional glass fibre composites, the fibres are loaded in the fibre direction, and therefore the properties of the fibre/matrix interface are of minor importance. However, the twisted and discontinuous fibres in plant fibre yarn composites should expectedly make the interface properties more important. Nevertheless, the obtained results cannot verify these expectations. This is furthermore supported by the estimated fibre properties in Table 4.17, which show that fibre stiffness and ultimate stress are slightly lower for the MAPP matrix composite than for the PP^D matrix composite. Thus, the reinforcement efficiency of He53 is in fact slightly reduced in the MAPP matrix composite.

TABLE 4.17. *Tensile properties of composites with different matrix types. Data are means ± stdv. (n=5). The composites were fabricated by film-stacking and a process temperature of 190 °C, and the conditioning humidity was uncontrolled. For the axial properties in brackets are given the estimated fibre properties as calculated by equations (4.53) and (4.54).*

Matrix type	Yarn type	V_f	V_p	Test. direc.	Stiffness (GPa)	Ultimate stress (MPa)	Strain at ultimate stress
PP^D	He53	0.415	0.057	0°	21.1 ± 0.9 (54.8)	214.5 ± 8.0 (553)	0.022 ± 0.001
MAPP		0.396	0.040	0°	20.1 ± 0.9 (45.8)	208.1 ± 6.4 (539)	0.019 ± 0.001
PP^D	He53	0.401	0.040	90°	1.8 ± 0.1	7.6 ± 0.8	0.023 ± 0.006
MAPP		0.346	0.026	90°	2.5 ± 0.1	16.3 ± 0.9	0.014 ± 0.004

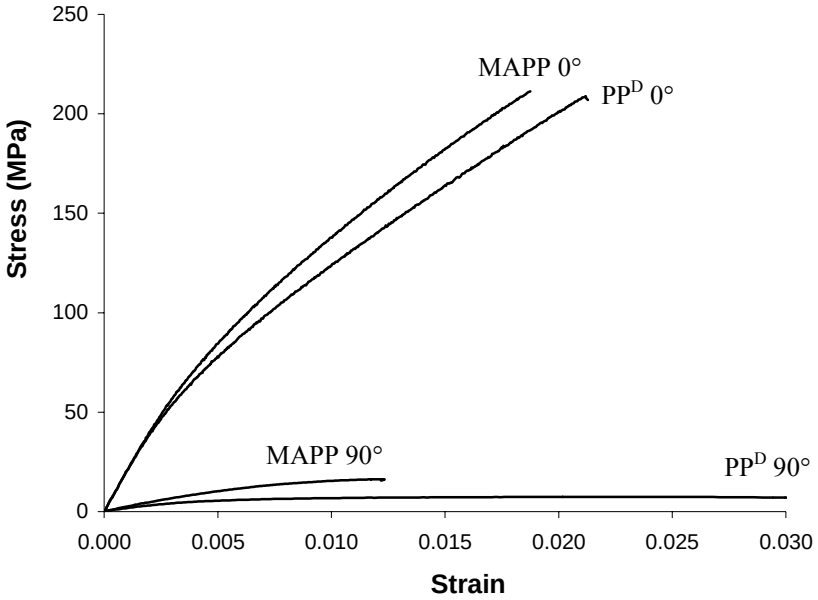

FIGURE 4.38. *Representative stress-strain curves of He53 composites with a PP^D or a MAPP matrix tested in the axial (0°) and transverse direction (90°). See specifications of composites in Table 4.17.*

Even though axial properties are not different between PP^D and MAPP matrix composites, Figure 4.39 shows that axial failure characteristics are radically different. For tensile specimens with a PP^D matrix the failure is characterised by several cracks along the fibres, whereas the specimens with a MAPP matrix fails by a single crack transverse to the fibres. This correlates well with the difference in fibre/matrix interface properties. In the PP^D matrix composite the cracks at failure are induced to progress along the weak interface between fibres and matrix. In the MAPP matrix composite the cracks are induced to progress directly through the fibres because of the strong fibre/matrix interface. Similar changes in failure characteristics as an effect of changes in fibre/matrix interface properties have also been observed for unidirectional glass and carbon fibre composites (Drzal and Madhukar 1993).

The failure characteristics for tensile specimens tested in the transverse direction are identical for PP^D and MAPP matrix composites; all specimens failed abruptly like the specimens in Figure 4.39B. However, Table 4.17 shows that transverse tensile properties are not identical for the two types of matrix composites (see also stress-strain curves in Figure 4.38). Transverse stiffness and ultimate stress are 2.5 GPa and 16 MPa, respectively, for the MAPP matrix composite, whereas they are 1.8 GPa and 8 MPa for the PP^D matrix composite. Moreover, transverse strain at ultimate stress is lower for the MAPP matrix composite. In an idealized model of transverse loading in unidirectional composites, the load is carried equally by fibres, matrix and fibre/matrix interface. Thus, transverse tensile properties are directly related to the properties of the fibre/matrix interface, and this correlates well with the measured larger transverse stiffness and ultimate stress of the MAPP matrix composite.

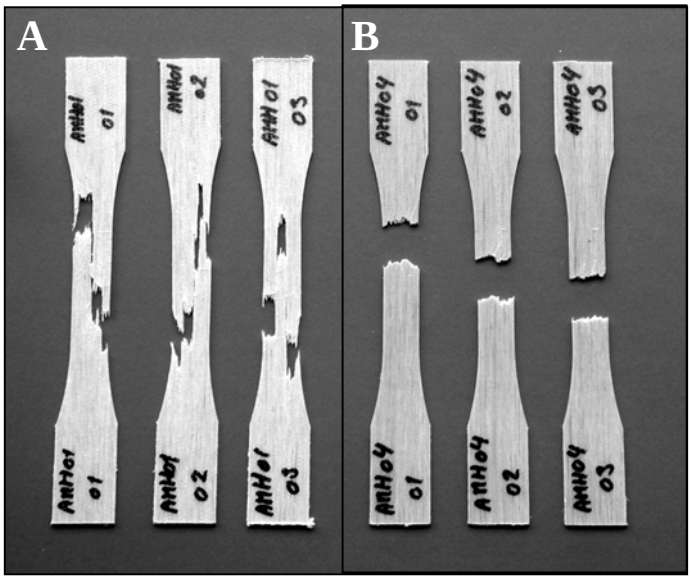

FIGURE 4.39. *Failure characteristics of (**A**) He53/PP^D and (**B**) He53/MAPP tensile specimens tested in the axial direction. See specifications of composites in Table 4.17.*

4.5.5 Fibre volume fraction

The tensile properties of aligned fibre composites are predominately affected by V_f and therefore this parameter needs to be accurately determined in order to assess the relatively smaller effect of other parameters. V_f can be determined directly by image analysis of polished composite cross-sections, such as the example shown in Figure 4.40. However, this requires that a number of assumptions are made to be able to optically distinguish between fibre, matrix and porosity parts in the images.

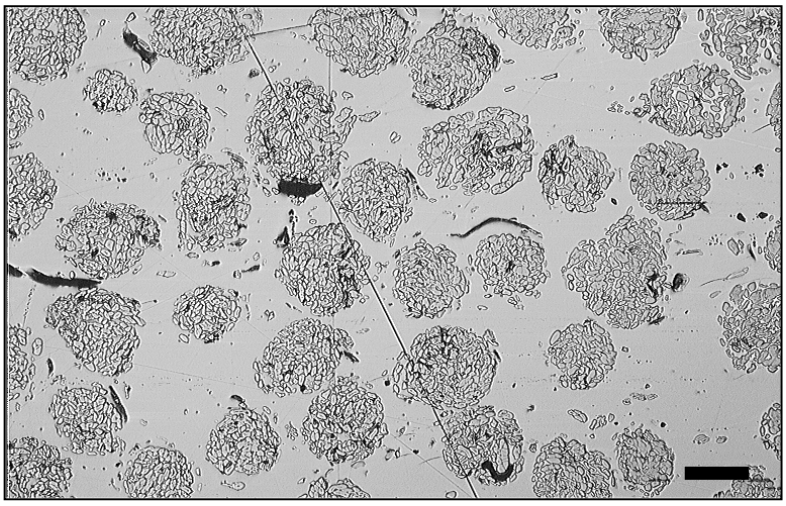

FIGURE 4.40. *OM image of a polished He53/PET composite cross-section. V_f is determined gravimetrically to be 0.31. The irregularly shaped black flecks appear not to be integrated parts of the composite, but are presumable impurities induced during the polishing process. Scale bar is 200 μm.*

Composite V_f is typically estimated indirectly from gravimetric and volumetric measurements of the composite laminate and its constituents. In one commonly applied method (Roe and Ansell 1985, Mohanty and Misra 1995, Oksman et al. 2002), V_f is estimated from the laminate volume (v_c), the laminate weight (m_c), the fibre weight (m_f), and the matrix density (ρ_m):

$$V_f = \frac{v_c - \frac{m_c - m_f}{\rho_m}}{v_c} \tag{4.39}$$

The method is fast and uncomplicated since it only requires knowledge of v_c, m_c and m_f, which are easily determined, and ρ_m which is normally given by the supplier. However, it is based on determination of the matrix volume, and therefore the estimated V_f includes the content of porosity in the composite laminate. Thus, for composites with low V_f (and low V_p) equation (4.39) is probably acceptable, but for composites with V_f approaching $V_{f\,(max)}$, the equation severely overestimates V_f (see Section 4.3). Consequently, V_f of aligned plant fibre composites has been reported in some studies to be above 0.70 (Hepworth et al. 2000, Rong et al. 2001), which even for unidirectional glass fibre composites is regarded as impracticable (Hull and Clyne 1996). A more accurate method to estimate composite V_f is based on determination of the fibre volume (Bisanda and Ansell 1991):

$$V_f = \frac{\frac{m_f}{\rho_f}}{v_c} \tag{4.40}$$

This method requires that ρ_f is accurately measured, and it must be assessed whether the absolute or apparent fibre density should be applied (see Subsection 4.1.2). The method is suitable if the fabricated laminate is perfectly quadrangular, but if it deviates from this shape the determination of v_c becomes inaccurate. Instead, equation (4.40) can be modified to apply for small laminate samples where laminate density (ρ_c) can be determined by the buoyancy method:

$$V_f = \frac{\frac{m_f}{\rho_f}}{v_c} = \frac{\frac{m_f}{\rho_f}}{\frac{v_c}{m_c}} \quad \Rightarrow \quad V_f = \frac{\rho_c}{\rho_f} W_f \tag{4.41}$$

This approach is the one applied in this study. With a thermosetting matrix, composite W_f cannot readily be determined, and must be approximated; e.g. by the area weight of the fibre assembly (Nordin and Berglund 2002). However, with a thermoplastic matrix, W_f can be determined by chemically dissolving the matrix material: e.g. PET is dissolved by hexafluoro-2-propanol, and PE and PP is dissolved by xylene. If commingled filament winding is used for fibre/matrix mixing, W_f can also be determined from the yarn linear densities of fibres and matrix (see equation (3.4), p. 46).

By rearranging equation (4.41), composite V_m can be calculated and subsequently composite V_p is determined by the volume fraction not taken up by the fibre and matrix parts:

$$V_m = \frac{\rho_c}{\rho_m}\left(1 - W_f\right) \quad ; \quad V_p = 1 - \left(V_f + V_m\right) \qquad (4.42)\ ;\ (4.43)$$

Based on a He47/PET composite laminate, Table 4.18 presents an example of the determination of composite V_f and V_p. The measured ρ_c is essentially identical for the three laminate samples. Likewise, ρ_f is also measured with a small variation (see Table 4.3, p. 58). Thus, an accurate determination of W_f is critical. Table 4.18 shows results of W_f determined by two methods. In method A, W_f was determined from the yarn linear densities of fibres and matrix (equation (3.4), p. 46), and it represents therefore a mean value for the entire laminate. In method B, W_f was determined for each of the samples by chemically dissolving the matrix, and they represent therefore local values. It can be observed that W_f determined by method B is larger than W_f determined by method A, and consequently, differences arise in the determined V_f and V_p. The difference in W_f determined by the two methods was observed for all laminates in this study. No arguments have been found to support that local values of W_f are consistently larger than the mean value of W_f. It is therefore deduced that the chemical dissolvement of the matrix in method B is insufficient and a small portion of matrix remained on the fibres, which tends to increase W_f. Consequently, method A has been applied to determine composite W_f.

TABLE 4.18. *Example of the determination of volume parts in a He47/PET composite laminate. Two methods were used to determine W_f. Equations (4.19)-(4.21) were used to calculate V_f and V_p. See text for more details.*

Sample	ρ_c	W_f		V_f		V_p	
no	(g/cm^3)	Method A	Method B	Method A	Method B	Method A	Method B
1	1.379		0.401		0.350		0.033
2	1.384	0.359	0.400	0.314	0.350	0.026	0.030
3	1.380		0.387		0.338		0.030
Mean	**1.381**	**0.359**	**0.396**	**0.314**	**0.346**	**0.026**	**0.031**
Stdv.	**0.002**		**0.008**		**0.007**		**0.002**

Shown in Figure 4.41 are representative stress-strain curves of He47/PET composites with different V_f. For composites tested in the axial direction the curves are shifted upwards as a function of V_f, but with identical strain at ultimate stress. However, for composites tested in the transverse direction the stress-strain curves are less consistently affected by V_f. The curves are almost identical at the two low values of V_f, but the curve at the high V_f is shifted downwards. Strain at ultimate stress (and strain at failure) is however nearly identical for all three curves. When aligned fibre composites are tested in the axial direction, the fibre and matrix parts are loaded in parallel and therefore they are strained equally. Thus, composite axial properties are governed by the stiff and strong fibres. This means that the stress-strain curves in Figure 4.41A are approaching the stress-strain curve of the fibres when composite V_f is increased, and moreover, composite strain at ultimate stress is directly related to fibre strain at ultimate stress. In contrast, when the composites are tested in the transverse direction, the fibre and matrix parts are loaded in serial and therefore they are stressed equally. Thus, composite transverse properties are governed by the less stiff and less strong matrix, and the effect of changes in V_f on these properties is therefore less straightforward to predict.

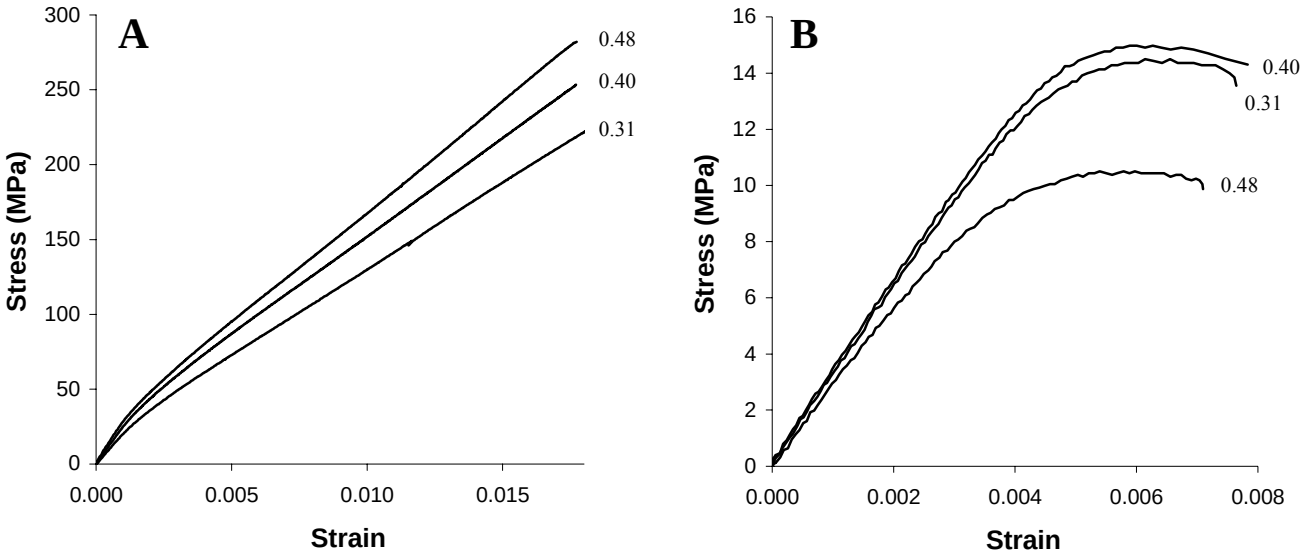

FIGURE 4.41. *Representative stress-strain curves of He47/PET composites with different V_f and tested in (**A**) the axial direction and (**B**) the transverse direction. See specifications of composites in Table 4.13.*

In conventional unidirectional and continuous composites, the traditional way to predict composite axial and transverse properties is to apply the simple "rule-of-mixtures":

$$E_x = V_f\ E_f + (1 - V_f)\, E_m \quad ; \quad \sigma_x = V_f\ \sigma_f + (1 - V_f)\, \sigma_m \qquad (4.44)\ ;\ (4.45)$$

$$E_y = \frac{E_f\ E_m}{(1 - V_f)\, E_f + V_f\ E_m} \quad ; \quad \sigma_y = \frac{\sigma_f\ \sigma_m}{(1 - V_f)\, \sigma_f + V_f\ \sigma_m} \qquad (4.46)\ ;\ (4.47)$$

The model is based on the assumptions of equal strain (equations (4.44) and (4.45)) and equal stress (equations (4.46) and (4.47)) of the fibre and matrix parts as mentioned above, and has proved to be a fairly good approximation to composite properties (Harris 1980, Hull and Clyne 1996). Three initiatives can however be proposed to improve the model:

1) Since fibres and matrix are equally strained in composites tested in the axial direction, it follows that the matrix is not strained to the point of ultimate stress. Consequently, σ_m in equation (4.45) must reflect the stress of the matrix strained to the point of composite failure (σ_{m*}) (Lilholt and Bjerre 1997, Oksman et al. 2002). Likewise, σ_m in equation (4.47) needs also to be adjusted. However, the matrix is strained non-uniformly within composites tested in the transverse direction (Hull and Clyne 1996), and this makes it difficult to select a single value of matrix stress. Thus, for reasons of simplicity, the same σ_{m*} used in equation (4.45) will be used in equation (4.47).

2) The model assumes that tensile properties of both fibres and matrix are isotropic. However, whereas this is an acceptable assumption for the matrix, the tensile properties of most fibre types (plant, carbon and aramid fibres, but not glass fibres) are significantly smaller in the transverse direction than in the axial direction. Consequently, the ratio of fibre anisotropy (*fa*), defined as the ratio between transverse and axial properties, must be multiplied with E_f and σ_m in equation (4.46) and (4.47). For practical reasons, experimental data on transverse fibre properties are limited. In a study on wood fibres, *fa* was estimated to be about 1/9 (Page et al. 1977), and in a study on jute fibres, *fa* was estimated to be about 1/7 (Cichocki and Thomason 2002). A ratio of 1/7 will be used for *fa* in this study.

3) The model assumes that the composites contain no porosity. In addition to the effect of a lower load bearing volume, porosity also affects the tensile properties by introducing stress concentrations in the loaded composite materials (Judd and Wright 1978, Varna et al. 1995). In a theoretical study by MacKenzie (1950) on spherical holes in materials, the effect of porosity on material stiffness was estimated by the equation:

$$E_p = E_d\, (1 - V_p)^2 \qquad (4.48)$$

where the subscripts p and d refer to the porous and the fully dense material, respectively. The same kind of correlation can be found in work by Schjødt-Thomsen and Pyrz (2000) on microcellular foams.

By including the above-proposed adjustments in equations (4.44)-(4.47), the complete and improved model is described by the equations:

$$E_x = \left(V_f\ E_f + \left(1 - V_f\right) E_m\right)\left(1 - V_p\right)^2 \tag{4.49}$$

$$\sigma_x = \left(V_f\ \sigma_f + \left(1 - V_f\right) \sigma_{m*}\right)\left(1 - V_p\right)^2 \tag{4.50}$$

$$E_y = \left(\frac{E_f\ fa\ E_m}{\left(1 - V_f\right) E_f\ fa + V_f\ E_m}\right)\left(1 - V_p\right)^2 \tag{4.51}$$

$$\sigma_y = \left(\frac{\sigma_f\ fa\ \sigma_{m*}}{\left(1 - V_f\right) \sigma_f\ fa + V_f\ \sigma_{m*}}\right)\left(1 - V_p\right)^2 \tag{4.52}$$

Shown in Figures 4.42-4.45 are experimental data of composites stiffness and ultimate stress plotted as a function of V_f. The four figures represent examples of the four different types of plant fibre yarns applied in this study. Also shown in the figures are the numerical outcome of equations (4.49)-(4.52) with V_p=0. This requires however knowledge of E_f and σ_f (E_m and σ_m were measured, see Subsection 4.5.4). These values were taken as the mean E_f and σ_f found by inserting the experimental data of composite stiffness and ultimate stress in the rearranged equations (4.49) and (4.50):

$$E_f = \frac{E_x \left(1 - V_p\right)^{-2} - \left(1 - V_f\right) E_m}{V_f} \quad ; \quad \sigma_f = \frac{\sigma_x \left(1 - V_p\right)^{-2} - \left(1 - V_f\right) \sigma_{m*}}{V_f} \tag{4.53) , (4.54}$$

The experimental data of composite stiffness and ultimate stress in Figures 4.42-4.45 were divided by $(1\text{-}V_p)^2$ to correct for the porosity, i.e. these data points are the expected experimental properties with V_p=0.

Figures 4.42-4.45 show that axial stiffness and ultimate stress of the composites are well predicted by the model. Moreover, transverse stiffness is also well predicted by the model. The model overestimates however transverse stiffness of the Fl64/PP^H composites (Figure 4.45). These composites were fabricated by film-stacking, which means that the fibres were less uniformly

distributed in the matrix, and this might explain their low transverse stiffness. Transverse ultimate stress of the composites is overestimated in all figures. These predictions can be improved by selecting a lower value of σ_{m*} in equation (4.52) (see considerations above), but at present no work have been done to validate such an adjustment.

Figures 4.42-4.45 show that the experimental axial stiffness and ultimate stress of the composites tend to deviate from the linear "rule-of-mixtures" relationship at high V_f, and this is corrected in the model by including composite V_p. The same deviations of axial properties at high V_f have also been observed in other studies of aligned plant fibre composites (Chawla and Bastos 1979, Roe and Ansell 1985, Sanadi et al. 1986, Bos et al. 1997), but no well-documented explanation has been given so far.

In Section 4.3 it is noted that V_f is limited by $V_{f(max)}$. From a practical point of view, this means that the axis of V_f in Figures 4.42-4.45 should end at $V_{f(max)}$, but to depict the model as a whole it was decided to extend the axis to 1.0. The estimated fibre stiffness and ultimate stress can be read from the endpoint of the predicted axial properties with V_p=0.

It can be concluded that the presented modified "rule-of-mixtures" model represents a valuable tool to predict composite properties from V_f and V_p. The good prediction of tensile properties of the composites verifies the application of the model to estimate fibre stiffness and ultimate stress from composite properties.

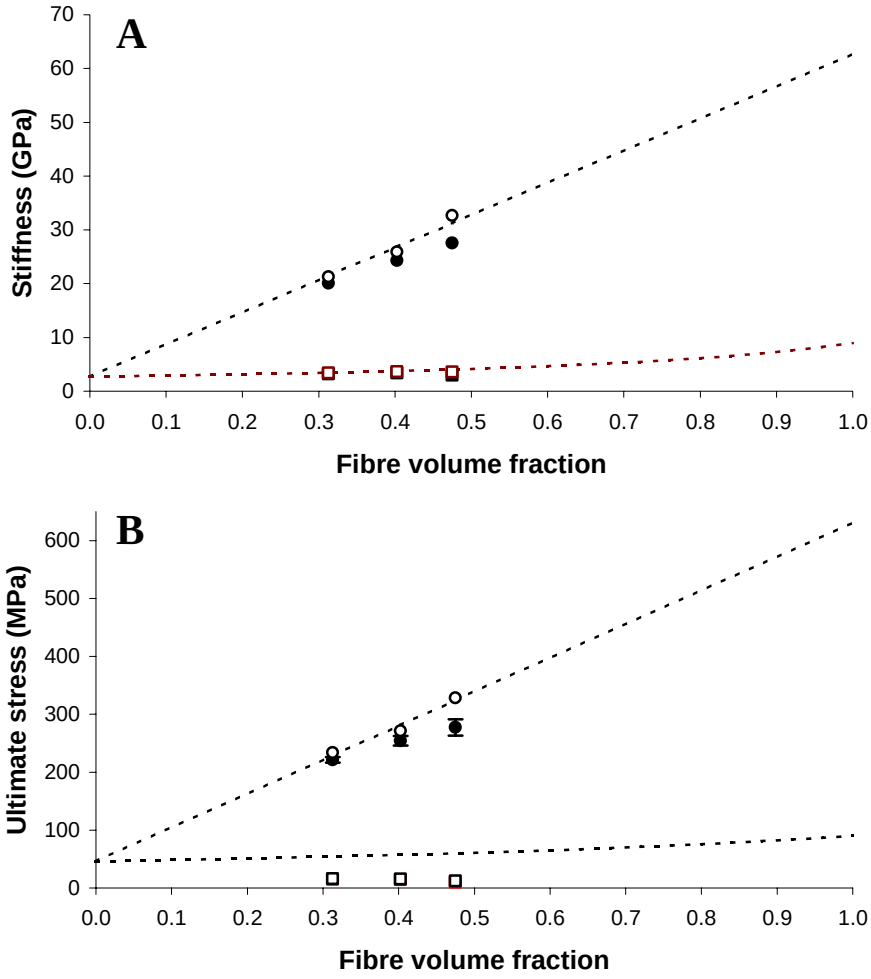

FIGURE 4.42. *Tensile (**A**) stiffness and (**B**) ultimate stress of He47/PET composites as a function of V_f. Shown are axial (o) and transverse (□) properties. Filled symbols are experimental properties and empty symbols are expected experimental properties with V_p=0. Dotted lines are the modified "rules-of-mixtures": equations (4.49)-(4.52) with V_p=0. See specifications of composites in Table 4.13.*

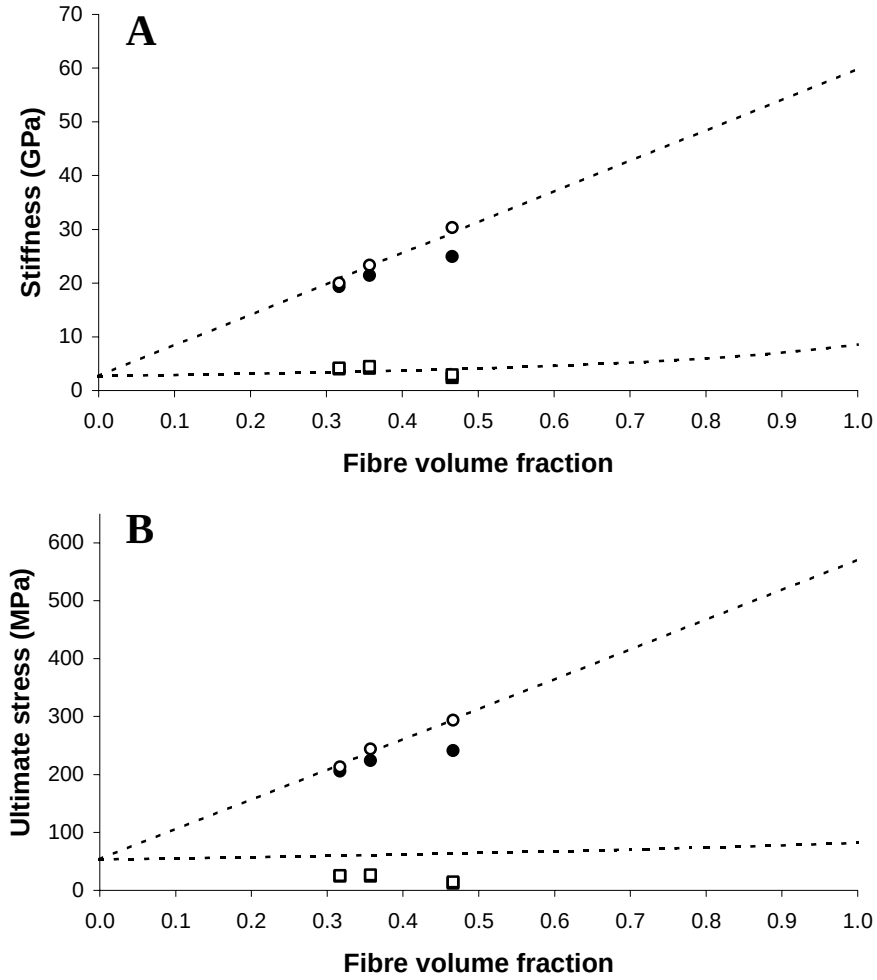

FIGURE 4.43. *Tensile (**A**) stiffness and (**B**) ultimate stress of He53/PET composites as a function of V_f. Shown are axial (o) and transverse (□) properties. Filled symbols are experimental properties and empty symbols are expected experimental properties with V_p=0. Dotted lines are the modified "rules-of-mixtures": equations (4.49)-(4.52) with V_p=0. See specifications of composites in Table 4.13.*

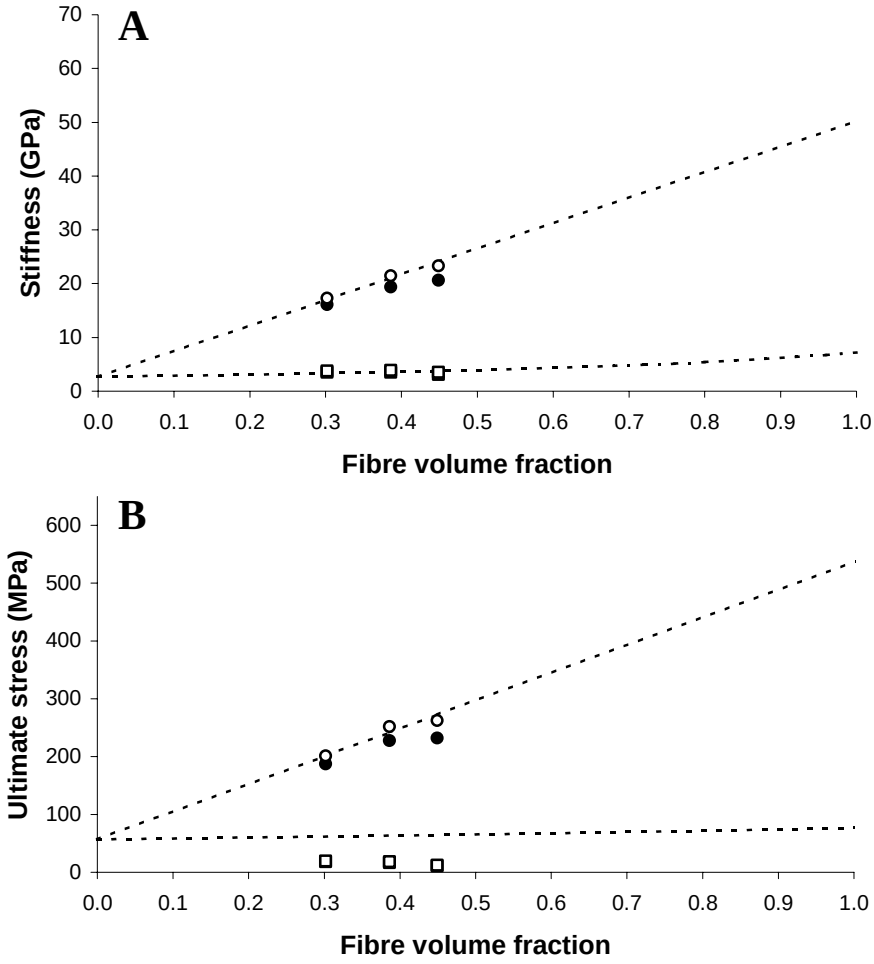

FIGURE 4.44. *Tensile (**A**) stiffness and (**B**) ultimate stress of He91/PET composites as a function of V_f. Shown are axial (o) and transverse (□) properties. Filled symbols are experimental properties and empty symbols are expected experimental properties with V_p=0. Dotted lines are the modified "rules-of-mixtures": equations (4.49)-(4.52) with V_p=0. See specifications of composites in Table 4.13.*

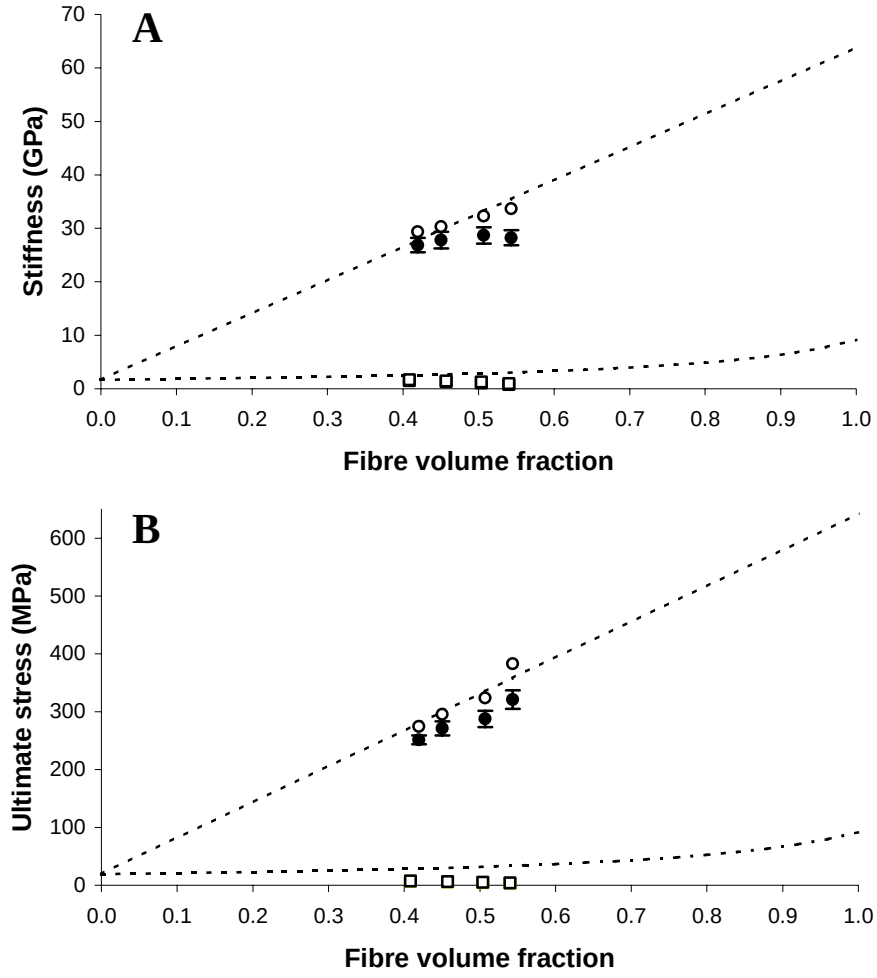

FIGURE 4.45. *Tensile (**A**) stiffness and (**B**) ultimate stress of Fl64/PP^H composites as a function of V_f. Shown are axial (o) and transverse (□) properties. Filled symbols are experimental properties and empty symbols are expected experimental properties with V_p=0. Dotted lines are the modified "rules-of-mixtures": equations (4.49)-(4.52) with V_p=0. See specifications of composites in Table 4.12.*

4.5.6 Process temperature

The fabrication of plant fibre composites with a thermoplastic matrix necessarily involves high process temperatures, and since plant fibres are not intended to sustain these harsh thermal conditions, the potential thermal degradation of the fibres must be expected to influence their tensile properties. In this respect the thermal degradation of cellulose is the main concern. This is a rather controversial subject, but it is generally accepted that thermal heating leads to cellulose chain scission; i.e. the degree of polymerisation is decreased (Gassan and Bledzki 2001 and references cited herein). In addition, the different thermal expansion coefficient of the various plant fibre chemical constituents means that the integrated cell wall structure is disrupted by elevated temperatures (Gassan and Bledzki 2001).

The above-mentioned changes in the chemical and physical structure of plant fibres explain the previously reported decrease in fibre tensile properties as a function of exposure temperature and duration (Brushwood 1988, Hornsby et al. 1997a, Wielage et al. 1999, Gassan and Bledzki 2001). Generally, it can be stated that plant fibre tensile properties start to deteriorate above about 180 °C. This is reflected by thermogravimetric studies of flax fibres (Hornsby et al. 1997a, Wielage et al. 1999, Van de Velde and Kiekens 2002). Below 180 °C there is hardly any loss of fibre mass, whereas the fibre mass is consecutively reduced above this temperature. The studies also show that above about 230 °C the fibre mass starts to decline dramatically, and this temperature might therefore be regarded as the maximum process temperature of plant fibre composites.

Yarn tensile properties of He47 and He53 processed at 180, 200 and 220 °C are presented in Table 4.19. For means of comparison, the results of the unprocessed yarns are also shown in the table. No clear and consistent effect of process temperature can be observed for apparent stiffness and strain at ultimate stress, except that stiffness is slightly reduced at 220 °C for both yarn types. Ultimate stress is however more consistently affected. For both yarn types it is generally decreased when the process temperature is increased; e.g. for He47, ultimate stress is decreased from 621 to 572 MPa when the process temperature is increased from 180 to 220 °C.

TABLE 4.19. *Tensile properties of yarn samples treated by different composite process conditions. Data are means ± stdv. (n=10).*

Yarn type	Process conditions	Stiffness (GPa)	Ultimate stress (MPa)	Strain at ultimate stress
He47	None	13.2 ± 2.1	658 ± 98	0.059 ± 0.007
	180 °C	14.5 ± 2.5	621 ± 61	0.061 ± 0.009
	200 °C	14.8 ± 2.2	568 ± 56	0.051 ± 0.007
	220 °C	12.0 ± 1.5	572 ± 67	0.057 ± 0.006
He53	None	9.3 ± 1.3	581 ± 63	0.081 ± 0.009
	180 °C	9.1 ± 1.1	533 ± 46	0.097 ± 0.011
	200 °C	10.6 ± 0.8	551 ± 53	0.082 ± 0.013
	220 °C	7.8 ± 0.9	494 ± 53	0.081 ± 0.006

Shown in Tables 4.20 and 4.21 are axial tensile properties of He47/PET and He47/PE composites processed at different temperatures. Ultimate stress of the composites is decreased when the process temperature is increased, which also is expected from the similar trend in yarn tensile properties. The decline in ultimate stress is most marked from 200 to 220 °C. The presented estimates of fibre ultimate stress reveal even more clearly the negative effect of process temperature. The tables show moreover that strain at ultimate stress of the composites is decreased when the process temperature is increased. Figure 4.46 shows representative stress-strain curves corresponding to the results in Tables 4.20 and 4.21. The three curves for each of the two types of composites are nearly identical irrespective of the process temperature; only the failure points are changed. This point towards that the effect of thermal degradation is mainly confined to the failure mechanisms in the fibres, and they fail prematurely in the composites at high process temperatures. Tables 4.20 and 4.21 show that stiffness of the composites is slightly increased, when the process temperature is increased. This is rather unexpected, but it might be related to the temperature dependent porosity of the composites (see below).

TABLE 4.20. *Axial tensile properties of He47/PET composites processed at different temperatures. The composites were fabricated by commingled filament-winding and conditioned at 65 % RH before testing. In brackets are given the estimated fibre properties as calculated by equations (4.53) and (4.54).*

Proc. temp. (°C)	V_f	V_p	Stiffness (GPa)	Ultimate stress (MPa)	Strain at ultimate stress
180	0.308	0.043	19.4 ± 0.4 (62.7)	244 ± 4 (748)	0.021 ± 0.0002
200	0.313	0.028	20.1 ± 0.6 (62.0)	221 ± 5 (646)	0.018 ± 0.0004
220	0.316	0.018	22.5 ± 0.5 (68.0)	170 ± 12 (489)	0.012 ± 0.0012

TABLE 4.21. *Axial tensile properties of He47/PE composites processed at different temperatures. The composites were fabricated by commingled filament-winding and conditioned at 65 % RH before testing. In brackets are given the estimated fibre properties as calculated by equations (4.53) and (4.54).*

Proc. temp. (°C)	V_f	V_p	Stiffness (GPa)	Ultimate stress (MPa)	Strain at ultimate stress
180	0.324	0.048	20.0 ± 0.2 (65.8)	193 ± 4 (634)	0.018 ± 0.0006
200	0.326	0.042	20.4 ± 0.5 (65.9)	180 ± 3 (581)	0.016 ± 0.0005
220	0.326	0.043	20.8 ± 0.3 (67.4)	136 ± 4 (439)	0.011 ± 0.0004

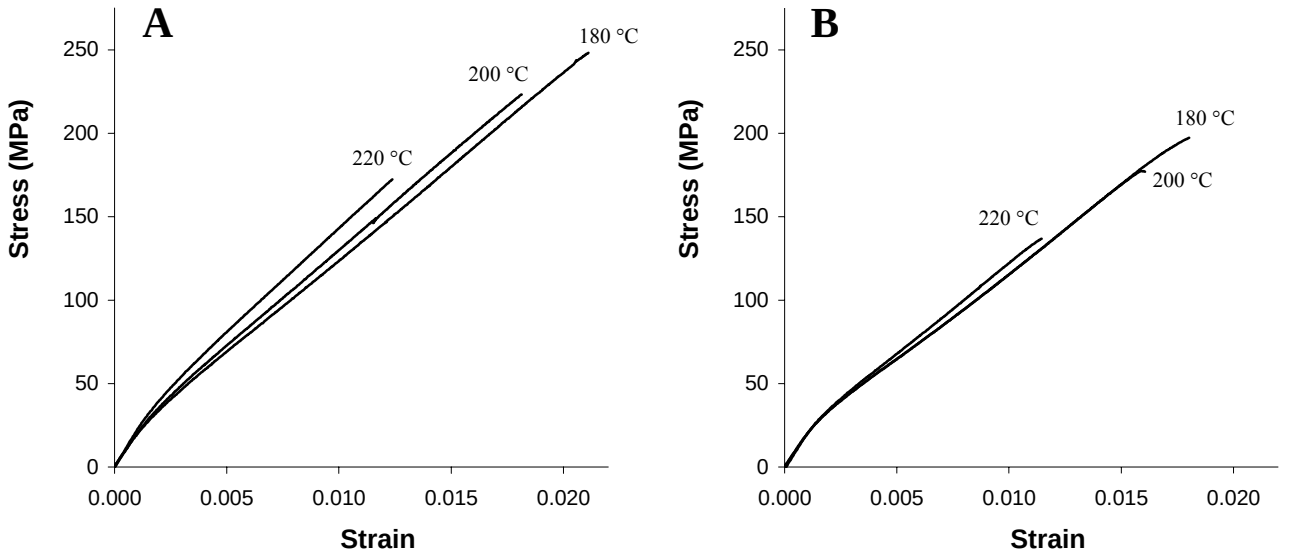

FIGURE 4.46. *Representative stress-strain curves of (**A**) He47/PET and (**B**) He47/PE composites fabricated with different process temperatures. See specifications of composites in Tables 4.20 and 4.21.*

Tables 4.20 and 4.21 show that porosity of the composites is decreased when the process temperature is increased. The change in porosity is most marked in the He47/PET composites; e.g. the porosity is decreased from 0.043 to 0.018 when the temperature is increased from 180 to 220 °C. A central controlling factor regarding composite porosity is matrix viscosity. Figure 4.47A shows results from measurements of PET and PE viscosity as a function of shear rate at the three isothermal conditions: 180, 200 and 220 °C. Viscosity of the two thermoplastics at all temperatures is characterised by shear-thinning, i.e. viscosity is decreased as a function of the shear rate. This is the typical rheological behaviour for thermoplastic polymer melts (Barnes et al. 1989). The effect of temperature on viscosity is however different between PET and PE. PET viscosity is markedly decreased when the temperature is increased, whereas PE viscosity is almost unaffected by the temperature. This is expected since the applied temperatures (180, 200 and 220 °C) are just above the melting temperature of PET ($T_m \approx 170$ °C; the exact T_m for PET is not known, see Section 3.1), but much above the melting temperature of PE (T_m=120 °C). The relationship between composite

porosity and matrix viscosity is shown in Figure 4.47B. In PET matrix composites, the porosity is linearly related to the logarithm of PET viscosity. In contrast, since PE viscosity is more or less unaffected by temperature, no such correlation can be observed for the PE matrix composites.

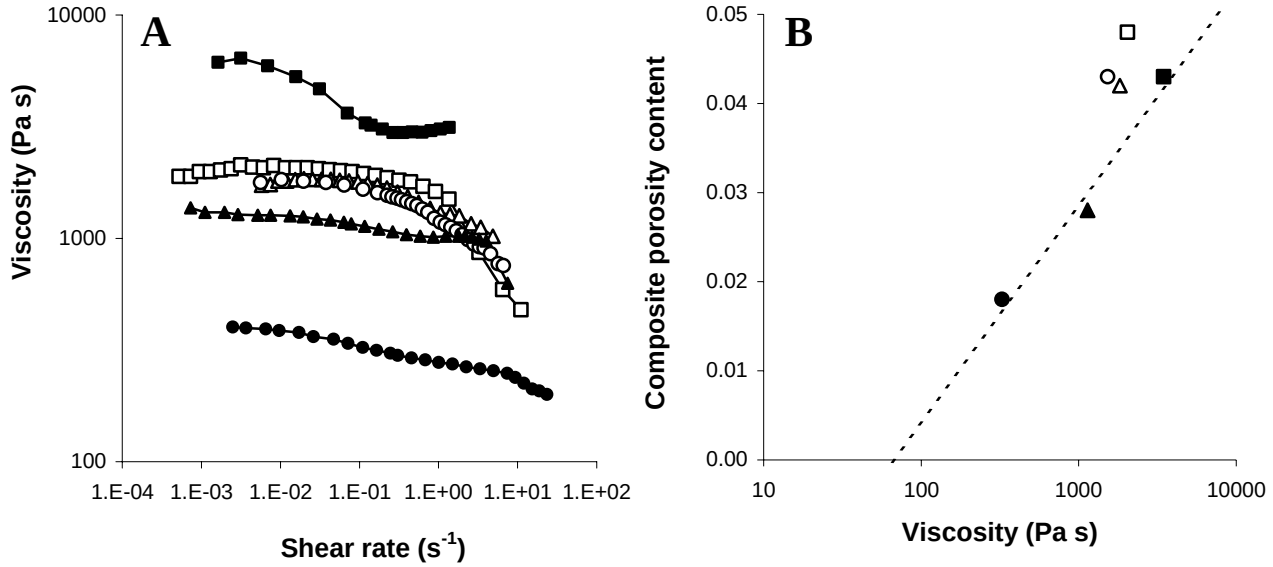

FIGURE 4.47. *Shown in (**A**) is viscosity as a function of shear rate for PET (filled symbols) and PE (empty symbols) at three temperatures: 180 °C (□), 200 °C (Δ) and 220 °C (o). Shown in (**B**) is porosity of He47 composites with PET or PE matrix as a function of matrix viscosity. The viscosity data in (**B**) are mean viscosity calculated from (**A**) in the shear rate interval 0.01-1.00 s^{-1}. The porosity data in (**B**) are from Tables 4.20 and 4.21. The regression line for PET in (**B**) is y=0.0105 ln x – 0.044 (R^2=0.98).*

Figure 4.47B suggest that if PET viscosity is furthermore reduced by increasing the temperature, composite porosity will approach zero at a viscosity of about 65 Pa s. Viscosity as a function of temperature can be estimated by the Arrhenius relationship given by the equation (Barnes et al. 1989):

$$\eta = a\, e^{-\frac{b}{T}} \qquad (4.55)$$

where η is viscosity (Pa s), T is absolute temperature (°K), and *a* and *b* are constants. Based on the experimental data, *a* and *b* are found to be 8.5 10^{-10} and –13174 for PET, and 60.8 and –1598 for PE, respectively. Figure 4.48 shows the determined Arrhenius relationships for PET and PE. According to the predictions, a process temperature of about 250 °C is required to reduce PET viscosity to 65 Pa s, and composite porosity can then be expected to approach zero. However, this needs yet to be verified. A temperature of 250 °C is larger than the stated maximum process temperature of plant fibre composites of about 230 °C, and ultimate stress of such composites can therefore be expected to be very low.

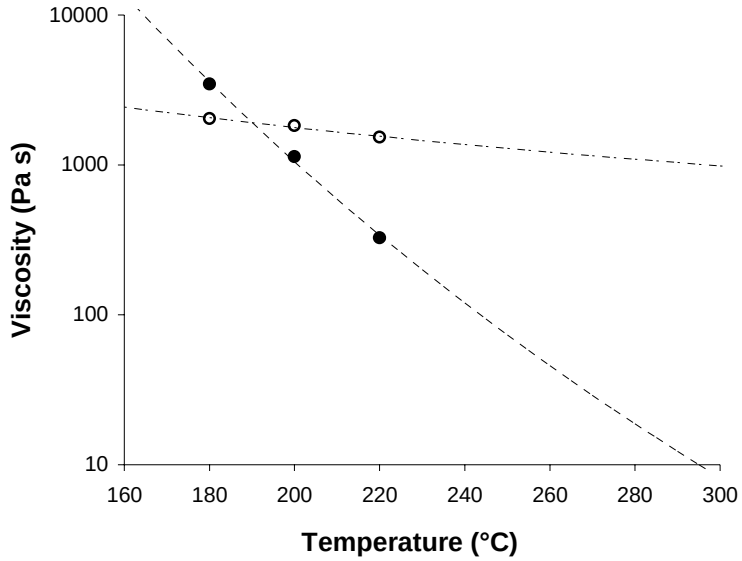

FIGURE 4.48. *Viscosity as a function of temperature for PET (filled symbols) and PE (empty symbols). The dotted lines are the theoretical Arrhenius relationships calculated by equation (4.55).*

4.5.7 Conditioning humidity

In wood technology it is general practice that wood samples are exposed to a controlled ambient air humidity before they properties are measured, and standard conditioning humidity is 65 % RH (Kollmann and Côté 1984). In contrast, most studies of plant fibre composites contain no such reference to a conditioning humidity.

It is shown in Section 4.4 that the water sorption capacity of the applied three thermoplastic matrix types (PET, PE and PP) is very low as compared to the hemp yarn fibres. Thus, the influence of conditioning humidity (or water content) on composite tensile properties is presumably primarily related to the fibres rather than the thermoplastic matrix. Investigations were performed in order to verify these expectations. Tensile specimens of pure PET, PE and PP were conditioned at two extreme humidity conditions (<10 % RH and >99 % RH) to assess the maximum effect of a changed water content. The measured tensile properties of these specimens are presented in Table 4.22, in addition to results from specimens conditioned at 65 % RH. The tensile properties of the three matrix types are generally unaffected by changes in the conditioning humidity below 65 % RH. However, at the high humidity (>99 % RH), strain at ultimate stress is decreased for all three matrix types. Moreover, ultimate stress is decreased and strain at failure is increased for PET at the high humidity. Thus, PET is the matrix type that is most affected by the high water content, and this correlates well with the measured largest water sorption capacity of PET (see Tables 4.9 and 4.10, p. 89). Shown in Figure 4.49 are representative stress-strain curves for PET corresponding to the results in Table 4.22. The curves reveal what is indicated in the table, i.e. the yielding point of PET is decreased at the high humidity, and failure occurs only after considerable plastic

deformation. Despite this change in tensile properties of PET at the high humidity, it will subsequently be assumed that for more moderate levels of humidities, the tensile properties of PET are unchanged. The results obtained at a conditioning humidity of 65 % RH will be used as representative tensile properties of PET.

TABLE 4.22. *Tensile properties of PET, PE and PP conditioned at different relative humidities. Data are means ± stdv. (n=7).*

Matrix type	Rel. hum. (%)	Stiffness (GPa)	Ultimate stress (MPa)	Strain at ultimate stress	Strain at failure	Poisson's ratio
PET	< 10	2.9 ± 0.1	63 ± 0.9	0.028 ± 0.001	0.029 ± 0.001	0.40 ± 0.02
	65	2.7 ± 0.1	60 ± 1.2	0.028 ± 0.001	0.030 ± 0.003	0.37 ± 0.02
	> 99	3.0 ± 0.1	48 ± 0.8	0.020 ± 0.001	0.064 ± 0.025	0.42 ± 0.02
PE	< 10	1.1 ± 0.1	18 ± 0.4	0.125 ± 0.013		0.53 ± 0.04
	65	1.1 ± 0.1	18 ± 0.3	0.131 ± 0.030	> 0.2	0.51 ± 0.02
	> 99	1.1 ± 0.1	18 ± 0.2	0.107 ± 0.008		0.47 ± 0.08
PP	< 10	1.6 ± 0.1	28 ± 0.3	0.091 ± 0.003		0.41 ± 0.02
	65	1.7 ± 0.1	28 ± 0.5	0.088 ± 0.017	> 0.2	0.41 ± 0.03
	> 99	1.6 ± 0.1	27 ± 0.9	0.063 ± 0.006		0.41 ± 0.02

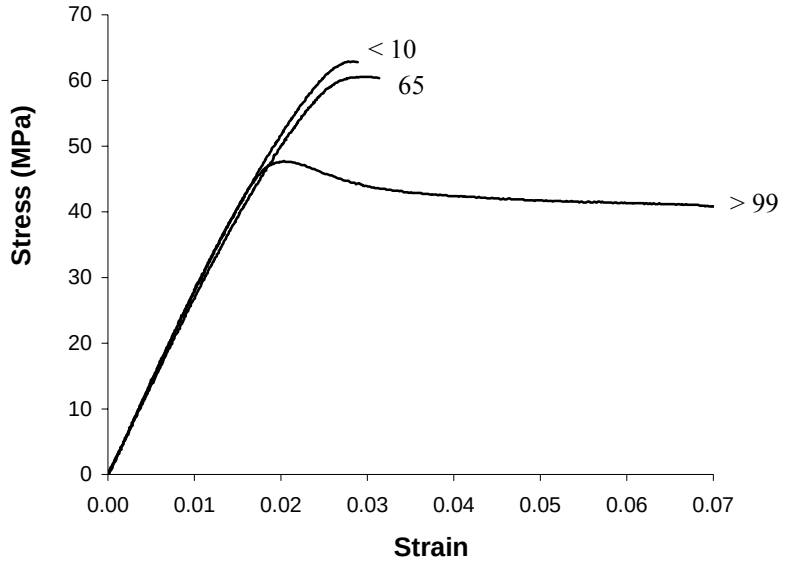

FIGURE 4.49. *Representative stress-strain curves of PET conditioned at different humidities (% RH).*

The results on yarn tensile properties of He53 conditioned at different humidities (35, 65, 85 and 100 % RH) are shown in Table 4.23. The corresponding water contents are shown in Table 4.5 (p. 65). The results demonstrate that for increasing levels of humidity (or water content); stiffness is decreased, ultimate stress is increased and strain at ultimate stress is increased. This can be accounted for in two ways: (i) by the direct effect of bound water in the fibre cell wall, and (ii) by the indirect effect of a changed fibre cross-sectional area; e.g. the larger fibre cross-sectional area at 85 % RH might explain the lower stiffness of the yarn (but not the larger ultimate stress). Equations (3.1) and (3.2) (p. 43) were used to re-calculate stiffness and ultimate stress of the yarn for a dry fibre cross-sectional area. These results are also shown in Table 4.23. Yarn stiffness is decreased as a function of the conditioning humidity even when it is based on a dry fibre cross-sectional area. Thus, the reduction in stiffness is a direct effect of cell wall bound water, and not an effect of an increased fibre cross-sectional area. Moreover, Table 4.23 shows that the increase in ultimate stress of the yarn becomes more pronounced when the counteracting effect of an increased fibre cross-sectional area is eliminated.

TABLE 4.23. *Yarn tensile properties of He53 conditioned at different humidities. Data are means ± stdv. (n=10). For stiffness and ultimate stress in brackets are given the properties calculated for a dry fibre cross-sectional area.*

Humidity. (% RH)	Stiffness (GPa)	Ultimate stress (MPa)	Strain at ultimate stress
35	10.6 ± 2.2 (11.4)	481 ± 58 (517)	0.064 ± 0.014
65	9.3 ± 1.3 (10.4)	581 ± 63 (647)	0.081 ± 0.009
85	9.0 ± 1.0 (10.6)	618 ± 54 (727)	0.115 ± 0.024
100*	6.3 ± 0.9 (7.8)	636 ± 95 (789)	0.172 ± 0.020

* *The yarn samples were submerged in water before testing.*

When the water content of plant fibres is increased, the original intermolecular hydrogen bonds in the cell wall are disrupted, and the mobility of the polymer chains are therefore increased. This plasticization effect of water might explain the measured decrease in stiffness and increase in strain at ultimate stress of He53 as shown in Table 4.23, but it can however not explain the increase in ultimate stress. In the textile industry it is well known that the breaking load of plant fibre yarns (e.g. hemp, flax and cotton) is increased as a function of the water content, whereas it is reduced in non-plant fibre yarns (e.g. wool and silk) (Furter1985). Plant fibres are designed to operate in a fully water saturated and swollen state, and because of their non-uniform chemical structure they tend to twist and attain irregular cross-sectional shapes when they are dried from these wet conditions. This applies in particular for cotton fibres that attain convoluted kidney-bean shaped cross-sections. Consequently, internal stresses are generated in the fibres, and this might explain

the reduction in ultimate stress when the water content is decreased (or the increase in ultimate stress when the water content is increased) (Postle 2004, pers. comm.) In contrast, in most other natural fibre types (e.g. wool and silk) the chemical structure is more uniform, which means that the fibre cross-sectional shape is more or less preserved when the water content is changed and internal stresses are therefore not generated. Thus, the reported reduction in ultimate stress of yarns based on these fibres can be assigned to the plasticization effect of bound water. Studies of cotton fibres have shown that ultimate stress is larger for fibres dried under tension, than for fibres dried with no tension (Zeronian et al. 1990, and references cited herein). In cotton fibres dried under tension, the untwisted and regular fibre cross-sectional shape of the wet fibres is preserved by stress relaxation, and accordingly ultimate stress is improved. Likewise, it has been reported that stiffness of various plant fibres (hemp, flax and jute) is improved when the fibres are dried under tension (Lilholt and Lawther 2000). Conclusively, it can be stated that the effect of a changed water content on plant fibre tensile properties can be assigned to two mechanisms: bound water plasticization and internal stresses. The effect of the two mechanisms is oppositely directed (Figure 4.50).

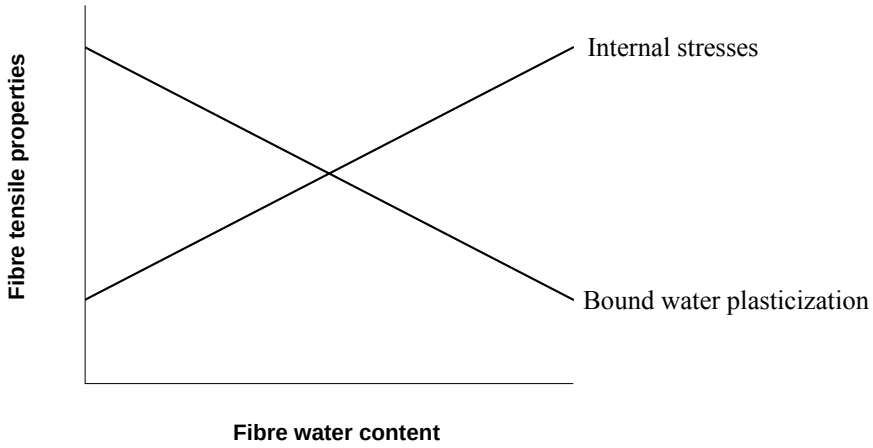

FIGURE 4.50. *The relation between fibre tensile properties (stiffness and ultimate stress) and fibre water content governed by two mechanisms: bound water plasticization and internal stresses.*

Axial tensile properties of He53/PET composites conditioned at different humidities (<35, 35, 65 and 85 % RH) are shown in Table 4.24. Stiffness is decreased and strain at ultimate stress is increased when the conditioning humidity is increased. Ultimate stress of the composites is unchanged at the three lower conditioning humidities, but is slightly decreased at 85 % RH. Based on plant fibre composites with a random fibre orientation, it has previously been reported that stiffness and ultimate stress are decreased when the composites are submerged in water (Hua et al. 1987, Kajaks et al. 2001, and references cited therein). Figure 4.51 shows representative stress-strain curves corresponding to the results in Table 4.24. In contrast to the relative small effect of process temperature on composite tensile properties (see Figure 4.46, p. 125), the different shape of

the stress-strain curves in Figure 4.51 underlines the profound effect of conditioning humidity on composite tensile properties.

TABLE 4.24. *Axial tensile properties of He53/PET composites conditioned at different humidities. The composites were fabricated by commingled filament-winding and a process temperature of 200 ℃. In brackets are given the estimated fibre properties as calculated by equations (4.53) and (4.54). Also shown is the fibre water content as presented in Table 4.5 for He53 processed at 200 ℃.*

Humidity (% RH)	$U_{f\,RH}$ (%)	V_f	V_p	Stiffness (GPa)	Ultimate stress (MPa)	Strain at ultimate stress
< 35*	2.4*	0.317	0.017	19.3 ± 0.7 (57.2)	206 ± 8 (556)	0.022 ± 0.0013
35	4.2	0.337	0.026	18.1 ± 0.6 (51.3)	200 ± 6 (510)	0.026 ± 0.0015
65	6.1	0.335	0.031	17.6 ± 0.7 (50.6)	205 ± 5 (533)	0.029 ± 0.0016
85	9.8	0.336	0.027	14.2 ± 1.1 (39.3)	191 ± 10 (482)	0.037 ± 0.0028

* *The conditioning humidity was uncontrolled, but presumable it was below 35 % RH (see Subsection 3.3.6). The fibre water content in this composite was estimated from the results of strain at ultimate stress. See text for more details.*

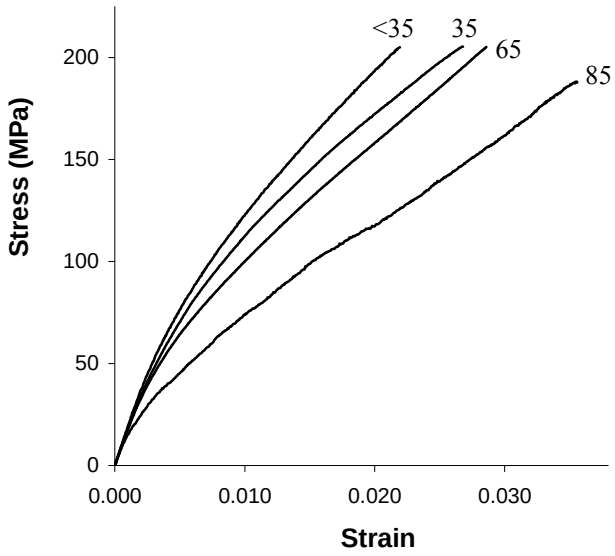

FIGURE 4.51. *Representative stress-strain curves of He53/PET composites conditioned at different humidities (% RH). See specifications of composites in Table 4.24.*

Also shown in Table 4.24 are the estimated fibre properties. Fibre stiffness is decreased when the conditioning humidity is increased, and this is expected from the similar trend in composite properties. Fibre ultimate stress is however decreased when the conditioning humidity is increased. At first sight, this is unexpected, since ultimate stress of the composites is almost unaffected by the conditioning humidity. However, the increase in strain at ultimate stress of the composites means

that σ_{m*} is increased as well (see Subsection 4.5.5). Thus, relatively less stress is carried by the fibres at the failure point, and this explains the decrease in fibre ultimate stress. Since both fibre stiffness and ultimate stress are decreased when the conditioning humidity is increased it is indicated that the dominating mechanism is bound water plasticization (see Figure 4.50).

Table 4.24 shows the expected water content of the hemp yarn fibres in the composites (results are from Table 4.5, p. 65). This implies however that the water sorption capacity of the embedded fibres is similar to fibres not restrained by a surrounding matrix (this is partly confirmed by the results in Subsection 4.4.2). Strain at ultimate stress is the tensile parameter most clearly affected by the conditioning humidity, and this parameter was therefore used to estimate the unknown fibre water content of the He53/PET composite with an uncontrolled conditioning humidity (<35 % RH). Based on linear regression between data of strain at ultimate stress and data of fibre water content, the unknown fibre water content was estimated to be 2.4 % ($R^2 = 0.997$).

Figure 4.52 shows the tensile properties of fibres, yarn and composites as a function of the fibre water content. The figure is a graphical representation of the results presented above; e.g. the opposite effect of a changed water content on ultimate stress of fibres and yarn is shown in Figure 4.52B. The regression lines in the figure are in good agreement with the experimental data. This is in particular true for stiffness and strain at ultimate stress (R^2>0.95) (Figures 4.52A and 4.52C). Thus, the figure suggests that the relationship between fibre water content and composite axial tensile properties can be modelled by a simple linear relationship. As an example, composite stiffness can be predicted by the equation:

$$E_{RH} = E_{65} - a\left(U_{65} - U_{RH}\right) \tag{4.56}$$

where the subscript RH is the conditioning humidity, and *a* is the slope of the regression line. In Figure 4.52A the slope of the regression line for composite stiffness is -0.6737, and E_{65} is measured to be 17.6 GPa. Subsequently, E_{35} and E_{85} can be calculated to be 18.8 and 15.1 GPa, respectively, which are in fairly good agreement with the experimental results shown in Table 4.24.

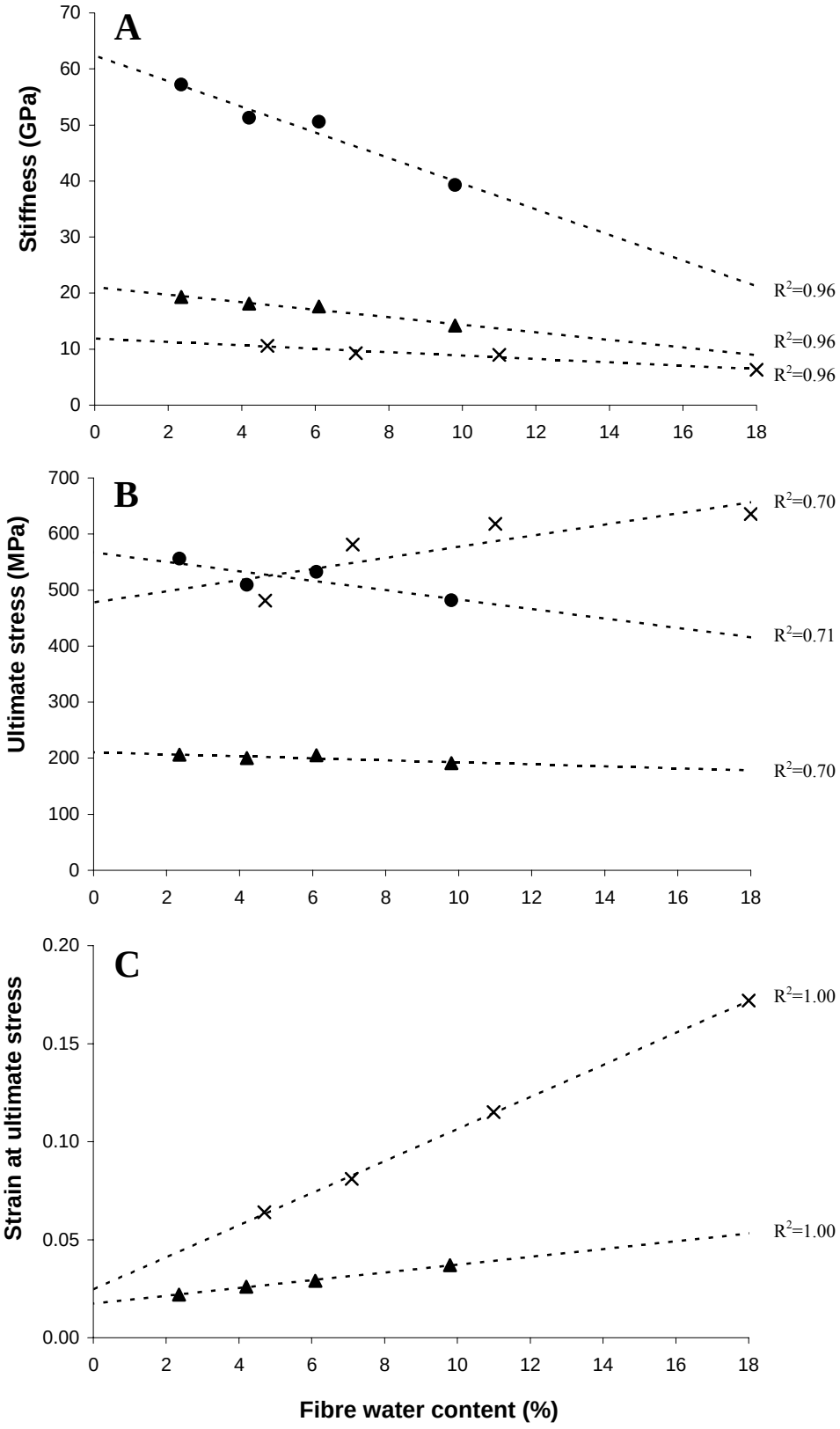

FIGURE 4.52. *Effect of fibre water content on (**A**) stiffness, (**B**) ultimate stress and (**C**) strain at ultimate stress for He53 fibres (estimated from composite properties) (●), He53 yarn (×) and He53/PET composites (▲). Dotted lines are regression lines.*

Table 4.25 shows that the transverse tensile properties He53/PET composites are slightly changed when the fibre water content is increased: stiffness and ultimate stress are decreased, whereas strain at ultimate stress is unaffected. The most obvious explanation for these findings would be changes in tensile properties of the PET matrix. However, as mentioned above, the properties of PET are unchanged below a conditioning humidity of 65 % RH. Instead, two mechanisms can be proposed to account for the results in the table: (i) it seems likely that the fibre/matrix compatibility is decreased when the fibre water content is increased; i.e. the adsorped water at the fibre surface acts as a separating agent at the fibre/matrix interface, and (ii) the composites were processed at a dry condition and the succeeding swelling of the fibres, because of water adsorption, might generate internal stresses at the fibre/matrix interface. Both of these mechanisms support that the transverse properties of the composites are decreased when the fibre water content is increased.

TABLE 4.25. *Transverse tensile properties of He53/PET composites conditioned at different relative humidities. The results are based on the same composite laminates as in Table 4.24.*

Rel. hum. (%)	U_{RH} (w%)	V_f	V_p	Stiffness (GPa)	Ultimate stress (MPa)	Strain at ultimate stress
< 35*	2.4*	0.317	0.017	4.0 ± 0.04	24.4 ± 0.5	0.009 ± 0.0005
35	4.2	0.337	0.026	3.5 ± 0.3	22.8 ± 1.7	0.012 ± 0.0005
65	6.1	0.335	0.031	3.5 ± 0.1	18.6 ± 0.4	0.008 ± 0.0007
85	9.8	0.336	0.027	2.9 ± 0.1	16.1 ± 0.4	0.009 ± 0.0005

* *See Table 4.24.*

5 CONCLUSIONS

Plant fibre yarn characteristics

The presented characterization of textile hemp yarns shows a number of findings, some of which make hemp yarn well suited for composite reinforcement.

The cellulose content of the hemp yarn fibres is about 90 w%, which is higher than previously reported cellulose contents of raw hemp fibres in the range 60-80 w%.

The cell wall density of the hemp yarn fibres is in the range 1.58-1.60 g/cm^3. The maximum density of cellulose-based fibres is 1.64 g/cm^3. The relative high density of the hemp yarn fibres is justified by their high cellulose content.

The luminar dimensions of the hemp yarn fibres are in the range 0-5 % of the fibre cross-sectional area. The small luminar dimensions means that the fibre density in composites is almost identical to the cell wall density of the fibres.

The hemp yarn fibres are inclined relative to the yarn axis with an angle of about 15° at the yarn surface. The corresponding mean inclination angle for all fibres in the yarn is estimated to be about 11°.

The hemp yarn fibres are well separated from each other; i.e. only few fibres are situated in bundles.

The water sorption capacity of the hemp yarn fibres is low as compared to raw hemp fibres; e.g. at 95 % RH the water content is about 15 % for hemp yarn fibres and it has previously been reported to be about 35 % for raw hemp fibres.

The tensile properties of the hemp yarn indicate the potential good tensile properties of the hemp yarn fibres. Ultimate stress of the hemp yarn is measured in the range 550-650 MPa.

Stiffness and ultimate stress of hemp yarn fibres are estimated from composite data (see below) in the ranges 50-65 GPa and 530-650 MPa, respectively.

Finally, it is shown that the properties of two batches of the same hemp yarn type, but bought with a time interval of two years, are most likely identical from a textile point of view; e.g. the same

breaking load and nearly the same fibre size distribution. However, small differences in water sorption capacity and stress-strain characteristics are detected between the two hemp yarn batches, and in relation to composite reinforcement this is more critical.

Compaction of plant fibre assemblies

The presented compaction behaviour of plant fibre assemblies shows that in comparison to glass fibres, the compactibility of plant fibres is lower, and moreover it is affected by the type of plant fibre. At a compaction pressure of 2.2 MPa, glass fibres are compacted to fibre volume fractions of 0.52 and 0.71 for assemblies with random and unidirectional fibre orientations, respectively. Likewise, plant fibres are compacted to fibre volume fractions in the ranges 0.28-0.38 and 0.52-56 for assemblies with random and unidirectional fibre orientations, respectively.

Based on cross-sectional observations of fibre assemblies, it is indicated that the compactibility of a fibre assembly is increased with the degree of fibre separation; i.e. the compactibility is largest for assemblies where the fibres are well separated from each other. The positive effect of fibre separation on the maximum obtainable fibre volume fraction in composites emphasizes the importance of an efficient defibration process.

The compactibility of plant fibre assemblies is improved by successive compaction cycles. The effect is most pronounced at the second compaction cycle. Thus, it is suggested that the maximum obtainable fibre volume fraction in composites can be notably increased if the fibre assembly is pre-compacted prior to composite fabrication.

Composite volumetric interaction

A model is shown to satisfactorily predict the interaction between volumes of fibres, matrix and porosity in aligned hemp yarn composites as a function of fibre weight fraction.

The porosity content is well predicted from experimental determined parameters such as the luminar dimensions and the compactibility of the hemp yarn fibres. In particular the compactibility of the fibres is found to be an important parameter. Composite porosity starts to increase dramatically when the fibre volume fraction approaches a certain maximum value, which is accurately predicted by the compactibility of the fibres.

The presented model is a valuable tool to predict the relationship between fibre volume fraction and porosity in plant fibre composites in general.

Composite water sorption

The water sorption properties of aligned hemp yarn composites were investigated. Different types of thermoplastics were applied as matrix.

The measurements of water sorption behaviour show that the diffusion coefficient of the hemp yarn fibres is much below the diffusion coefficients of the thermoplastic matrix and the composites. However, the small diffusion distance in the fibres means that water is rapidly sorped by the fibres despite their low diffusion coefficient.

The rate of water diffusion in the composites is found to be largest in the length direction (i.e. along the fibres), as compared to the width and thickness directions (transverse to the fibres). Moreover, the diffusion rate in the thickness direction is initially below the diffusion rate in the width direction. Thus, different diffusion coefficients must be assigned to each of the three directions.

A model is presented to exemplify how water diffusion in the three directions contributes to the total water content in composite samples with different geometries. It is shown that the low diffusion coefficient in the thickness direction restricts even more the use of the one-dimensional Fickian diffusion model to laminate samples with large planar dimensions.

Water diffusion in the composites is found to deviate from Fickian diffusion. The water content as a function of time is at first well predicted by the Fickian diffusion model, and an apparent equilibrium water content is approached, but then the water content starts to increase and reaches a notable larger equilibrium. This so-called two-stage diffusion behaviour is a well-known phenomenon in synthetic fibre composites, and theoretical models have previously been reported to explain the underlying mechanisms.

It is indicated that the water adsorption capacity of the hemp yarn fibres is reduced in the composites; i.e. the fibres are restrained from swelling by the surrounding matrix. This is beneficial with respect to the water related dimensional stability of the composites.

The dimensional swelling/shrinkage of the composites at humidities 35 and 85 % RH, with respect to a reference condition of 65 % RH, is relative small. For composites with a fibre volume fraction of 0.43, the dimensional changes in the length, width and thickness directions are –0.1, 0.9 and 1.1 % at 85 % RH. Likewise, the dimensional changes in the three directions are –0.0, -0.5 and –0.7 % at 35 % RH. Thus, at these two extreme ambient air humidities, the dimensional changes in the width and thickness directions are in the range ± 0.5-1.1 %, whereas the dimensions in the length direction are almost unchanged.

For composites with high fibre content, the dimensional swelling/shrinkage is well predicted from the product of density and water content of the composites. This simple predictability of the water-related dimensional changes is important with respect to an industrial use of aligned plant fibre composites.

It is found that the thermoplastic matrix shrinks when water is adsorped. This explains that the dimensional swelling of composites with low fibre content is lower than predicted (see above).

Finally, it is documented that internal interfacial cracks are generated in composites conditioned at 85 % RH.

Composite tensile properties

The tensile properties of aligned hemp yarn composites were investigated. Different types of thermoplastics were applied as matrix.

Generally, the measured tensile properties of the composites are superior to previously reported properties of aligned plant fibre composites. For composites with fibre volume fraction in the range 0.30-0.34, stiffness is in the range 16-20 GPa and ultimate stress is in the range 190-220 MPa.

The tensile properties of the composites are highly affected by the testing direction; e.g. ultimate stress is reduced from 205 to 125 MPa at an off-axis angle of only 10°. The off-axis properties are well modelled by a planar model of a homogenous and orthotropic material. It is shown that composite shear properties are predominantly governed by matrix shear properties.

The reinforcement efficiency is different between types of hemp yarn. Even for two batches of the same type of hemp yarn bought with a time interval of two years, the reinforcement efficiency is not identical. With a fibre volume fraction of about 0.32, the difference in tensile properties of composites reinforced with the two hemp yarn batches is about 2 GPa for stiffness and about 15 MPa for ultimate stress. This underlines a critical aspect in the use of plant fibres; i.e. their properties are less controllable in comparison to the properties of synthetic fibres.

A good correlation is found between yarn properties and composite properties. Thus, measurement of yarn properties might be a fast and reliable method to predict composite properties. However, more investigations are needed to elucidate the underlying mechanical mechanisms.

The axial tensile properties of the composites are affected only little by the degree of fibre/matrix compatibility. Even for composites with a strong fibre/matrix bonding, no clear improvements in

axial properties are observed, but the failure characteristics of the composites are changed dramatically. In contrast, the transverse tensile properties of the composites are markedly affected by the degree of fibre/matrix compatibility. In composites with a strong fibre/matrix bonding, the transverse stiffness and ultimate stress are increased, whereas strain at ultimate stress is decreased.

The degree of fibre/matrix compatibility is found to affect the content of porosity in the composites. Porosity is decreased when the degree of fibre/matrix compatibility is increased. This indicates that the composites contain porosities located at the fibre/matrix interface regions, which also is supported from microscopic observations.

For composites with large fibre volume fraction (and large porosity content), it is observed that the axial tensile properties are overestimated by the commonly applied "rule-of-mixtures" model. To account for this situation a modified and improved model is presented, which includes the effect of porosity on composite tensile properties. The improved model is shown to accurately predict the axial stiffness and ultimate stress of the composites. Transverse stiffness is also well predicted by the model. The model is a valuable tool to estimate fibre properties from composite properties; i.e. for composites with a given yarn type, almost identical fibre tensile properties are calculated irrespective of fibre volume fraction, porosity and matrix type.

The process temperature used for composite fabrication is shown to affect the tensile properties of the composites; e.g. when process temperature is increased from 180 to 220 °C, stiffness is increased from 19 to 23 GPa, ultimate stress is decreased from 240 to 170 MPa, and strain at ultimate stress is decreased from 0.021 to 0.012. Generally, the results emphasize the importance of a low process temperature. The small increase in composite stiffness might be explained by the process temperature dependent porosity of the composites (see below). The measured stress-strain curves are nearly identical irrespective of the process temperature, only the failure point is changed. Thus, it is indicated that the effect of thermal degradation is mainly confined to the failure mechanisms in the hemp yarn fibres, and they fail prematurely in composites processed at high temperatures.

The porosity of the composites is decreased when the process temperature is increased; e.g. when process temperature is increased from 180 to 220 °C, porosity is decreased from 0.043 to 0.018. This is explained by the decrease in matrix viscosity. Composite porosity is found to be linearly related to the logarithm of matrix viscosity.

The level of conditioning humidity (i.e. the water content of the composites) is shown to affect the tensile properties of the composites; e.g. when conditioning humidity is increased from 35 to 85 %

RH, stiffness is decreased from 18 to 14 GPa, and strain at ultimate stress is increased from 0.026 to 0.037. Ultimate stress is more or less unaffected by the conditioning humidity. It is hypothesised that the change in tensile properties of the composites is governed by water plasticization of the hemp yarn fibres. The relationship between water content of the fibres and tensile properties of the composites is well modelled by a simple linear relationship. Overall, the results underline that plant fibre composites need to be carefully conditioned before testing, if comparisons of tensile properties are to be made between series of experiments.

6 FUTURE WORK

On the background of the presented results and considerations in this study a number of issues are proposed for future work.

- Development of methods to fabricate aligned plant fibre semi-products. Since plant fibre yarns are rather expensive (see Table 2.6, p. 27), they are not appropriate fibre semi-products for commercial composite materials. Moreover, plant fibre yarns are intended to be used in textile applications, and their properties are therefore not optimised with respect to composite reinforcement.
- Establishment of a correlation between density and cellulose content of plant fibres (see considerations in Subsection 4.1.2). Both of these parameters are important with respect to plant fibre composites, and such a correlation has not previously been documented.
- Prediction of fibre tensile properties from yarn tensile properties. A closely related issue is prediction of composite tensile properties from yarn tensile properties. It is shown in this study that yarn tensile properties are well correlated with composite tensile properties (see Figure 4.34, p. 105). However, the underlying mechanical mechanisms need yet to be revealed.
- Water sorption properties of plant fibre composites. Although this is an important aspect in the use of plant fibre composites it has received limited attention in previous studies. This study presents a number of interesting findings with respect to directional diffusion coefficients, dimensional changes and internal cracks (see Section 4.4), but more investigations are needed. Particularly, it would be interesting to study the water related dimensional changes of the composites as a function of time. This might provide the necessary information in order to explain the two-stage diffusion behaviour observed for the composites in this study.
- Determination of bound water density. In this study bound water density is assumed to be equal to liquid water density (see considerations in Subsection 2.2.3). However, it seems likely that bound water density is not constant, but varies with the water content of the fibres. Appendix B presents a potential method for the determination of bound water density.
- Investigation of off-axis tensile properties of aligned plant fibre composites. The presented results in Subsection 4.5.2 might form a basis for further investigations, in which more parameters are included; e.g. fibre content, porosity and fibre/matrix interface properties.

REFERENCES

Alvarez V.A., Fraga A.N. and Vázquez A. (2004). Effects of the moisture and fiber content on the mechanical properties of biodegradable polymer-sisal fiber biocomposites. Journal of Applied Polymer Science. 91: 4007-4016.

American Society of Testing and Materials. (1980). Annual book of ASTM standards. Part 35. D792. Specific gravity and density of plastics by displacement.

American Society of Testing and Materials. (1981). Annual book of ASTM standards. Part 32. D2256. Breaking load (strength) and elongation of yarn by the single-strand method.

American Society of Testing and Materials. (1981). Annual book of ASTM standards. Part 32. D2260. Conversion factors and equivalent yarn numbers measured in various numbering systems.

Anagnost S.E., Mark R.E. and Hanna R.B (2002). Variation of microfibril angle within individual tracheids. Wood and Fiber Science. 34: 337-349.

Andersen T.L. (1997). Development of a rapid press consolidation technique for continuous fibre reinforced thermoplastic composites. In the Proceedings of the 18th Risoe International Symposium on Materials Science. Polymeric Composites – Expanding the Limits. Eds. S.I. Andersen et al. Risoe National Laboratory, Roskilde, Denmark. p. 237-244.

Andersen T.L. and Lilholt H. (1999). Natural fibre composites: Compaction of mats, press consolidation and material quality. Ed. J. Renard. In the Proceedings of the 7th Euro-Japanese Symposium, Paris, France. p. 1-12.

Andersen T.L. and Plackett D. (2002). Polymer composite product, a process for the manufacture thereof and use of the product. International Application Number: PCT/DK02/00085. International Publication Number: WO 02/064670 A1. International Publication Date: 22 August 2002.

Ashby M.F. (1997). Materials selection in mechanical design. Butterworth-Heinemann, Oxford, United Kingdom. ISBN 0 7506 2727 1. Cited in Kandachar (2002).

Avramidis S. (1997). The basics of sorption. In the Proceedings of An International Conference on Wood-Water Relations. Ed. Hoffmeyer P. June 1997. Copenhagen, Denmark. p. 3-16.

Barkas W.W. (1949). The swelling of wood under stress. A discussion of its hygroscopic, elastic and plastic properties. Department of Scientific and Industrial Research, Forest Products Research Laboratory, USA.

Barnes H.A., Hutton J.F. and Walters K. (1989). An introduction to rheology. Elsevier Science. Amsterdam, The Netherlands.

Barton S.J. and Pritchard G. (1994). The moisture absorption characteristics of crosslinked vinyl terminated polyethers compared with epoxies. In Polymers for Advanced Technologies. Wiley, New York, USA. Vol. 5, p. 245-252.

Beil N.B. and Roberts W.W. (2002). Modeling and computer simulation of the compressional behaviour of fiber assemblies. Part I: Comparison to van Wyk's theory. Textile Research Journal. 72: 341-351.

Bhuiyan M.T.R. and Sobue N.H.N. (2001). Effect of intermittent heat treatment on crystallinity in wood cellulose. Journal of Wood Science. 47: 336-341.

Bisanda E.T.N. and Ansell M.P. (1991). The effect of silane treatment on the mechanical and physical properties of sisal-epoxy composites. Composites Science and Technology. 41: 165-178.

Bledzki A.K., Sperber V.E. and Faruk O. (2002). Natural and wood fibre reinforcement in polymers. Rapra Review Reports. Vol. 13; No. 8.

Blikstad M., Sjöblom P.O.W. and Johannesson T.R. (1988). Long-term moisture absorption in graphite/epoxy angle-ply laminates. In Environmental Effects of Composite Materials. Technomic, Lancaster, United Kingdom. p. 107-121.

Bonniau P. and Bunsell A.R. (1984). A comparative study of water absorption theories applied to glass epoxy composites. In Environmental effects of composite materials. Ed. G. S. Springer. Technomic, Lancaster, United Kingdom. p. 209-229.

Booth J.E. (1975). Textile mathematics. Volume two. The Textile Institute, Manchester, United Kingdom.

Bos H.L., Oever M.J.A. and Peters O.C.J.J. (1997). The influence of fibre structure and deformation on the fracture behaviour of flax fibre reinforced composites. In the Proceedings of the 4th International Conference on Deformation and Fracture of Composites. p. 499-504.

Bos H.L., van den Oever M.J.A. and Peters O.C.J.J. (2002). Tensile and compressive properties of flax fibres for natural fibre reinforced composites. Journal of Materials Science. 37: 1638-1692.

Broge J.L. (2000). Natural fibers in automotive components. Automotive Engineering International. 108: 120-.

Brühlmann F., Leupin M., Erismann K.H. and Fiechter A. (2000). Enzymatic degumming of ramie bast fibers. Journal of Biotechnology. 76: 43-50.

Brushwood D.E. (1988). Effects of heating on chemical and physical-properties and processing quality of cotton. Textile Research Journal. 58: 309-317.

Cai L.W. and Weitsman Y. (1994). Non-Fickian moisture diffusion in polymeric composites. Journal of Composite Materials. 28: 130-54.

Cantero G., Arbelaiz A., Llano-Ponte R. and Mondragon I. (2003b). Effect of fibre treatment on wettability and mechanical behaviour of flax/polypropylene composites. Composites Science and Technology. 63: 1247-1254.

Cantero G., Arbelaiz A., Mugika F., Valea A. and Mondragon I. (2003a). Mechanical behavior of wood/polypropylene composites: Effects of fibre treatments and ageing processes. Journal of Reinforced Plastics and Composites. 22: 37-50.

Carnaby G.A. and Grosberg P. (1976). The tensile behaviour of staple-fibre yarns at small extensions. Journal of Textile Institute. 9: 299-308.

Chawla K.K. and Bastos A.C. (1979). The mechanical properties of jute fibers and polyester/jute composites. In the Proceedings of the 3rd International Conference on Mechanical Behaviour of Materials. Cambridge, England. p. 191-196.

Cichocki F.R. and Thomason J.L. (2002). Thermoelastic anisotropy of a natural fiber. Composites Science and Technology. 62: 669-678.

Clemons C.M. (2000). Woodfiber-plastic composites in the United States – History and current and future markets. In the Proceedings of the 3rd International Wood and Natural Fibre Composites Symposium. Kassel, Germany. September, 2000. p. 1-7.

Creasy T.S. (2000). A method of extracting Weibull survival model parameters from filament bundle load/strain data. Composites Science and Technology. 60: 825-832.

Davies G.C. and Bruce D.M. (1997). A stress analysis model for composite coaxial cylinders. Journal of Materials Science. 32: 5425-5437.

Dobel J. (2002). The future of airlaid forming. Nonwovens World. June-July. p. 53-56.

Donaghy J.A., Boomer J.H. and Haylock R.W. (1992). An assessment of the quality and yield of flax fiber produced by the use of pure bacterial cultures in flax rets. Enzyme Microbiological Technology. 14: 131-134.

Drzal L.T. and Madhukar M. (1993). Fiber-matrix adhesion and its relationship to composite mechanical properties. Journal of Materials Science. 28: 569-610.

Eichhorn S.J., Baillie C.A., Zafeiropoulos N., Mwaikambo L.Y., Ansell M.P., Dufresne A., Entwistle K.M., Herrera-Franco P.J., Escamilla G.C., Groom L., Hughes M., Hill C., Rials T.G. and Wild P.M. (2001). Review. Current international research into cellulosic fibres and composites. Journal of Materials Science. 36: 2107-2131.

Ellison G.C. and McNaught R. (2000). The use of natural fibres in nonwoven structures for applications as automotive component substrates. Research and Development Report. Ministry of Agriculture Fisheries and Food Agri – Industrial Materials. Reference NF0309. London, United Kingdom.

Entwistle K.M. and Terrill N.J. (2000). The measurement of the micro-fibril angle in softwood. Journal of Materials Science. 35: 1675-1684.

Eriksen M. and Pallesen B.E. (2002). New generation airforming for flax and hemp. Nonwovens World. June-July. p. 80-84.

Evans W.J., Isaac D.H., Suddell B.C. and Crosky A. (2002). Natural fibres and their composites: A global perspective. In the Proceedings of the 23rd Risoe International Symposium on Materials Science. Sustainable Natural and Polymeric Composites. Eds. Lilholt H. et al. Risoe National Laboratory, Roskilde, Denmark. p. 1-14.

Furter R. (1985). Strength and elongation testing of single and ply yarns. The Textile Institute, Manchester, United Kingdom.

Gamstedt E.K, Berglund L.A. and Peijs T. (1999). Fatigue mechanisms in unidirectional glass-fibre-reinforced polypropylene. Composites Science and Technology. 59: 759-768.

Gassan J. and Bledzki A.K. (1999a). Alkali treatment of jute fibers: Relationship between structure and mechanical properties. Journal of Applied Polymer Science. 71: 623-629.

Gassan J. and Bledzki A.K. (1999b). Effect of cyclic moisture absorption desorption on the mechanical properties of silanized jute-epoxy composites. Polymer Composites. 20: 604-611.

Gassan J. and Bledzki A.K. (1999c). Influence of fiber surface treatment on the creep behavior of jute fiber-reinforced polypropylene. Journal of Thermoplastic Composite Materials. 12: 388-398.

Gassan J. and Bledzki A.K. (2001). Thermal degradation of flax and jute fibers. Journal of Applied Polymer Science. 82: 1417-1422.

Gassan J., Chate A. and Bledzki A.K. (2001). Calculation of elastic properties of natural fibers. Journal of Materials Science. 36: 3715-3720.

Goering H.K. and van Soest P.J. (1970). Forage fiber analyses (apparatus, reagents, procedures, and some applications). Agricultural Research Service – United States. Department of Agriculture. USDA, Washington DC. 1-20.

Grosberg P. and Iype C. (1999). Yarn production. Theoretical aspects. The Textile Institute, Manchester, United Kingdom.

Gutowski T.G., Cai Z., Bauer S., Boucher D., Kingery J. and Wineman S. (1987). Consolidation experiments for laminate composites. Journal of Composite Materials. 21: 650-669.

Harris B. (1980). The mechanical behaviour of composite materials. Symposia of the Society for Experimental Biology. Cambridge University Press, United Kingdom. p. 37-73.

Hepworth D.G., Bruce D.M., Vincent J.F.V. and Jeronimidis G. (2000). The manufacture and mechanical testing of thermosetting natural fiber composites. Journal of Materials Science. 35: 293-298.

Hepworth D.G., Hobson R.N., Bruce D.M. and Farrent J.W. (2000). The use of unretted hemp fibre in composite manufacture. Composites: Part A. 31: 1279-1283.

Hobson R.N., Hepworth D.G. and Bruce D.M. (2001). Quality of fibre separated from unretted hemp stems by decortification. Journal of Acricultural Engineering Research. 78: 153-158.

Hornsby P.R., Hinrichsen E. and Tarverdi K. (1997a). Preparation and properties of polypropylene composites reinforced with wheat and flax straw fibres. Part I. Fibre characterization. Journal of Materials Science. 32: 443-449.

Hornsby P.R., Hinrichsen E. and Tarverdi K. (1997b). Preparation and properties of polypropylene composites reinforced with wheat and flax straw fibres. Part II. Analysis of composite microstructure and mechanical properties. Journal of Materials Science. 32: 1009-1015.

Hua L., Zadorecki P. and Flodin P. (1987). Cellulose fiber-polyester composites with reduced water sensitivity (1) – Chemical treatment and mechanical properties. Polymer Composites. 8: 199-202.

Hull D. and Clyne T.W. (1996). An Introduction to Composite Materials. 2nd edition. Cambridge University Press, Cambridge, United Kingdom.

International Organization for Standardization. (1972). Methods for determination of breaking load and elongation at the breaking load of single strands. International Standard ISO 2062.

Israelachhvili J.N. (1991). Intermolecular and surface forces. 2nd edition. Academic Press, London, United Kingdom. Chapter 8.

Judd N.C.W. and Wright W.W. (1978). Voids and their effects on the mechanical properties of composites – an appraisal. SAMPE Journal. January/February: 10-14.

Kajaks J.A., Reihmane S.A., Bulmanis V.N. and Lejnieks J.E. (2001). Effect of water on the physicomechanical properties of composites containing low-density polyethylene and linen yarn production waste. Mechanics of Composite Materials. 37: 167-170.

Kalaprasad G., Joseph K., Thomas S. and Pavithran C. (1997). Theoretical modelling of tensile properties of short sisal fiber-reinforced low-density polyethylene. Journal of Materials Science. 32: 4261-4267.

Kandachar P. (2002). Opportunities for product development for industrial applications in polymers reinforced with natural fibres. In the Proceedings of the 23rd Risoe International Symposium on Materials Science. Sustainable Natural and Polymeric Composites. Eds. Lilholt H. et al. Risoe National Laboratory, Roskilde, Denmark. p. 15-33.

Karmaker A.C. and Hinrichsen G. (1991). Processing and characterization of jute fiber reinforced thermoplastic polymers. Polymer Plastics Technology and Engineering. 30: 609-629.

Karus M., Kaup M. and Ortmann S. (2002). Use of natural fibres in the German and Austrian automotive industry. Market survey 2002: Status, analysis and trends. Nova-Institute GmbH, Hürth, Germany.

Keller A., Leupin M., Mediavilla V. and Wintermantel E. (2001). Influence of the growth stage of indutrial hemp on chemical and physical properties of the fibres. Industrial Crops and Products. 13: 35-48.

Khalil H.P.S.A., Ismail H., Rozman H.D. and Ahmad M.N. (2001). The effect of acetylation on interfacial shear strength between plant fibres and various matrices. European Polymer Journal. 37: 1037-1045.

Klein W. (1998). The technology of short-staple spinning. 2nd ed. The Textile Institute, Manchester, United Kingdom.

Kollmann F.F.P. and Côté W.A. (1984). Principles of wood science and technology. Volume I: Solid wood. Springer-Verlag Berlin, Heidelberg, Germany.

Kumar P. (1986). Mechanical properties of jute fibres and their composites. Indian Journal of Technology. 24: 29-32.

Lilholt H. (2002). Strength of cellulose and fibres. In the Proceedings of the 23rd Risoe International Symposium on Materials Science. Sustainable Natural and Polymeric Composites. Eds. Lilholt H. et al. Risoe National Laboratory, Roskilde, Denmark. p. 225-230.

Lilholt H. and Bjerre A.B. (1997). Composites based on jute-fibres and polypropylene matrix, their fabrication and characterization. In the Proceedings of the 18th Risoe International Symposium on Materials Science. Polymeric Composites – Expanding the Limits. Eds. S.I. Andersen et al. Risoe National Laboratory, Roskilde, Denmark.

Lilholt H. and Lawther J.M. (2000). Natural organic fibres. In Comprehensive Composite Materials (6 vols). Eds. A. Kelly and C. Zweben. Elsevier Science. Vol. 1, chap. 10, p. 303-325.

Lilholt H., Toftegaard H., Thomsen A.B. and Schmidt A.S. (1999). Natural composites based on cellulosic fibres and polypropylene matrix – their processing and characterisation. In the Proceedings of the 12th International Conference on Composite Materials, Paris, France. Paper no 1115.

Lomov S.V. and Verpoest I. (2000). Compression of woven reinforcements: A mathematical model. Journal of Reinforced Plastic Composites. 19: 1329-1350.

Lu J.Z., Wu Q. and McNabb H.S. (2000). Chemical coupling in wood fiber and polymer composites: A review of coupling agents and treatments. Wood and Fiber Science. 32: 88-104.

Lu X., Zhang M.Q., Rong M.Z., Shi G. and Yang G.C. (2003). All-plant fiber composites. II: Water absorption behavior and biodegradability of unidirectional sisal fiber reinforced benzylated wood. Polymer Composites. 24: 367-379.

Lystrup A. (1998). Hybrid yarn for thermoplastic fibre composites. Risø-R-1034 (EN). Risoe Report, Risoe National Laboratory, Roskilde, Denmark.

MacKenzie J.K. (1950). The elastic constants of a solid containing spherical holes. Proceedings of Physical Society. B63:2-.

Marcovich N.E., Reboredo M.M. and Aranguren M.I. (1999). Moisture diffusion in polyester-woodflour composites. Polymer. 40: 7313-7320.

Mishra S., Mohanty A.K., Drzal L.T., Misra M., Parija S., Nayak S.K. and Tripathy S.S. (2003). Studies in mechanical performance of biofibre/glass reinforced polyester hybrid composites. Composites Science and Technology. 63: 1377-1385.

Mishra S., Naik J.B. and Patil Y.P. (2000). The compatibilising effect of maleic anhydride on swelling and mechanical properties of plant-fiber reinforced novolac composites. Composites Science and Technology. 60: 1729-1735.

Mohanty A.K. and Misra M. (1995). Studies on jute composites – A literature review. Polymer Plastics Technology and Engineering. 34: 729-792.

Mohanty A.K., Misra M. and Hinrichsen G. (2001). Biofibres, biodegradable polymers and biocomposites: An overview. Macromolecular Materials and Engineering. 276/277: 1-24.

Mott L. (1995). Micromechanical properties and fracture mechanisms of single wood pulp fibers. Ph.d.-thesis. University of Maine. Maine, USA.

Munksgaard J. (1961). Garnfremstilling. In Textilbogen. Håndbog i Textil Varekundskab. Ed. P. Sterm. Martins Forlag, Copenhagen, Denmark.

Muzzy J.D. (2000). Thermoplastics – Properties. In Comprehensive Composite Materials (6 vols). Eds. A. Kelly and C. Zweben. Elsevier Science. Vol. 2, chap. 2.

Myers G.E., Chahyadi I.S., Coberly C.A. and Ermer D.S. (1991). Wood flour/polypropylene composites: Influence of maleated polypropylene and process and composition variables on mechanical properties. International Journal of Polymeric Materials. 15: 21-44.

Neville A.C. (1993). Biology of fibrous composites. Development beyond the cell membrane. Cambridge University Press, USA.

N-fibrebase. Database on the internet: www.n-fibrebase.net. By nova-Institute, Hürth, Germany.

Niklas K.J. (1992). Plant Biomechanics. An engineering approach to plant form and function. The University of Chicago Press. USA.

Nishiyama Y., Langan P. and Chanzy H. (2002). Crystal structure and hydrogen-bonding system in cellulose Iβ from synchrotron X-ray and neutron fiber diffraction. Journal of American Chemical Society. 124: 9074-9082.

Nordin L.O. and Berglund L.A. (2002). Polymer composites based on paper fibres. In the Proceedings of the 23rd Risoe International Symposium on Materials Science. Sustainable Natural and Polymeric Composites. Eds. Lilholt H. et al. Risoe National Laboratory, Roskilde, Denmark. p. 273-279.

O'Sullivan A.C. (1995). Modelling of cellulose-molecule interactions. Ph.d.-thesis. University of Wales, United Kingdom.

Oksman K. (2000). Mechanical properties of natural fibre mat reinforced thermoplastic. Applied Composite Materials. 7: 403-414.

Oksman K. (2001). High quality flax fibre composites manufactured by the resin transfer moulding process. Journal of Reinforced Plastics and Composites. 20: 621-627.

Oksman K., Wallström L., Berglund L.A. and Filho R.D.T. (2002). Morphology and mechanical properties of unidirectional sisal-epoxy composites. Journal of Applied Polymer Science. 84: 2358-2365.

Page D.H., El-Hosseiny F., Winkler K. and Lancaster A.P.S. (1977). Elastic modulus of single wood pulp fibers. Tappi. 60: 114-117.

Parikh D.V., Calamari T.A., Sawhney A.P.S., Blanchard E.J., Screen F.J., Myatt J.C., Muller D.H. and Stryjewski D.D. (2002). Thermoformable automotive composites containing kenaf and other cellulosic fibers. Textile Research Journal. 72: 668-672.

Peijs T. (2002). Novel concepts for obtaining sustainable composites based on synthetic polymers. In the Proceedings of the 23rd Risoe International Symposium on Materials Science. Sustainable Natural and Polymeric Composites. Eds. Lilholt H. et al. Risoe National Laboratory, Roskilde, Denmark. p. 61-75.

Perry D.R. (1985). Identification of textile materials. 7th ed. The Textile Institute, Manchester, United Kingdom.

Postle R. (2004). Faculty of Science, University of New South Wales, Sydney, Australia. Pers. comm.

Pratten N.A. (1981). Review. The precise measurement of the density of small samples. Journal of Materials Science. 16: 1737-1747.

Reussman T., Mieck P., Grützner R. and Bayer R. (1999). The recycling of polypropylene reinforced with natural fibres. Kunststoffe Plast Europe. 89: 80-84.

Riccieri J.E., Hecker De Carvalho L. and Vázquez A. (1999). Interfacial properties and initial step of the water sorption in unidirectional unsaturated polyester/vegetable fiber composites. Polymer Composites. 20: 29-37.

Robinson R. (1996). The great book of hemp. Park Street Press, Main, USA.

Robson D., Hague J., Newman G., Jeronimidis G. and Ansell M. (1993). Survey of natural materials for use in structural composites as reinforcement and matrices. The Biocomposites Centre, University of Wales, United Kingdom. EC/4316/92. Crown Copywright.

Roe P.J. and Ansell M.P. (1985). Jute-reinforced polyester composites. Journal of Materials Science. 20: 4015-4020.

Romhány G., Karger-Kocsis J. and Czigány T. (2003). Tensile fracture and failure behavior of technical flax fibers. Journal of Applied Polymer Science. 90: 3638-3645.

Rong M.Z., Zhang M.Q., Liu Y., Yang G.C. and Zeng H.M. (2001). The effect of fiber treatment on the mechanical properties of unidirectional sisal-reinforced epoxy composites. Composites Science and Technology. 61: 1437-1447.

Rowell R.M. (1986). A simplified procedure for the acetylation of hardwood and softwood flakes for flakeboard production. Journal of Wood Chemistry Technology. 6: 427-448.

Salisbury F.B. and Ross C.W. (1992). Plant Physiology. Fourth edition. Wadsworth Inc. California, USA.

Salmén L. (1997). The sorption behaviour of wood. In the Proceedings of An International Conference on Wood-Water Relations. Ed. Hoffmeyer P. June 1997. Copenhagen, Denmark. p. 33-44.

Sanadi A.R., Prasad S.V. and Rohatgi P.K. (1986). Sunhemp fibre-reinforced polyester. Journal of Materials Science. 21: 4299-4304.

Sankari H.S. (2000). Comparison of bast fibre yield and mechanical fibre properties of hemp (*Cannabis sativa* L.) cultivars. Industrial Crops and Products. 11: 73-84.

Schjødt-Thomsen J. and Pyrz R. (2000). Stress-strain modelling of microcellular materials. Proceedings of the 3rd Nordic Meeting on Materials and Mechanics, Rebild Bakker, Denmark. p. 201-212.

Shah A.N. and Lakkad S.C. (1981). Mechanical properties of jute-reinforced plastics. Fibre Science and Technology. 15: 41-46.

Siau J.F. (1995). Wood: Influence of moisture on physical properties. Department of Wood Science and Forest Products, Virginia Polytechnic Institute and State University, USA.

Simácek P and Karbhari V.M. (1996). Notes on the modeling of preform compaction: I. Micromechanics at the fiber bundle level. Journal of Reinforced Plastic Composites. 15: 86-122.

Skaar C. (1972). Water in wood. Syracuse University Press, New York, USA.

Skaar C. (1988). Wood-water relations. Springer-Verlag Berlin Heidelberg, Germany.

Sridhar M.K., Basavarappa G., Kasturi S.G. and Balasubramanian N. (1984). Mechanical properties of jute-polyester composites. Indian Journal of Technology. 22: 213-215.

Stout H.P. (1988). Fibre and yarn quality in jute spinning. The Textile Institute, Manchester, United Kingdom.

Strømdahl K. (2000). Water sorption in wood and plant fibres. Ph.d.-thesis. Department of Civil Engineering, Technical University of Denmark. Series R: no 78.

Sugiyama J., Vuong R. and Chanzy H. (1991). Electron diffraction study on the two crystalline phases occurring in native cellulose from an algal cell wall. Macromolecules. 24: 4168-4175.

Svensson N., Shishoo R. and Gilchrist M. (1998). Manufacturing of thermoplastic composites from commingled yarns – a review. Journal of Thermoplastic Composite Materials. 11: 22-56.

Thomason J.L. and Adzima L.J. (2001). Sizing up the interphase: an insider's guide to the science of sizing. Composites: Part A. 32: 313-321.

Thomsen A.B., Schmidt A.S., Toftegaard H., Pedersen W.B., Woidemann A. and Lilholt H. (1999). Natural plant fibre composites based on wet-oxidised wheat straw and polypropylene. In the Proceedings of the 6th Symposium of Renewable Resources for the Chemical Industry. Bonn, Germany. p. 762-771.

Thygesen A., Madsen F.T., Lilholt H., Felby C. and Thomsen A.B. (2002). Changes in chemical composition, degree of crystallisation and polymerisation of cellulose in hemp fibres caused by pre-treatments. In the Proceedings of the 23rd Risoe International Symposium on Materials Science.

Sustainable Natural and Polymeric Composites. Eds. Lilholt H. et al. Risoe National Laboratory, Roskilde, Denmark. 315-323.

Toll S. (1998). Packing mechanics of fiber reinforcements. Polymer Engineering Science. 38: 1337-1350.

Tsai S.W. and Hahn H.T. (1980). Introduction to composite materials. Technomic Publishing Company, Connecticut, USA.

Van de Velde K. and Kiekens P. (2002). Thermal degradation of flax: The determination of kinetic parameters with thermogravimetric analysis. Journal of Applied Polymer Science. 83: 2634-2643.

Van de Weyenberg I., Ivens J., De Coster A., Kino B., Baetens E. and Verpoest I. (2003). Influence of processing and chemical treatment of flax fibres on their composites. Composites Science and Technology. 63: 1241-1246.

van Wyk C.M. (1946). Notes on the compressibility of wool. Journal of Textile Institute. 37: T285-T292.

Varna J., Joffe R. and Berglund L.A. (1995). Effect of voids on failure mechanisms in RTM laminates. Composites Science and Technology. 53: 241-249.´

Vignon M.R., Dupeyre D. and Garcia-Jaldon C. (1996). Morphological characterization of steam-exploded hemp fibers and their utilization in polypropylene-based composites. Bioresource Technology. 58: 293-215.

Wadsö L. (1993). Studies of water vapor transport and sorption in wood. Ph.d.-thesis. Building Materials, Lund University, Sweden.

Wang H.M., Postle R., Kessler R.W. and Kessler W. (2003). Removing pectin and lignin during chemical processing of hemp for textile applications. Textile Research Journal. 73: 664-669.

Weatherwax and Tarkow (1968). Importance of penetration and adsorption compression of the displacement fluid. Forest Products Journal. 18: 44-46. Cited from Skaar (1972).

Weitsman Y.J (2000). Effects of fluids on polymeric composites - A review. In Comprehensive Composite Materials (6 vols). Eds. A. Kelly and C. Zweben. Elsevier Science. Vol. 2, chap. 11, p. 369-401.

White N.M. and Ansell M.P. (1983). Straw-reinforced polyester composites. Journal of Materials Science. 18: 1549-1556.

Wielage B., Lampke T., Marx G., Nestler K. and Starke D. (1999). Thermogravimetric and differential scanning calorimetric analysis of natural fibre and polypropylene. Thermochimica Acta. 337: 169-177.

Young R.A. and Rowell R.M. (1986). Cellulose. Structure, modification and hydrolysis. John Wiley & Sons, New York, USA.

Zafeiropoulos N.E., Baillie C.A. and Hodgkinson J.M. (2002a). Engineering and characterisation of the interface in flax fibre/polypropylene composite materials. Part II. The effect of surface treatments on the interface. Composites: Part A. 33: 1185-1190.

Zafeiropoulos N.E., Williams D.R., Baillie C.A. and Matthews F.L. (2002b). Engineering and characterisation of the interface in flax fibre/polypropylene composite materials. Part I. Development and investigation of surface treatments. Composites: Part A. 33: 1083-1093.

Zeidman M. and Sawhney P.S. (2002). Influence of fiber length distribution on strength efficiency of fibers in yarn. Textile Research Journal. 72: 216-220.

Zeronian S.H., Kawabata H. and Alger K.W. (1990). Factors affecting the tensile properties of nonmercerized and mercerized cotton fibers. Textile Research Journal. 60: 179-183.

Zhou J. and Lucas J.P. (1995). The effects of a water environment on anomalous absorption behavior in graphite/epoxy composites. Composites Science and Technology. 53: 57-64.

SYMBOLS AND ABBREVIATIONS

β	Hygroexpansion coefficient (%/%)
σ	Ultimate stress (MPa)
ρ	Density (g/cm^3)
τ	Shear stress (MPa)
ν	Poisson's ratio
η	Viscosity (Pa s)
σ_{m*}	Matrix stress at the point of composite failure (MPa)
a	Fitting parameter/constant
b	Fitting parameter/constant
d	Diffusion distance (m)
D	Diffusion coefficient (m^2/s) or Absolute dimensions of laminate samples (mm)
E	Stiffness (GPa) or Degree of water saturation
fa	Ratio of fibre anisotropy (transverse properties/axial properties)
Fl64	Flax yarn with a linear density of 64 tex
G	Shear stiffness (GPa)
He47	Hemp yarn with a linear density of 47 tex
He53	Hemp yarn with a linear density of 53 tex
He91	Hemp yarn with a linear density of 91 tex
L	Absolute length of laminate samples (mm) or Pitch (mm)
m	Absolute mass (g)
MAPP	Maleated polypropylene, foils
n	Sample size
p	Water vapour pressure (kPa)
P	Compaction pressure (MPa)
PE	Polyethylene, filament yarn
PET	Polyethyleneterephthalate, filament yarn
PP	Polypropylene, filament yarn
PP^D	Polypropylene, foils
PP^H	Polypropylene, foils
r	Fibre or yarn radius (µm)
RH	Relative humidity (%)
S	Swelling or shrinkage (%)
T	Absolute temperature (°K) or Absolute thickness of laminate samples (mm)
t½	Halftime to saturation (hours)
tex	Linear density (g/1000 m)
u	Water content, fractional
U	Water content (%)
U*	Relative water content (%)
U_{fs}	Water content at the fibre saturation point (%)
v	Absolute volume (cm^3)

v%	Volume percentage (%), calculated with respect to dry volume
V	Volume fraction
$V_{f\,(max)}$	Maximum obtainable fibre volume fraction
V_{f*}	Fibre volume fraction of composites with no porosity
V_L	Lumen volume fraction of fibres
$V_{p\,(1)}$	Porosity component
W	Weight fraction or Absolute width of laminate samples (mm)
w	Width of gap at the fibre/matrix interface (μm)
w%	Weigth percentage (%), calculated with respect to dry mass

Frequently used subscripts

0	Dry condition
c	Composite
f	Fibres
m	Matrix
p	Porosity
RH	Conditioning relative humidity
v	Volume
w	Water
x	Direction along fibres, axial direction (0°)
y	Direction perpendicular to fibres, in plane direction, transverse direction (90°)
z	Direction perpendicular to fibres, through thickness direction

A.1 APPENDIX A

THE EFFECT OF BOUND WATER COMPRESSION ON THE DETERMINATION OF PLANT FIBRE DENSITY

The determination of plant fibre density by pycnometry is based on four gravimetric measurements (Figure A.1): the empty pycnometer (C1), the water filled pycnometer (C2), the pycnometer containing the dry fibres (C3), and the pycnometer filled with both fibres and water (C4). From these measurements the following quantities are calculated:

$$m_{f0} = C3 - C1 \quad ; \quad m_w = C2 - C1 \quad ; \quad m_{w*} = C4 - C3$$

where m_{f0} is mass of the dry fibres, m_w is mass of the maximum amount of water in the pycnometer and m_{w*} is mass of the reduced amount of water in the pycnometer owing to the fibre volume. The fibre dry density (ρ_{f0}) is then calculated by the standard equation:

$$\rho_{f0} = \frac{m_{f0}\ \rho_w}{m_w - m_{w*}} \quad \Rightarrow \quad \rho_{f0} = \frac{m_{f0}}{\frac{m_w}{\rho_w} - \frac{m_{w*}}{\rho_w}} \tag{A.1}$$

where ρ_w is density of liquid water. However, because of the hygroscopic nature of the plant fibres, m_{w*} represents a mass with a density equal to a mixture of liquid water density and bound water density (ρ_{wb}). Thus, the resulting density (ρ_{w*}) can be calculated from the weight fractions of the two types of water:

$$\frac{1}{\rho_{w*}} = W_{wb}\ \frac{1}{\rho_{wb}} + W_w\ \frac{1}{\rho_w} \quad \Rightarrow \quad \frac{1}{\rho_{w*}} = \frac{m_{f0}\ u_{fs}}{m_{w*}}\ \frac{1}{\rho_{wb}} + \left(1 - \frac{m_{f0}\ u_{fs}}{m_{w*}}\right)\frac{1}{\rho_w} \tag{A.2}$$

where W is weight fraction, and u_{fs} is the fibre saturation point (i.e. the water content at which the fibres are fully saturated with bound water, but contain no free water). Thus, the modified water density predicted by equation (A.2) needs to be incorporated in equation (A.1), in order to include the density of bound water in the calculations of fibre dry density:

$$\rho_{f0} = \frac{m_{f0}}{\frac{m_w}{\rho_w} - \frac{m_{w*}}{\rho_{w*}}} \tag{A.3}$$

Based on raw data from the measurement of dry density of a sample of hemp fibres (He53) an example can be calculated using the standard equation (A.1) and the modified equation (A.3). The measurements were performed at 22.8 °C and the following quantities were determined:

$m_{f0} = C3 - C1 = 21.3841 - 20.5649 = 0.8192$ g

$m_{w} = C2 - C1 = 45.658 - 20.5649 = 25.0931$ g

$m_{w*} = C4 - C3 = 45.9661 - 21.3841 = 24.5820$ g

$\rho_{w} = 0.997585501$ g/cm^3 (tabulated)

When these quantities are inserted into the standard equation (A.1) the calculated dry density of the hemp yarn fibres is 1.5989 g/cm^3. To use the modified equation (A.3) requires knowledge of two more parameters, the fibre saturation point (u_{fs}) and the density of bound water (ρ_{wb}). From the determined sorption isotherm of hemp yarn fibres in Figure 4.7 (p. 64) the fibre saturation point can be approximated to be about 0.18. In a study of wood fibres the density of bound water was estimated to be about 1.017 g/cm^3 (Weatherwax and Tarkow 1968). Subsequently, the dry density of the hemp fibres, using the modified equation (A.3), is calculated to be 1.5901 g/cm^3, which is slightly below the density calculated by the standard equation. Thus, by including the effect of bound water compression, the determined dry density is decreased. In the given example, the difference between the two equations is within the range of normal measuring errors, and consequently equation (A.1) is acceptable.

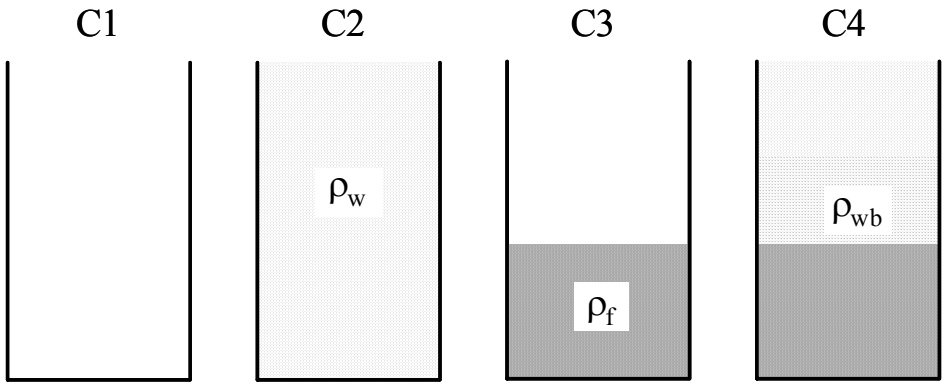

FIGURE A.1. *Diagram showing how the four gravimetric parameters C1-C4 are related to the content of the pycnometer.*

A.2 APPENDIX B

OSMOTIC GRADIENT METHOD FOR THE DETERMINATION OF PLANT FIBRE VOLUME

By selecting different aqueous salt solutions as displacement mediums in the pycnometric method described in Appendix A, the equilibrium volume of plant fibres can be determined at different ambient relative humidities. This approach can also supply information of bound water density as a function of the water content of the fibres.

All of the following experimental procedures should be performed under strictly isothermal conditions. Initially, the density of different saturated salt solutions (ρ_s) is determined from gravimetric measurements of the empty pycnometer (C1), the water-filled pycnometer (C2), and the pycnometer filled with a given salt solution ($C2^*$) (see Figure A.1):

$$\rho_s = \left(C2^* - C1\right) \frac{\rho_w}{\left(C2 - C1\right)} \tag{A.4}$$

where ρ_w is the tabulated density of water. The relative humidity of the different salt solutions is determined with a calibrated sensor.

The water sorption isotherm of the fibres is determined. Optimally, the data points of the isotherm should coincide with the relative humidities of the selected salt solutions; otherwise the water content at a given relative humidity is determined by interpolation.

The volume (v_f) of the fibres at a given relative humidity is determined from gravimetric measurements of the pycnometer containing the dry fibres (C3) and the pycnometer filled with both the fibres and a salt solution ($C4^*$):

$$\frac{1}{v_f} = \frac{\rho_s}{\left(C2^* - C1\right) - \left(\left(C4^* - C1\right) - \left(1 + u_{RH}\right)\left(C3 - C1\right)\right)} \tag{A.5}$$

where u_{RH} is the fibre water content at the relative humidity established by the salt solution. By repeating this procedure for different salt solutions a relationship between volume and relative humidity is established. Knowing how both the fibre volume and the fibre mass is changing with the relative humidity, the bound water density can be calculated at different fibre water contents.

The usability of the method has not yet been tested in practice, and it should therefore be regarded as a basis for further development.

A.3 APPENDIX C

ESTIMATION OF CRYSTALLINE CELLULOSE DENSITY

Native cellulose, or cellulose I, is the only one of the existing six different polymorphs of cellulose, which is found in nature (Nishiyama et al. 2002). Its crystalline structure has been a much-debated issue since it initially was documented by Carl von Nägeli in 1858 (Young and Rowell 1986), and moreover, recent evidence has been provided for the existence of two forms of native cellulose, cellulose Iα and Iβ (Nishiyama et al. 2002). It is generally accepted that cellulose Iβ dominates in evolutionary higher plants [4]. Its crystal unit cell is monoclinic (i.e. it has tree axes of different lengths and one non-90° angle) and is constructed from five cellobiose units ($C_{12}H_{20}O_{10}$): four at the edges and a central one, which is shifted by a distance of 0.25 cellobiose units in the chain direction (Figure A.2) (Sugiyama et al. 1991, Nishiyama et al. 2002).

The effective mass of the unit cell is two cellobiose units which equals 1.077 10^{-21} g $\left(= 1.661 \cdot 10^{-24}\ \text{g/u} \cdot 2 \cdot \left(12 \cdot 12.011\ \text{u} + 20 \cdot 1.008\ \text{u} + 10 \cdot 16.000\ \text{u}\right)\right)$. The dimensions of the unit cell (a, b and c) and the non-90° angle (γ) have been measured repeatedly in the past, however, with some minor variations. In a recent study, high resolution synchrotron X-ray diffraction was applied to determine the crystal structure of the unit cell, and the reported dimensions for a, b, and c were 0.778 nm, 0.820 nm and 1.038 nm, respectively, with a non-90° angle of 96.5° (Nishiyama et al. 2002). Subsequently, the volume of the unit cell is calculated to be 0.658 10^{-21} cm^3 $\left(= 0.778\ \text{nm} \cdot 0.820\ \text{nm} \cdot 1.038\ \text{nm} \cdot \cos\left(96.5° - 90°\right) \cdot 10^{-21}\right)$. Thus, the estimated density of crystalline cellulose Iβ is 1.64 g/cm^3.

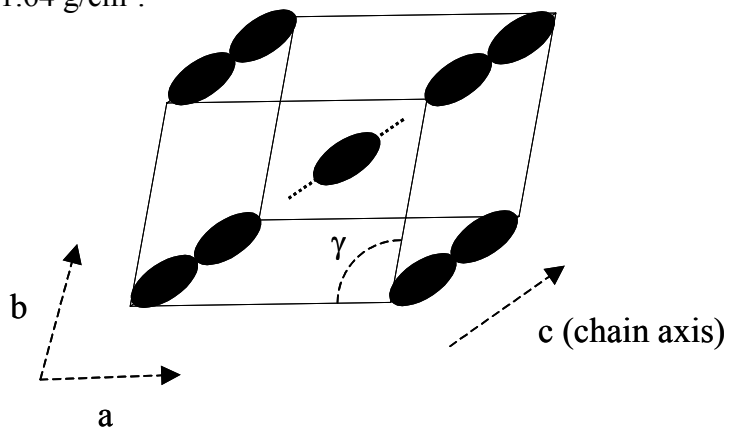

FIGURE A.2. *The crystal unit cell of cellulose Iβ. The ellipses represent the glucose molecules of the cellobiose units. The two half glucose molecules in the central chain are omitted for reasons of clarity.*

4. It has been reported by Sugiyama et al. (1991) that the difference in density between cellulose Iα and Iβ is very small (< 0.02 g/cm^3), and the contribution of cellulose Iα to the calculated density of crystalline cellulose can therefore be neglected.

A.4 APPENDIX D

ESTIMATION OF THE MEAN FIBRE ANGLE IN A RING SPUN YARN

In the operation of twist insertion in ring spinning (see Figure 2.15, p. 25), the initial filament of parallel fibres is converted into a helical yarn structure where the fibres are inclined with an angle to the yarn axis. However, the fibres are twisted around the yarn axis, and therefore the inclination angle of a given fibre depends on its radial position in the yarn cross-section; at the periphery the fibres are having larger inclination angles than in the yarn interior (see Figure 4.4, p. 61) (Klein 1998). The principles of the following estimation of the mean fibre angle are depicted in Figure A.3. The estimation is based on three assumptions:

- The fibres in the untwisted filament are all parallel.
- The fibres are distributed uniformly in the yarn cross-section.
- The yarn cross-section is circular.

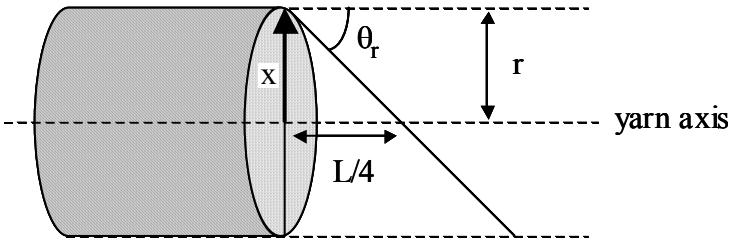

FIGURE A.3. *The principles in the estimation of the mean fibre angle.*

Since the fibres are twisted around the yarn axis it means that the length in the yarn direction of a single twist (L; denoted *pitch*) is identical for all fibres, and it can be calculated from the yarn radius (r) and the fibre angle [5] at the yarn surface (θ_r):

$$L = 4\ r\ \tan\left(\frac{\pi}{2} - \theta_r\right) \tag{A.6}$$

At a given radial distance from the yarn axis (x), the fibre angle (θ_x) can be calculated for all fibres located at this radial position:

$$\theta_x = \frac{\pi}{2} - \tan^{-1}\left(\frac{L}{4\ x}\right) \tag{A.7}$$

5. All angles in equations (A.6)-(A.12) are in radians.

The proportional contribution of θ_x to the overall mean fibre angle is obtained by multiplying it with the ratio: $2\pi x/\pi r^2$, and consequently, the mean fibre angle (θ_{mean}) is given by the integral equation:

$$\theta_{mean} = \frac{\pi}{2} - \int_0^r \frac{2\pi x}{\pi r^2} \tan^{-1}\left(\frac{L}{4x}\right) dx \qquad (A.8)$$

The integral is resolved to give an analytical expression of the mean fibre angle:

$$\theta_{mean} = \frac{\pi}{2} - \int_0^r \frac{2\pi x}{\pi r^2} \tan^{-1}\left(\frac{L}{4x}\right) dx \Rightarrow$$

$$\theta_{mean} = \frac{\pi}{2} - \frac{2}{r^2}\int_0^r x \tan^{-1}\left(\frac{L}{4x}\right) dx \quad \text{(see equation A.11)} \Rightarrow$$

$$\theta_{mean} = \frac{\pi}{2} - \frac{2}{r^2}\left(\left[\tfrac{1}{2}x^2 \tan^{-1}\left(\frac{L}{4x}\right)\right]_0^r - \int_0^r \tfrac{1}{2}x^2 \frac{1}{1+(L/4x)^2}\frac{L}{4}\left(-\frac{1}{x^2}\right) dx\right) \Rightarrow$$

$$\theta_{mean} = \frac{\pi}{2} - \frac{2}{r^2}\left(\left[\tfrac{1}{2}x^2 \tan^{-1}\left(\frac{L}{4x}\right)\right]_0^r - \int_0^r -\frac{x^2 L}{8x^2 + L^2/2} dx\right) \Rightarrow$$

$$\theta_{mean} = \frac{\pi}{2} - \frac{2}{r^2}\left(\left[\tfrac{1}{2}x^2 \tan^{-1}\left(\frac{L}{4x}\right)\right]_0^r - \left(-\frac{L}{8}\int_0^r \frac{x^2}{x^2 + (L/4)^2} dx\right)\right) \quad \text{(see equation A.12)} \Rightarrow$$

$$\theta_{mean} = \frac{\pi}{2} - \frac{2}{r^2}\left(\tfrac{1}{2}r^2 \tan^{-1}\left(\frac{L}{4r}\right) + \frac{L}{8}\left(r - \frac{L}{4}\tan^{-1}\left(\frac{4r}{L}\right)\right)\right) \Rightarrow$$

$$\theta_{mean} = \frac{\pi}{2} - \frac{2}{r^2}\left(\tfrac{1}{2}r^2 \tan^{-1}\left(\frac{L}{4r}\right) + \frac{Lr}{8} - \frac{L^2}{32}\tan^{-1}\left(\frac{4r}{L}\right)\right) \Rightarrow$$

$$\theta_{mean} = \frac{\pi}{2} - \left(\tan^{-1}\left(\frac{L}{4r}\right) + \frac{L}{4r} - \frac{L^2}{16r^2}\tan^{-1}\left(\frac{4r}{L}\right)\right) \qquad (A.9)$$

By inserting equation (A.6) into equation (A.9), r and L are eliminated and it is demonstrated that θ_{mean} is a function of θ_r only:

$$\theta_{mean} = \frac{\pi}{2} - \left(\tan^{-1}\left(\tan\left(\frac{\pi}{2} - \theta_r\right)\right) + \tan\left(\frac{\pi}{2} - \theta_r\right) - \left(\tan\left(\frac{\pi}{2} - \theta_r\right)\right)^2 \tan^{-1}\left(\frac{1}{\tan(\pi/2 - \theta_r)}\right)\right) \Rightarrow$$

$$\theta_{mean} = \frac{\pi}{2} - \left(\left(\frac{\pi}{2} - \theta_r\right) + \tan\left(\frac{\pi}{2} - \theta_r\right) - \left(\tan\left(\frac{\pi}{2} - \theta_r\right)\right)^2 \theta_r\right) \Rightarrow$$

$$\theta_{mean} = \theta_r - \tan\left(\frac{\pi}{2} - \theta_r\right) + \left(\tan\left(\frac{\pi}{2} - \theta_r\right)\right)^2 \theta_r \qquad (A.10)$$

Figure A.4 shows the mean fibre angle as a function of the surface fibre angle as calculated by equation (A.10). For surface fibre angles between 0° and 40° the relationship is almost linear with a coefficient of regression of 0.999 and a slope of 0.7. Thus, for surface fibre angles below 40°, the mean fibre angle can be approximated by multiplying the surface angle with 0.7; e.g. for a surface fibre angle of 20.0°, the approximated mean fibre angle is 14.0°, whereas the calculated mean fibre angle is 13.6°.

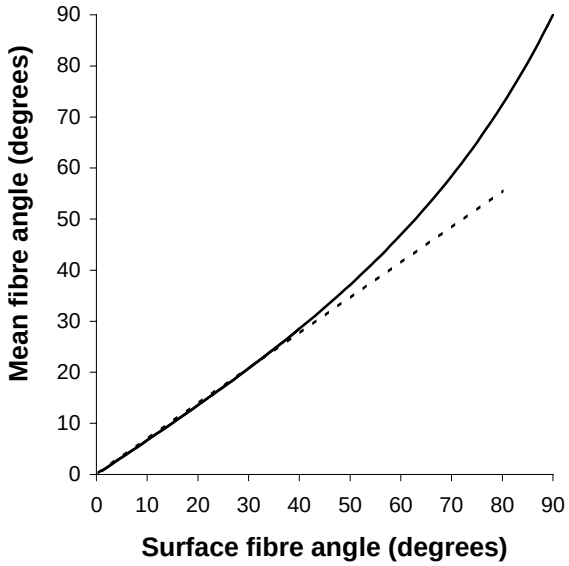

FIGURE A.4. *Relationship between mean fibre angle and surface fibre angle. Dotted line is a regression line (y=0.695x; R^2=0.999) for surface fibre angles between 0° and 40°.*

Supporting equations used in the resolution of equation (A.9):

$$\frac{d}{dx}\tan^{-1}(u) = \frac{1}{1+u^2}\frac{du}{dx} \tag{A.11}$$

$$\int \frac{x^2}{x^2+a^2}\,dx = x - a\,\tan^{-1}\left(\frac{x}{a}\right) \tag{A.12}$$

A.5 APPENDIX E

EQUILIBRIUM MASS AND DIMENSIONS OF LAMINATE SAMPLES IN WATER SORPTION EXPERIMENT

- The presented data are mean ± stdv. with a sample size of 5 for mass (m) and 10 for the three dimensions: length (L), width (W) and thickness (T). The dimensions were measured at two locations for each sample.
- The applied hemp yarn type for all laminates was He53. See Table 4.8 (p. 78) for more specifications of the laminates.

TABLE A.1. *Results for laminate samples initially conditioned at 65 % RH and then conditioned at 35 % RH.*

Matrix type	Mass (g) and Dim. (mm)	Fibre volume fraction				
		0	**0.21**	**0.33**	**0.38**	**0.43**
PET	m_{65}	0.5905 ± 0.0094	0.5699 ± 0.0070	0.6762 ± 0.0180	0.7437 ± 0.0103	0.7781 ± 0.0100
	m_{35}	0.5888 ± 0.0093	0.5664 ± 0.0069	0.6709 ± 0.0181	0.7377 ± 0.0102	0.7710 ± 0.0100
	L_{65}	14.832 ± 0.127	14.808 ± 0.121	15.036 ± 0.032	15.043 ± 0.032	15.020 ± 0.064
	L_{35}	14.812 ± 0.132	14.802 ± 0.121	15.040 ± 0.032	15.040 ± 0.034	15.017 ± 0.063
	W_{65}	14.796 ± 0.062	15.074 ± 0.0046	15.157 ± 0.041	15.240 ± 0.131	15.262 ± 0.058
	W_{35}	14.775 ± 0.062	15.027 ± 0.050	15.096 ± 0.040	15.170 ± 0.132	15.179 ± 0.059
	T_{65}	2.092 ± 0.045	1.919 ± 0.014	2.186 ± 0.053	2.399 ± 0.016	2.494 ± 0.028
	T_{35}	2.086 ± 0.044	1.911 ± 0.015	2.176 ± 0.050	2.385 ± 0.017	2.477 ± 0.029
PE	m_{65}	0.3690 ± 0.0020		0.5421 ± 0.0039		
	m_{35}	0.3686 ± 0.0020		0.5375 ± 0.0038		
	L_{65}	14.914 ± 0.058		14.986 ± 0.050		
	L_{35}	14.897 ± 0.062		14.985 ± 0.049		
	W_{65}	14.957 ± 0.124		15.115 ± 0.035		
	W_{35}	14.946 ± 0.117		15.050 ± 0.037		
	T_{65}	1.788 ± 0.015		2.185 ± 0.010		
	T_{35}	1.788 ± 0.017		2.172 ± 0.010		

TABLE A.1. CONTINUED.

Matrix type	Mass (g) and Dim. (mm)	Fibre volume fraction				
		0	0.21	0.33	0.38	0.43
PP	m_{65}	0.3790 ± 0.0025		0.5585 ± 0.0093		
	m_{35}	0.3786 ± 0.0026		0.5534 ± 0.0093		
	L_{65}	14.941 ± 0.141		15.049 ± 0.047		
	L_{35}	14.931 ± 0.148		15.048 ± 0.047		
	W_{65}	14.949 ± 0.039		15.177 ± 0.055		
	W_{35}	14.929 ± 0.024		15.106 ± 0.037		
	T_{65}	1.918 ± 0.024		2.268 ± 0.020		
	T_{35}	1.915 ± 0.023		2.256 ± 0.021		

TABLE A.2. *Results for laminate samples initially conditioned at 65 % RH and then conditioned at 85 % RH.*

Matrix type	Mass (g) and Dim. (mm)	Fibre volume fraction				
		0	0.21	0.33	0.38	0.43
PET	m_{65}	0.5981 ± 0.0117	0.5696 ± 0.0071	0.6740 ± 0.0092	0.7439 ± 0.0080	0.7781 ± 0.0106
	m_{85}	0.5995 ± 0.0117	0.5750 ± 0.0071	0.6827 ± 0.0093	0.7546 ± 0.0082	0.7904 ± 0.0108
	L_{65}	14.978 ± 0.090	14.827 ± 0.050	15.046 ± 0.048	15.088 ± 0.040	14.983 ± 0.033
	L_{85}	14.968 ± 0.082	14.815 ± 0.051	15.032 ± 0.047	15.075 ± 0.038	14.972 ± 0.033
	W_{65}	14.853 ± 0.085	15.079 ± 0.044	15.184 ± 0.044	15.323 ± 0.113	15.235 ± 0.108
	W_{85}	14.844 ± 0.087	15.138 ± 0.043	15.287 ± 0.043	15.448 ± 0.113	15.374 ± 0.110
	T_{65}	2.083 ± 0.032	1.923 ± 0.008	2.189 ± 0.034	2.378 ± 0.019	2.489 ± 0.029
	T_{85}	2.082 ± 0.033	1.931 ± 0.009	2.202 ± 0.034	2.399 ± 0.019	2.517 ± 0.026
PE	m_{65}	0.3644 ± 0.0102		0.5383 ± 0.0074		
	m_{85}	0.3646 ± 0.0102		0.5459 ± 0.0069		
	L_{65}	14.975 ± 0.098		14.991 ± 0.045		
	L_{85}	14.968 ± 0.101		14.969 ± 0.043		
	W_{65}	14.824 ± 0.313		15.123 ± 0.072		
	W_{85}	14.817 ± 0.315		15.212 ± 0.075		
	T_{65}	1.780 ± 0.023		2.162 ± 0.037		
	T_{85}	1.779 ± 0.019		2.177 ± 0.038		

TABLE A.2. CONTINUED.

Matrix type	Mass (g) and Dim. (mm)	Fibre volume fraction				
		0	**0.21**	**0.33**	**0.38**	**0.43**
PP	m_{65}	0.3764 ± 0.0073		0.5516 ± 0.0037		
	m_{85}	0.3768 ± 0.0072		0.5599 ± 0.0037		
	L_{65}	14.925 ± 0.100		15.080 ± 0.048		
	L_{85}	14.921 ± 0.107		15.084 ± 0.095		
	W_{65}	14.835 ± 0.137		15.166 ± 0.063		
	W_{85}	14.820 ± 0.128		15.263 ± 0.120		
	T_{65}	1.924 ± 0.017		2.228 ± 0.027		
	T_{85}	1.924 ± 0.020		2.248 ± 0.030		

A.6 APPENDIX F

PARAMETRIC VARIABLES OF COMPOSITES
IN TENSILE TESTING EXPERIMENT

Testing direction: All composites were tested in the axial (0°) and in the transverse (90°) direction. The intermediate off-axis angles (10°, 20°, 30°, 45° and 60°) were tested only for a single combination of parametric variables: commingled filament-winding; He53; PET; 0.3-0.4; 200 °C; 65 % RH.

Fibre/matrix mixing: Film-stacking

		Yarn type				Matrix type				Fibre volume fraction			Process temperature (°C)					Conditioning humidity (% RH)			
		He47	He53	He91	Fl64	PET	PE	PP	MAPP	0.2-0.3	0.3-0.4	0.5-0.6	180	190	200	210	220	35	65	85	Uncon.
Yarn type	He47																				
	He53							X	X		X			X							X
	He91							X			X	X	X	X	X	X					X
	Fl64							X			X	X		X							X
Matrix type	PET																				
	PE																				
	PP		X	X	X						X	X	X	X	X	X					X
	MAPP		X								X			X							X
Fibre volume fraction	0.2-0.3																				
	0.3-0.4																				
	0.4-0.5		X	X	X			X	X				X	X	X	X					X
	0.5-0.6			X	X			X						X							X
Process temperature (°C)	180			X				X				X									X
	190		X	X	X			X	X			X	X								X
	200			X				X				X									X
	210			X				X				X									X
	220																				
Conditioning humidity (% RH)	35																				
	65																				
	85																				
	Uncon.		X	X	X			X	X		X	X	X	X	X	X					

Fibre/matrix mixing: Commingled filament-winding

		Yarn type				Matrix type				Fibre volume fraction				Process temperature (°C)				Conditioning humidity (% RH)			
		He47	He53	He91	Fl64	PET	PE	PP	MAPP	0.2-0.3	0.3-0.4	0.4-0.5	0.5-0.6	180	190	200	210	220	35	65	85	Uncon.
Yarn type	He47					X	X				X	X		X		X		X		X		
	He53					X	X	X		X	X	X	X			X		X	X	X	X	X
	He91					X				X	X	X				X				X		
	Fl64																					
Matrix type	PET	X	X	X						X	X	X	X	X		X		X	X	X	X	X
	PE	X	X								X			X		X		X		X		
	PP		X								X					X				X		
	MAPP																					
Fibre volume fraction	0.2-0.3		X	X		X										X				X		
	0.3-0.4	X	X	X		X	X	X						X		X		X	X	X	X	X
	0.4-0.5	X	X	X		X										X		X		X		X
	0.5-0.6		X			X												X		X		
Process temperature (°C)	180	X				X	X				X									X		
	190																					
	200	X	X	X		X	X	X		X	X	X							X	X	X	X
	210																					
	220	X	X			X	X				X	X	X					X		X		X
Conditioning humidity (% RH)	35		X			X					X					X						
	65	X	X	X		X	X	X		X	X	X	X	X		X		X				
	85		X			X					X					X						
	Uncon.		X			X					X	X				X		X				

A.7 APPENDIX G

TENSILE PROPERTIES OF COMPOSITES

- The presented data are mean ± stdv. with a sample size of 4-6.
- The table legends present the parametric variables by the order:
  Fibre/matrix mixing; Testing direction; Yarn type; Matrix type; Fibre volume fraction; Process temperature; Conditioning humidity
- The parameters in bold in the table legends are the variable parameters.
- It should be noted that strain at ultimate stress measured in the transverse direction is not identical to strain at failure (see Figure 4.35, p. 106).

TABLE A.3. *Film-stacking; 0 ° and 90 °; He91; PP^H; **V_f**; **Process temperature**; Uncontrolled*

V_f	V_p	Stiffness		Ultimate stress		Strain at ultimate stress	
		0°	90°	0°	90°	0°	90°
180 °C							
0.451	0.107	20.2 ± 1.4		191.8 ± 16.9		0.020 ± 0.002	
190 °C							
0.445	0.047	23.2 ± 1.5		205.6 ± 13.1		0.018 ± 0.002	
0.428	0.045		1.4 ± 0.1		6.3 ± 0.2		0.042 ± 0.013
0.474	0.060	22.8 ± 1.7		232.9 ± 13.5		0.023 ± 0.002	
0.488	0.080		1.1 ± 0.1		5.0 ± 0.4		0.053 ± 0.023
0.485	0.055	23.1 ± 1.2		219.0 ± 8.3		0.020 ± 0.001	
0.516	0.081	21.5 ± 1.4		239.3 ± 9.2		0.024 ± 0.002	
0.512	0.087		0.9 ± 0.2		4.0 ± 0.2		0.038 ± 0.020
0.542	0.107	17.8 ± 1.7		247.2 ± 6.8		0.026 ± 0.001	
0.544	0.102		0.6 ± 0.04		3.4 ± 0.1		0.062 ± 0.014
200 °C							
0.487	0.047	23.3 ± 1.7		215.4 ± 8.3		0.018 ± 0.001	
210°C							
0.499	0.051	25.4 ± 1.3		216.2 ± 16.5		0.016 ± 0.001	

TABLE A.4. *Film-stacking; 0°and 90°; He53; **Matrix type**; 0.4-0.5; 190 °C; Uncontrolled*

V_f	V_p	Stiffness		Ultimate stress		Strain at ultimate stress	
		0°	90°	0°	90°	0°	90°
PP^D							
0.415	0.057	21.1 ± 0.9		214.5 ± 8.0		0.022 ± 0.001	
0.401	0.040		1.8 ± 0.1		7.6 ± 0.8		0.023 ± 0.006
MAPP							
0.396	0.040	20.1 ± 0.9		208.1 ± 6.4		0.019 ± 0.001	
0.346	0.026		2.5 ± 0.1		16.3 ± 0.9		0.014 ± 0.004

TABLE A.5. *Film-stacking; 0°and 90°; Fl64; PP^H; **V_f**; 190 °C; Uncontrolled*

V_f	V_p	Stiffness		Ultimate stress		Strain at ultimate stress	
		0°	90°	0°	90°	0°	90°
0.420	0.044	26.9 ± 1.4		251.1 ± 7.7		0.015 ± 0.001	
0.408	0.048		1.5 ± 0.1		6.5 ± 0.3		0.020 ± 0.006
0.450	0.042	27.8 ± 1.6		271.2 ± 11.9		0.016 ± 0.001	
0.457	0.057		1.3 ± 0.02		5.6 ± 0.2		0.024 ± 0.005
0.507	0.058	28.7 ± 1.5		287.5 ± 13.9		0.018 ± 0.001	
0.504	0.068		1.1 ± 0.04		4.4 ± 0.2		0.038 ± 0.015
0.543	0.084	28.2 ± 1.4		320.7 ± 16.1		0.019 ± 0.001	
0.540	0.079		0.8 ± 0.1		3.4 ± 0.2		0.038 ± 0.016

TABLE A.6. *Comm. filament-winding; He53; PET; **V_f**; **Process temperature**; Uncontrolled*

V_f	V_p	Stiffness		Ultimate stress		Strain at ultimate stress	
		0°	90°	0°	90°	0°	90°
200 °C							
0.317	0.017	19.3 ± 0.7	4.0 ± 0.04	205.9 ± 8.0	24.4 ± 0.5	0.022 ± 0.001	0.009 ± 0.001
0.357	0.042	21.4 ± 1.6	4.1 ± 0.02	223.9 ± 8.2	24.4 ± 0.2	0.021 ± 0.001	0.009 ± 0.001
0.466	0.094	24.9 ± 0.8	2.4 ± 0.2	240.9 ± 7.1	12.0 ± 0.6	0.022 ± 0.002	0.010 ± 0.001
220 °C							
0.236	0.019	16.7 ± 0.7	4.0 ± 0.1	127.5 ± 9.9	22.8 ± 2.7	0.013 ± 0.002	0.007 ± 0.002
0.312	0.031	19.6 ± 0.3	4.1 ± 0.1	159.3 ± 12.6	22.9 ± 2.4	0.014 ± 0.002	0.007 ± 0.001
0.369	0.012	22.2 ± 0.6	4.3 ± 0.01	186.5 ± 13.1	22.1 ± 1.8	0.015 ± 0.002	0.006 ± 0.001
0.431	0.024	24.7 ± 1.1	4.3 ± 0.1	215.0 ± 9.4	23.0 ± 1.2	0.016 ± 0.002	0.007 ± 0.001
0.477	0.072	27.1 ± 1.0	3.6 ± 0.3	251.0 ± 13.9	16.3 ± 1.0	0.018 ± 0.002	0.006 ± 0.001

TABLE A.7. *Comm. filament-winding; 0 ° and 90 °; He53; PET;* V_f*;* ***Process temperature****; 65 % RH*

V_f	V_p	Stiffness		Ultimate stress		Strain at ultimate stress	
		0°	90°	0°	90°	0°	90°
200 °C							
0.205	0.017	12.7 ± 0.3	3.3 ± 0.1	159.4 ± 3.1	20.8 ± 0.3	0.030 ± 0.001	0.009 ± 0.001
0.335	0.031	17.6 ± 0.7	3.5 ± 0.1	204.7 ± 5.0	18.8 ± 0.2	0.029 ± 0.002	0.008 ± 0.001
0.430	0.027	18.8 ± 1.0	3.6 ± 0.1	223.8 ± 7.2	17.3 ± 0.6	0.031 ± 0.002	0.008 ± 0.001
220 °C							
0.506	0.174	19.0 ± 1.4	0.8 ± 0.1	231.4 ± 15.1	4.3 ± 0.5	0.030 ± 0.003	0.011 ± 0.002
0.508	0.136	18.1 ± 0.6	0.8 ± 0.3	220.9 ± 9.7	4.5 ± 0.5	0.031 ± 0.002	0.011 ± 0.004

TABLE A.8. *Comm. filament-winding; 0 ° and 90 °; He53; PET; 0.3-0.4; 200 °C;* ***Conditioning humidity****[*]*

V_f	V_p	Stiffness		Ultimate stress		Strain at ultimate stress	
		0°	90°	0°	90°	0°	90°
35 % RH							
0.337	0.026	18.1 ± 0.6	3.5 ± 0.3	200.0 ± 6.2	22.8 ± 1.7	0.026 ± 0.002	0.012 ± 0.001
85 % RH							
0.336	0.027	14.2 ± 1.1	2.9 ± 0.1	191.2 ± 10.0	16.1 ± 0.4	0.037 ± 0.003	0.009 ± 0.001

** See results for 65 % RH in Table A.7 row 2.*

TABLE A.9. *Comm. filament-winding;* ***Testing direction****[*]**; He53; PET;0.3-0.4; 200 °C; 65 % RH*

V_f	V_p	Stiffness	Ultimate stress	Strain at ultimate stress
10°				
0.338	0.023	16.4 ± 1.6	124.0 ± 5.6	0.017 ± 0.002
20°				
0.338	0.023	9.3 ± 1.0	72.1 ± 3.2	0.015 ± 0.002
30°				
0.338	0.023	7.5 ± 0.9	49.3 ± 2.2	0.010 ± 0.001
45°				
0.338	0.024	4.8 ± 0.4	31.3 ± 1.3	0.009 ± 0.001
60°				
0.336	0.027	3.6 ± 0.1	24.2 ± 0.6	0.009 ± 0.001

[*] See results for 0 ° and 90 ° in Table A.7 row 2.

TABLE A.10. *Comm. filament-winding; 0 ° and 90 °; He53;* ***Matrix type**** *; 0.3-0.4; 200 °C; 65 % RH*

V_f	V_p	Stiffness		Ultimate stress		Strain at ultimate stress	
		0°	90°	0°	90°	0°	90°
PE							
0.319	0.034	15.8 ± 0.3	1.8 ± 0.1	161.2 ± 2.7	6.2 ± 0.2	0.027 ± 0.002	0.028 ± 0.007
PP							
0.322	0.036	15.4 ± 0.4	2.0 ± 0.1	172.7 ± 5.0	7.0 ± 0.5	0.030 ± 0.001	0.024 ± 0.003

* *See results for PET in Table A.7 row 2.*

TABLE A.11. *Comm. filament-winding; 0 ° and 90 °; He47; PET;* ***V_f; Process temperature****; 65 % RH*

V_f	V_p	Stiffness		Ultimate stress		Strain at ultimate stress	
		0°	90°	0°	90°	0°	90°
180 °C							
0.308	0.043	19.4 ± 0.4	3.1 ± 0.1	244.1 ± 3.9	12.9 ± 0.9	0.021 ± 0.0002	0.006 ± 0.002
200 °C							
0.313	0.028	20.1 ± 0.6	3.2 ± 0.1	221.3 ± 5.1	15.1 ± 0.3	0.018 ± 0.0004	0.006 ± 0.0003
0.402	0.032	24.3 ± 0.9	3.4 ± 0.1	254.3 ± 8.2	14.3 ± 0.5	0.018 ± 0.001	0.006 ± 0.0001
0.475	0.081	27.6 ± 0.6	3.0 ± 0.1	277.3 ± 14.0	10.2 ± 0.7	0.018 ± 0.001	0.006 ± 0.001
220 °C							
0.316	0.018	22.5 ± 0.5	3.4 ± 0.01	169.8 ± 11.8	16.3 ± 0.9	0.012 ± 0.001	0.005 ± 0.001
0.406	0.023	26.1 ± 0.6	3.5 ± 0.1	204.3 ± 10.6	14.6 ± 1.3	0.013 ± 0.001	0.005 ± 0.001
0.494	0.043	28.8 ± 0.4	3.4 ± 0.1	221.5 ± 5.9	13.2 ± 0.5	0.013 ± 0.001	0.006 ± 0.0004

TABLE A.12. *Comm. filament-winding; 0 ° and 90 °; He47; PE; 0.3-0.4;* ***Process temperature****; 65 % RH*

V_f	V_p	Stiffness		Ultimate stress		Strain at ultimate stress	
		0°	90°	0°	90°	0°	90°
180 °C							
0.324	0.048	19.9 ± 0.2	1.6 ± 0.1	192.9 ± 4.4	5.3 ± 0.2	0.018 ± 0.001	0.041 ± 0.010
200 °C							
0.326	0.042	20.4 ± 0.5	1.6 ± 0.04	179.8 ± 2.7	5.3 ± 0.2	0.016 ± 0.001	0.042 ± 0.009
220 °C							
0.326	0.043	20.8 ± 0.3	1.5 ± 0.1	136.2 ± 4.1	5.0 ± 0.02	0.011 ± 0.0004	0.037 ± 0.004

TABLE A.13. *Comm. filament-winding;0° and 90°; He91; PET;* V_f*; 200°C; 65 % RH*

V_f	V_p	Stiffness		Ultimate stress		Strain at ultimate stress	
		0°	90°	0°	90°	0°	90°
0.302	0.035	16.1 ± 0.4	3.5 ± 0.04	187.4 ± 7.7	18.0 ± 0.4	0.024 ± 0.001	0.006 ± 0.0003
0.386	0.049	19.4 ± 0.2	3.5 ± 0.03	227.8 ± 6.0	16.4 ± 0.1	0.024 ± 0.001	0.006 ± 0.0002
0.449	0.060	20.6 ± 0.2	3.1 ± 0.1	231.9 ± 3.4	10.8 ± 0.6	0.024 ± 0.0002	0.007 ± 0.001

Evaluation of properties of unidirectional hemp/polypropylene composites – influence of fiber content and fiber/matrix interface variables

Bo Madsen [a,b,*], Tom Andersen [a], David Plackett [c] and Hans Lilholt [a]

[a] Materials Research Department, Risø National Laboratory, 4000 Roskilde, Denmark

[b] Department of Civil Engineering, Technical University of Denmark, 2800 Lyngby, Denmark

[c] Danish Polymer Centre, Technical University of Denmark, 2800 Lyngby, Denmark

Abstract

Filament-wound textile hemp yarn was used in combination with unmodified or maleated polypropylene films to produce plates of unidirectional composites. The material quality was characterized by fiber and porosity content as well as by tensile mechanical properties. With a matrix of unmodified polypropylene, the composite axial strength and stiffness were recorded in excess of 200 MPa and 20 GPa, respectively, values which were only weakly correlated with composite fiber content. In contrast, the corresponding values in the transverse direction were less than 10 MPa and 2 GPa, respectively, and were negatively correlated with composite fiber content. With a matrix of maleated polypropylene transverse tensile properties were significantly increased with the axial ones being unaffected. The research demonstrated the feasibility of obtaining composites based on hemp yarn with very good tensile properties in one direction. The use of maleated polypropylene as matrix component reduced the anisotropy of the unidirectional composites.

Introduction

From both ecological and engineering points of views the use of non-wood plant fibers as reinforcement in composite materials contains some attracting perspectives. As opposed to wood fibers, which are a well-established natural source component in composite production, plant fibers are a more rapidly renewable resource (one year for hemp against at least thirty years for softwoods) with improved mechanical properties (1). The majority of studies, examining the properties of plant fiber composites, are based on techniques directly adopted from the production of wood fiber composites, i.e. moulding of randomly oriented fibers in a binder matrix resulting in materials with quasi-isotropic physical/mechanical properties. Indeed, these studies have shown that plant fibers offer a good

alternative to wood fibers in composite production (2-4). However, to fully utilize the great potential of natural fibers as composite reinforcement requires control of fiber orientation. With wood fibers, methods to control fiber orientation in the composite are practically limited by their relative small lengths (about 3 mm for softwood) (1). In contrast, plant fibers are generally longer (10-15 mm for hemp fibers) and are most often situated in bundles, which further more increase length (1). The longer length of plant fibers eases the handling process and therefore different approaches can be applied to align the fibers; hand lay-up of fibers (5-12,19), filament-winding of textile yarns (13-15) or use of woven fabrics (16-18). The method employed in this study is filament winding of textile hemp yarn in order to produce unidirectional fiber configurations. Most data available on properties of aligned plant fiber composites are mechanical data measured in the fiber direction (5-12) whereas only a few studies have attempted to investigate off-axis properties (13,19). With the perspective of using plant fiber composites in construction applications data on off-axis properties are crucial since there is almost always a component of the structural loads in an angle to the fibre axis. Presented in this paper are preliminary results of a larger study set out to investigate the physical and mechanical behavior of plant fiber composites with controlled fiber orientations.

Methods and materials

In this paper experimental details of two independent studies of unidirectional hemp/polypropylene composites are presented with their respective objectives.

Influence of fiber content variable on composite properties

Unidirectional composites of textile difilament twisted hemp yarn (Linificio e Canapificio Nazionale, Italy; Nm 20/2) and unmodified polypropylene, PP_H (Hoechst Folien; Trespaphan NNA, film; thickness 0.025 mm) were manufactured with fiber contents in the range 40-60 vol.%. The objectives were to determine the optimal fibre content and to characterize any dependency of mechanical behavior on fiber content.

Influence of fiber/matrix interface variable on composite properties

Unidirectional composites of textile monofilament hemp yarn (Linificio e Canapificio Nazionale, Italy; Nm 20/1) in combination with either unmodified polypropylene, PP_D (Dow; H1710-05; granulate) or maleated polypropylene, MAPP (Uniroyal Chemical; Polybond 3002; granulate) were manufactured aiming at a fiber content of 40 vol.%. Prior to the experiment the two types of polypropylene

granulates were extruded into films of 0.15 mm thickness. The objective was to characterize the mechanical behavior as a function of quality of the fiber/matrix interface.

Fabrication and characterization

With a custom-built winding-machine the hemp yarn was wound on to metal frames (400x400 mm) with 1 mm sideward steps per rotation producing fiber assemblies with high yarn alignment and controlled uniform thickness. Polypropylene matrix films were combined with the fiber assemblies by a film-stacking technique and processed by vacuum heating (190 ºC, 15 min) and press consolidation (200 kN, 1 min) (20). The rectangular dimensions of the manufactured composite laminate plates were 240x300 mm, with a thickness varying in the range 1.8-2.4 mm, depending on the actual fibre/matrix ratio. Composite and fiber densities were determined from the immersion method (Archimedes principle). From using xylene to dissolve the polymer matrix and applying gravimetric measurements, the exact fiber and matrix volume fractions were calculated. Composite porosity content was estimated as the volume fraction not taken up by the fiber and matrix components (4). The composite plates were cut out into standard dumbbell shaped test specimens (180x25 mm with gaugesection 30x15 mm) in both the axial (0^o) and transverse (90^o) fiber direction. Mechanical tensile tests were performed at room temperature on an Instron machine with crosshead speed 2 mm/min and loadcell 10 kN. Displacements were measured with two extensometers centred on each side of the test specimens. Nominal ultimate strength (MPa), nominal stiffness (GPa, linear regression between 0-0.1% deformation) and failure elongation (%) were determined from the stress-strain curves. Polished composite cross-sections were mounted under a light microscope to examine material microstructure.

Results

Prior to the experiments the tensile properties of unreinforced matrix material were measured for all three types of polypropylenes used in the studies, PP_H, PP_D and MAPP, giving values of (i) strength 28.1, 27.7 and 29.2 MPa, (ii) stiffness 1.5, 1.6 and 1.8 GPa and (iii) failure elongation 6.0, 9.6 and 8.8%. These results demonstrate that the properties of the three polypropylene types are practically identical with MAPP having only slightly higher values for strength and stiffness and PP_H having lower values for failure elongation.

Influence of fiber content variable on composite properties

Good quality unidirectional hemp/PP_H composites with fiber volume fractions ranging from 44 to 55% were manufactured. Composite microstructure was examined by light microscopy demonstrating good

fibre/matrix intermixing with an acceptably small porosity content indicated by the limited extent of dark areas on cross-sections (Figure 1). However, manufacture of composites having fiber contents below 44 vol.% or above 55 vol.% were characterized by either many interlaminar yarn displacements or by the poor degree of fiber/matrix intermixing, respectively, and therefore these laminates were discarded.

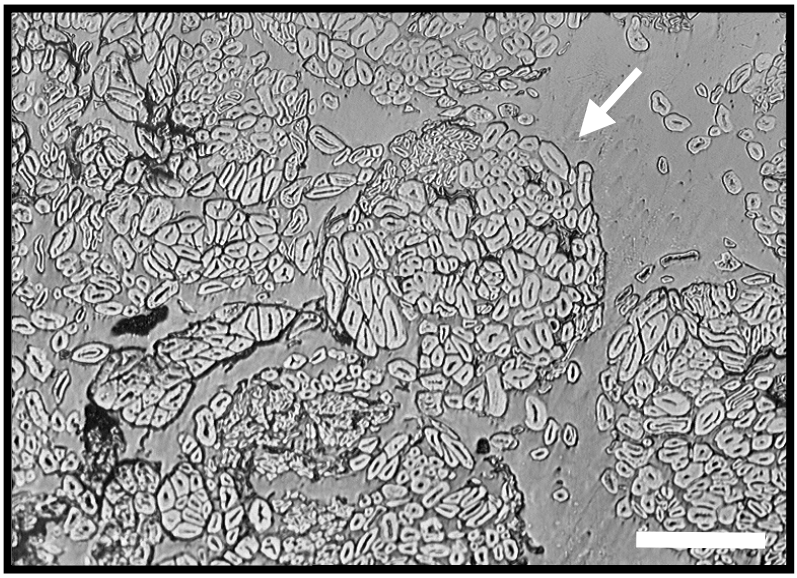

Figure 1. Light microscopy micrograph of hemp/PP_H axial cross-section showing yarn fiberbundles (arrow) and single separated hemp fibers intermixed with the PP_H matrix. Note also dark areas, which is a possible indication of porosity. Fiber content is 48 vol.% and scale bar is 100 μm.

Table 1. Porosity and tensile properties of unidirectional hemp/PP_H composites with different fiber contents. Composite density was determined in the range 1.16-1.19 g/cm^3 increasing with the actual fiber content. Data are given as means (± stdv.) with sample size n=3 and n=5 for porosity content and tensile properties respectively.

Fiber content (vol. %)	**Porosity (vol. %)**	**Strength (MPa)**		**Stiffness (GPa)**	
		Axial	Transverse	Axial	Transverse
44.7	4.5 ± 0.3	205.6 ± 13.1		23.2 ± 1.5	
43.1	4.3 ± 0.5		6.28 ± 0.21		1.36 ± 0.06
47.7	5.6 ± 0.7	232.9 ± 13.5		22.8 ± 1.7	
49.1	7.6 ± 1.1		5.00 ± 0.38		1.12 ± 0.07
51.9	7.8 ± 0.4	239.3 ± 9.2		21.5 ± 1.4	
51.6	8.3 ± 1.3		3.95 ± 0.16		0.89 ± 0.16
54.6	10.3 ± 2.0	247.2 ± 6.8		17.8 ± 1.7	
54.7	9.9 ± 0.8		3.35 ± 0.11		0.55 ± 0.04

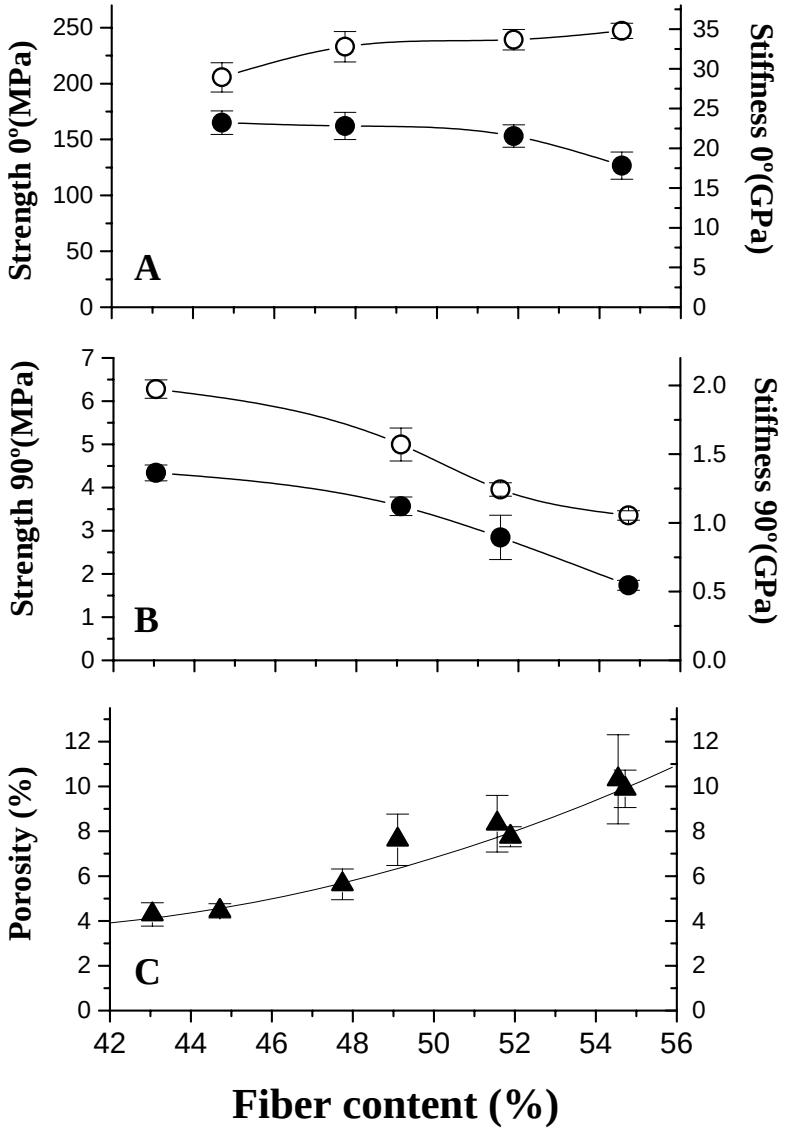

Figure 2. Tensile strength (O) and stiffness (l) of unidirectional hemp/PP_H composites as a function of fiber content tested in the (A) axial and (B) transverse fiber direction. (C) shows composite porosity content of the eight laminates presented in (A) and (B).

Physical and mechanical data sampled from composite plates grouped by four different levels of fiber contents (44, 48, 52 and 55 vol.%) are presented in Table 1 and graphically illustrated in Figure 2. In the axial fiber direction tensile strength and stiffness were differently affected by composite fiber content (Figure 2A). The data indicate that strength is increasing slightly with fiber content most notably in the range 44-48 vol.%. In contrast, stiffness is decreasing slightly with fiber content most notably in the range 52-55 vol.%. For the transverse tensile properties both strength and stiffness are

considerably lower than the strength and stiffness of unreinforced PP_H and are clearly decreasing as function of composite fiber content (Figure 2B). No consistent correlation could be found between composite fiber content and failure elongation in either the axial or the transverse testing direction (results not shown). The data were scattered with measured grand means ± stdv. of 2.3 ± 0.4% and 4.9 ± 1.9% in the axial and transverse fiber direction, respectively. The porosity content was shown to be positively correlated with the composite fiber content with values of approximately 4 vol.% at low fiber contents and approximately 10 vol.% at high fiber contents (Figure 2C). This tendency was confirmed by light microscopy observations on composite cross-sections.

Table 2. Tensile properties (mean ± stdv., n=5) of unidirectional hemp composites with a matrix of one of two types of polypropylenes, PP_D or MAPP. For all composite plates fiber content was approximately 41 vol.% (40.8 ± 0.9) with a porosity content of approximately 4 vol.% (4.1 ± 0.9).

Matrix	**Strength (MPa)**		**Stiffness (GPa)**		**Failure elongation (%)**	
	Axial	Transverse	Axial	Transverse	Axial	Transverse
PP_D	214.5 ± 8.0		21.5 ± 0.9		2.2 ± 0.1	
PP_D		7.6 ± 0.8		1.8 ± 0.1		4.9 ± 0.8
MAPP	208.1 ± 6.4		20.1 ± 0.9		1.9 ± 0.1	
MAPP		16.3 ± 0.9		2.5 ± 0.1		1.5 ± 0.6

Influence of fiber/matrix interface variable on composite properties

In the axial fiber direction no improvements in tensile strength and stiffness were observed when replacing matrix PP_D with matrix MAPP with only a small decrease in failure elongation (Table 2; Figure 3). However, although the axial mechanical properties did not change, failure characteristics did change dramatically (Figure 4). With matrix PP_D failure of the test specimens were characterized by a ductile fracture mode with progressing cracks moving along the fibers taking several milliseconds before the specimens were finally separated. In contrast, failure of test specimens with a matrix of MAPP were characterized by a brittle fracture mode with a single crack moving perpendicular to the fibers and completed within a few milliseconds. These two different failure characteristics are a good qualitative indication of improvements in fiber/matrix interface when using matrix MAPP. Testing the composites in the transverse fiber direction showed a considerable change in mechanical properties with tensile strength increasing about 100%, stiffness increasing about 40% and failure elongation decreasing about 70% when replacing matrix PP_D with matrix MAPP (Table 2; Figure 3). Failure

characteristics (not shown) were identical with the two matrix types, both were characterized by a brittle fracture mode resembling the one seen for the axial direction with matrix MAPP (Figure 4B).

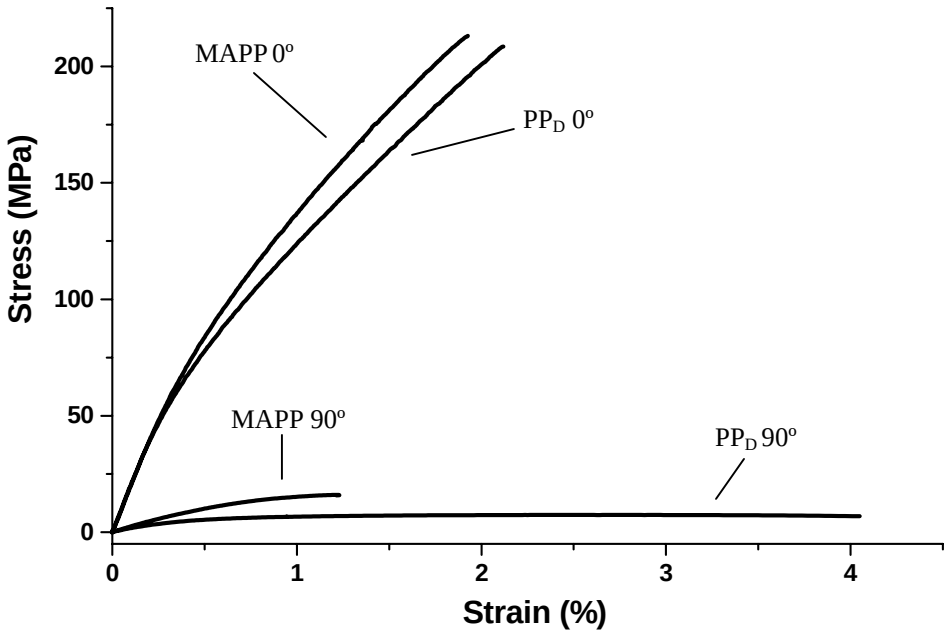

Figure 3. Representative stress-strain curves of unidirectional hemp composites with a matrix of PP$_D$ or MAPP tested in the axial (0°) or transverse (90°) fiber direction.

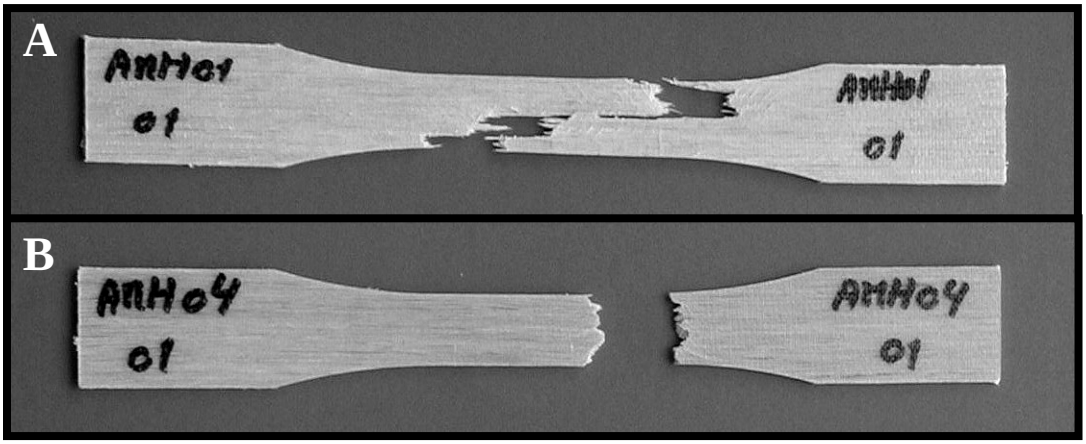

Figure 4. Representative examples of failure characteristics of unidirectional (A) hemp/ PP$_D$ and (B) hemp/MAPP composites tested in the axial fiber direction. Size of test specimens is 180x25 mm.

Discussion

Influence of fiber content variable on composite properties

Other studies investigating properties of unidirectional plant fiber composites with a fiber content variable have found that axial tensile properties follows a rule of mixtures relationship (5-8,11,15,19), a relationship observed with more traditionally composites such as glassfiber/polyester. However, our results could not confirm such a strong positive linear response of axial properties with fiber content. We only observed weak correlations with strength increasing and stiffness decreasing. On the other hand, we observed a clear correlation of composite porosity content with fiber content, and this may partly explain the deviations of tensile properties from a rule of mixtures relationship; by increasing levels of porosity, material inhomogenities are induced with a negative effect on composite mechanical properties. Moreover, we only varied the fiber content in a relatively small range and this might possibly have distorted the overall correlations. For the transverse properties both composite tensile strength and stiffness were clearly decreasing with fiber content, a correlation which too is a deviation from the expected positive relationship. In addition to the effect of porosity content, this deviation may be explained by the relatively weak interface bonding between the hemp fibers and the PP_H matrix, which results in a poor transfer of stress between fibers and matrix. According to the above considerations we found that the optimal fibre content is about 50 vol.% resulting in composites with properties, (i) porosity content 7%, (ii) axial tensile strength 235 MPa and stiffness 23 GPa and (iii) transverse tensile strength 5 MPa and stiffness 1 GPa (values are interpolated from figure 2). The large anisotropy for the unidirectional hemp fiber composites shows the potential for strong materials when the composites are loaded in the fiber direction, but shows also the weakness for loads in off-axis and in particular transverse directions. Attempts to counteract this weakness by e.g. a random distribution of fiber orientations by using fiber mats, will not be very efficient because the properties of such a composite will be dominated by the transverse properties. The fiber efficiency factor for a random mat is 1/3, which is smaller than for a linear mixture of longitudinal and transverse properties, where the factor is 1/2. This is also borne out by a set of experimental results for flax fiber composites (unpublished), where the strength in the fiber direction is about 300 MPa, in the transverse direction about 5 MPa, and for a random mat composite about 30 MPa.

Influence of fiber/matrix interface variable on composite properties

From the literature it is well documented that using MAPP as a coupling agent in natural fiber reinforced polymer composites considerably improve mechanical properties (21 and references cited

herein). Therefore, as expected, results from this study showed that in unidirectional hemp composites the replacement of matrix PP_D with matrix MAPP changed the failure characteristics in the axial fiber direction and increased transverse tensile properties; both of these phenomena can be explained by the effect of improved quality of the fiber/matrix interface. When a material is stressed by increasing tensile load cracks will start to develop in the weakest areas (most often at the outside edge) and progress along a path of weak areas inside the material. The different axial failure characteristics observed with matrix PP_D and with matrix MAPP are therefore merely an indication of a change in the path of weak areas. Due to the relatively poor fiber/matrix interface in composites with matrix PP_D cracks will progress along the weak interface between fiber and matrix. In composites with matrix MAPP the fiber/matrix interface quality is improved and this will induce the cracks to progress directly through the fibers. This change in failure characteristics as a function of quality of fiber/matrix interface has also been observed in many other unidirectional composites based on e.g. glass and carbon fibers (22). The reason for the nearly identical axial strength and stiffness of composites with matrix PP_D and with matrix MAPP is that in axial tension of a continuous unidirectional composite most of the applied load is carried by the fibers, independent of the quality of fiber/matrix interface. In contrast, in transverse tension load is carried equally by fibers, matrix and fiber/matrix interface and therefore the transverse tensile properties are seen to be directly affected by quality of fiber/matrix interface. Processing of natural plant fibers, such as hemp fibers, into textile yarns most often requires the application of some kind of finishing, such as soaps or oils. Observations (unpublished) indicate that this was also the case for the hemp yarn used in this study. When using a coupling agent, such as maleated polypropylene to improve bonding between the polar plant fibers and the nonpolar polymer, removal of the finishing by some dewaxing technique optimizes the quality of the fiber/matrix interface (17). Therefore, in the case of this study, dewaxing of the hemp yarn prior to composite processing would most probably have resulted in even better transverse tensile properties when using a matrix of MAPP.

Conclusion

Filament winding was shown to be a suitable method for manufacturing unidirectional hemp yarn reinforced polypropylene composites with tensile strength and stiffness in the axial direction exceeding 200 MPa and 20 GPa, respectively. Transverse tensile properties were found to be negatively correlated with composite fiber content, whereas composite porosity content was positively correlated.

Replacing unmodified polypropylene with maleated polypropylene improved transverse properties and dramatically changed failure characteristics in the axial direction.

Acknowledgements

This work was partly supported by the Danish Research Councils (project: "Characterisation and application of plant fibres for new environmentally friendly products"), and by the Danish Research Agency of the Ministry of Research (project: "High performance hemp fibres and improved fibre network for composites"). The authors thank Henning Frederiksen for the determinations of composite fiber and porosity content.

References

1. Robson, D. and J. Hague. 1995. A comparison of wood and plant fiber properties. Proceedings of Woodfiber-Plastic Composites Conference, Madison, Wisconsin, USA 41-46.
2. Robson, D., J. Hague, G. Newman, G. Jeronimidis and M. Ansell. 1993. Survey of natural materials for use in structural composites as reinforcement and matrices. Crown Copywright, The Biocomposites Centre, University of Wales.
3. Mohanty, A.K. and M. Misra. 1995. Studies on jute composites – a literature review. Polymer Plastics Technology and Engineering 34(5):729-792.
4. Lilholt, H. and A.B. Bjerre. 1997. Composites based on jute-fibres and polypropylene matrix, their fabrication and characterisation. In 'Proceedings of the 18th Risø International Symposium on Materials Science: Polymeric Composites – Expanding the limits, Risø National Laboratory, Denmark. 411-423.
5. Pal, S.K., D. Mukhopadhyay, S.K. Sanyal and R.N. Mukherjea. 1988. Studies on process variables for natural fiber composites – effect of polyesteramide polyol as interfacial agent. Journal of Applied Polymer Science 35:973-985.
6. Kalaprasad, G., K. Joseph, S. Thomas and C. Pavithran. 1997. Theoretical modelling of tensile properties of short sisal fibre-reinforced low-density polyethylene composites. Journal of Materials Science 32:4261-4267.
7. Sanadi, A.R., S.V. Prasad and P.K. Rohatgi. 1986. Sunhemp fibre-reinforced polyester. Part I. Analysis of tensile and impact properties. Journal of Materials Science 21:4299-4304.
8. White, N.M. and M.P. Ansell. 1983. Straw-reinforced polyester composites. Journal of Materials Science 18:1549-1556.
9. Hepworth, D.G., D.M. Bruce, J.F.V. Vincent and G. Jeronimidis. 2000. The manufacture and mechanical testing of thermosetting natural fibre composites. Journal of Materials Science 35:293-298.
10. Hepworth, D.G., R.N. Hobson, D.M. Bruce and J.W. Farrent. 2000. The use of unretted hemp fibre in composite manufacture. Composites Part A 31:1279-1283.
11. Roe, P.J. and M.P. Ansell. 1985. Jute-reinforced polyester composites. Journal of Materials Science 20(11):4015-4020.

12. Bos, H.L., M.J.A. van den Oever and O.C.J.J. Peters. 1997. The influence of fibre structure and deformation on the fracture behaviour of flax fibre reinforced composites. 4th International Conference on Deformation and Fracture of Composites 429-504.
13. Sridhar, M.K., G. Basavarappa, S.G. Kasturi and N. Balasubramanian. 1984. Mechanical properties of jute-polyester composites. Indian Journal of Technology 22(6):213-215. (Cited in ref. 3).
14. Shah, A.N. and S.C. Lakkad. 1986. Fibre Sci. Technology 15:41-. (Cited in ref. 3).
15. Chawla, K.K. and A.C. Bostos. 1979. Proceedings of Third International Conference on Mechanical Behaviour of Materials, Pergamon Press, Cambridge 3:191-. (Cited in ref. 3).
16. Herrmann, A.S., J. Nickel and U. Riedel. 1997. Construction materials based upon biologically renewable resources – from components to finished parts. Polymer Degradation and Stability 59:251-261.
17. Gassan, J. and A.K. Bledzki. 1997. The influence of fiber-surface treatment on the mechanical properties of jute-polypropylene composites. Composites Part A 28:1001-1005.
18. Gassan, J. and A.K. Bledzki. 1999. Effect of cyclic moisture adsorption desorption on the mechanical properties of silanized jute-epoxy composites. Polymer Composites 20(4):604-611.
19. Kumar, P. 1986. Indian Journal of Technology 24:29-. (Cited in ref. 3).
20. Andersen, T.L. and H. Lilholt. 1999. Natural fibre composites: Compaction of mats, press consolidation and material quality. In 'Proceedings of the 7th Euro-Japanese Symposium'. Ecole des Mines de Paris. 1-12.
21. Myers, G.E., I.S. Chahyadi, C.A. Coberly and D.S. Ermer.1991. Wood flour/polypropylene composites: Influence of maleated polypropylene and process and composition variables on mechanical properties. International Journal of Polymeric Materials 15:21-44.
22. Drzal, L.T. and M. Madhukar. 1993. Fibre-matrix adhesion and its relationship to composite mechanical properties. Journal of Materials Science 28:569-610.

Available online at www.sciencedirect.com
SCIENCE DIRECT®
Composites Science and Technology 63 (2003) 1265–1272
COMPOSITES SCIENCE AND TECHNOLOGY
www.elsevier.com/locate/compscitech

Physical and mechanical properties of unidirectional plant fibre composites—an evaluation of the influence of porosity

Bo Madsen[a,b,*], Hans Lilholt[a]

[a]Materials Research Department, Risoe National Laboratory, 4000 Roskilde, Denmark
[b]Department of Civil Engineering, Technical University of Denmark, 2800 Lyngby, Denmark

Received 10 November 2002; accepted 21 February 2003

Abstract

Unidirectional composites were made from filament wound non-treated flax yarns and polypropylene foils. With increasing composite fibre weight fractions from 0.56 to 0.72, porosity fractions increased from 0.04 to 0.08; a theoretical model was fitted to the data in order to describe the composite volumetric interaction between contents of fibre, matrix and porosity. In the model two porosity components were proposed, a process governed component and a structurally governed component. The composite axial stiffness and strength were in the range 27–29 GPa and 251–321 MPa, respectively. A modified version of the "rule-of-mixtures", supplemented with parameters of composite porosity content and anisotropy of fibre properties, were developed to improve the prediction of composite tensile properties.

Keywords: A. Polymer-matrix composites (PMCs); B. Porosity; B. Mechanical properties; Natural fibres

1. Introduction

Some aspects of plant fibre composites have gained considerable scientific interest, i.e. methods of extracting the fibres from the plants in order to preserve their good mechanical properties, methods to increase the compatibility between the polar lignocellulosic fibres and the nonpolar polymeric matrix, and measurements of interface properties [for examples see Refs. 1–10]. Thus, so far, most studies have primarily focused on the fibre and matrix component of the composites, and ignored the existence of the third component, the porosity. Porosity, which is defined as air-filled cavities inside an otherwise continuous material, is a most often unavoidable component in all composite materials, caused by the mixing and consolidation of two discrete material components. With most synthetic composite materials, such as glass/polyester and carbon/epoxy, considerable knowledge has been built up over the years in order to control and optimise the fabrication process, and consequently the porosity content is normally relative low (<2%) [25]. However, with plant fibre composites, the fabrication techniques are not yet that developed, and the natural origin of the fibre component necessarily induces an element of variation into the composites; both factors cause the porosity component to make a noteworthy contribution to the overall composite volume in plant fibre composites [11,19,26]. Knowing that porosity has a direct effect on composite physical and mechanical properties [12,16–17,24] underlines the need for more studies including this component into the overall material characterisation.

Another important parameter regarding composite material properties is fibre anisotropy. In many studies it is assumed that the mechanical properties of both fibre and matrix components are isotropic, meaning that the properties are independent of the direction of loading. However, with most fibres (e.g. carbon and aramid, but not glass), stiffness and strength in the axial direction are significantly larger than stiffness and strength in the transverse direction. For practical reasons, almost all available experimental data on fibre mechanical properties relate to the axial direction, whereas only few studies show data on transverse fibre properties. In one study of jute fibres, the ratio between transverse and axial stiffness has been estimated to be about 1/7 [18].

* Corresponding author. Tel.: +45-4677-5805; fax: +45-4677-5758.
E-mail address: bo.madsen@risoe.dk (B. Madsen).

0266-3538/03/$ - see front matter © 2003 Elsevier Science Ltd. All rights reserved.
doi:10.1016/S0266-3538(03)00097-6

Based on unidirectional flax/polypropylene composites, this paper presents theoretical and experimental studies of (i) the volumetric interaction in composite materials and (ii) the effect of porosity and fibre anisotropy on composite mechanical properties. Initially, the necessary theory behind these studies is introduced.

1.1. Composite volumetric interaction

Assuming that on a macroscopic scale a composite material can be divided into three volumetric components, fibre, matrix and porosity, then the total volume of the composite equals the summation of these individual volumes:

$$v_c = v_f + v_m + v_p \tag{1}$$

where v is volume and the subscripts c, f, m and p denotes composite, fibre, matrix and porosity, respectively. By applying the concepts of volume and weight fractions, Eq. (1) can be rewritten into

$$\begin{aligned} v_c &= \frac{m \cdot W_f}{\rho_f} + \frac{m \cdot W_m}{\rho_m} + V_p \cdot v_c \Rightarrow \\ v_c \cdot (1 - V_p) &= \frac{m \cdot W_f}{\rho_f} + \frac{m \cdot W_m}{\rho_m} \\ \Rightarrow\ v_c &= \frac{\dfrac{m \cdot W_f}{\rho_f} + \dfrac{m \cdot W_m}{\rho_m}}{1 - V_p} \end{aligned} \tag{2}$$

where m is mass of the composite, ρ is density, W is weight fraction and V is volume fraction. The expressions for fibre and matrix volume fractions can then be evaluated

$$V_f = \frac{v_f}{v_c} = \frac{\dfrac{W_f}{\rho_f}}{\dfrac{W_f}{\rho_f} + \dfrac{W_m}{\rho_m}} \cdot (1 - V_p) \tag{3}$$

$$V_m = \frac{v_m}{v_c} = \frac{\dfrac{W_m}{\rho_m}}{\dfrac{W_f}{\rho_f} + \dfrac{W_m}{\rho_m}} \cdot (1 - V_p) \tag{4}$$

Instead of assuming that the porosity content is a fixed constant, which would make the model very restricted, it is assumed that porosity is a variable function of the fibre weight fraction. Moreover, we hypothesise that the total porosity content is the summation of two independent components each created by their own specific mechanism. In the first component, called $V_{p(proc)}$, the porosities are created during the processing of the composites; an example of porosities included in $V_{p(proc)}$ is the porosities created at the fibre/matrix interface. In the second component, called $V_{p(struc)}$, the porosities can be assigned to a structural mechanism. Results from compaction tests on plant fibre assemblies [13,14] have shown that there is a limit to the degree of compaction, ranging between 30 and 60% depending on different factors, such as fibre type and fibre orientation. Consequently, fabrication of composites with a fibre volume content above a particular limit will lead to porosities because of this incomplete compaction of the fibre assemblies. Both components, $V_{p(proc)}$ and $V_{p(struc)}$, are a function of the fibre content, but whereas $V_{p(proc)}$ is assumed to increase throughout the entire range of fibre contents, $V_{p(struc)}$ is zero below the particular compaction limit.

The introduction of a new function, based on the fibre weight fraction,

$$\alpha = \frac{(1 - W_f) \cdot \rho_f}{W_f \cdot \rho_m} \tag{5}$$

and the incorporation of $V_{p(proc)}$ and $V_{p(proc)}$ into Eqs. (3) and (4) will complete the model of composite volumetric interaction,

$$V_f = \frac{1}{1 + \alpha} \cdot \left(1 - \left(V_{p(proc)} + V_{p(struc)}\right)\right) \tag{6}$$

$$V_m = \frac{\alpha}{1 + \alpha} \cdot \left(1 - \left(V_{p(proc)} + V_{p(struc)}\right)\right) \tag{7}$$

1.2. Effect of porosity and fibre anisotropy on composite mechanical properties

In conventional unidirectional and continuous composites, the traditional way to predict composite axial stiffness (E_1) and transverse stiffness (E_2) is to apply the simple "rule-of-mixtures" [15],

$$E_1 = V_f \cdot E_f + (1 - V_f) \cdot E_m \tag{8}$$

$$E_2 = \frac{E_f \cdot E_m}{(1 - V_f) \cdot E_f + V_f \cdot E_m} \tag{9}$$

The same equations can be used for strength properties (σ), by replacing E with σ.

Even though, the model has proved to be a good approximation to composite properties, the user should be aware of the assumptions made in the model. One assumption is that composite porosity content is equal to zero. Besides the effect of lowering the composite load bearing volume, porosity also affect the composite mechanical properties by introducing stress concentrations into the material. Based on a theoretical study by MacKenzie [16] on adding spherical holes into materials, the effect of porosity on material stiffness can be approximated by,

$$E_p = E_d \cdot (1 - V_p)^2 \tag{10}$$

where the subscripts d and p denotes the fully dense material and the porous material, respectively. The

same kind of correlation can be found in work by Schjødt-Thomsen and Pyrz [17] on microcellular foams.

Another assumption made in the "rule-of-mixtures" is that the mechanical properties of both the fibre and matrix components are isotropic, which implies that axial stiffness is equal to transverse stiffness. However, as pointed out above, for most fibres the axial properties are radically larger than the transverse properties. Consequently, to further improve the "rule-of-mixtures", the fibre stiffness in Eq. (9) needs to be multiplied with the ratio of fibre anisotropy (*fa*), defined as the ratio between transverse and axial properties.

The complete and improved model is described by the following equations:

$$E_1 = (V_f \cdot E_f + (1 - V_f) \cdot E_m) \cdot (1 - V_p)^2, \quad (11)$$

$$E_2 = \left(\frac{(E_f \cdot fa) \cdot E_m}{(1 - V_f) \cdot (E_f \cdot fa) + V_f \cdot E_m} \right) \cdot (1 - V_p)^2 \quad (12)$$

2. Materials and methods

Unidirectional composites of textile monofilament flax yarn (Linificio e Canapificio Nazionale, Italy; Nm 16/1) in combination with foils of unmodified polypropylene (PP; Hoechst Folien, Germany; Trespaphan NNA; density 0.91 g/cm^3; thickness 0.025 mm) were manufactured with fibre weight fractions in the range 0.50–0.75. With a custom-built winding-machine the flax yarn was wound on to metal frames (400×400 mm) with 1 mm sideward steps per rotation producing fibre assemblies with high yarn alignment and controlled uniform thickness. Polypropylene matrix foils were combined with the fibre assemblies by a film-stacking technique and processed by vacuum heating (190 °C, 15 min) and press consolidation (2.2 MPa, 1 min) [13]. The rectangular dimensions of the manufactured composite laminates were 240×300 mm, with a thickness varying in the range 1.8–2.4 mm, depending on the actual fibre/matrix ratio. Composite and fibre densities were determined by the buoyancy method (Archimedes principle) using water as the displacement medium. It should be noted that the central cavity of the fibres, the so-called lumen, was not included in the determined densities. The exact weight fractions of fibre and matrix were determined by dissolving the PP matrix with xylene and applying gravimetric measurements. Based on data for densities and weight fractions, the volume fractions of fibre and matrix were calculated. Composite porosity content was estimated as the volume fraction not taken up by the fibre and matrix components [19]. The composite laminates were cut into standard dumbbell shaped test specimens (180×25 mm with gaugesection 30×15 mm) in both the axial and transverse fibre directions. Tensile tests were performed at room temperature on an Instron tensile machine with crosshead speed 2 mm/min and loadcell 10 kN. Strains were measured with two extensometers centred on each side of the test specimens. Nominal ultimate strength (MPa) and nominal stiffness (GPa, linear regression between 0 and 0.1% strain) were determined from the stress–strain curves.

3. Results

In this study 8 composite laminates were manufactured with fibre volume fractions in the range 0.41–0.55 and with porosity in the range 0.04–0.08 (Table 1). Density (mean ± S.D., $n = 12$) of the flax fibres was 1.54 ± 0.01 g/cm^3. Composite axial mechanical properties were measured in the range 27–29 GPa and 251–321 MPa for stiffness and strength, respectively, values which were considerably above the data for the transverse testing direction (Table 2). Fig. 1 shows a representative polished cross-section of a composite laminate demonstrating that apparently the lumen in most of the fibres is collapsed and therefore the determined composite porosity content can mainly be assigned to regions outside the fibres (e.g. at the fibre/matrix interface).

In an ideal composite with no porosity the volumetric interaction between volume fractions of fibre and matrix can be modelled by using Eqs. (6) and (7) and setting $V_{p(proc)} = V_{p(struc)} = 0$. In Fig. 2A the numerical outcome of the model has been plotted as a function of

Table 1
Physical properties of the fabricated composite laminates

Laminate No.	Density (g/cm^3)	Fibre weight fraction	Porosity volume fraction	Fibre volume fraction	Matrix volume fraction
1a	1.14	0.574 (0.018)	0.038 (0.010)	0.426 (0.015)	0.537 (0.022)
1b	1.13	0.564 (0.015)	0.042 (0.006)	0.414 (0.012)	0.544 (0.018)
2a	1.16	0.604 (0.008)	0.036 (0.007)	0.457 (0.005)	0.508 (0.011)
2b	1.15	0.619 (0.005)	0.050 (0.005)	0.464 (0.005)	0.486 (0.007)
3a	1.19	0.667 (0.009)	0.051 (0.008)	0.514 (0.005)	0.435 (0.013)
3b	1.18	0.670 (0.005)	0.061 (0.008)	0.511 (0.006)	0.428 (0.007)
4a	1.19	0.715 (0.006)	0.077 (0.005)	0.551 (0.004)	0.372 (0.009)
4b	1.19	0.709 (0.007)	0.071 (0.003)	0.548 (0.006)	0.381 (0.009)

Data in table are means (S.D.) with a sample size of 3 for each laminate.

Table 2
Mechanical properties of the fabricated composite laminates

Laminate No.	Stiffness (GPa)		Strength (MPa)	
	Axial	Transverse	Axial	Transverse
1a	26.9 (1.4)		251.1 (7.7)	
1b		1.54 (0.01)		6.50 (0.31)
2a	27.8 (1.6)		271.2 (11.9)	
2b		1.31 (0.02)		5.60 (0.22)
3a	28.7 (1.5)		287.5 (13.9)	
3b		1.12 (0.04)		4.41 (0.16)
4a	28.2 (1.4)		320.7 (16.1)	
4b		0.83 (0.09)		3.37 (0.16)

Data in table are means (S.D.) with a sample size of 5 for each laminate.

the fibre weight fraction (W_f) together with the experimentally determined volume fractions. As the composites contain some porosity it is anticipated that the model does not fit the experimental data very well, and that it tends to overestimate both the fibre and the matrix volume fractions. Therefore, in order to improve the model prediction the actual porosity content should enter the equations. In Fig. 2B, by focusing on the porosity data and by applying the concept that the total porosity consists of the two independent components created by two different mechanisms ($V_{p(proc)}$ and $V_{p(struc)}$, see introduction), a summation of these components are fitted to the experimental data. For simplicity the two components have been modelled by linear functions:

$$V_{p(proc)} = 0.06 \cdot W_f \tag{13}$$

$$V_{p(struc)} = 0.32 \cdot W_f - 0.20 \quad \text{for} \quad W_f > 0.625$$
$$\text{else} \quad V_{p(struc)} = 0 \tag{14}$$

These linear functions can then enter the volumetric interaction model [Eqs. (6) and (7)] to give the numerical output shown in Fig. 2C. From the figure it is clear that the model is a suitable tool to predict composite volumetric interaction.

The mechanical properties are plotted in Fig. 3; the fitting (dotted lines) of the uncorrected "rule-of-mixtures" [Eqs (8) and (9)] to the experimental data of stiffness and strength, makes a fairly rough estimation of composite properties. Consequently, the model shows some deviations from the experimental data: (i) it fails to predict composite axial properties at high fibre contents and (ii) composite transverse properties are all below the prediction of the model. In order to explain some of these deviations, porosity content and fibre anisotropy are included in the corrected "rule-of-mixtures" [Eqs. (11) and (12)]. Composite porosity content is assumed to be equal to the summation of the linear functions of $V_{p(proc)}$ and $V_{p(struc)}$ [Eqs. (13) and (14)]

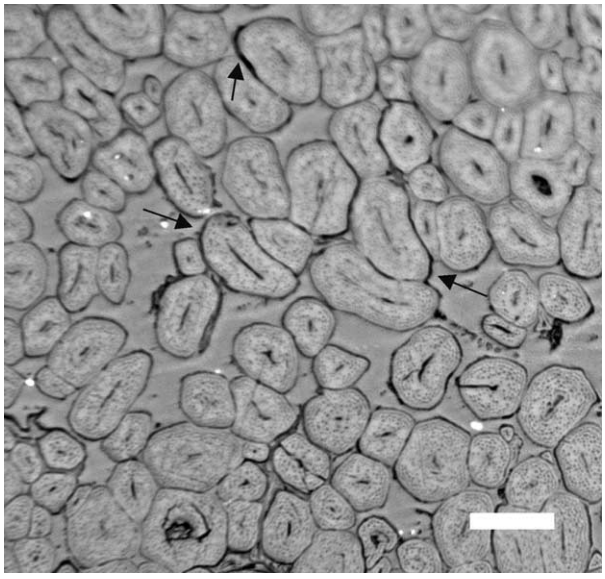

Fig. 1. Light microscope image of a polished flax/PP composite (laminate 1b) at a right angle to the fibre direction. Arrows show examples of porosities at the fibre/matrix interface. Scale bar is 20 μm.

estimated in Fig. 2B. Well-documented data on the anisotropic nature of plant fibre mechanical properties are limited to a single study on jute fibres where the ratio between transverse and axial fibre stiffness is determined to be about 1/7 at room temperature [18]. Because of the lack of other available information, the same fibre anisotropy ratio of 1/7 is applied in this study, assuming that the mechanical behaviour of flax and jute fibres (both lignocellulosic fibres) are closely related and that the anisotropic nature of strength and stiffness fibre properties is about equal. The corrected model improves the prediction of composite axial properties (Fig. 3, full lines). An improvement that is particularly obvious for axial stiffness, but can also be justified for axial strength. On the other hand, only rather small improvements are observed in predicting composite transverse properties, they are all still below the lines of the model, indicating that these deviations can not be fully explained by either composite porosity or fibre anisotropy. The "knee-point" of the corrected "rule-of-mixtures" at about 0.48 fibre volume fraction is correlated with the "knee-point" of V_p at 0.62 fibre weight fraction (Fig. 2C). It means that after this point, the structural porosity component starts to increase and therefore a further increase in fibre content does not improve composite properties much. Moreover, it should be noted that the corrected model in Fig. 3 ends at about 0.82 fibre volume fraction, which corresponds to the maximum attainable fibre volume fraction estimated in the volumetric interaction model (Fig. 2C). The acceptable fit between experimental data of axial properties and the corrected "rule-of-mixtures" verifies the application of the model [Eq. (11)] to approximate axial fibre stiffness and strength to be about 60 GPa and 600 MPa, respectively.

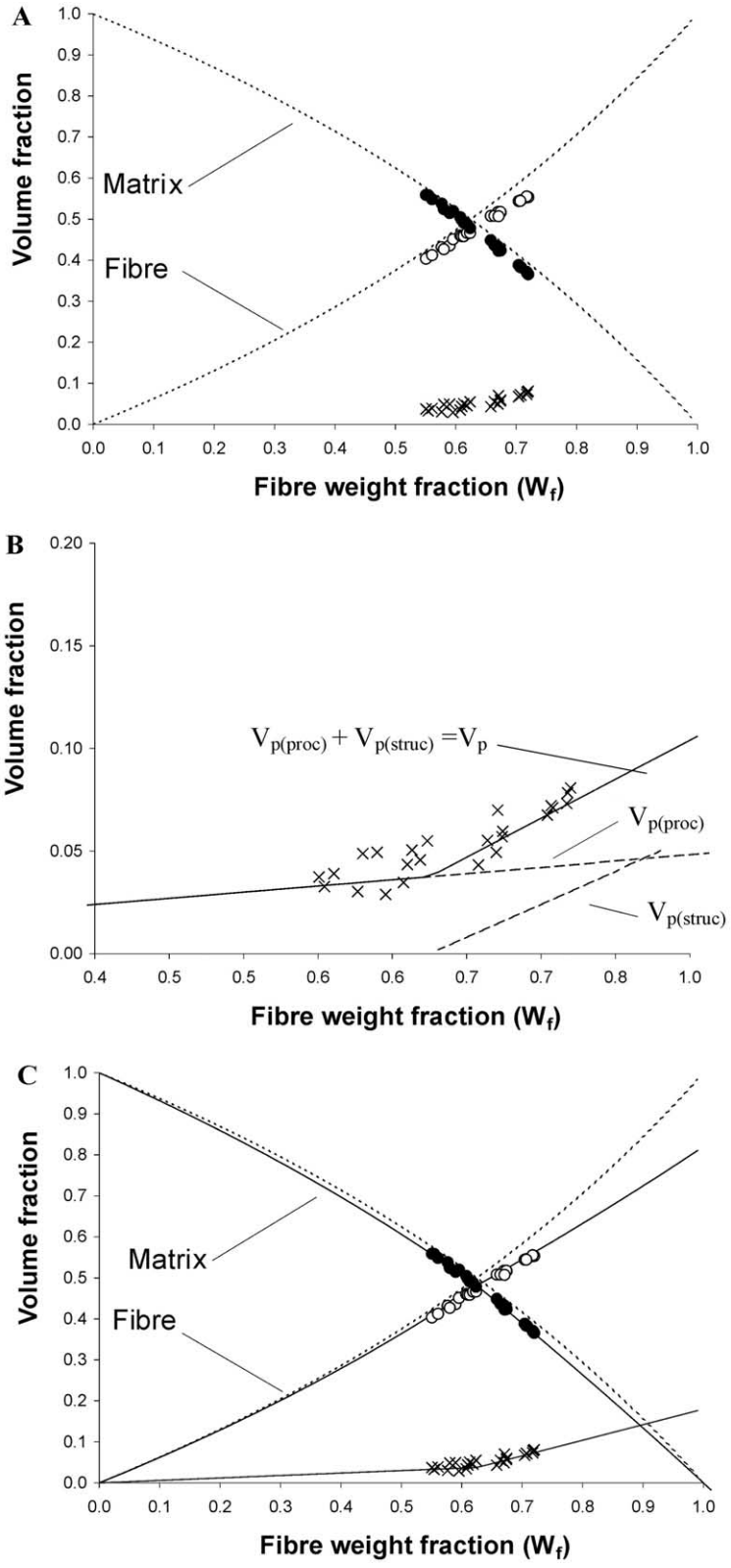

Fig. 2. Composite volumetric interaction. (A) Shows experimental data of volume fractions of (○) fibre, (●) matrix and (×) porosity as a function of composite fibre weight fraction, together with the numerical outcome (dotted lines) of Eqs. (6) and (7) with no porosity ($V_{p(proc)} = V_{p(struc)} = 0$). Note that the theoretical lines are overpredicting the fibre and matrix volume fractions. (B) Is focusing on the experimental data of porosity from (A). The summation (full line) of the two components of porosity ($V_{p(proc)}$ and $V_{p(struc)}$, dashed lines) has been fitted to the porosity data. (C) Is a resume of (A) and (B), supplemented with the numerical outcome (full lines) of Eqs. (6) and (7) when the linear functions from (B) for $V_{p(proc)}$ and $V_{p(struc)}$ are entered into these equations.

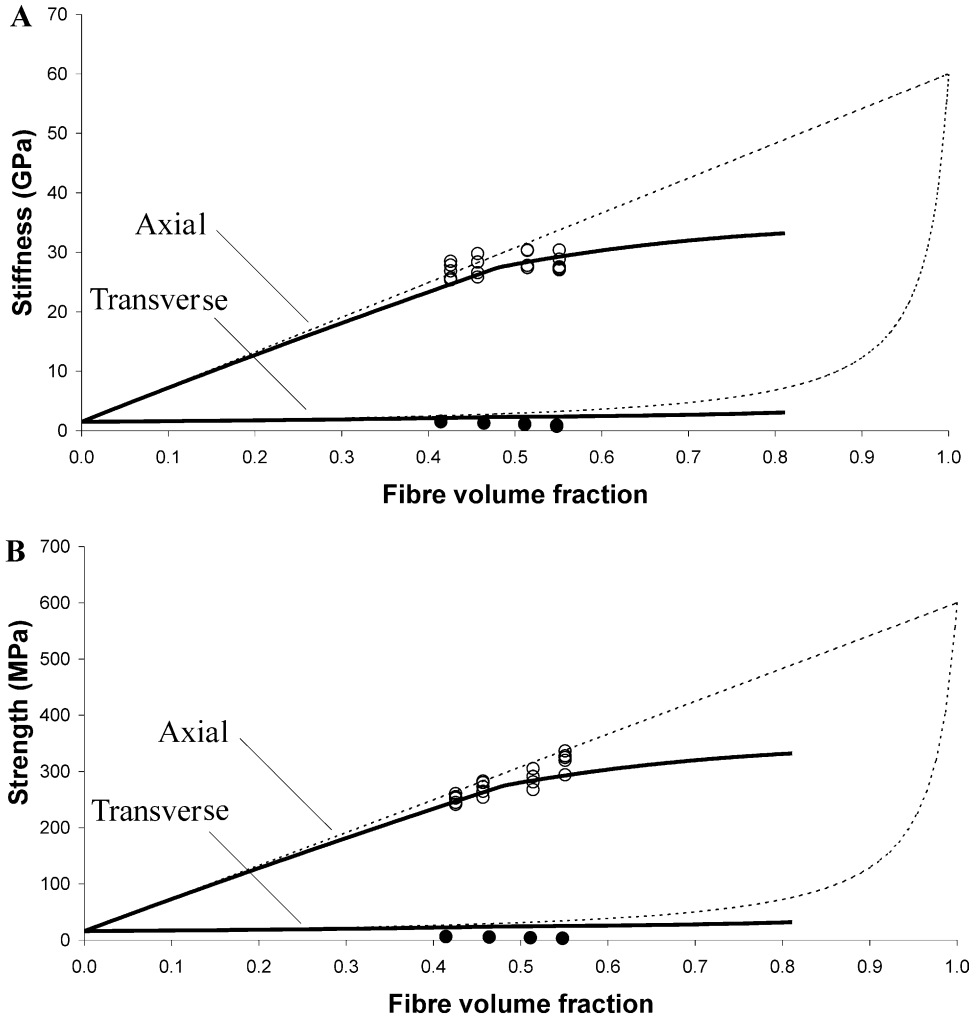

Fig. 3. Composite mechanical properties. Experimental data of (○) axial and (●) transverse properties of (A) stiffness and (B) strength are plotted as a function of composite fibre volume fraction. Dotted lines are the uncorrected "rule-of-mixtures" [Eqs. (8) and (9)] fitted to the experimental data and full lines are the corrected "rule-of-mixtures" [Eqs. (11) and (12)], using the porosity content approximated in Fig. 2B and a fibre anisotropy ratio of 1/7.

4. Discussion

The two models introduced in this study are validated by results based on unidirectional plant fibre composites processed by filament winding and film-stacking techniques. Unfortunately, the combination of these two techniques induces some limits to the composite fibre content. With too high a fibre content the degree of intermixing between the flax fibres and the matrix PP gets very poor and with too low a fibre content the flow of the PP matrix starts introducing many intralaminar fibre displacements. As a consequence, the actual processing techniques limit the composite fibre content to the range from about 0.55 to 0.75 fibre weight fraction. Since the main experimental parameter investigated in this paper is composite fibre content, the narrow process window makes model validation somewhat limited. Consequently, even though both models are based on some well-accepted materials relations, and as such do not need much support, there is a need for more data for validation. Therefore, the aim of future experiments is to widen up the process window by applying different processing techniques, such as commingled filament winding.

The volumetric interaction model presented in this paper is a general model, which can be applied to all kinds of composite materials. It is based on some simple mathematical equations based on the concepts of constant mass and volume. Despite its simplicity it underlines a fundamental aspect in composite volumetric interaction: the correlation between fibre volume fraction and fibre weight fraction is not only governed by fibre and matrix density, but is also affected by porosity. The understanding of this aspect becomes important in the context of composite fabrication. In the fabrication process, for practical reasons, fibre weight fraction is most often used as a way of controlling composite fibre content. However, because most mechanical properties

are directly governed by volume and not by mass of the material, there is a need to convert fibre weight fraction into fibre volume fraction, a conversion which requires data on fibre and matrix density, as well as data on composite porosity.

Other studies measuring axial mechanical properties of unidirectional plant fibre composite have also observed deviations from the rule of mixtures relationship at high composite fibre content [20–23]. However, so far, no attempts have been made to present a well-documented explanation. The quantitative correlation between the deviations and the composite porosity content, presented in this paper, is a valuable tool for assessing how porosity affect composite mechanical properties.

5. Conclusions

Unidirectional flax/PP composites were fabricated with a moderate porosity content and good mechanical properties in the fibre direction. The correlation between volume content of fibre, matrix and porosity was modelled by simple mathematical formulas emphasising the strong effect of porosity on composite volumetric interaction. By including composite porosity content and fibre anisotropy a corrected version of ''rule-of-mixtures'' was developed. With high fibre volume content (and high porosity content) this corrected version improved the prediction of composite axial properties, but failed to fully predict transverse properties.

Acknowledgements

This work was partly supported by the Danish Research Councils (project: ''Characterisation and application of plant fibres for new environmentally friendly products''), and by the Danish Research Agency of the Ministry of Research (project: ''High performance hemp fibres and improved fibre network for composites''). The authors thank Henning Frederiksen for the determinations of composite physical properties.

References

[1] Hobson RN, Hepworth DG, Bruce DM. Quality of fibre separated from unretted hemp stems by decortication. J Agric Engng Res 2001;78(2):153–8.
[2] Candilo MD, Ranalli P, Bozzi C, Focher B, Mastromei G. Preliminary results of tests facing with the controlled retting of hemp. Industrial Crops and Products 2000;11:197–203.
[3] Kymäläinen H-R, Hautala M, Kuisma R, Pasila A. Capillarity of flax/linseed (*Linum usitatissimum* L.) and fibre hemp (*Cannabis sativa* L.) straw fractions. Industrial Crops and Products 2001;14:41–50.
[4] Thomsen AB, Bohn V, Nielsen KV, Pallesen B, Jørgensen MS. Effect of chemical-physical pre-treatment processes on hemp fibres. Industrial Crops and Products [submitted].
[5] Gassan J, Gutowski VS. Effects of corona discharge and UV treatments on the properties of jute-fibre epoxy composites. Comp Sci Technol 2000;60:2857–63.
[6] Bisanda ETN, Ansell MP. The effect of silane treatment on the mechanical and physical properties of sisal-epoxy composites. Comp Sci Technol 1991;41:165–78.
[7] Hill CAS, Khalil HPSA. Effect of fiber treatments on mechanical properties of coir or oil palm fiber reinforced polyester composites. J Appl Polym Sci 2000;78:1685–97.
[8] Khalil HPSA, Ismail H, Rozman HD, Ahmad MN. The effect of acetylation on interfacial shear strength between plant fibres and various matrices. Eur Polym J 2001;37:1037–45.
[9] Joseph K, Varghese S, Kalaprasad G, Thomas S, Prasannakumari L, Koshy P, et al. Influence of interfacial adhesion on the mechanical properties and fracture behaviour of short sisal fibre reinforced polymer composites. Eur Polym J 1996;32(10):1243–50.
[10] Felix JM, Gatenholm P. The nature of adhesion in composites of modified cellulose fibers and polypropylene. J Appl Polym Sci 1991;42:609–20.
[11] Lilholt H, Toftegaard H, Thomsen AB, Schmidt AS. Natural composites based on cellulosic fibres and polypropylene matrix—their processing and characterisation. In: Proceedings of the 12th international conference on composite materials, Paris, France, 1999 [Paper No. 1115].
[12] Judd NCW, Wright WW. Voids and their effects on the mechanical properties of composites—an appraisal. SAMPE Journal 1978;January/February:10–14.
[13] Andersen TL, Lilholt H. Natural fibre composites: compaction of mats, press consolidation and material quality. In: Proceedings of the 7th Euro-Japanese symposium, Paris, France, 1999. p. 1–12.
[14] Lilholt H, Madsen B. Compaction of plant fibre assemblies [in preparation].
[15] Hull D, Clyne TW. An introduction to composite materials. 2nd ed. UK: Cambridge University Press; 1996.
[16] MacKenzie JK. The elastic constants of a solid containing spherical holes. Proc Phys Soc 1950;B63:2.
[17] Schjødt-Thomsen J, Pyrz R. Stress-strain modelling of microcellular materials. In: Proceedings of the 3rd Nordic meeting on materials and mechanics, Rebild Bakker, Denmark, 2000. p. 201–12.
[18] Cichocki FR, Thomason JL. Submitted to special Comp Sci Tech conference issue of An International Conference on Eco-Composites, Queen Mary, University of London, UK, 2001.
[19] Lilholt H, Bjerre AB. Composites based on jute-fibres and polypropylene matrix, their fabrication and characterisation. In: Proceedings of the 18th Risø international symposium on materials science: polymeric composites—expanding the limits. Denmark: Risø National Laboratory; 1997. pp. 411–23.
[20] Sanadi AR, Prasad SV, Rohatgi PK. Sunhemp fibre-reinforced polyester. J Mater Sci 1986;21:4299–304.
[21] Bos HL, Oever MJA, Peters OCJJ. The influence of fibre structure and deformation on the fracture behaviour of flax fibre reinforced composites. In: Proceedings of the 4th international conference on deformation and fracture of composites, 1997. pp. 499–504.
[22] Roe PJ, Ansell MP. Jute-reinforced polyester composites. J Mater Sci 1985;20:4015–20.
[23] Chawla KK, Bastos AC. The mechanical properties of jute fibers and polyester/jute composites. In: Proceedings of third international conference on mechanical behaviour of materials. Cambridge, UK: Pergamon Press; 1979. pp. 191–196.
[24] Varna J, Joffe R, Berglund LA. Effect of voids on failure mechanisms in RTM laminates. Comp Sci Technol 1995;53:241–9.

[25] Lystrup A. Hybrid yarn for thermoplastic fibre composites. Risø-R-1034 (EN). Roskilde, Denmark: Risø National Laboratory; 1998.
[26] Madsen B, Andersen T, Plackett D, Lilholt H. Evaluation of properties of unidirectional hemp/polypropylene composites—influence of fiber content and fiber/matrix interface variables. In: Proceedings of the 6th international conference on wood-fiber-plastic composites, Madison, Wisconsin, USA; 2001 [in press].

COMPACTION OF PLANT FIBRE ASSEMBLIES IN RELATION TO COMPOSITE FABRICATION

Bo Madsen[*, **] and Hans Lilholt[*]

[*]Materials Research Department, Risoe National Laboratory,
4000 Roskilde, Denmark
[**]Department of Civil Engineering, Technical University of Denmark,
2800 Lyngby, Denmark

ABSTRACT

The compaction behaviour of various plant fibre assemblies is presented, showing that in comparison to glass fibres, the compactibility of plant fibres is lower and moreover it is affected by the type of fibre. Based on assembly cross-sections it is indicated that differences in the structural fibre arrangement, called fibre dispersion, is a possible explanation for the observed non-uniform compaction behaviour, with the highly dispersed and regular glass fibres at one extreme and the jute fibres clustered together into irregular bundles at the other. Results from fibre assemblies compacted in successive cycles, reveal a considerable change in compaction behaviour at the second cycle, which in effect reduces the necessary compaction stress for obtaining maximum compaction, and in addition this effect is shown to be most pronounced for the plant fibre assemblies of lowest compactibility. Finally, based on an example of unidirectional hemp/PET composites, a good correlation is established between the maximum obtainable fibre volume fraction predicted from the compaction behaviour and the maximum measured fibre volume fraction of the composite, at the same consolidation stress. Beyond this limiting fibre volume fraction of 0.54 the composite porosity content starts to increase dramatically.

1. INTRODUCTION

In relation to composite fabrication, the compactibility of the fibre assembly may set the limits of reinforcement efficiency, and is therefore a topic which must be treated with special attention. In the literature several studies have addressed the derivation of suitable models for compaction (for examples see Gutowski, Cai, Bauer, Boucher, Kingery and Wineman 1987; Simácek and Karbhari 1996; Toll 1998; Lomov and Verpoest 2000; Beil and Roberts 2002). Many of these are modifications of a power-law relationship first proposed by van Wyk (1946) based on a 3D randomly oriented fibre assembly,

$$P = K\,E\left(V_f^3 - V_{f0}^3\right) \tag{1}$$

where P is the compaction stress, V_f is the fibre volume fraction, V_{f0} is the fibre volume fraction of the uncompacted assembly, E is the fibre stiffness and K is an empirical parameter which accounts for fibre geometry, fibre orientation and other fibre characteristics. In general, although the various models offer an acceptable fit to the experimental data, at least one adjustable parameter must be approximated. With plant fibres assemblies, the large variation of the parameters normally assigned to the compaction mechanisms, i.e. fibre orientation, fibre aspect ratio and fibre stiffness, and the difficulties of their determinations, makes the compactibility less straightforward to predict as compared to assemblies of synthetic fibres (e.g. glass or carbon fibres), where the distributions of these parameters are more narrow and simple to determine (Toll 1998). Moreover, the critical assumption of the fibres being uniformly packed employed in many theoretical models is certainly more questionable with plant fibre assemblies due to the above mentioned broad distribution of fibre characteristics. Thus, the compactibility of any given type of plant fibre assembly must be expected to be unique, and needs to be documented in order to approximate the maximum V_f at a given level of consolidation stress applied for composite fabrication. The consequence of aiming for a higher V_f than the maximum V_f can be recognized from the work by Madsen and Lilholt (2002) presenting an equation for the volumetric interaction in a composite material,

$$V_f = \frac{1}{1+\alpha}\left(1 - V_p\right) \qquad \text{where} \quad \alpha = \frac{\left(1 - W_f\right)\rho_f}{W_f\,\rho_m} \tag{2}$$

where ρ is density, W is weight fraction, V is volume fraction and the subscripts f, m and p denotes fibre, matrix and porosity, respectively. The equation demonstrates how V_f is related to not only W_f but also to V_p. Therefore, if W_f is exceeding a certain value, corresponding to the maximum V_f, the resultant space would, due to the low $W_m = 1 - W_f$, not be filled out by the matrix, but instead V_p is increased.

This paper presents the results from an experimentally based study investigating the compactibility of a range of plant fibre assemblies differed by fibre type, fibre orientation and fibre length. By applying glass fibre assemblies as a reference, it aims to demonstrate that generally, the compactibility of a plant fibre assembly is lower than the compactibility of a synthetic fibre assembly, and that the irregular bundled arrangement of plant fibres is a likely factor accounting for this difference. Moreover, it aims to demonstrate how the compactibility of a fibre assembly can be applied to predict the volumetric interaction in a composite material. As the perspective of this study is composite fabrication, where the compaction stress typically is controlled, the compactibility is presented in the form of deformation-load curves, in contrast to the load-deformation curves presented in most other studies (see equation (1)) where the perspective is the underlying compaction mechanisms.

2. MATERIALS AND METHODS

2.1 Fibre assemblies. An outline of the different types of commerciel fibre products applied in this study is presented in Table 1, together with specifications given by the suppliers. Moreover, the table shows the different fibre assembly configurations obtained from these products; unidirectional (UD) and randomly oriented (RD). UD fibre assemblies (340x140 mm^2) with uniform thickness and high fibre alignment were fabricated by filament-winding of yarns onto metal frames. RD fibre assemblies were obtained in two ways: (i) by cutting a non-woven mat into rectangular dimensions (180x140 mm^2) and stacking it, or (ii) by cutting the yarn into

average lengths of 2, 10 or 50 mm, soaking them in a water-filled container (180x140x60 mm^3), manually stirring the fibre suspension to obtain uniform packing and random fibre orientation, hand-pressing the assembly to a thickness of about 20 mm, and drying it.

Table 1. An outline of the applied fibre products and the configurations of the fibre assemblies obtained from these products (unidirectional, UD; randomly oriented, RD).

Fibre type	**Product type**	**Supplier**	**Specifications**	**Configurations of fibre assemblies**	
				UD	**RD**
Hemp	Yarn	Lignificio, I	nm 20/1; 58 tex	X	X
Flax	Yarn	Lignificio, I	nm 16/1; 64 tex	X	
Glass	Yarn	Ahlstrom, UK	1200 tex	X	
Hemp	Non-woven mat	Mülhmeier GmbH, D	320 g/m^2; No binder		X
Flax	Non-woven mat	Mülhmeier GmbH, D	350 g/m^2; No binder		X
Jute	Non-woven mat	JP Plant Fibre, UK	230 g/m^2; No binder.		X
Glass	Non-woven mat	Monofiber, DK	300 g/m^2; 4% binder by weight; 50 mm rovings of 15 tex		X

The theoretical thickness of the fully compacted solid fibre assembly (T, mm), referred to as the *bulk thickness*, was calculated according to the equation,

$$T = \frac{M}{A\rho}10^3 \tag{3}$$

where M is the weight (g) of the assembly dried for at least 24 h under vacuum at 20°C, A is the assembly area (mm^2) and ρ is the dry fibre density (g/cm^3). The precision of determination of weight and linear dimensions was ±0.05 g and ±0.5 mm, respectively. Fibre density with a precision of about ±0.02 g/cm^3 was determined by the buoyancy method (ASTM D792) where water was used as the displacement medium, ensuring that only the density of the solid fibre material was measured. By controlling the weight of the assembly, the bulk thickness was controlled, and unless otherwise noted it was adjusted to be close to 2 mm.

2.2 Compaction of fibre assemblies. The compactibility of the fibre assemblies was measured using an Instron testing machine with settings: load cell 100 kN, crosshead speed 2 mm/min and sampling rate 5 data point/s. The press area was 180x140 mm^2, which gave a maximum compaction stress of about 4 MPa. The precision of the recorded data was ±0.0025 mm for the crosshead positions and ±0.005 kN for the loads. The compliance of the system and the zero position of the crosshead with no gap between the press platens were determined in tests with no assemblies. By correcting for the compliance and the zero position, data of crosshead position was converted to distance between the press platens (d), and subsequently the fibre volume fraction (V_f) was calculated according to the equation,

$$V_f = \frac{T}{d} \tag{4}$$

From equation (3) and (4) it can be observed that the precision of the determined V_f is improved with the assembly weight, the assembly area, the fibre density and the distance between the press platens. With an assembly of weight 75.0 g, area 180.0x140.0 mm^2, fibre density 1.50 g/cm^3 and distance above 2.8 mm (corresponding to a maximum V_f of about 0.7), and by using the precisions of the relevant parameters as stated above, it can be calculated that the absolute precision of the determined V_f was better than ±0.01.

Two different compaction tests were performed:

- Single compaction, where the fibre assembly was loaded until maximum stress a single time. This test was applied in order to investigate the validity of the experimental procedure, as well as the compactibility of the different types of assemblies.
- Multiple compaction, where the fibre assembly was loaded-unloaded between zero and maximum stress in four succeeding compaction cycles. This test was applied in order to investigate how the rearrangment of the fibre network that takes place during a compaction cycle was affecting the compactibility at the following compaction cycle.

For each of the compaction tests, the V_f - stress relationship was measured for the loading part and is subsequently denoted as the compaction behaviour. To quantitative analyse the results, a power law function was fitted to the V_f - stress relationship by the least squares method,

$$V_f = a\,P^b \tag{5}$$

where P is the compaction stress (MPa) and a and b are the two adjustable fitting parameters.

2.3 Cross-sections of fibre assemblies. Composite laminates of RD fibre assemblies were fabricated by film-stacking, using unmodified polypropylene foils (PP; Hoechst Folien, Germany; density 0.91 g/cm^3; thickness 0.025 mm) as the matrix component, followed by vacuum heating (190°C, 10 min) and press consolidation (2.2 MPa, 1 min). The laminates were cut into small rectangular samples and their cross-sections were polished and observed by light microscope.

2.4 Composite volume and weight fractions. Unidirectional hemp yarn composite laminates with W_f in the range from 0.3 to 0.7 were fabricated by commingled filament-winding using polyethyleneterephthalate yarn (PET; Trevira Neckelmann, Denmark, density 1.34 g/cm^3; 57 tex) as the matrix component. The hemp/PET assemblies were processed by vacuum heating (220°C, 15 min) and press consolidation (2.2 MPa, 1 min). The volumetric and gravimetric components of the laminates were determined by a method, described in detail by Lilholt and Bjerre (1997). In short, composite density was determined by the buoyancy method (ASTM D792), and the exact W_f was determined by dissolving the PET matrix with hexafluoro-2-propanol. Based on data for W_f and densities for fibre and matrix, V_f and V_m were calculated. V_p was estimated as the volume fraction not taken up by the fibre and matrix components.

3. RESULTS

3.1 Fibre densities. Table 2 shows the results from the ρ_f determinations of the commercial fibre products. Generally, the single measurements only deviated slightly from the mean values with an overall precision of about ±0.02 g/cm^3. The importance of the small variations in these measurements is emphasized by noticing that ρ_f is a key parameter in the determination of V_f. Moreover, it can be observed that in the case of hemp and flax fibres the mean densities were lower and the deviations were larger for fibres from the mat products relative to fibres from the

yarn products, which among other factors can be attributed to a higher content of impurities (e.g. low density shives) visually observed in the mats.

Table 2. Results from measurements of fibre density (n=4).

Fibre type	Product type	Fibre density (g/cm^3)			
		Mean	**Stdv.**	**Min.**	**Max.**
Glass	Yarn	2.682	0.016	2.664	2.696
Glass	Non-woven mat	2.416	0.013	2.403	2.430
Hemp	Yarn	1.560	0.003	1.555	1.562
Hemp	Non-woven mat	1.518	0.019	1.490	1.534
Flax	Yarn	1.562	0.013	1.543	1.574
Flax	Non-woven mat	1.493	0.029	1.456	1.517
Jute	Non-woven mat	1.523	0.008	1.515	1.534

3.2 Single compaction tests. The validity of the experimental procedure applied for the compaction tests was verified by measuring a number of the same type of fibre assemblies. As an example, in Fig. 1, the results are shown from 5 assemblies of UD hemp fibres differing in bulk thickness in the range from 1.4 to 3.5 mm, and 4 assemblies of RD jute fibres differing in numbers of mat layers in the range from 4 to 14. The small scatter of the curves validates the experimental procedure and concomitantly it excludes any effect of bulk thickness and layer-layer interaction. The compaction curves generally resemble a power law function, as expected from equation (1), where V_f is rapidly increasing at low stress levels and thereafter it tends to gradually approach an asymptotic V_f beyond the experimentally used maximum stress of 4 MPa.

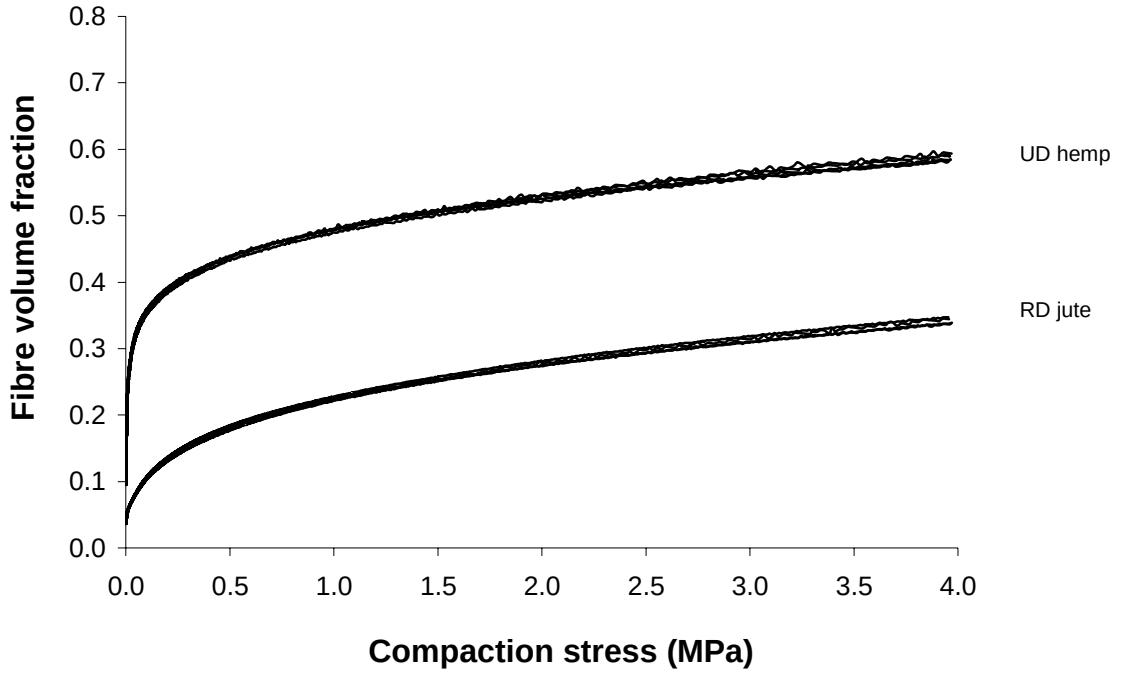

Fig. 1. Compaction behaviour of 5 assemblies of UD hemp fibres and 4 assemblies of RD jute fibres.

The compaction behaviour measured for all the different types of fibre assemblies is presented in Fig. 2. For the UD assemblies the glass fibres are compacted considerably more than the flax fibres, which in turn are compacted slightly more than the hemp fibres, a difference which is numerically exemplified by a V_f of 0.71, 0.56 and 0.54 at 2.2 MPa, respectively. Compared with the aligned fibre assemblies, the curves for the RD fibre assemblies are shifted downwards. At a given stress level, the compactibility is decreased for the assemblies in the order: glass, hemp yarn, flax, hemp, jute, and this can be numerically exemplified at 2.2 MPa, where V_f is 0.52, 0.43, 0.38, 0.35 and 0.28, respectively. Besides their different vertical positions, the exact shape of the compaction curves in the figure is also different, with the UD glass fibres at one extreme and the RD jute fibres at the other; this is illustrated in Fig. 3, which shows how the exponent *b* of the fitted power law function (equation (5)) varies for the UD and RD assemblies. Recognizing that *b* is a shape controlling parameter that is inversely related to how fast the curves approach their asymptotic values, the figure shows that for both the UD and RD assemblies, in comparison with the plant fibres, the glass fibres are more rapidly approaching their maximum obtainable V_f, which likewise can be visually assessed from the compaction curves. Moreover, for the RD assemblies the increase in *b* follows the same assembly order as for the decreased compactibility.

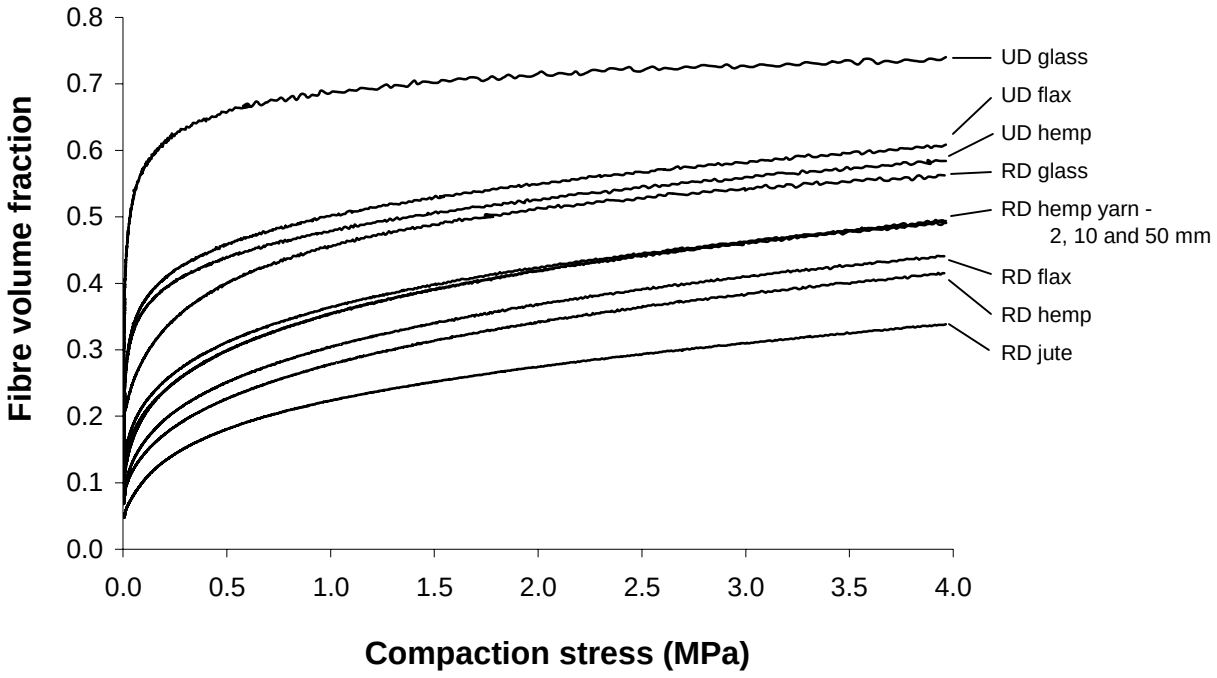

Fig. 2. Compaction behaviour in single compaction tests for all the different types of tested fibre assemblies.

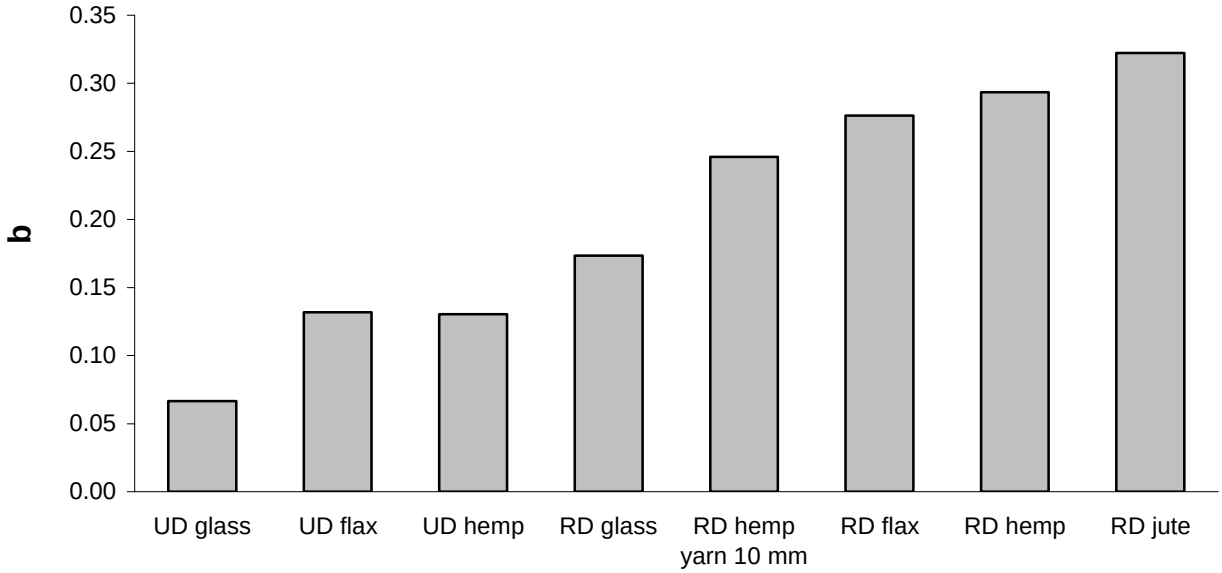

Fig. 3. The exponent *b* of the fitted power law function for all the tested UD and RD fibre assemblies.

The nearly identical compaction behaviour of the RD hemp yarn assemblies shown in Fig. 2, with mean yarn lengths of 2, 10 and 50 mm, points towards the fact that differences in the fibre length distribution can not explain the unequal compaction behaviour of the commercial plant fibre mats, where the fibre lengths are visually observed to be distributed between 1 and 10 mm, but with no clear difference between the mats. Another factor, which can be suspected to be important for the compaction behaviour is the fibre dispersion. Fig. 4 shows representative cross-sections of the RD assemblies, and it clearly illustrates how the fibres are dispersed differently between the assemblies. Even if the cross-sectional area of the elementary fibres are about the same, with the glass fibres being sligthly smaller than the plant fibres, the fibres are more or less clustered together into irregular bundles depending on the assembly type. From the images it can roughly be assessed that the fibre bundle cross-sectional area is increasing by the assembly order: glass, hemp yarn, flax, hemp, jute, an order which resembles the one for the decreased compactibility.

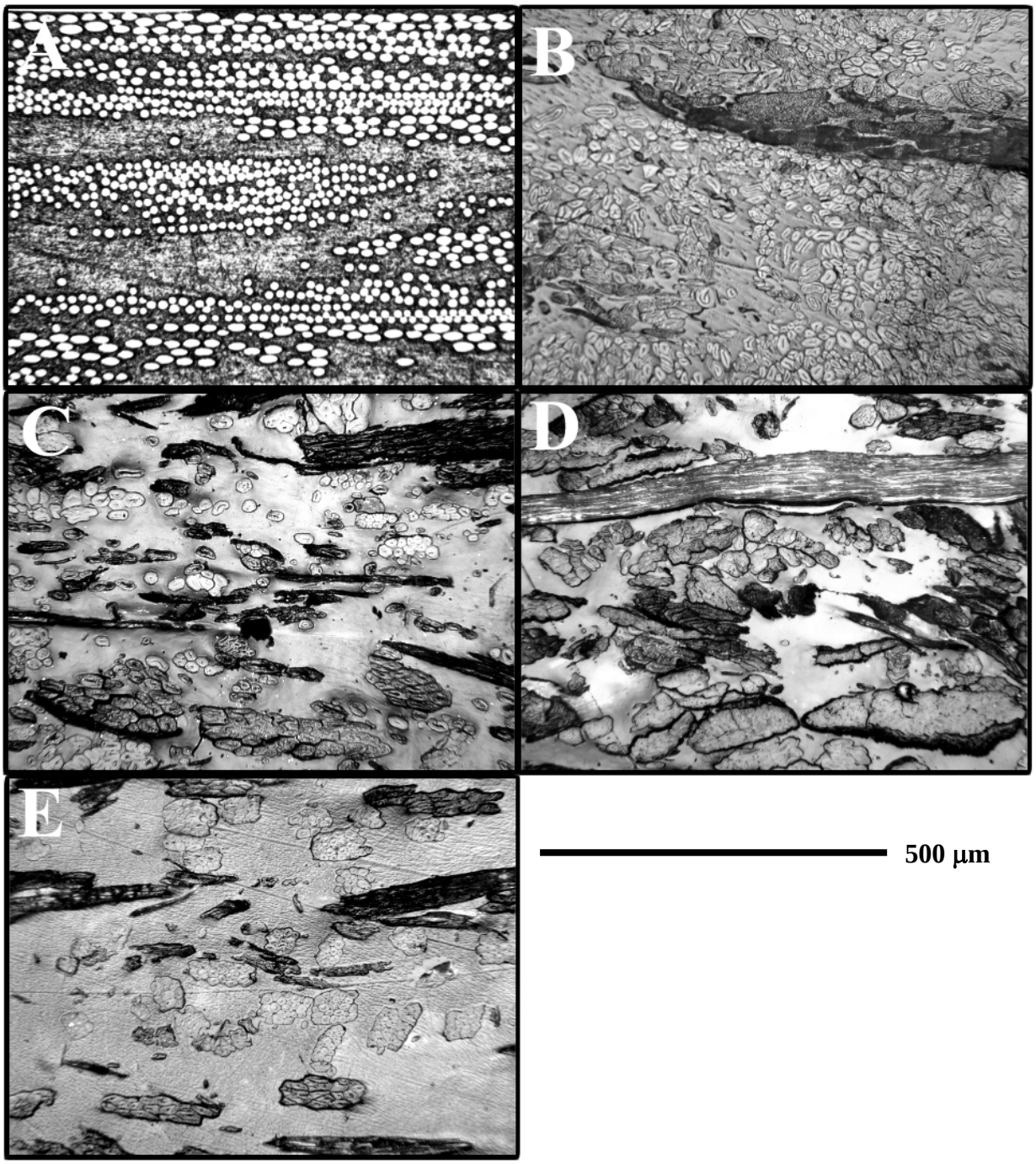

Fig. 4. Light microscope images showing representative cross sections of RD fibre assemblies: (A) glass, (B) hemp yarn 10 mm, (C) flax, (D) hemp and (E) jute.

3.3 Multiple compaction tests. The results from multiple compaction tests of UD and RD hemp fibre assemblies are shown in Fig. 5, and this demonstrates that for intermediary levels of stress the compactibility was increased with the compaction cycle number. The largest increase was observed at the second cycle, but the effect was gradually deminishing at the third and fourth cycle. It should be noted that the asymptotic value of the 4 curves seems not to be affected by the multiple compaction, and this points towards the fact that any difference between the curves is reflected by the exponent *b* of the fitted power law function (equation (5)). Fig. 6 shows *b* as a function of the cycle number determined for all the UD and RD assemblies, and it

demonstrates that *b* is lowered considerably at the second cycle whereafter only a small decrease can be observed at the third and fourth cycle. For the RD assemblies the decrease of *b* at the second cycle is much more marked than for the UD assemblies, and moreover, it is interesting to note that the relatively high values of *b* for all the RD plant fibre assemblies at the first cycle are getting close to the value of *b* for the RD glass fibre assembly at the second cycle.

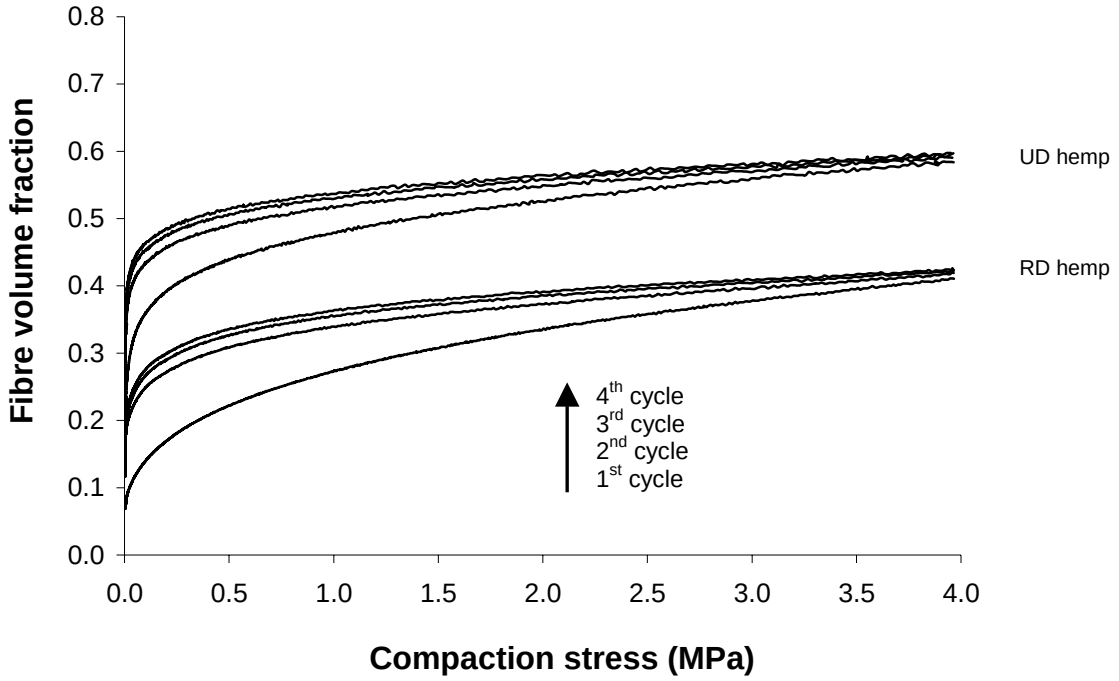

Fig. 5. Compaction behaviour of a UD and a RD hemp fibre assembly measured in multiple compaction tests. The numbering of the curves corresponding to the four successive compaction cycles follows the direction of the arrow.

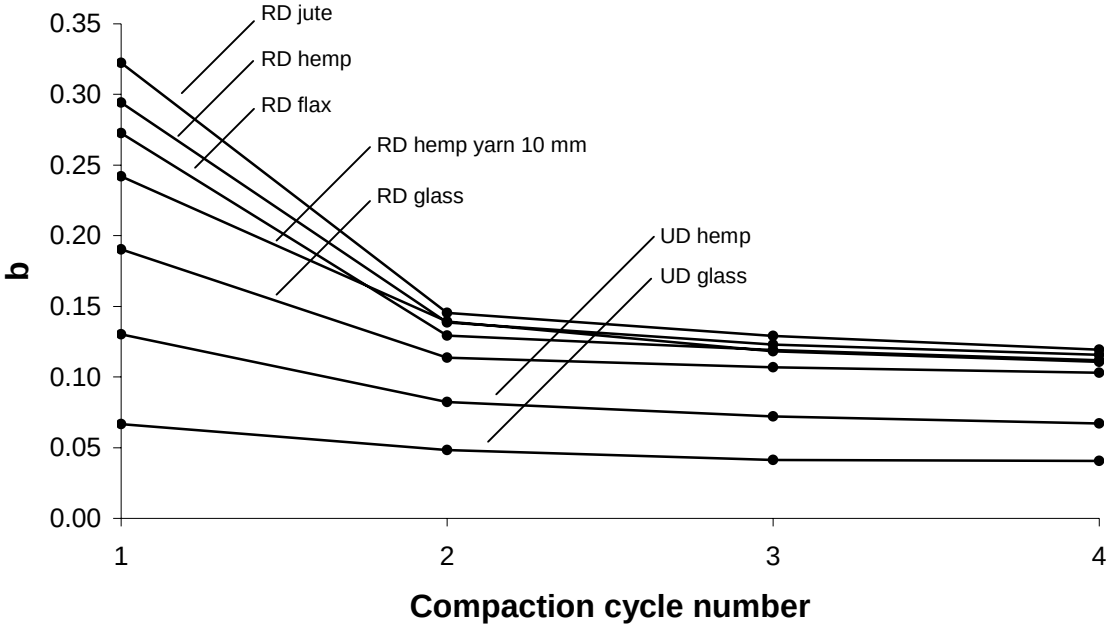

Fig. 6. The exponent *b* of the fitted power law function as a function of the compaction cycle number for the UD and RD fibre assemblies.

3.4 Volumetric interaction of composites. A diagram of the measured V_f against W_f of the fabricated unidirectional hemp/PET composites is presented in Fig. 7. The dotted line designates a V_f on 0.54 at a consolidation stress of 2.2 MPa, as read from the compaction curve in Fig. 2. The diagram clearly reveals a good accordance between the maximum obtainable V_f predicted from the compaction behaviour of the UD hemp fibre assembly and the measured V_f of the composites.

In addition, the ideal relationship between V_f and W_f, as predicted by equation (2) when the porosity content, V_p, is equal to zero, is plotted. The figure demonstrates that V_f starts to deviate from the ideal line when the value of W_f, corresponding to the maximum V_f, is approached, and at the same time the measured values of V_p starts to increase from the basal level.

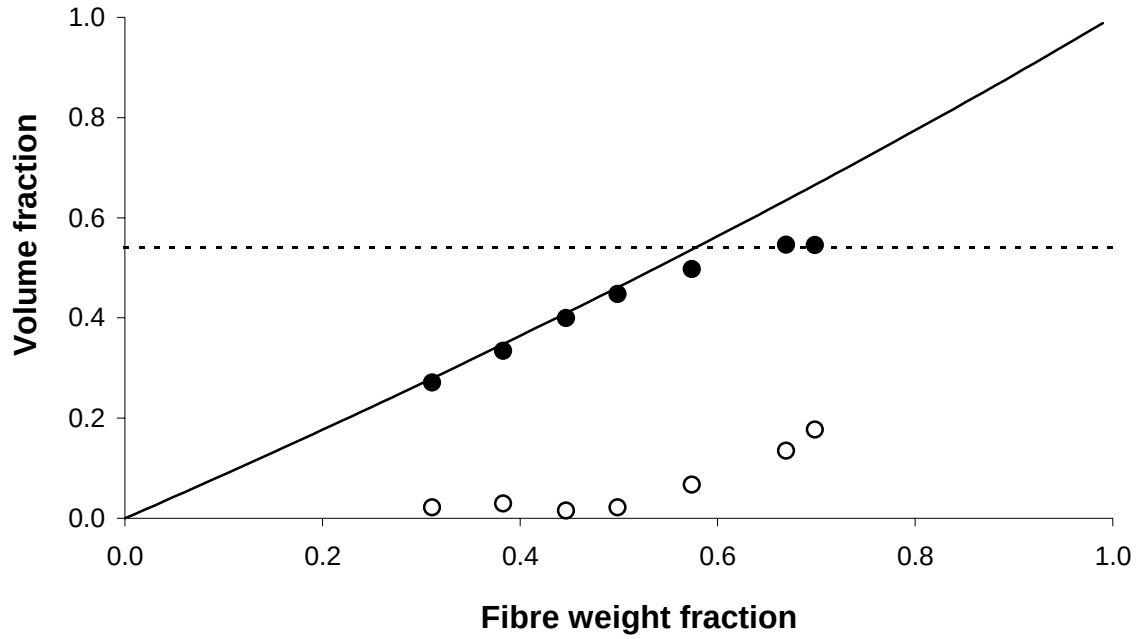

Fig. 7. The fibre volume fraction (filled symbols) and the porosity (open symbols) plotted as a function of the fibre weight fraction of unidirectional hemp/PET composite laminates. The full line designates the ideal relationship with no porosity as predicted from equation (2). The dotted line designates the maximum obtainable fibre volume fraction of 0.54 as read from the compaction curve in Fig. 2.

4. DISCUSSION

The good reproducibility of the measurements of compaction behaviour as documented in Fig. 1, gives support to the estimated precision of V_f on ±0.01, and more importantly it validates the use of only a few replicates for each of the tested experimental conditions. Thus, measurement of fibre assembly compactibility is a fast and reliable method to obtain an overall quantitative assessment of the structural organisation of a fibre network, without having to determine each of the many structural parameters, such as fibre orientation and fibre dispersion, and in fact because of its simplicity the method is utilised by the textile industry to control fabric quality (Toll 1998).

As expected from common sense of packing, the results showed that compactibility of the fibre assemblies was positively correlated with the fibre alignment. However, the observed effect of

fibre type, the glass fibres being considerable more easy to compact than the plant fibres, requires some profound explanation. In general, the stiffness of plant fibres must be considered to be lower than the stiffness of glass fibres, and this would in fact point towards a higher compactibility of the plant fibres (see equation (1)), meaning that apparently some other parameters must be working against the effect of stiffness. Small deviations of the fibre orientation are another possible explanation to account for the observed differences between the fibre types. For the UD assemblies the glass fibres are continuous and parallel and therefore these assemblies are essentially unidirectional; the hemp and flax fibres, on the other hand, are smaller discontinuous fibres twisted around each other, which increases the degree of misalignment and this could account for some of the reduced compactibility of the UD plant fibre assemblies. The same kind of explanation could be given for the RD assemblies, which implies that the fibre orientation in the jute assemblies, showing the lowest compactibility, should be close to random, whereas it should be less random in the glass fibre assemblies. However, the equal compaction results of the RD hemp yarn assemblies made manually in the laboratory, and therefore probably with a highly variable fibre orientation distribution, indicates that differences in the fibre orientation is not the main parameter explaining the different compaction behaviour of the RD assemblies. As already mentioned, the identical results of the three RD hemp yarn assemblies moreover demonstrate that the effect of the fibre length on the compaction behaviour can be ignored, which is as expected since the high fibre aspect ratio, even for relative short fibre lengths, means that a large number of contact points occur per fibre making the exact fibre length less important (Toll 1998). Thus, by neglecting the effect of the above-mentioned parameters, the negative correlation between the fibre bundle cross-sectional area and the assembly compactibility, as presented in this paper, indicates that fibre dispersion might be the main parameter explaining the difference in compactibility of the RD assemblies. In relation to fabrication of plant fibre composites the apparent positive effect of fibre dispersion on the maximum obtainable V_f highlights the efficiency of the defibration process applied to divide the larger fibre bundles into elementary fibres.

The presented results of the exponent b of the fitted power law function show that the exact shape of the compaction curves varies between the fibre assemblies, which means that to obtain maximum compaction different values of compaction stress need to be applied. The observation of a positive correlation between b and the fibre dispersion, identical to the one for the compactibility, only gives more support to the above-mentioned hypothesis. In Toll (1998), based on micro mechanical considerations, a power law for the load-deformation relationships, with an exponent n of 5 is presented to model the compaction behaviour of RD assemblies with a perfect fibre dispersion. In the same paper experimental data is presented of the compaction of RD assemblies with a less ideal fibre dispersion, and it is showed that a smaller exponent n of 3.5 must be applied to fit these data to a power law function. It should be noted that when the more typical load-deformation relationships are reported the exponent n corresponds to the inverse value of the exponent b given in this study. Thus, the value of b of 0.18 (1/0.18 = 5.6) for the RD glass assemblies and the larger values of b of around 0.30 (1/0.3 = 3.3) for the RD plant fibre assemblies with the larger fibre bundles, compare very well with the exponents reported by Toll (1998).

The results of multiple compaction are consistent with a study by Gutowski et al. (1987) on UD carbon fibre assemblies, showing a similar change of the compaction behaviour at the second compaction cycle but only minor changes at the subsequent cycles. As can be recognised from Fig. 5, the interpretation of the results from multiple compaction depends of the applied maximum compaction stress. If for instance the curves ended at 1 MPa it would have seemed obvious to conclude that the curves were shifted upwards as an effect of the successive compactions, and that the asymptotic V_f equally might increase. However, as can be realised

from Fig. 5, the four curves seem to share the same asymptotic V_f, which also can be confirmed by the nearly identical values of a from the fitted power law function (results not presented), and therefore the only difference between the curves is the shape as reflected by the exponent b. In relation to composite fabrication the observed decrease of b at the second compaction cycle means that by precompacting the fibre assembly prior to composite consolidation, the consolidation stress can be reduced without lowering the maximum V_f. Moreover, the results show that the decrease of b is largest for the RD plant fibre assemblies of lowest compactibility and this makes precompaction of these assemblies even more relevant.

The importance of measurements of compaction behaviour in order to optimise composite properties is illustrated by the presented volumetric interaction of UD hemp/PET composites with a variable W_f. The same good resemblance of the maximum obtainable V_f as predicted from the compaction behaviour and as measured from the composites, is presented in the work by Andersen and Lilholt (1999) based on RD jute/PP composites. The compaction of a fibre assembly during the composite consolidation process adds a few more parameters, which might influence the compaction behaviour, such as temperature and lubrication.

ACKNOWLEDGEMENT

This work was partly supported by the Danish Research Councils (project: "Characterisation and application of plant fibres for new environmentally friendly products"), and by the Danish Research Agency of the Ministry of Science (project: "High performance hemp fibres and improved fibre network for composites"). The authors thank Henning Frederiksen for the determinations of fibre densities and composite physical properties.

REFERENCES

Andersen, T.L., and Lilholt, H. (1999). Natural fibre composites: Compaction of mats, press consolidation and material quality. Ed. J. Renard, Proceedings of the 7th Euro-Japanese Symposium, Paris. p. 1-12.

Beil, N.B., and Roberts, W.W. (2002). Modeling and computer simulation of the compressional behaviour of fiber assemblies. Part I: Comparison to van Wyk's theory. Tex. Res. J. 72, 341-351.

Gutowski, T.G., Cai, Z., Bauer, S., Boucher, D., Kingery, J., and Wineman, S. (1987). Consolidation experiments for laminate composites. J. Comp. Mater. 21, 650-669.

Lilholt, H., and Bjerre, A.B. (1997). Composites based on jute-fibres and polypropylene matrix, their fabrication and characterisation. Eds. S.I. Andersen et al, Proceedings of the 18th Risø International Symposium on Materials Science: Polymeric Composites – Expanding the limits, Risø National Laboratory. p. 411-423.

Lomov, S.V., and Verpoest, I. (2000). Compression of woven reinforcements: A mathematical model. J. Reinforced Plast. Comp. 19, 1329-1350.

Madsen, B., and Lilholt, H. (2002). Physical and mechanical properties of unidirectional plant fibre composites – an evaluation of the influence of porosity. Comp. Sci. Tech. In press.

Simácek, P., and Karbhari, V.M. (1996). Notes on the modeling of preform compaction: I-Micromechanics at the fiber bundle level. J. Reinforced Plast. Comp. 15, 86-122.

Toll, S. (1998). Packing mechanics of fiber reinforcements. Polym. Eng. Sci. 38, 1337-1350.

van Wyk, C.M. (1946). Note on the compressibility of wool. J. Tex. Inst. 37, T285-T292.